BOEM2016-050

Use of Finite-Volume Modeling and the Northeast Coastal Ocean Forecast System in Offshore Wind Energy Resource Planning

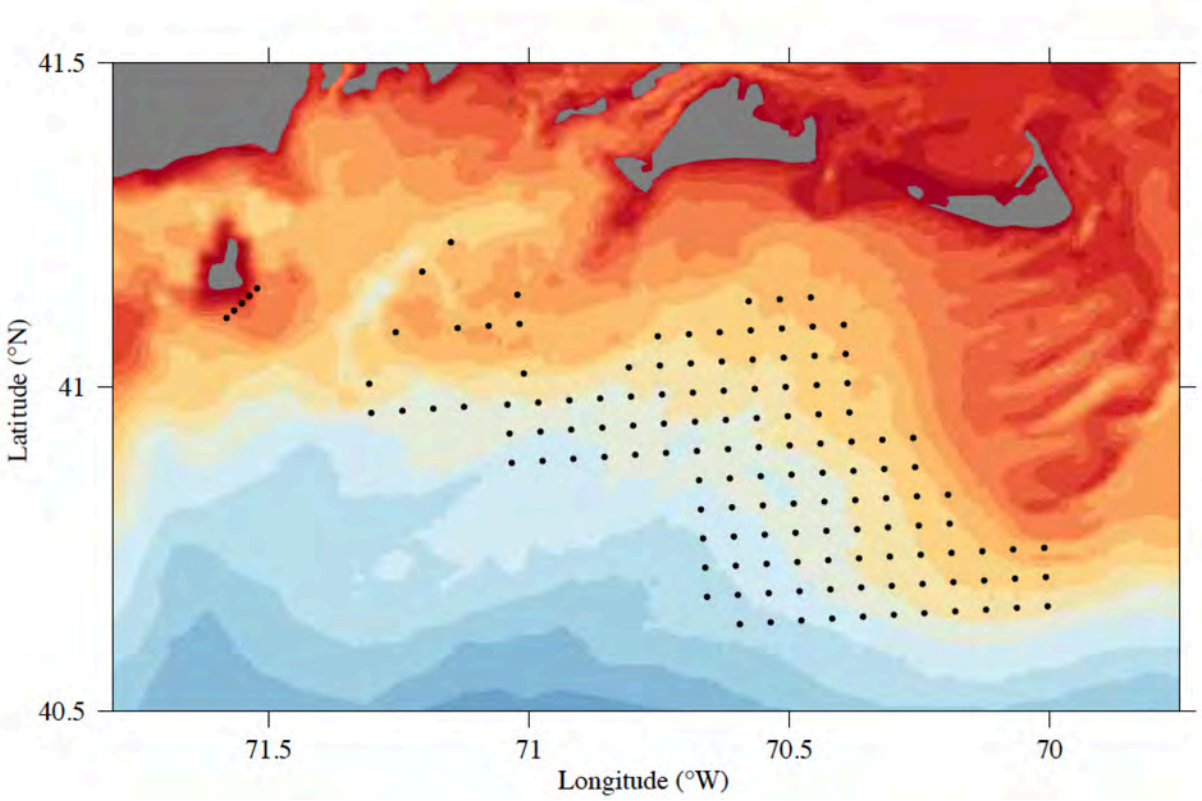

U.S. Department of the Interior
Bureau of Ocean Energy Management
Office of Renewable Energy Programs
www.boem.gov

BOEM
Bureau of Ocean Energy Management

BOEM 2016-050

Use of Finite-Volume Modeling and the Northeast Coastal Ocean Forecast System in Offshore Wind Energy Resource Planning

Authors

Changsheng Chen
Robert C Beardsley
Jianhua Qi
Huichan Lin

Prepared under BOEM Contract
M14PS00040
by
School for Marine Science and Technology
University of Massachusetts-Dartmouth
New Bedford, MA 02744

Department of Physical Oceanography
Woods Hole Oceanographic Institution
Woods Hole, MA 02542

Published by
U.S. Department of the Interior
Bureau of Ocean Energy Management
Office of Renewable Energy Programs
45600 Woodland Road, VAM-OREP
Sterling, VA 02166

July 2016

DISCLAIMER

This report was prepared under contract between the Bureau of Ocean Energy Management (BOEM) and University of Massachusetts-Dartmouth. This report has been technically reviewed by BOEM and has been approved for publication. Approval does not signify that the contents necessarily reflect the views and policies of BOEM, nor does mention of trade names or commercial products constitute endorsement or recommendations for use. It is, however, exempt from review and in compliance with BOEM editorial standards.

REPORT AVAILABILITY

You will be able to obtain this report from BOEM by writing to the following addresses.

U.S. Department of the Interior
Bureau of Ocean Energy Management
Office of Renewable Energy Programs
45600 Woodland Road, VAM-OREP
Sterling, VA 20166
Phone: 703.787.1553
Fax: 703.787.1708

To download a PDF of this report, please go to the U.S. Department of the Interior, Bureau of Ocean Energy Management, Environmental Studies Program Information System (ESPIS) website and search OCS Study BOEM 2016-050.

CITATION

Changsheng Chen, R. C. Beardsley, J. Qi and H. Lin, 2016. Use of Finite-Volume Modeling and the Northeast Coastal Ocean Forecast System in Offshore Wind Energy Resource Planning. Final Report to the U.S. Department of the Interior, Bureau of Ocean Energy Management, Office of Renewable Energy Programs. BOEM 2016-050. 131pp.

ABOUT THE COVER

Cover photo (Image of local bathymetry with possible locations of wind turbines). The figure is rescaled from Figure 2.2 in the report.

EXECUTIVE SUMMARY

The Bureau of Safety and Environmental Enforcement (BSEE), the United State Department of the Interior (DOI), on behalf of the Bureau of Ocean Energy Management (BOEM), has contracted the Marine Ecosystem Dynamics Modeling Laboratory (MEDML), School of Marine Science and Technology (SMAST), University of Massachusetts-Dartmouth (UMASSD) to conduct modeling experiments for the purpose of assessing the possible impacts of future offshore wind energy facilities on the small-scale coastal and regional physical environmental processes: evaluating the potential changes in ocean circulation patterns throughout the water column and determining what geographic areas and depths may be most affected by the installation of wind turbines as well as influences on biological processes (e.g., larval transport).

The physical environments in the offshore wind facility development region are generally stratified, in which the flow is generated and controlled by tidal, wind forcing and surface heat flux over time scales in the range of hourly to interannual time regimes. This region is frequently influenced by nor'easter storms during winter through spring and is occasionally struck by hurricanes, with no average or mean events that can represent such a large variation in atmospheric forcing. This contract work has been focused on storm-induced short-term variability: with objectives aimed at assessing the extreme impacts of the offshore wind facility on the local and regional physical environment under severe weather conditions. The February 1978 Nor'easter storm (a hundred-year storm) and the August 1991 Hurricane Bob (a H2 hurricane when passing over the offshore wind farm region) were selected as representatives of extratropical and tropical storms.

Built on the Northeast Coastal Ocean Forecast System (NECOFS), the MEDML/SMAST/UMASSD has developed a high-resolution, subdomain FVCOM model and nested it with the regional NECOFS. This subdomain model is named "NS-FVCOM", with a computational domain covering Nantucket Shoals (NS), Nantucket Sound, Buzzard Bay, Narragansett Bay, Block Island and Long-Island Sound. The domain was configured with the unstructured triangular grid with a horizontal resolution of up to 1.5 m for the case including wind turbines. NS-FVCOM is fully coupled with the FVCOM surface wave model named "NS-SWAVE".

The influences of future offshore wind energy resources were estimated by calculating the difference of model-computed surface elevation, vertically averaged velocity (proportional to the volume transport), near-surface and near-bottom velocities, significant wave height, and bottom stress between the model runs with and without wind turbines. The experiments were first made by running the coupled NS-FVCOM and NS-SWAVE model system with the inclusion of wave-current interaction, and then either the hydrodynamic simulation with NS-FVCOM only or the surface wave simulation with NS-SWAVE only was conducted to examine the roles of wave-current interaction in the change of the storm-induced physical environment under the conditions without and with wind turbines. The purpose of running the model under different dynamical setups is to quantitatively estimate the relative contribution of wave-current interaction to

hydrodynamics variables and significant wave heights under the conditions without and with wind turbines.

For the February 1978 Nor'easter case, the model results show that the influence of the deployment of offshore wind turbines on the physical environment varies in space; not only locally inside the wind turbine facility area but can also be regional. It is generally small in the surface elevation, but can be significant in the transport, near-surface and near-bottom velocities, and significant wave height. Inside the wind turbine facility area, the mean and maximum changes are ~ 0.04 and ~ 0.08 m for the surface elevation, while they can be ~ 0.34 and ~ 5.53 m for the significant wave height, ~ 0.03 and ~ 2.09 m/s for vertically averaged velocity, ~ 0.04 and ~ 0.86 m/s for the near-surface velocity, and ~ 0.04 and ~ 0.66 m/s for the near-bottom velocity. The change in the bottom stress is also relatively small with a mean of ~ 0.05 N/m^2, but its maximum can be locally up to ~ 2.30 N/m^2. Near the surface, a cyclonic circulation with a magnitude of ~ 0.10-0.20 m/s can form around the wind turbine facility area and multiple small-scale cyclonic eddies can be generated between wind turbines. Near the bottom, the existence of wind turbines can intensify the offshore flow during the storm by a magnitude up to ~ 0.20-0.30 m/s. The change in the flow direction can be as large as 80°-170°. The changes in the region outside the wind turbine facility area can be in the same order of magnitude as inside the wind turbine facility area. The influence can be extended to the outer shelf and coastal region. Over the shelf region where the water is stratified, the change in the velocity exhibits a two-layer structure, being opposite in direction near the surface and bottom. As a result of cancellation, the influence does not cause a significant change in the vertically averaged velocity and thus transport. The existence of offshore wind turbines can significantly enhance the significant wave height over the outer shelf during the storm, with a maximum up to ~ 2.35 m.

For the August 1991 Hurricane Bob case, the model results also suggest that the influence of the deployment of the offshore wind turbines can have a regional impact. The change is generally small in the surface elevation and vertically averaged velocity, but can be significant in surface waves, and near-surface and near-bottom velocities. The wind turbine-induced influence exhibits a significant spatial variation. The maximum change can be ~ 12.6 (3.5) m for the significant wave height, ~1.4 (1.1) m/s for the near-surface velocity, and ~1.0 (0.6) m/s for the near-bottom velocity inside (outside) the offshore wind turbine facility area, respectively. The change in the bottom stress is generally small inside the offshore wind turbine facility area, but significant around the edge of the wind turbines' boundary, around islands, and near the coast in the shallow region outside the wind turbine facility. The maximum change can be up to 6 and 7 N/m^2 inside and outside the wind turbine facility area, respectively.

The model experiments imply that the wind turbine facility on the eastern shelf of Block Island can cause more significant local and regional impacts than offshore wind facilities over the outer shelves off Massachusetts and Rhode Island. Inside the wind turbine facility area, the maximum change during the nor'easter storm and hurricane cases can be ~ 0.2-0.4 m for the surface elevation, ~ 3.5-7.3 m for the significant wave

height, ~ 0.7-1.7 m/s for the vertically averaged, near-surface and near-bottom velocities, and ~ 16.8-28.2 N/m^2 for the bottom stress.

The possible impact of the change in the local and regional physical environments due to the offshore wind facility development on larval transports was examined by particle-tracking experiments. In these experiments, fish larvae were treated as individual passive particle tracers and released outside and within the wind turbine facility areas. The same numbers of particles were released at the same locations for the case without the wind turbines, and the change of spatial dispersion was estimated by the difference between the larval dispersion rates between the cases with and without wind turbines. The results show that during the storm events the deployment of wind turbines in the proposed offshore region will not have a significant influence on the southward larval transport from the upstream Georges Bank and Nantucket Shoals areas to the Mid-Atlantic Bight, although it can cause a relatively large cross-shelf larval dispersion. The mean of the change in the spatial dispersion rate through the wind turbine region was in the range of $0.01\text{-}0.44\times10^5$ m^2/s, with a maximum value up to 1.6×10^5 m^2/s. This maximum value was the same order of magnitude as the maximum dispersion rate of the particles that were released in the case without wind turbines.

Table of Contents

1. Introduction

1.1 Project Overview

1.1.1 Objectives

The objective of this project is to use the Northeast Coastal Forecast System (NECOFS), which was developed and is being operated by our team [the Marine Ecosystem Dynamics Modeling Laboratory (MEDML), School of Marine Science and Technology (SMAST), University of Massachusetts-Dartmouth], to assess "the mesoscale effects of offshore wind resource facilities on oceanic environmental conditions and habitat." The project has selected a proposed area of offshore wind energy development within the NECOFS domain to develop a high-resolution subdomain FVCOM with the inclusion of the proposed wind turbines. This subdomain FVCOM is nested to NECOFS and driven through the boundary conditions derived from the NECOFS hindcast hydrodynamic field and by the surface forcing derived from the NECOFS mesoscale meteorological model (MM5 or WRF) products. A series of simulations were conducted with an aim at providing a comprehensive assessment of the impact of wind energy resource facilities on temporal and spatial variability of the circulation, mixing, and larval transports over local and regional scales. BOEM will use the high-resolution model-produced physical fields from this project to *a*) assess the possible impact of the offshore wind construction in particular geographic regions along the U.S. northeast coast on biological processes (e.g., spawning and larval transport) and *b*) evaluate the potential changes in ocean circulation patterns throughout the water column and determine what geographic areas and depths may be most affected by the installation of wind turbines.

1.1.2 Required Tasks

Following RFP No. M14PS00040, BOEMS requires that the experiments be made in the U.S. Northeast Atlantic Region covering from Massachusetts to New Jersey (C3. A); "starting with the outer continental shelf off Massachusetts and Rhode Island and, if time allows, continuing down the shelf to New Jersey (C3: Task 2)." Six tasks are required to complete, including:

Task 1: Provide overall project coordination and management including 1) a post-award meeting with BOEM within two weeks of contract award in the BOEM office in Herndon, VA with BOEM staff and 2) manage project plan and coordinates. For this meeting, the UMASSD team must provide: *a*) agenda to participants prior to the meeting; *b*) draft an action plan to participants prior to meeting; *c*) meeting summary to participants with one week of the meeting; and *d*) revised action plan to Contracting Officer's Representative (COR): Ms. Callie Hall (listed in F.6).

Task 2: The UMASSD team is required to "develop a numerical finite-volume coastal ocean model for designated wind energy areas of the U.S. Northeast Atlantic Coast, starting with the outer continental shelf off Massachusetts and Rhode Island and, if time

allows, continuing down the shelf to New Jersey. Refine the modeling grid of the study area, including the fitting of bottom topography and the fitting of irregular geometric coastlines, island complexes, and barriers, from a priori turbine scenarios within proposed wind energy areas along the U.S. Northeast Atlantic Coast. Turbine scenarios may be found within the Multi- Purpose Marine Cadastre National Viewer Tool (csc.noaa.gov/mmcviewer.com), using the layers of "Active Renewable Energy Leases" and "BOEM Wind Planning Areas."

Task 3: The UMASSD team is required to "conduct wave-current interaction modeling experiments with particular analysis of the impacts of storms, hurricanes, and Nor-easters on bottom stress within the study area."

Task 4: The UMASSD team is required to "refine NECOFS model grids, up to a few meters, with the introduction of individual wind turbines and wind farms in the study area. Create a new, refined subdomain grid including possible wind turbines. Process and implement high-resolution bathymetric data into the refined grid. Configure and test the sub-grid model for stability. The final product should be a well-calibrated sub-grid FVCOM specific to the project (including placement of wind turbines within the study area and accounting for storm events within the study area)."

Task 5: Prepare and submit draft final and revised final report. The report will summarize the results from Tasks 2-4 with clear, concise writing following the format and organization agreed upon between the Program Manager (PM) and the BOEM prior to preparation. First, prepare and submit a draft final report and then submit a revised final report with taking BOEM's comments into consideration. No permission is given to distribute any components of the report to any parties prior to final acceptance by BOEM. If a need arises to do it, the UMASSD team must obtain the written approval from the COR in BOEM.

Task 6: All submissions of peer-revised journal articles, abstracts for oral presentations for conferences, must be submitted to the BOEM COR for review and comment prior to submission. "All publications and oral presentation must contain an acknowledgement of BOEM funding that reads: Study funding was provided by the U.S. Department of the Interior, Bureau of Ocean Energy Management, Environmental Studies Program, Washington, DC under Contract Number M14PS00040." Contract number to be filled in at time of award. An acknowledgement page of this statement needs to be incorporated into the PowerPoint slides.

1.2 Physical Background

The wind, wave, ocean current (tidal currents) and solar energies are the clean renewable energy resources that the Bureau of Ocean Energy Management (BOEM) is considering to issue leases for energy production on the Outer Continental Shelf (OCS). BOEM has been working together with individual state agencies to identify potential leasing areas for the offshore wind facilities. Over the U.S. Northeast Atlantic Region extending from Massachusetts to Virginia, five areas are proposed (Figure 1.1).

According to the OCS Lands Act, BOEM is required to "balance the nation's energy needs with the protection of human, marine and coastal environments" (cited from section C.1 of RFP No. M14PS00040).

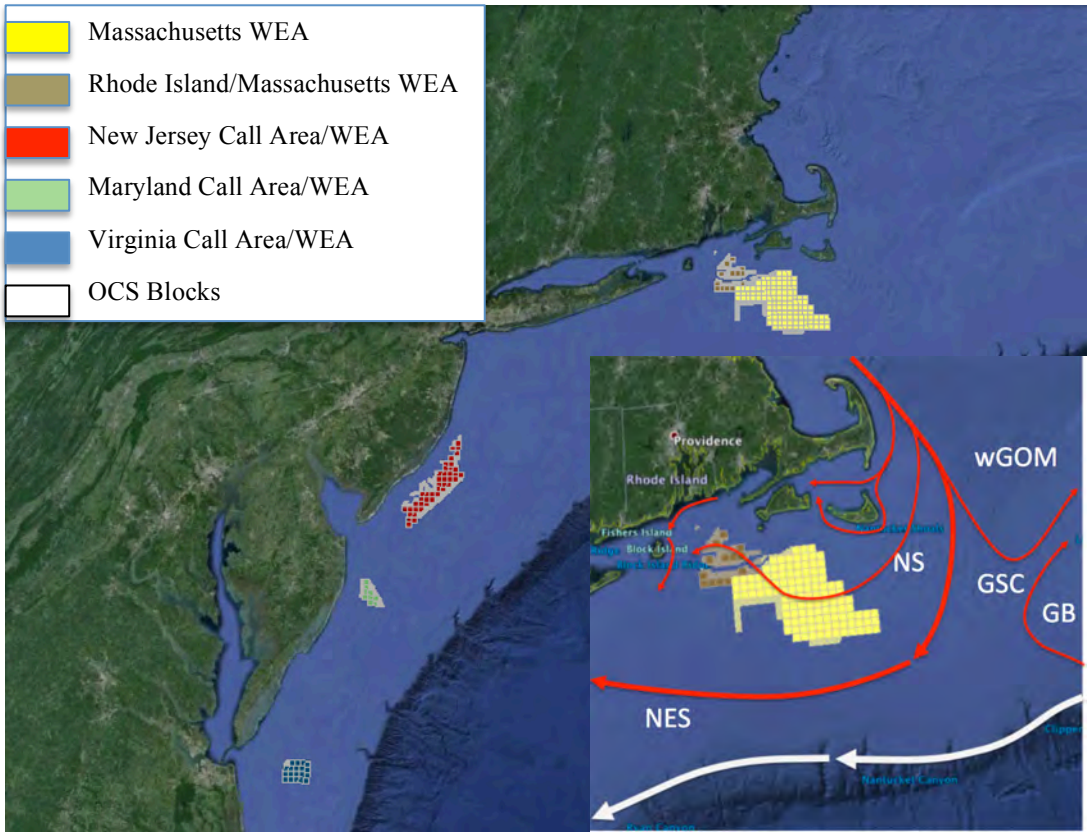

Figure 1.1: Existing lease areas identified by BOEM for the offshore wind facilities downloaded from http://www.boem.gov/ Renewable-Energy-Program-Mapping-and-Data/. Right-lower panel is an enlarged view of the lease areas in the federal waters of Massachusetts and Rhode Island overlapped with the schematic pattern of water currents from the Cape Cod coast on the north (red color arrows) and southern Georges Bank (GB) on the east (a white arrow). wGOM: western Gulf of Maine; NS: Nantucket Shoals; GSC: Great South Channel; NES: New England Shelf.

The physical environments in the offshore wind facility development region are generally stratified, in which the flow is generated and controlled by tidal and wind forcing. This region is frequently influenced by the nor'easter storms during winter through spring and is occasionally struck by hurricanes. The tidal elevation is dominated by the semidiurnal M_2 tide, with a tidal energy convergence zone on the southeast of Nantucket Island (NI), where the southward propagating tidal energy flux from the western Gulf of Maine (wGOM) along the Cape Cod (CC) meets the northeastward tidal energy flux from the eastern New England Shelf (NES) (Chen et al., 2011). The interaction between these two tidal waves results in a relative permanent minimum surface elevation in the region. The amplitude of the M_2 tidal elevation has a maximum of 0.3-0.4 m, decreases toward the northeast, and reaches a minimum over the southeast Nantucket Shoals (Shearnan and Lentz, 2004, Chen et al., 2011). In contrast, the depth-

averaged tidal current amplitude increases toward the northeast and reaches a maximum of > 0.6 m/s near Nantucket Island (Chen et al., 2011).

This shelf is a typical flow-through system in which the subtidal currents are generally characterized by a westward flow. This flow originates from two distinct water sources: a) the southward coastal current along CC and b) the westward slope current along the shelf break where the density front is located (Figure 1.1). Around the eastern shelf off Block Island where the coastal wind turbines were deployed, the subtidal current is characterized by around-island clockwise southward flow. This around-island flow can be tracked back to the near-coastal current over the Rhode Island shelf and the eastward flow from the Block Island Sound that is bifurcated on the western shelf off Block Island (Sun et al., 2016). The speed of the around-island clockwise flow is about 0.05-0.2 cm/s.

The shelf off Massachusetts and Rhode Island is often influenced by severe weather conditions due to hurricanes (tropical cyclones) and nor'easter storms (extratropical cyclones) (Bernier and Thompson, 2006; Chen et al., 2013a and Beardsley et al., 2013). Strong winds of hurricanes and nor'easter storms generate high surface waves, and the resulting wave-current interaction can directly affect the water movement and bottom sediment transport over the shelf. In the past 30 years, two hurricanes and more than 15 notable nor'easter storms have swept through the coast of Massachusetts and Rhode Island. Hurricane Bob, with peak marine winds up to 54 m/s (~ 100 mph), was a very strong tropical storm that moved up the U.S. east coast and crossed over southern New England on 19-20 August 1991. The February 1978 nor'easter was the strongest extratropical storm that struck the region of Nantucket Shoals and Sound in the 20th century, with peak marine winds up to 38-49 m/s (~ 86-111 mph). This nor'easter had the same strength as an hurricane. The Cape Wind Associates, LLC selected this nor'easter as a test case to assess the storm-induced potential impact of the wind energy facilities on the local marine environment in Nantucket Sound. The October 1991 extratropical cyclone (the "Perfect Storm" or "Halloween Nor'easter of 1991") produced strong winds (peak gusts above 27 m/s) and > 8-m waves during high tides (1.2 m above normal) (McCown, 2008). More recently, the December 27 2010 nor'easter (Freedman, 2010) produced sustained peak winds above 23 m/s and > 6-m waves above high tides along the Massachusetts coast (Beardsley et al., 2013). The recent February 8-9 2013 nor'easter (the "Blizzard of 2013"), a super winter storm formed by the merger of a warm moist Mid-Atlantic low and a cold northeast low, caused a snowfall of > 25 inches (0.6 m) and a storm surge of ~ 1.3-1.5 m in the Boston area (Freedman, 2013).

1.3 Biological Background

The U.S. northeast continental shelf supports a number of very important fisheries. For example, the sea scallops (*Placopecten magellanicus*) harvested in this area account for some 28% of all scallop production worldwide (Naidu and Robert, 2006), with roughly 50 million pounds of sea scallop worth over $500 million being landed in New Bedford annually. As with many marine living resources, the scallop fishery stocks are subject to environmental changes and exploitation pressure, which can lead to fluctuations in fishery landings. Recently we have collaborated with Dr. Kevin

Stokesbury's team at UMASSD to combine scallop abundance data from the last ten-year (2003-2012) video surveys with NECOFS-computed bottom temperatures. The results clearly show that the abundance distribution is strongly geographically related, with a high correlation between bottom temperature and benthic habitats (Figure 1.2). Although sea scallops are a sedentary species with limited ability to migrate (Posgay, 1981; Melvin et al., 1985), their pelagic larvae are easily advected by ocean currents, which results in effective connection between geographically-separated populations between Georges Bank and the Mid-Atlantic Bight (Tian et al., 2009). The two offshore wind energy development areas (labeled WEAs in Figure 1.1) in federal waters south off Massachusetts and Rhode Island include part of Nantucket Shoals and the adjacent New England Shelf waters, in an area of relatively low abundance of scallops (Figure 1.2). This area, however, is close to a region where the southward flow from the Cape Cod coast and the westward flow from the southern Georges Bank and shelf break merges and flows to the Mid-Atlantic Bight (see the right-lower panel in Figure 1.1).

One concern of the fisheries community is on the impact that the mesoscale flow produced by an offshore wind resource facility can change the water transport connection between the Georges Bank/Gulf of Maine and the Mid-Atlantic Bight, and thus affect the scallop landings in the Mid-Atlantic Bight. Nantucket Shoals is a region of high tidal energy dissipation, where the southward-propagating tidal energy flux from the western Gulf of Maine along Cape Cod meets the northeastward tidal energy flux from the eastern New England Shelf (Chen et al., 2011). Dynamics controlling the sediment transport in this region are complicated. It is unknown whether or not an offshore wind facility located on the western side of this convergence zone can alter the tidal energy flux from the New England Shelf, and thus cause a change on sediment distribution around this area. In addition, an array of wind turbines can produce mesoscale or even small-scale eddies around the wind facility area. As a result, the turbine-generated flow can enhance vertical and lateral mixing, and thus cause a change in sediment transport and distribution. Since scallop larval settlement and recruitment depend critically on its habitat, it is imperative to assess the possible potential impacts of offshore wind resource facilities on local and regional environments and provide an optimal design with a balance between our nation's renewable energy development and commercial fisheries.

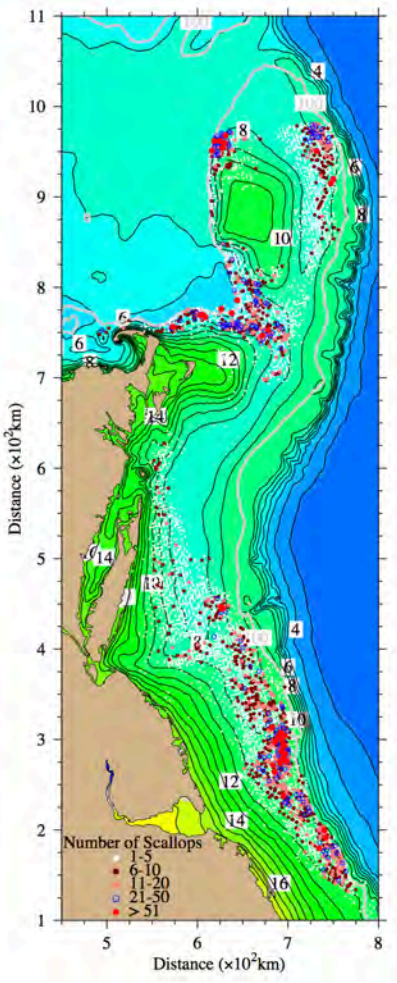

Figure 1.2: Relationship between distributions of scallop abundance observed from scallop video survey and bottom water temperature on the U.S. Northeast Continental Shelf.

1.4 Modeling update-NECOFS

We have developed the Northeast Coastal Ocean Forecast System (NECOFS) as one component of the NOAA IOOS-funded Northeastern Regional Association of Coastal and Ocean Observing Systems (NERACOOS). NECOFS is an integrated atmosphere/surface wave/ocean forecast model system designed for the northeast U.S. coastal region, covering a computational domain from the Delaware Shelf to the eastern end of the Scotian Shelf, including the New England Shelf (NES), Georges Bank (GB) and the Gulf of Maine (GOM). NECOFS was placed in experimental forecast operations in late 2007.The present system includes 1) a community mesoscale meteorological

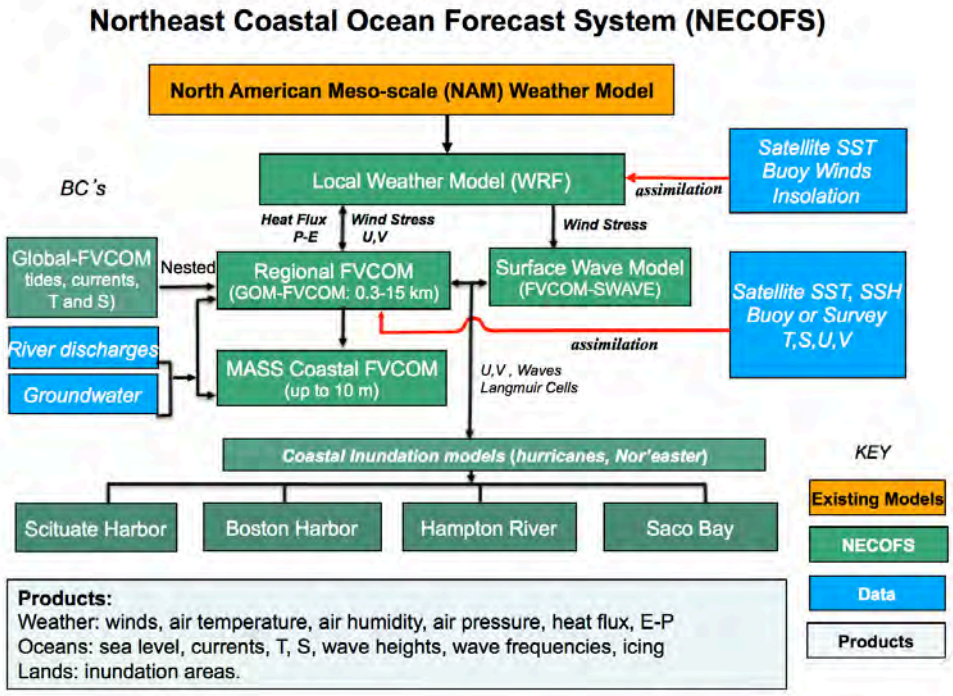

Figure 1.3: Schematic chart of NECOFS.

model named "Weather Research and Forecasting (WRF)"; 2) the 3rd version regional FVCOM with the computational domain covering the Gulf of Maine/Georges Bank/New England Shelf region (GOM3-FVCOM); 3) the unstructured-grid surface wave model (GOM3-SWAVE) modified from SWAN (Qi et al., 2009) with the same domain as GOM3-FVCOM; 4) the Mass Coastal FVCOM with the inclusion of estuaries, inlets, harbors and intertidal wetlands; and 5) three subdomain wave-current coupled FVCOM inundation forecast systems in Scituate, MA; Boston Harbor, MA; and Hampton-Seabrook Estuary, NH (Figures 1.3 and 1.4).

The GOM3-FVCOM grid features unstructured triangular meshes with horizontal resolution of ~ 0.3-25 km and a hybrid terrain-following vertical coordinate (with a total of 45 layers, 10 and 5 uniform layers near the surface and bottom, respectively, in regions deeper than 225 m with a transfer to a sigma-coordinate in the shallow continental and coastal regions. The thickness of the uniform layers is 5 m, so the hybrid coordinate

transition occurs at locations where all layers have uniform thickness of 5 m. The Mass Coastal FVCOM grid is configured with triangular meshes with horizontal resolution up to ~ 10 m, and 10 layers in the vertical. The Scituate, Boston Harbor and Hampton-Seabrook Estuary inundation model grids include both the water and land with horizontal resolution up to ~ 5-10 m and 10 vertical layers.

GOM3-FVCOM is driven by surface forcing from the output of the WRF model configured for the region (with a 9-km resolution), the COARE3 bulk air-sea flux algorithms, tidal forcing constructed using five constituents (M_2, S_2, N_2, K_1 and O_1) on the open boundary, and local river discharges. The GOM3-SWAVE is driven by the same WRF wind field with wave forcing at the boundary nested to the Wave Watch III (WWIII). The Wave Watch III is set up for a northwestern Atlantic region and run at the same time when the WRF forecast is carried out. The Mass Coastal FVCOM and three inundation models are connected with GoM3-FVCOM through "one-way" nesting in the common boundary zones. The Mass coastal FVCOM is driven by the same surface forcing as GOM3-FVCOM. The nesting boundary conditions for the inundation models include both hydrodynamics and waves provided by GOM3-FVCOM and GOM3-SWAVE. NECOFS was placed in experimental forecast operations in late 2007 and the daily 3-day forecast product can be accessed and viewed on the NECOFS Web Map Server addressed: (http://134.88.229.220:8080/fvcomwms/).

The updated version of FVCOM (called FVCOM 3.1.6) is a fully coupled current-ice-wave-sediment-ecosystem model system. This version has been optimized to run efficiently in parallel on multi-processor computers using the MPI (Message Passing Interface) software. In addition to the surface wave model FVCOM-SWAVE, other modules useful in our contract work include FVCOM-NH (a non-hydrostatic version of FVCOM (Lai et al., 2010), the mass-conservative multi-domain nesting module, VisIt - the DOE Oak Ridge National Laboratory model visualization interactive tool that allows users to monitor model performance during model runs and post-process the model output data, FVCOM-SED (an unstructured-grid version of the USGS structured-grid community sediment model developed by Warner et al. (2008)), 4-D nudging, OI and Kalman Filters for data assimilation (Chen et al., 2009a), and unstructured-grid versions of the EPA's WASP, Army Corps of Engineers' CE-QUAL-ICE, and HydroQual's RCA (HydroQual, 1993, Chen et al., 2013b) water quality models**.** FVCOM 3.1.6 has been distributed to users (e.g., the NOAA National Ocean Survey (NOS) Center for Operational Oceanographic Products and Services (CO-OPS) for development of a forecast system for the northern Gulf of Mexico shelf), with public release with the 3rd version of the new user manual.

The 37-year (1978-2014) hindcast simulation of NECOFS was conducted using a global-regional nested FVCOM system with the core models of Global-FVCOM and GOM3-FVCOM (Figure 4). Global-FVCOM is a fully atmosphere-ice-surface wave-ocean coupled primitive equation unstructured-grid ocean model that is driven by 1) astronomical tidal forcing with eight constituents (M_2, S_2, N_2, K_2, K_1, P_1, O_1 and Q_1), 2) surface wind stress, 3) net heat flux at the surface plus shortwave irradiance in the water column, 4) surface air pressure gradients, 5) precipitation (P) minus evaporation (E), and

6) river discharge (Gao et al., 2011, Chen et al., 2016). The updated version of Global-FVCOM features a horizontal resolution of ~ 2 km (measured by the length of the longest edge of a triangular cell) within the Canadian Archipelago, shelf-break and coastal regions to ~ 50 km in the interior open ocean. The vertical grid features a total of 45 layers (Chen et al., 2009b, 2016). In regions with depth greater than 225 m, 10 uniform layers (5-m thick) are used near the surface and 5 uniform layers (5-m thick) near the bottom respectively to better resolve these boundary layers. In shelf and coastal regions of depth less than 225 m, a sigma distribution with a uniform layer thickness is used. The coordinate transition thus occurs smoothly at a depth of 225 m where all layers have a uniform thickness of 5 m. GOM3-FVCOM was driven by one-way nesting with Global-FVCOM. Global-FVCOM has been run with assimilation of SST, SSH on a daily basis and T/S profiles on a monthly basis for 1978-2013 *(*http://202.121.66.105:8000/fvcom

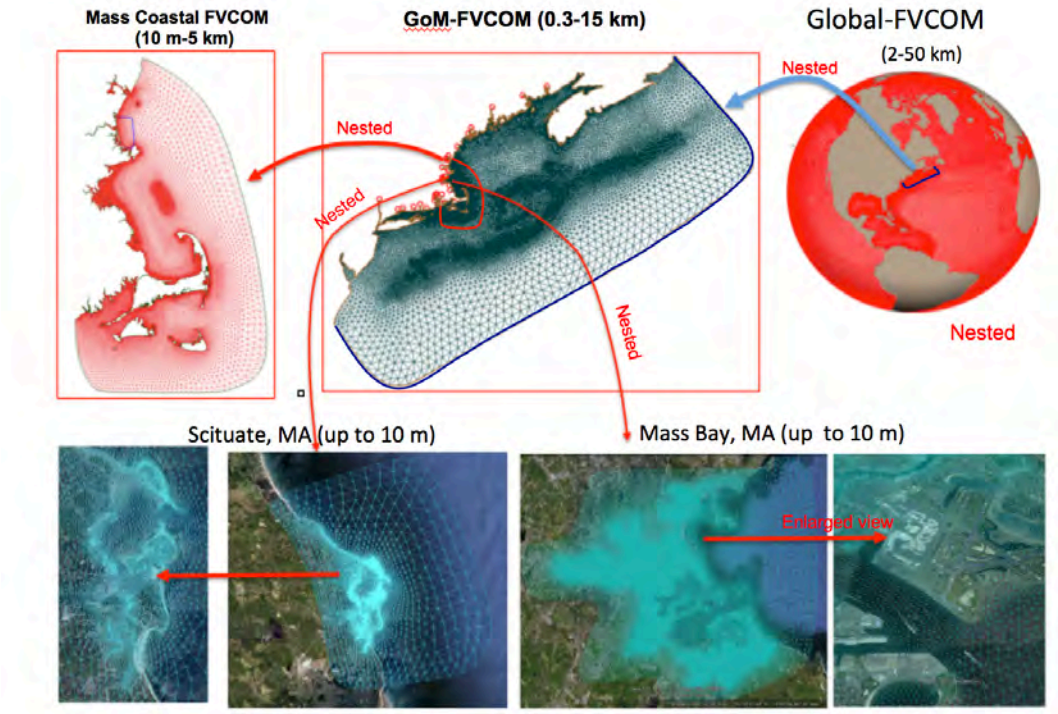

Figure 1.4: Global-regional-estuarine-wetland nested unstructured grids of NECOFS including Global-FVCOM, GOM3-FVCOM, Mass Coastal FVCOM and Scituate-Mass Bay FVCOM inundation models. Global-FVCOM is run in the hindcast application nested with GoM3-FVCOM.

wms/*)*. A 37-year NECOFS hindcast product is now available on the NECOFS Web Map Server (http://134.88.229.220:8080/fvcomwms/). An hourly hindcast database housed at SMAST includes meteorological and oceanic components. The meteorological database includes hourly fields of key physical variables (wind velocity, air pressure, precipitation minus evaporation, shortwave radiation, longwave radiation, sensible and latent heat fluxes, and air temperature). The oceanic database contains hourly fields of three-dimensional water currents, temperatures and salinity, and surface wave conditions. Both databases will consist of a collection of standard NetCDF files. For more information

about the Global-FVCOM and GOM3-FVCOM model structure and results, see http://www.fvcom.smast.umassd.edu/.

We have validated NECOFS hindcast fields by comparing the results with many available observations including 1) water level measurements at tidal gauges, 2) temperature and salinity in the water column, and 3) the surface current measurements made using CODAR from 2000 to 2008. The model-data comparison results are uploaded on the NECOFS server: http: //fvcom.smast.umassd.edu/Data/FVCOM/ NECOFS/Archive/Seaplan_model_validation/. Some of validation results have been published in peer-reviewed journals, which include Cowles et al. (2008) for vertical mixing and subtidal currents; Chen et al. (2011) for tidal elevations and currents; Li et al. (2015) for water stratification and spatial/temporal variability; and Sun et al. (2016) for CODAR-derived surface currents over periods within 2000-2008. NECOFS was also validated for the storm-induced surges and coastal inundation by hindcasting flooding caused by the extratropical storm (nor'easter) that swept New England on December 27, 2010 (Chen et al., 2013a; Beardsley et al., 2013) and the storm surge caused by the 1991 Hurricane Bob (Sun et al., 2013). All these experiments were made with the inclusion of the wave-current interaction process. Model-predicted water elevation and significant wave heights were compared directly to observed elevation at coastal tidal gauges and buoys available in the model domain. The model was capable of reproducing the observed peaks and oscillations and strong waves before, during, and after hurricane and nor'easters passed these coastal stations.

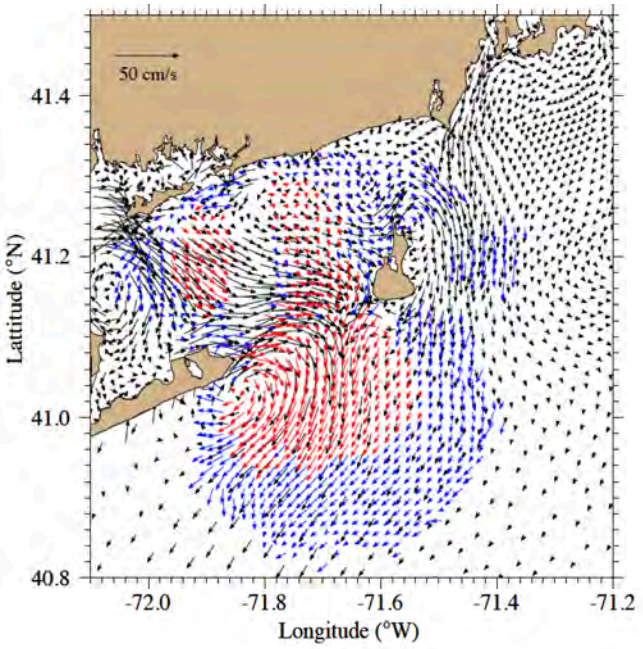

Figure 1.5: an example of FVCOM and CODAR-derived monthly averaged surface currents in January over 2000-2008. Black arrows: FVCOM-computed; red arrows: CODAR-derived at high-quality data points; blue arrows: CODAR-derived at all grid points.

An example illustrated in Figure 1.5 is from the comparison of the GOM3-FVCOM-computed and CODAR-derived surface flow field over the 2000-2008 in the northern Mid-Atlantic Bight. The results highlight the capability of FVCOM in reproducing spatially highly variable currents over the shelf system without assimilating the current data in the model (Sun et al., 2016). Our work has demonstrated that with accurate resolution of complex bathymetry and land geometry, the GOM3-FVCOM nested with Global-FVCOM is capable of accurately simulating the temporal and spatial variability of currents over the U. S. Northeast Atlantic Shelf.

The NECOFS is driven with the boundary condition forcing through the output of Global-FVCOM. The Global-FVCOM was validated via observational current data collected on either fixed location mooring or neutrally buoyant floats in the Arctic Ocean, Canadian Archipelago, and North Atlantic Ocean/Greenland Sea. The good agreements were reported in the comparison with observational data, which convinced us that the boundary condition forcing provided by Global-FVCOM to NECOFS is realistic and reliable. The results have been summarized and published on (or submitted to) peer reviewed scientific journals (Chen et al., 2016; Zhang et al., 2016a, b; and Zhang et al, 2016).

This model-data integrated product provides us with a unique database for the ocean environment over the U.S. northeast shelf, which can be used to drive a high-resolution subdomain model for the purpose of assessing the impact of offshore wind resource facilities on the local and regional marine environments. In particular, for emerging areas of offshore wind resource energy development, the Bureau of Ocean Energy Management (BOEM) requires adequate assessment of the impact of proposed future wind energy facilities on small-scale coastal (local) and regional offshore physical and biological environmental processes. Incorporating individual wind turbines and other wind energy resource facilities within a validated modeling system for the U.S. northeast outer continental shelf that includes 37 years (1978-2014) of the data for hindcasting scenarios and forecasting capabilities enables BOEM to use detailed simulations to more accurately assess the impacts that proposed wind energy facilities may have on affected environments (as mandated by the National Environmental Policy Act (NEPA)) over local and regional scales. As the team who developed and is now operating NECOFS, we have conducted the work requested in BOEM RFP No. M14PS00040 by developing a subdomain, turbine-resolving high-resolution FVCOM and using it to assess how the physical presence of wind turbines and other facilities will alter the oceanic currents, waves, and mixing in the lease areas under known surface wind conditions. Such assessments have provided us with a realistic evaluation of potential impacts of the offshore wind energy facility on the marine environment.

2. Methods

2.1 High-resolution NS-FVCOM-NECOFS nesting model

We have selected the region over the OCS off Massachusetts and Rhode Island as the study site and created a high-resolution subdomain FVCOM model nested to the regional NECOFS GOM3-FVCOM domain. Initially, the high-resolution subdomain FVCOM model only covered the OCS region off Nantucket Shoals (NS), so that we named this model "NS-FVCOM". On the project kick-off meeting, the Contracting Officer's Representative (COR) Ms. Callie Hall suggested that we extend our high-resolution domain to cover Block Island, Block Island Sound, Long-Island Sound and inner-shelf further west along the southern coast of Long Island. Following the COR's suggestion, we extended NS-FVCOM domain westward to cover the suggested regions. The "NS-FVCOM" used for the contract work is referred to the upgraded version with the inclusion of the shelf off Massachusetts, Rhode Island, Block Island, Block Island Sound

and Long-Island Sound.

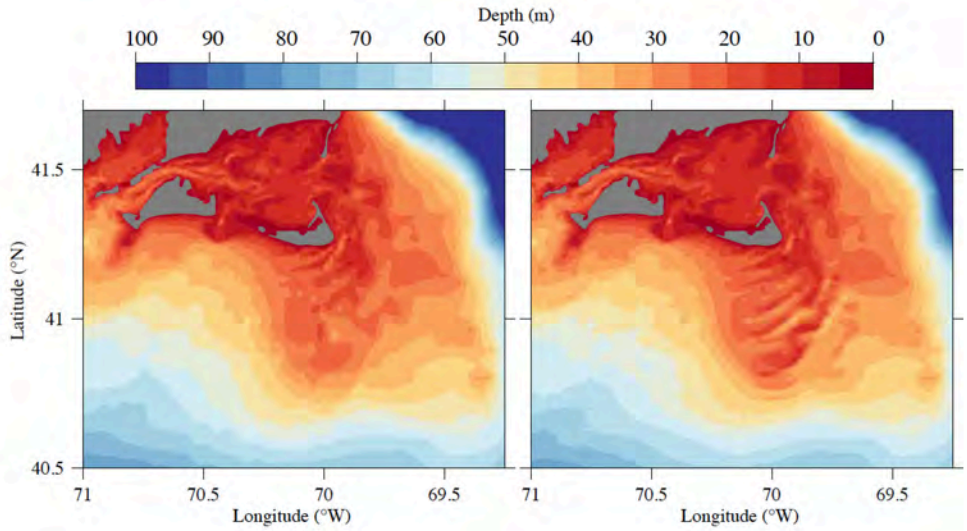

Figure 2.1: Comparison of bathymetries used in regional GOM3-FVCOM (left) and local high-resolution NS-FVCOM (right).

An effort was made to collect the high-resolution bathymetry over Nantucket Shoals, south and east of Martha's Vineyard, and Rhode Island Sound. The data were combined with our existing NECOFS regional bathymetry database. The bathymetry in the OCS off

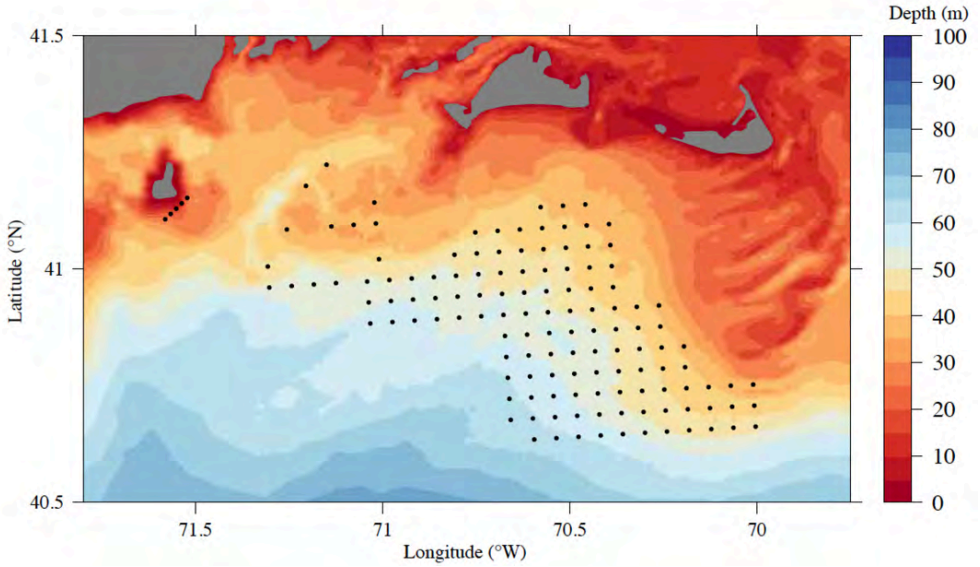

Figure 2.2: Illustration of the locations of wind turbines included in NS-FVCOM.

Massachusetts and Rhode Island is relatively flat. As the resolution is increased, the detailed structure of the seabed is resolved. Figure 2.1 illustrates the difference between bathymetries used in the regional GOM3-FVCOM and the local high-resolution subdomain NS-FVCOM.

2.1.1 Model grids

We first set up the high-resolution subdomain grid of NS-FVCOM for the case without the inclusion of wind turbines and upgraded it by adding wind turbines. The computational domains configured for both the cases were the same. For the case without wind turbines, the domain was constructed using the unstructured triangles with a total node number of 63483 and a total cell number of 124034. The horizontal resolution was up to ~ 33 m. 11 σ-levels (10 layers) with an uniform thickness was specified in the vertical, which produced a vertical resolution of 4 m on the 40-m isobath and up to ~ 0.5 m on the 5-m isobath. At the time this contract started, we had no specific information about what types of wind turbines would be proposed to be constructed in the possible leasing area over the OCS off Massachusetts and Rhode Island. In Nantucket Sound, Cape Wind Associates (CWA) is proposing to "construct and operate a 130-turbine Wind Park in central Nantucket Sound along with a submarine electrical transmission cable

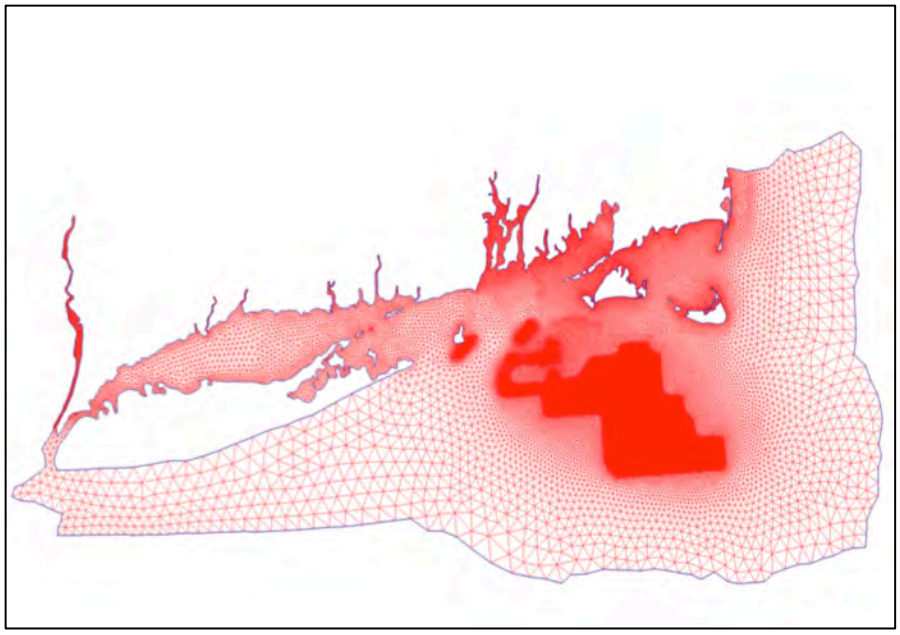

Figure 2.3: The high-resolution subdomain NS-FVCOM grid with the inclusion of 135 wind towers. The line is the boundary nesting to the GOM3-FVCOM.

system interconnecting the Wind Park with the onshore electrical grid. Each wind turbine generator (WTG) will have a tower diameter of approximately 16 feet (FT), and will be installed in a grid with a minimum spacing of 0.34 nautical miles (NM) by 0.54 NM." (Cited from the report of project No. E159-501.16 entitled "Revised Navigational Risk Assessment. Cape Wind Project Nantucket Sound" and prepared for Cape Wind Associates, LLC). We checked the BOEM website (http://www.boem.gov) and determined the numbers of the turbines by counting nodes on the grid map of the proposed offshore wind facilities shown in Figure 1.1. 135 turbines equaled to the total number of that grid: 117 in the Massachusetts Water blocks and 18 in the Rhode Island blocks (Figure 2.2). We used the Google map ruler to measure the distance between nodes, and determined the separation scale. We used the same approach to measure the

distance around the Block Island block. The Rhode Island block included 5 wind turbines (which have been already installed) on the eastern shelf of Block Island. When we added wind turbines into the NS-FVCOM, we considered a tower diameter of ~ 5 m (with a circumference of ~ 15.7 m). The distance between centers of two towers was measured by the design map posted on the BOEM website, which was about ~ 5 km in the Mass waters and Rhode Island waters connected to the Mass waters and ~ 2.5 km around Block Island. The boundary of individual towers was constructed with about 12-13 triangular cells, which provided the reasonable resolving of the circular shape of a tower with a resolution of ~ 1.3 m around the circle boundary. The shortest side length of a triangular cell measured the resolution. The cell resolution changed from ~ 1.3 m to ~ 8 m over a distance of 10 m from the tower edge and then to 200-300 m at the middle point between two towers. In the case with inclusion of wind turbines, the grid contained a total node number of 293,418 and a total cell number of 582,951 cells. The vertical configuration was the same as the case without wind turbines.

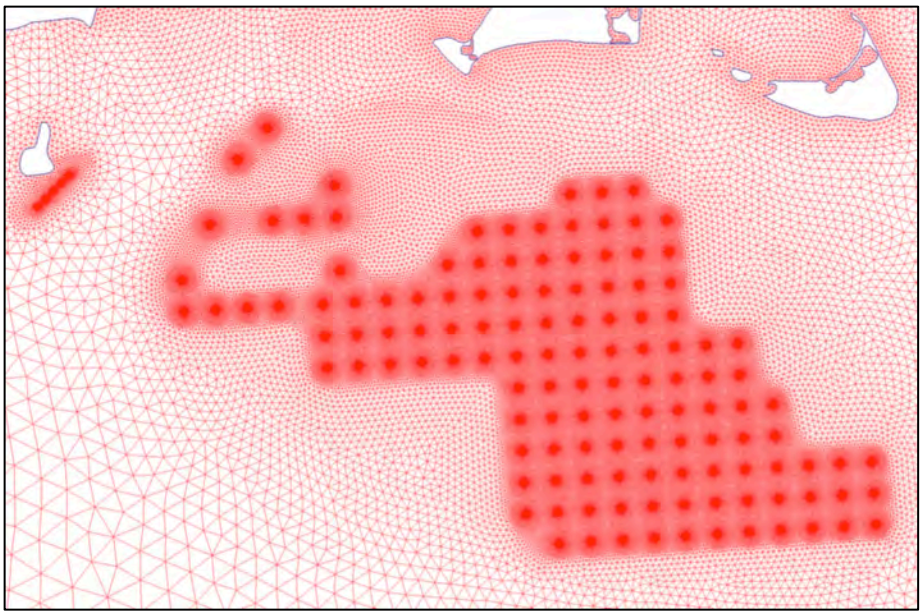

Figure 2.4: Enlarged view of the high-resolution grid with the inclusion of 135 wind towers.

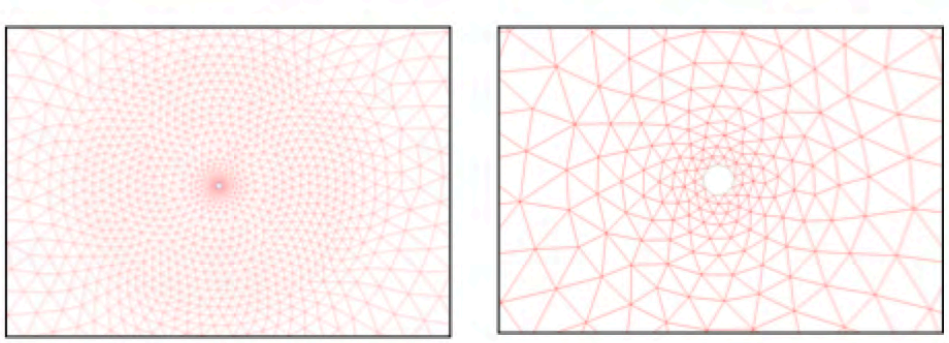

Figure 2.5: Enlarged view of the model grid around an individual wind tower with a diameter of 5 m. The horizontal resolution around the tower's edge is 1.3 m.

The current grid of GOM3-FVCOM over Nantucket Shoals and adjacent OCS WEA areas has only a resolution of 0.5 to 5 km. The new subdomain NS-FVCOM developed for this project has significantly improved the resolution in the proposed offshore wind energy facility areas to resolve the size of wind turbines. Figures 2.3-2.5 are included here to illustrate the high-resolution grid configured in NS-FVCOM with the inclusion of wind turbines.

2.1.2 Forcing and boundary conditions

The high-resolution NS-FVCOM and NS-SWAVE system is a fully wave-current coupled hydrodynamic model driven by surface forcing (wind stress, surface heat flux plus short-wave irradiance, precipitation minus evaporation) with lateral boundary conditions specified through one-way nesting with GOM3-FVCOM and GOM3-SWAVE. GOM3-FVCOM provides the initial and boundary conditions for hydrodynamics variables (the sea level, velocity, temperature, salinity, horizontal diffusion coefficient and vertical eddy viscosity), while GOM3-SWAVE provides the boundary conditions for surface waves (wave height, wave energy spectral data).

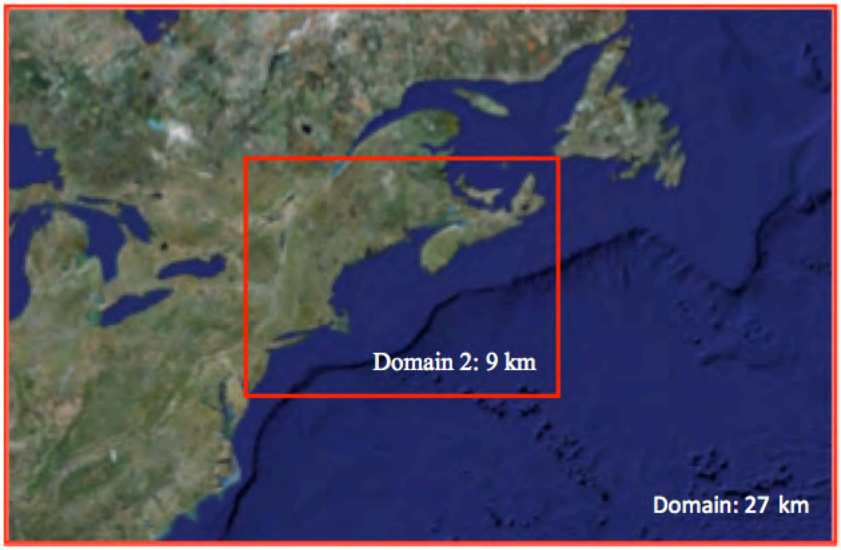

Figure 2.6: Illustration of the NECOFS-WRF domains. The output of the WRF model in domain 2 was used to drive GOM3-FVCOM and NS-FVCOM.

The surface forcing data are provided by the hindcast data-assimilated fields of the WRF (Weather Research and Forecast) model or MM5. The WRF model is a mesoscale numerical weather prediction system developed principally by the National Center for Atmosphere Research (NCAR) through collaboration with other government agencies (http://wrf-model.org/index.php). MM5 is the fifth-generation mesoscale regional weather model developed by NCAR/Penn State (Dudhia et al., 2003) for community use. MM5 covers the period 1978-2006 and WRF covers the period 2007-present. Both models feature the non-hydrostatic dynamics, terrain-following sigma-coordinate, variable domain and spatial resolution, multiple grid nesting, 4-D data assimilation, and several planetary boundary layer (PBL) modules to represent turbulent mixing over the

ground and ocean (Grell et al., 1993). In NECOFS, the WRF model is configured with a "regional" domain (covering the Northeast U.S.) and a "local" domain (covering the Scotian Shelf/GOM/GB/New England Shelf) with horizontal grid spacing of 30 and 10 km, respectively (Figure 2.6). 31 non-uniform sigma levels were specified in the vertical, with a design to have finer resolution in the PBL. WRF uses the hydrostatic North American Mesoscale weather model fields as initial and boundary conditions. These two models were coupled through the two-way nesting approach. To improve the model-based surface wind stress and heat flux estimates, we have implemented the COARE 3.0 bulk algorithm (Fairall et al., 1996, 2003) to NECOFS-WRF/MM5 to re-calculate the air-sea heat flux and wind stress. We have also integrated all coastal NDBC and C-MAN surface weather data in the local domain through 4-D data assimilation.

In the hurricane simulation, we used the combined winds and air pressures from a hurricane model and WRF/MM5. The detailed formulation of the hurricane model was given in Sun et al. (2013) and a brief description is repeated here. The surface wind of the hurricane is calculated using the asymmetric formulation given as

$$\vec{V} = \vec{V}_{\text{sym}} + \left(\frac{1/R_{\max}}{1 + (\frac{r}{R_{\max}})^2} \right) \cdot \vec{V}_{\text{path}} \quad , \qquad (1)$$

where $\vec{V}_{\text{sym}}$ is the symmetric hurricane wind vector at the 10-m height above the sea surface, $R_{\max}$ is the radius of maximum winds, r is the radial distance from the hurricane center, and $\vec{V}_{\text{path}}$ is the moving velocity vector of the hurricane center (Bretschneider, 1972; Jelesnianski, 1966; Powell and Black, 1990; Pasch and Avila, 1992; Houston et al., 1999; Phadke et al, 2003). The air pressure of the hurricane is defined as the sum of the surrounding dynamics pressure (P_d) and the hurricane center air pressure (P_c), i.e.,

$$P = P_c + P_d, \qquad (2)$$

where P_c is given from the observed hurricane records and P_d is determined by solving its gradient equation in the form of

$$\frac{\partial P_d}{\partial r} = \rho_{\text{air}} \left(\frac{V_{\text{sym}}^2}{r} + f V_{\text{sym}} \right) \qquad (3)$$

where V_{sym} is the magnitude of $\vec{V}_{\text{sym}}$, f is the Coriolis parameter and ρ_{air} is the air density (Vickery et al., 2000).

The WRF and hurricane wind and air pressure fields are merged in the radial distance relative to the hurricane center. Inside the radial region of $r \leq 1.5\, R_{\max}$, the WRF /MM5 wind and air pressure are completely replaced by hurricane model-predicted wind and air pressure. The radial distance between $1.5\, R_{\max}$ and $3.0\, R_{\max}$ defines the transition zone, in which the wind and air pressure fields are determined by a linear weight averaging of WRF and hurricane model fields. The weight for the hurricane field (WRF) is 1(zero) at

1.5 R_{max} and linearly decreases (increases) to zero (1) at 3.0 R_{max}. Outside of 3.0 R_{max}, only the WRF/MM5 fields are used. This method was validated by comparing the model-predicted wind and air pressures at coastal buoys (Sun et al., 2013).

The nesting boundary of NS-FVCOM consists of boundary cells with two boundary lines connected by triangle's nodes. FVCOM contains three types of one-way nesting boundaries: direct, indirect, and relaxed. In this contract work, we used the direct nesting method. Following this method, we first re-ran the large domain GOM3-FVCOM, output all variables at nodes (surface elevation, temperature, salinity, vertical velocity) and cell centers (horizontal velocity) at every time step, and saved these variables as a nesting boundary file. This nesting boundary file was then used to specify the hydrodynamic boundary condition for NS-FVCOM. It should be noted here that the surface elevation in the nesting boundary file contains both tidal and subtidal components. Similarly, we also re-ran GOM3-SWAVE to create the initial and boundary conditions of surface waves for NS-SWAVE. The nesting boundary file created by GOM3-SWAVE contains a wave spectral density array at the nodes of boundary cells. In the NS-SWAVE run, the wave parameters consist of numbers of 20 frequency bins and 36 direction bins. Therefore, at each boundary node, the wave spectral density is a matrix array with a size of 20×36. All experiments were made with the hydrostatic version of FVCOM.

2.2 Design of numerical experiments

This contract work is focused on the assessment of the impact of the offshore wind turbine facility on the marine environment under extratropical and tropical storm conditions. For this purpose, we have selected the February 1978 Nor'easter storm, a hundred-year storm, to represent the extratropical storm and the August 1991 Hurricane Bob to represent the tropical storm. The experiments were made for these two cases, with the aim at assessing the maximum short-term impacts of storms and hurricanes on the local and regional circulation, surface elevation, waves and bottom stress in the study area. A brief description of the weather and wave conditions during these two events is

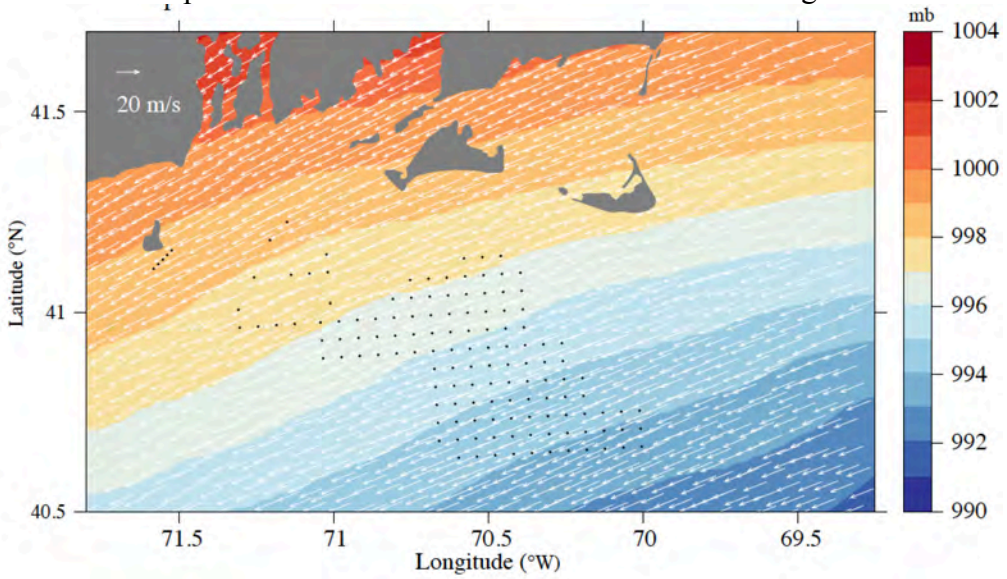

Figure 2.7: Distribution of the wind velocity vectors at the 10-m height (m/s) and the sea surface air pressure (mb) at 03:00:00 GMT, February 7, 1978.

given next.

2.2.1 The February 1978 nor'easter storm

In January through February 1978, the northerly or northeasterly (blowing from the north) wind prevailed over the entire New England Shelf. The outbreak of a nor'easter storm (called the "Blizzard of 78") appeared on February 5 and lasted for about 4 days. A peak northeasterly wind occurred at 03:00:00 GMT February 7. During this storm, the maximum wind exceeded 20 m/s, with gusts up to ~ 50 m/s (Altimari, 1998; Earls and Dukakis, 2008).

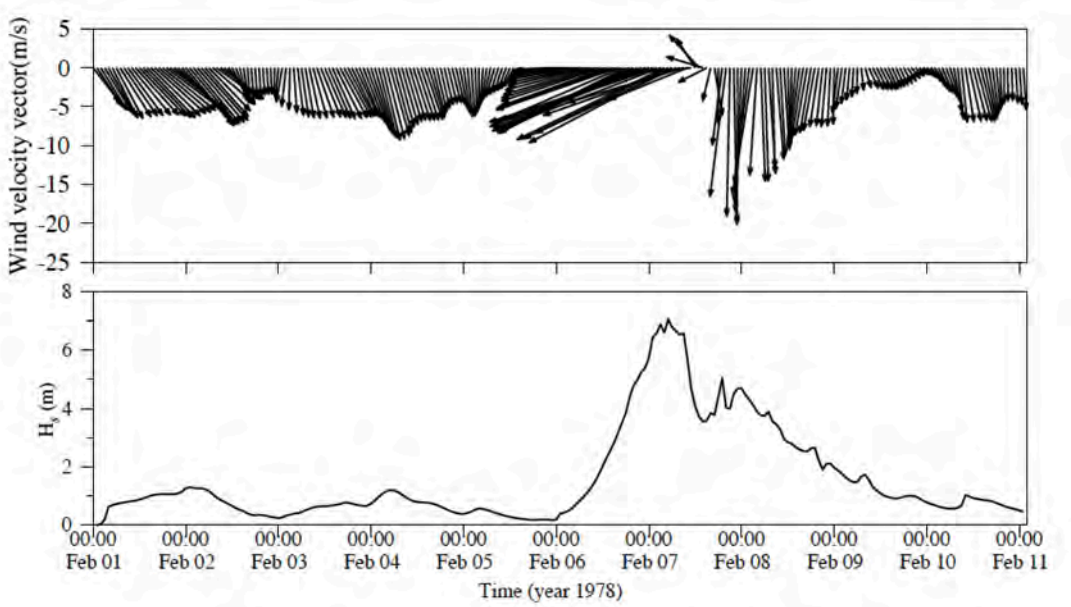

Figure 2.8: Time series of the wind velocity vectors (m/s) and significant wave height Hs (m) over the period of February 1-11, 1978.

The MM5-computed winds showed that this storm produced a strong northeasterly wind over the entire New England Shelf. The center of the pressure low was located over the outer shelf, and the air pressure contours over the New England Shelf were almost parallel to the coastline (Figure 2.7). Over the proposed offshore wind turbine region, during that nor'easter storm period, the spatial variation scale of the wind was small, so that the wind exhibited spatial uniformity. The GOM3-SWAVE-computed significant wave height showed that this storm produced strong surface waves with a significant wave height of >7.0 m over the shelf off Massachusetts and Rhode Island (Figure 2.8). The wave height started increasing rapidly on February 6, reached a maximum at 03:00:00 GMT February 7, and then decreased as the winds weakened.

2.2.2 The August 1991 Hurricane Bob

Hurricane Bob moved up the U.S. east coast and crossed over southern New England and the Gulf of Maine on 19-20 August 1991 (Figure 2.9). "It originally appeared as a

low-pressure area in the Atlantic Ocean near the Bahamas (74.3°W, 25.6°N) at 00:00 GMT August 16 1991. The depression steadily intensified, and became a tropical storm 18 hours later. The storm continued to strengthen as it moved northwestward and became "Hurricane Bob" at 77.10°W, 29.00°N at 18:00 GMT August 17. Hurricane Bob initially moved northeastward and brushed the North Carolina shelf between 18:00 GMT August 18 through 00:00 GMT August 19, during which it reached H3 with maximum sustained winds of 51.4 m/s. Around 18:00 GMT August 19, Hurricane Bob had weakened to H2 and made landfall near Newport, Rhode Island. Shortly thereafter, it rapidly deteriorated to a tropical storm and moved across the Gulf of Maine towards Maine and Canada, dissipating finally west of Portugal on August 29 after a long transit across the North Atlantic Ocean" (Sun et al., 2013). This was the largest tropical storm landing over the Rhode Island coast, with a wind-induced significant wave height of ~ 20 m. The storm produced an onshore strong current and mixing over Nantucket Shoals and the New England Shelf.

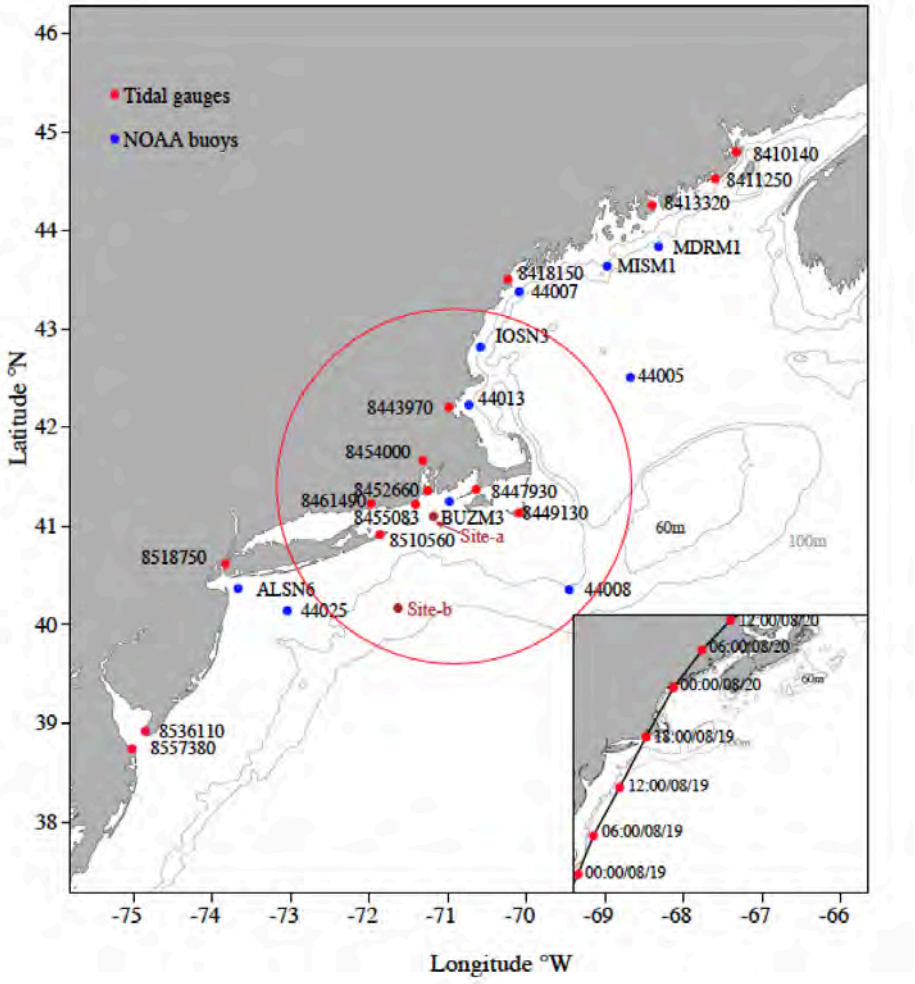

Figure 2.9: Locations of coastal buoys and tidal gauges in the computational domain for Hurricane Bob-induced storm surge simulation. Red dots: tidal gauges and blue dots: NOAA buoys. Orange dots: sites selected to display vertical profiles of water temperature and velocity. The subfigure in the right-lower corner shows the path of Hurricane Bob from 00:00 GMT August 19 to 12:00 GMT August 20.

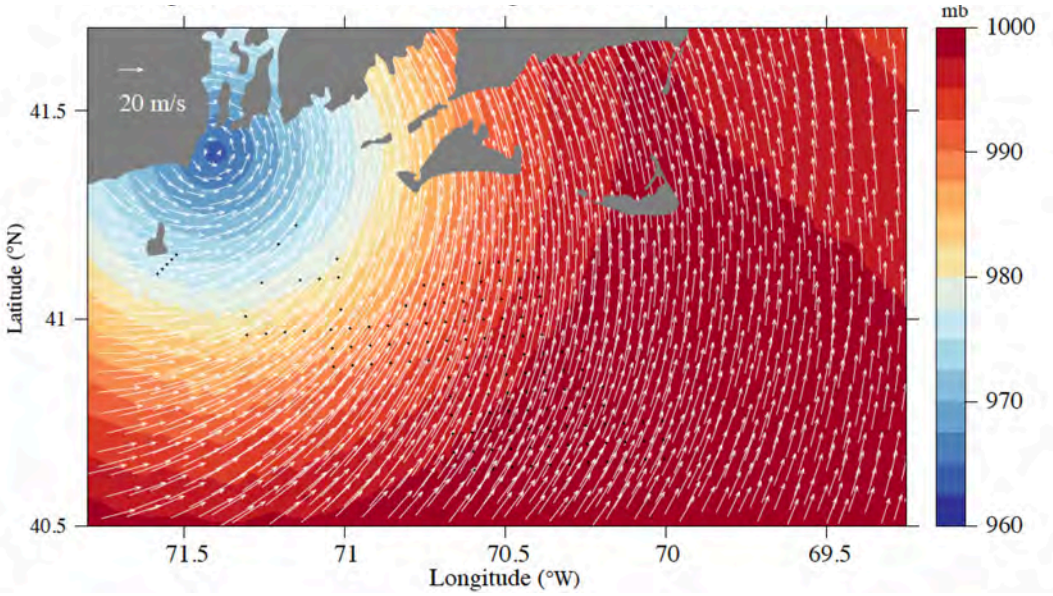

Figure 2.10: Snapshot of the distribution of the sea surface air pressure and wind vectors at the 10-m height over the New England Shelf at 18:00:00 GMT August 19 1991.

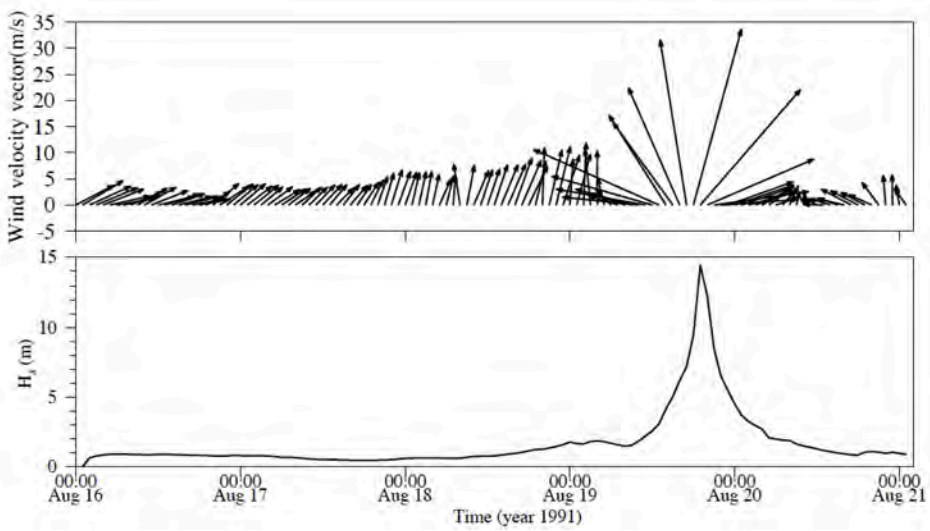

Figure 2.11: Time series of the MMS/hurricane wind model-simulated wind velocity vector at the 10-m height above the mean sea level (m/s) and significant wave height (m) during the August 1991 Hurricane Bob event.

Sun et al. (2013) used the combined hurricane and MM5 model to simulate the fields of the surface wind, heat flux, precipitation minus evaporation and air pressure over the local domain region of MM5. Using this meteorological model output to drive the GOM3-FVCOM and FVCOM SWAVES coupled model, they simulate the surface waves, oceanic currents, temperature/salinity and vertical mixing in the GOM3-FVCOM domain. The hurricane model was established based on a symmetric wind field, with a correction to resolving the hurricane moving induced asymmetric wind through input time series of the central eye air pressure and location and maximum wind speed taken from the NWS 6-hourly records (Phadke et al., 2003; Jelesnianski, 1966). The model has

successfully simulated the storm surge caused by Hurricane Bob (Sun et al., 2013). Model-predicted water elevation was compared directly to observed elevations at 15 coastal tidal gauges available in the model domain (Figure 2.9). The model was capable of reproducing the observed peaks and oscillations before, when, and after the hurricane passed these coastal stations.

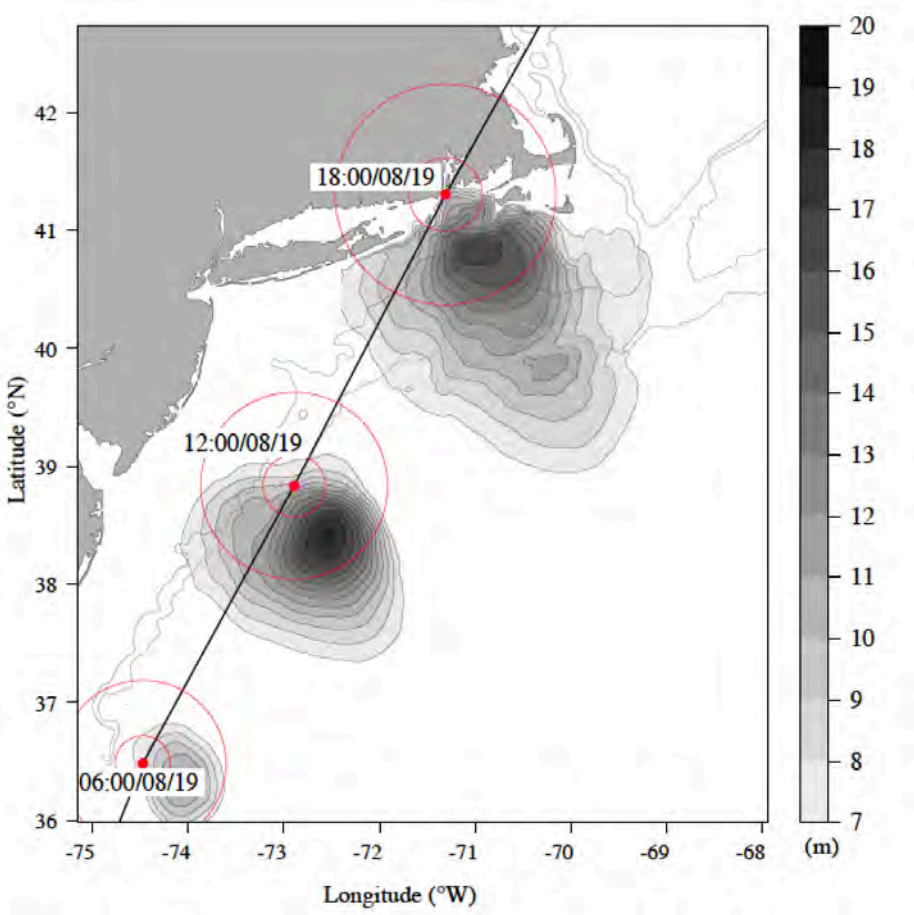

Figure 2.12: Spatial distributions of model-predicted significant wave heights along the track of Hurricane Bob at 06:00, 12:00 and 18:00 GMT August 19, 1991. The red circles centered at each site are drawn with radii equal to 1.0 R_{max} and 3.0 R_{max}, where R_{max} is the radius of the maximum wind velocity. This figure was adopted from Figure 4 in Sun et al. (2013).

We include here four figures from our previous simulation results to highlight the major finding. Figure 2.10 shows a snapshot of the distribution of the sea surface air pressure and wind vectors at the 10-m height above the sea surface over the New England Shelf at 18:00:00 GMT August 19, 19991. At that time, the center of Hurricane Bob had reached the inner shelf of Narragansett Bay, Rhode Island, and the entire continental shelf was covered by the strong southwesterly wind with a maximum of ~ 30 m/s or higher.

Figure 2.11 shows the time series of the wind velocity vector and significant wave height within the proposed offshore wind turbine region over the outer shelf of Nantucket

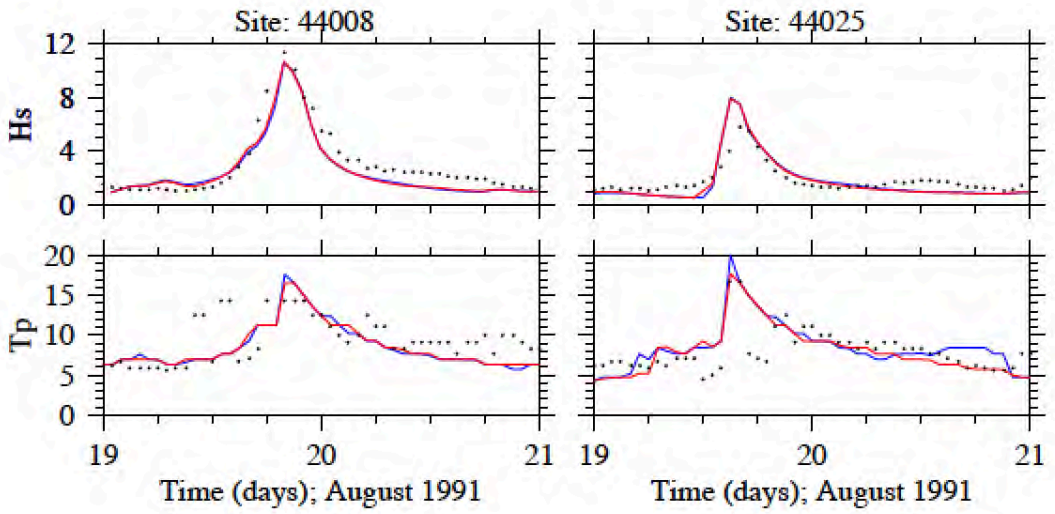

Figure 2.13: Comparisons between MM5/hurricane model-simulated and observed wind speeds, wind directions, and air pressures at Buoy 44008 and BUZM3 during August 19-21. Black dots: observed; red line: MM5-calculated; blue line: calculated using the MM5-hurricane model combined fields. This figure was adapted from Figure 3 in Sun et al. (2013).

Shoals. Then Hurricane Bob moved towards the Narragansett Bay coast on the left side of the proposed offshore wind turbine region, so that the maximum wind over the shelf occurred around 18:00:00 GMT, August 19, at which time the surface waves reached a maximum significant wave height of >14.0 m.

Figure 2.12 shows the distributions of the FVCOM-SWAVE-simulated significant wave height along the pathway of Hurricane Bob. These distributions clearly show that the surface waves were higher on the right side of the hurricane center, with its maximum value occurring in the area between 1.0 R_{max} and 3.0 R_{max}. As Hurricane Bob moved northeastward onto the Rhode Island and Massachusetts shelf, the significant wave height significantly increased. Hurricane Bob's pathway was located on the left side area of the proposed offshore wind turbine zones over the continental shelf, the proposed offshore wind turbine zones experienced the maximum surface wave with a significant wave height of >15 m. Therefore, the Hurricane Bob case can provide us with an extreme situation with the maximum impact of the hurricane-induced surface waves on the proposed offshore wind turbine area.

Figure 2.13 shows the model-data comparisons of the wind speed, wind direction and air pressure at meteorological buoys BUZM3 and 44008 during Hurricane Bob. BUZM3 is a buoy deployed at the entrance of Buzzards Bay. When Hurricane Bob moved towards Newport, Rhode Island, the closest distance of BUZM3 from the storm center was 0.49 R_{max}. At this site, the observed maximum wind speed at 10-m height exceeded 30 m/s. At that time, the air pressure dropped to a minimum of 986 mb. The observed wind speed, wind direction and air pressure during the Hurricane Bob event was well captured by the hurricane and MM5 combined wind model. Buoy 44008 was located over the Nantucket

Shoals. When Hurricane Bob arrived over the Rhode Island shelf, the closest distance of Buoy 44008 from the storm center was 3.9 R_{max}. Even though it is a relatively far distance from the maximum wind area of Hurricane Bob, the observed wind speed still exceeded 20 m/s. The observed wind speed, wind direction and air pressure were reasonably captured by the MM5.

Figure 2.14 shows the comparison of time series of model-computed and observed significant wave heights and peak periods at Buoys 44008 and 44025. Buoy 44008 was located on the right side of the hurricane track, where the maximum observed significant wave height was close to ~ 12 m. Buoy 44025 was located on the left side of the hurricane track, where the observed significant height was about 5.6 m lower than at Buoy 44008. Both significant wave heights and peak periods observed at these two buoy sites were captured by FVCOM-SWAVE.

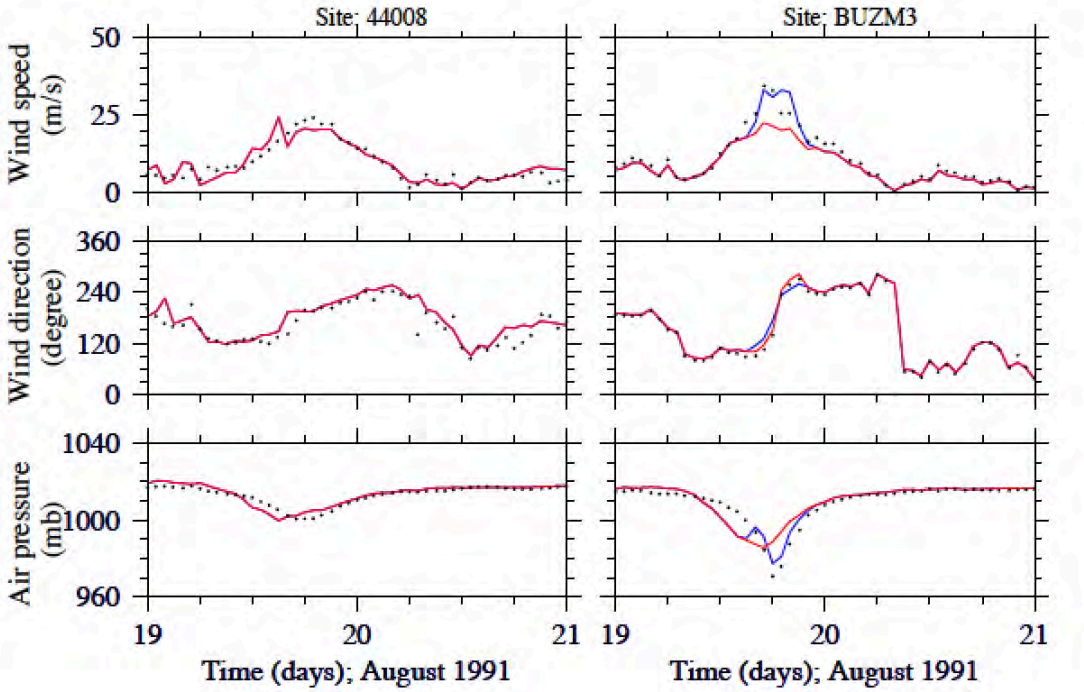

Figure 2.14: Comparisons between FVCOM-SWAVES-computed and observed significant wave heights and peak periods during August 19-21 at Buoys 44008 and 44025. Black dots: observed; red line: calculated without inclusion of wave-current interaction; blue line: calculated with inclusion of wave-current interaction. This figure was adapted from Figure 5 in Sun et al. (2013).

2.2.3 Case studies

Three experiments were made for each storm case: 1) hydrodynamics only (Exp#1), 2) waves only (Exp#2) and 3) hydrodynamics-waves coupled with inclusion of wave-current interaction (Exp#3). In each experiment, we ran the model under the conditions without and with the inclusion of wind turbines. The differences in the results between these two conditions are defined as the change caused by the deployment of wind

turbines. We will first describe the Exp#3 results, and then Exp#1 and Exp#2. The purpose of conducting Exp#1 and Exp#2 is to distinguish the relative contributions of hydrodynamics and wave dynamics to the marine environment change due to the wind turbine deployment.

2.2.3.1 Hydrodynamics only (Exp#1)

The experiments for hydrodynamics only refer to the model run using NS-FVCOM without the inclusion of surface waves, i.e., FVCOM-SWAVE is not included. The NS-FVCOM has the same parameter configuration as GOM3-FVCOM, with the MY level 2.5 turbulent closure model for vertical mixing (Mellor and Yamada, 1982) and Smagorinsky turbulence parameterization for horizontal diffusion (Smagorinsky, 1963). Forcing variables, boundary conditions, and simulation periods are listed in Table 2.1.

Table 2.1: Parameter setup for Exp#1

February 1978 nor'easter storm		
Items	**Sources**	**Contents**
Surface forcing	MM5	Wind stress, net heat flux, short-wave irradiance, P-E
Boundary condition	GOM3-FVCOM	Surface elevation, temperature, salinity, 3-D velocity, vertical viscosity and horizontal diffusion coefficient
Initial condition	GOM3-FVCOM	Surface elevation, temperature, salinity, 3-D velocity, vertical viscosity and horizontal diffusion coefficient
Simulation period	00:00 February -00:00 February 11, 1978.	
FVCOM setup	Mode-split	
Time step	Without turbines: External time step: 0.4 seconds; internal time step: 4.0 seconds. With turbines: External time step: 0.02 seconds; internal time step: 0.1 seconds.	
August 1991 Hurricane Bob		
Items	**Sources**	**Contents**
Surface forcing	MM5/hurricane model	Wind stress, net heat flux, short-wave irradiance, P-E, air pressure
Boundary condition	GOM3-FVCOM	Surface elevation, temperature, salinity, 3-D velocity, vertical viscosity and horizontal diffusion coefficient
Initial condition	GOM3-FVCOM	Surface elevation, temperature, salinity, 3-D velocity, vertical viscosity and horizontal diffusion coefficient
Simulation period	00:00 August 16 -00:00 August 21, 1991.	

FVCOM setup	Mode-split
Time step	Without turbines: External time step: 0.3 seconds; internal time step: 3.0 seconds. With turbines: External time step: 0.02 seconds; internal time step: 0.1 seconds.

2.2.3.2 Waves only (Exp#2)

The experiments for the surface wave only refer to the model run using FVCOM-SWAVE without the inclusion of the feedback from wave-current interaction. FVCOM-SWAVE is driven by the surface wind stress with the initial and boundary conditions specified by the large regional GOM3-SWAVE. The wind forcing used in Exp#2 is the same as those in Exp#1. The semi-implicit version of NS-SWAVE is used in Exp#2. For the February 1978 nor'easter storm case, the time step is 60 seconds under the condition without wind turbines and 12 seconds under the condition with wind turbines. For the August 1991 Hurricane Bob case, the time step is 30 seconds under the condition without turbines and 10 seconds under the condition with turbines. The simulation periods for these two storms are the same as those used for Exp#1. The wave parameters specified in NS-SWAVE is listed in Table 2.2.

Table 2.2: Wave Parameters used in NS-SWAVE

Direction	Full circle
Direction bins (number)	36
Frequency bins (number)	20
Lowest discrete frequency (Hz)	0.05
Highest discrete frequency (Hz)	0.5
Bottom friction formulation	Jonswap

2.2.3.3 Hydrodynamics-waves coupled (Exp#3)

The experiments for hydrodynamics-wave coupled with wave-current interaction refer to the model run using the coupled NS-FVCOM and NS-SWAVE system. SWAVE is coupled with FVCOM through radiation stress in the hydrodynamic momentum equations. These radiation stress terms and computational algorithms were described in detail in Warner et al. (2008), Mellor (2011), and Wu et al. (2011). The surface wind stress is calculated using a quadratic slip surface boundary condition with the surface drag coefficient given as

$$C_d = \left[\kappa / \ln\left(\frac{10}{z_0}\right)\right]^2 \qquad (4)$$

where the von Karman constant $\kappa = 0.41$ and z_o is the sea surface roughness calculated using Donelan's parameterization (Donelan et al., 1993) given as

$$z_o = 3.7\times10^{-5}\,\frac{U_{10}^2}{g}\left(\frac{U_{10}}{C_p}\right)^{0.9} \qquad (5)$$

where C_p is the phase velocity of the peak frequency wave, U_{10} is the 10-m wind speed and U_{10}/C_p is defined as the wave age. The bottom stress is calculated using the bottom boundary layer model implemented in Warner et al. (2008). The BBL code used in this coupling was adopted from the code developed by Warner et al. (2008) and converted to an unstructured-grid finite-volume version using the FVCOM framework.

The surface forcing used in Exp#3 is the same as that used in Exp#1. The boundary and initial conditions are the combined files of the nesting boundary and initial conditions for Exp#1 and Exp#2. The time steps to run NS-FVCOM and NS-SWAVE are the same as those used for Exp#1 and Exp#2, and coupling is done with the step time determined by the time steps used to run NS-SWAVE.

2.3 Lagrangian particle-tracking experiments

The particle-tracking in the 3-D flow field is conducted solving the following time integration equation in the form of

$$P_n(\vec{x}, t + \Delta t) = P_n(\vec{x}_t, t) + \int_t^{t+\Delta t} \vec{v} dt \qquad (6)$$

where $P(\vec{x}, t + \Delta t)$ and $P(\vec{x}_t, t)$ are the locations of the nth particle at $t+\Delta t$ and t; $\vec{v}$ is the 3-D velocity vector. The advective distance is calculated by a modified fourth-order Runge-Kutta time-stepping scheme with second-order accuracy (Chen et al., 2003). No horizontal and vertical random walk processes are included in the tracking.

The particle-tracking experiments are conducted for both the February 1978 nor'easter storm and the August 1991 Hurricane Bob cases. In each case, the tracking is carried out under the conditions without and with wind turbines, respectively.

For the February 1978 nor'easter storm case, the particle-tracking experiments are made over the period from 00:00:00 GMT February 1 1978 to 00:00:00 GMT February 11 1978. The particles are initially released in the outside and inside regions of offshore wind turbines. In each region, 100 particles are released at the sea surface and traced with a time step of 120 seconds. The outside region is defined as a box with longitudes of 69.5°- 69.0°W and latitudes of 40.65° - 41.1° N. The inside region is defined as a box with longitudes of 70.8° -70.1° W and latitudes of 40.7° - 41.25° N.

For the August 1991 Hurricane Bob case, the particle-tracking experiments are made over the period from 00:00:00 GMT August 16 1991 to 00:00:00 August 21 1991. The particles are also initially released in the outside and inside regions of offshore wind turbines and tracked with the time step of 120 seconds. A total number of particles in each region are also 100. The outside region is defined as a box with longitudes of 71.12°- 70.36°W and latitudes of 40.3° - 40.46° N. The inside region is defined as a box with longitudes of 70.8° -70.1° W and latitudes of 40.7° - 41.25° N.

3. Results

Results described here include the model runs of NS-FVCOM and NS-SWAVE under the conditions without and with the inclusion of wind turbines. The purposes of these two types of experiments are aimed at 1) understanding the marine environment condition occurring during nor'easter storms and hurricanes and 2) how this condition can be changed after wind turbines are added. Here we first describe the results for the condition without wind turbines and then results with wind turbines.

3.1 The February 1978 nor'easter storm case

The results obtained from three types of experiments are described here. They are the model runs with 1) the coupled NS-FVCOM and NS-SWAVE system, 2) the NS-FVCOM only and 3) the NS-SWAVE only. The first experiment includes wave-current interaction; the second experiment only considers the hydrodynamic process without the feedback from surface waves; and the third experiment is only for surface waves. The discussions of second and third experiments are focused on identifying and quantifying the contribution of wave-current interaction to the model-computed surface elevation, currents, waves and bottom stress. In each experiment, we have run the model for the cases without and with wind turbines and then calculate the differences.

3.1.1 NS-FVCOM and NS-SWAVE coupled simulation

3.1.1.1 Without wind turbines

During the February 1978 nor'easter event, driven by the strongly northeasterly wind, the entire New England shelf was dominated by the westward flow, with a zonal-paralleling distribution of surface elevation. The northeasterly wind reached a maximum at around 03:00:00 GMT February 7, at which the strongest westward flow occurred, and the water moved westward along the contour of the surface elevation (Figure 3.1). In the shelf region where the deployment of offshore wind turbines is proposed, the water mainly came from two sources: 1) the strong southward flow from the Cape Code coast and 2) the northwestward flow from the outer shelf. The vertically averaged velocity in the region was ~ 0.4-0.6 cm/s. The strong northeasterly wind provided an energetic vertical mixing near the surface, which caused the water to be vertically well mixed near the coastal region and in Nantucket Sound, but the water remained stratified over the mid- and outer shelve where the deployment of offshore wind turbines is proposed. As a result, the current varied significantly in the vertical: intensified near the surface and decreased rapidly towards the bottom beneath the surface mixed layer (Figure 3.2). The near-surface current exhibited the same spatial distribution pattern as the vertically averaged current, with a maximum velocity of > 1.0 m/s. Near the bottom, the flow was dominated by an offshore flow with an averaged magnitude of ~ 0.2-0.3 m/s. A convergence flow zone was identified near the bottom in the outer shelf region where the southward offshore flow encountered the northwestward flow from the outer shelf break.

The strong northeasterly wind also generated large surface waves over the New England Shelf, with significant wave height decreasing towards the coast (Figure 3.3). At the time that the peak wind occurred, the significant wave height over the shelf off Massachusetts and Rhode Island was in the range of 6-8 m. Corresponding to the surface wind and waves, the bottom stress was large in the vertically well-mixed region around Nantucket Sound and Block Island, but remained low in the offshore region where the deployment of wind turbines is proposed. The value of the bottom stress between the 40- and 60-m isobaths was in the range of 0.1-0.6 N/m^2, with a relatively large value of ~0.6 N/m^2 occurring around the 50-m isobaths. During this storm, the bottom stress around and in Nantucket Sound as well as Block Island exceeded 1.6 N/m^2.

3.1.1.2 With wind turbines

Under the same forcing and boundary conditions, the distributions of surface elevation and currents remain the same pattern after wind turbines are added. If only looking at the contour images, no significant difference can be seen in the surface elevation after turbines are included (Figure 3.4: upper panel). In the wind turbine facility area, the vertically averaged currents exhibited some local variations between individual turbines. However, these variations do not change the dominant westward flow feature (Figure 3.4: lower panel). Similar patterns are also true for the near-surface and near-bottom currents (Figure 3.5), but velocity magnitudes and direction are changed remarkably. Near the surface and bottom, after wind turbines are added, the flow is locally intensified within and around the wind turbine facility area. The convergence zone at the encounter zone between the offshore and northwest currents is strengthened. In addition, the near-bottom southward flow over the southern shelf off Nantucket Island is also significantly intensified.

Similarly, the surface waves remain the same spatial distribution pattern after wind turbines are added. The most significant changes occur in the turbine region and neighbor outer shelf area (Figure 3.6: upper panel), where the local variation of significant wave height is increased after turbines are added. As a result of the flow intensification near the bottom, the bottom stress increases significantly in the wind turbine facility area, especially around the 50-m isobaths (Figure 3.6: lower panel). In this case, the change of the bottom stress is mainly caused by the intensification of the velocity near the bottom and wave-current interaction. The importance of the wave-current interaction will be discussed in sections 3.12 and 3.13.

3.1.1.3 Differences

We estimated the impact of wind turbines on the marine environment by calculating the difference between model-computed surface elevations, vertically averaged currents, near-surface and near-bottom currents, significant wave heights and bottom stresses for the cases with and without the inclusion of wind turbines. The change in surface elevation is relatively small. At the time of the maximum wind, the difference of surface elevation is generally < 0.1 m (Figure 3.7: upper panel). In the wind turbine facility area, the surface elevation difference is ~ 0.05 m, with a value of ~ 0.08 cm in a small portion

of the area. The difference in the vertically averaged velocity shows that adding the offshore wind turbines can produce a cyclonic circulation with a magnitude of ~ 0.1-0.2 m/s plus multiple small-scale cyclonic eddies around and inside the wind turbine facility area (Figure 3.7: lower panel). This cyclonic circulation pattern also appears for the near-surface flow but not near the bottom, implying that this circulation forms as a result of the influence of turbines on the wind-induced westward currents (Figure 3.8). Adding wind turbines can produce a large spatial flow variation near the bottom: the offshore and onshore flow can be significantly intensified locally, with a magnitude up to ~ 0.2-0.3 m/s.

Our experiments with and without the inclusion of wind turbines clearly show that the influence of offshore wind turbines can not only affect the currents within the turbine region, but also over the neighboring shelf. This is clearly evident in the northern shelf and western slope regions outside the wind turbine facility area, where relatively large velocity differences are found near the surface and near the bottom. Since the water is stratified, the change in the velocity direction has an opposite sign between the surface and bottom (Figure 3.8). As a result of cancellation, these influences will not cause a significant change in the vertically averaged velocity and thus volume transport (Figure 3.7: lower panel).

Although the spatial distribution of significant wave height remained the same pattern after wind turbines are added, the difference in magnitude is significant. At the time of the maximum wind, the difference in the significant wave height can be up to 0.9-1.0 m or higher around and within the wind turbine region (Figure 3.9: upper panel). The influence of wind turbines on the surface waves also exhibits a regional impact. Adding offshore wind turbines can cause the significant wave height to be increased by as much as $\geq$ 1.0 m the outer New England Shelf and near the Cape Cod coast, and decreased by as much as 0.4 m or lower ($\leq$-0.4 m).

After wind turbines are added, the change in the bottom stress around and inside the offshore wind turbine region is relatively small, except near the isobath convergence zone between 40 and 50 m and around Block Island (Figure 3.9: lower panel). We have included Section 3.3 to describe the model results in the Block Island region. The increase of the bottom stress inside the offshore wind turbine facility area (excluding the turbines around Block Island) is in an order of 0.05 N/m^2, but the maximum in a local area can be > 2.0 N/m^2. The noticeable changes on the northwestern shelf of Cape Cod and Great South Channel are due to the regional impact of wind turbines on surface waves and currents described in Figures 3.7-3.8.

3.1.2 Hydrodynamic simulation with NS-FVCOM

The hydrodynamic simulation refers to the model run with NS-FVCOM, in which the surface waves are not included. We conducted this experiment for two purposes: 1) to check if the features found in the case with the wave-current interaction are applicable for the case with hydrodynamic simulation only; and 2) to quantitatively estimate the relative contribution of the wave-current interaction by calculating the difference between the

cases with and without the inclusion of wave-current interaction. The difference is defined as residual values by using the results with the wave-current interaction minus the results with the hydrodynamic simulation only.

3.1.2.1 Without wind turbines

Under the condition without wind turbines, the model-simulated surface elevation, vertically averaged velocity, the near-surface and near-bottom velocity, and bottom stress exhibit the same spatial distribution and temporal variation as those obtained from the model run with the inclusion of wave-current interaction. The major difference is in the magnitude. The difference in surface elevation is larger in Nantucket Sound where the water is shallow and currents are strong and small in the New England Shelf where the bottom bathymetry is relatively deep and flat. For example, at the time of the maximum wind (03:00:00 February 7 1978), the value of the difference can be up to 0.2 m or larger in Nantucket Sound, but is about ~ 0-0.05 m over the shelf where the water depth is deeper than 40 m (Figure 3.10). This means that driven by the same external forcing, the model-calculated surface elevation can be 0.2 m higher in the case with wave-current interaction.

The difference in the vertically averaged velocity mainly occurs on the eastern and southern shelf off Nantucket Island and in Nantucket Sound, with a value up to 1.0 m/s or larger (Figure 3.11). Over the New England Shelf, where the water depth is deeper than 40 m, wave-current interaction shows little influence on the vertically averaged flow field. This difference found in the vertically averaged velocity is consistent with the difference in surface elevation, suggesting that the wave-current interaction tends to increase the convergence of the transport in and around Nantucket Sound during this storm.

The contribution of wave-current interaction to the velocity is more obvious near the surface than near the bottom. Near the surface, the wave-current interaction not only changed the current direction, but also weakened the cyclonic flow on the eastern shelf of Nantucket Shoals by intensifying southwestward flow (Figure 3.12). At the time of the maximum wind, the difference can be up to 1.0 m/s or larger over the eastern shelf of Nantucket Shoals. The contribution of wave-current interaction is smaller in the deeper region, with the range of 0.1-0.2 m/s over the shelf where the water depth is deeper than 40 m. Near the bottom, the effects of wave-current interaction are more significant in and around Nantucket Sound, but generally small in the offshore shelf region where the water depth is deeper than 40 m (Figure 3.13). The difference can be up to 0.5 m/s or larger in Nantucket Sound, but less than 0.05 m/s in the offshore shelf region.

Compared with the results for the case with the inclusion of wave-current interaction, the model-computed bottom stress in the hydrodynamic simulation without surface waves is significantly smaller around and in Nantucket Sound where the wave-current interaction-induced currents are strong. The difference can exceed 0.6 N/m^2 (Figure 3.14). The difference is relatively small in the offshore region. In the shelf region where

the water depth is deeper than 40 m, the difference is ~ 0.1-0.2 N/m^2 or smaller, although it can be > 0.6 N/m^2 locally.

3.1.2.2 With wind turbines

Under the condition with wind turbines, the model-simulated surface elevation, vertically averaged velocity, near-surface and near-bottom velocity and bottom stress remain the same spatial distribution and temporal variation patterns as those obtained from the model run with the inclusion of wave-current interaction. The effects of wave-current interaction to surface elevation and velocity are almost the same as those shown for the model run under the condition without wind turbines, except small-scale variations in magnitudes and directions inside the wind turbine facility area (Figures 3.15-3.18).

3.1.2.3 Difference

The differences of the surface elevation and vertically average velocity between the case with and without wind turbines for the experiment with hydrodynamics only are almost identical to those found for the experiment with wave-current interaction (Figure 3.20). That is also true for the near-surface and near-bottom velocity as well as the bottom stress (Figures 3.21 and 3.22). This suggests that even if we do not include wave-current interaction, the differences found between the cases with and without wind turbines remain unchanged.

3.1.3 Surface wave simulation with NS-SWAVE

The surface wave simulation refers to the model run with NS-SWAVE only, in which the wave-current interaction process is not taken into account. We conduct this experiment for two purposes: 1) to check if the spatial distribution and temporal variation of the significant wave height and wave propagation direction found in the case with wave-current interaction are applicable for the surface wave simulation case without the inclusion of feedback influence due to wave-current interaction; and 2) to quantitatively estimate the relative contribution of wave-current interaction to surface waves by calculating the difference between the cases with and without the inclusion of wave-current interaction. The difference is defined as residual values by using the results with wave-current interaction minus the results with the surface wave simulation only.

3.1.3.1 Without wind turbines

The model-simulated significant wave height and propagation direction for the case without the inclusion of the feedback effect of wave-current interaction has the same spatial distribution and temporal variation patterns as those described in the wave simulation using the NS-FVCOM and NS-SWAVE coupled model. The model shows that surface waves mainly propagate westward in the offshore shelf region and southwestward in Nantucket Sound, Buzzard Bay and Narragansett Bay. The wave-current interaction can cause higher waves in Nantucket Sound and over the eastern shelf

of Nantucket Shoals, and lower in the offshore shelf region (Figure 3.23). In the region where the significant wave height difference is higher, the difference is in the range of 0-0.3 m, with a maximum value of > 1.0 m at some local sites. In the region where the significant wave height difference is lower, the difference can be ~ -0.8 m, occurring around the 50-m isobaths.

3.1.3.2 With wind turbines

The model-simulated significant wave height and propagation direction for the case with NS-SWAVE only exhibit the same spatial distribution and temporal variation patterns as those described in the model run with the inclusion of wave-current interaction. This indicates that the major finding for the changes in surface waves described in Section 3.1 is applicable for the case without the inclusion of feedback effect resulting from wave-current interaction. Differed from the case without wind turbines, the impact of wave-current interaction on the significant wave is more significant within and around the wind turbine facility area in addition to the eastern shelf of Nantucket Sound and Nantucket Shoals (Figure 3.24). The difference can be 0.5 m higher or lower. The change of the significant wave height resulted from the wave-current interaction is regional, not only in the wind turbine facility area, but also over the outer shelf.

3.1.3.3 Difference

The difference of the significant wave height between the cases with and without wind turbines for the experiment with waves only significantly differs from that found for the experiment with wave-current interaction. If we do not consider the feedback effect of wave-current current interaction on surface waves, the model shows that the deployment of wind turbines will not have a significant influence on surface waves in the wind turbine facility area except near the coastal area (Figure 3.25). However, when wave-current interaction is taken into account, the model suggests that the surface waves can be significantly changed in and around the wind turbine facility area, with a difference of > 1.0 m (Figure 3.9). This result implies that the influence of wind turbines is more significant on surface waves than surface elevation due to the enhanced wave-current interaction in and around that region.

3.2 The August 1991 Hurricane Bob

Following the same strategy as those used in the February 1978 nor'easter storm case, the results described here are also based on three types of experiments: 1) the coupled NS-FVCOM and NS-SWAVE system, 2) the NS-FVCOM only and 3) the NS-SWAVE only. The numerical experiments are made with model runs under hydrostatic approximation, with the understanding of the limitation in resolving hurricane-induced high-frequency internal waves and local convection. This approximation should be sufficient, since during extratropical and tropical storm events, we believe, the energies of high-frequency internal waves are significantly weaker than wind-induced surface waves, and wind-induced vertical mixing is more energetic than cooling-induced local convection.

3.2.1 NS-FVCOM and NS-SWAVE coupled simulation

3.2.1.1 Without wind turbines

The model-predicted sea elevation and currents in the refined grid NS-FVCOM remain the same as that found in the GOM3-FVCOM described in Sun et al (2013). As shown in Figure 2.11, during Hurricane Bob, the maximum wind over the shelf off Massachusetts and Rhode Island occurred around 18:00:00 GMT August 19. At that time, Hurricane Bob was close to the land, which caused the high storm surge along the coast of Massachusetts and Rhode Island, especially in Buzzard Bay, MA (Figure 3.26: upper panel). Compared with that in the coastal region, the surface elevation over the shelf was relatively low and flat, with small cross-isobath gradient. Correspondingly, the vertically averaged currents were dominated by an onshore flow, which was strong near the coastal region and relatively weak over the shelf where the deployment of offshore wind turbines is proposed (Figure 3.26: lower panel). The average velocity was larger than 1.0 m/s near the coast, while was ~ 0.05-0.10 m/s over the shelf where the water depth is deeper than 50 m.

Over the shelf, the response of the flow to the cyclonic hurricane wind featured a two-layer dynamics structure. The southerly wind pushed the water onshore near the surface, and in turn it caused the water to move offshore near the bottom (Figure 3.27). The existence of this two-layer feature was due to vertical stratification, which was discussed in detail in Sun et al. (2013).

The spatial distribution and temporal variation of the significant wave height were controlled fully by the surface wind. At 18:00:00 GMT August 19, the significant wave height had a maximum core in the strongest wind area and decreased radially from that core, with a minimum value of 9.0 m and a maximum value of >14.0 m over the shelf (Figure 3.28: upper panel).

The distribution of the bottom stress was also similar to currents and significant wave height: with the largest value in the shallow region where the currents were strongest, and the relatively large value over the shelf where surface waves were high (Figure 3.28: lower panel). The bottom stress was in the range of 0.1-0.5 N/m^2 over the shelf between the 40- and 50-m isobaths at the time of maximum wind passage.

3.2.1.2 With wind turbines

The surface elevation and vertically averaged currents remain similar after wind turbines are added. The surface elevation contours are almost parallel to local isobaths, with relatively small cross-isobath gradient over the shelf at the time of the maximum wind. The spatial distribution of surface elevation is almost identical in the cases with and without wind turbines (Figure 3.29: upper panel). No significant change is found in the vertically averaged velocity, either (Figure 3.29: lower panel). This is dynamically consistent with surface elevation, since the change of surface elevation is proportional to

the spatial change of the vertically averaged velocity, especially over the shelf where bathymetry is relatively flat.

The velocities near the surface and bottom also remain the same spatial patterns and temporal variations after wind turbines are added (Figure 3.30). The velocity within the wind turbines facility area is slightly reduced

The spatial distribution and temporal variation of significant wave height are very similar to those found in the case without wind turbines (Figure 3.31: upper panel). However, the bottom stress changes significantly within the wind turbine facility area between 40- and 50-m isobaths (Figure 3.31: lower panel). It is reduced considerably in the bathymetry divergence zone and becomes stronger around the northern edge of the wind turbine facility area along the 40-m isobath.

3.2.1.3 Differences

No significant difference is found in surface elevation and vertically averaged velocity inside and outside the wind turbine facility area over the shelf except around Block Island and the water passages between Nantucket Island and Martha's Vineyard Island and Buzzard Bay (Figure 3.32). The surface elevation can be changed by about ~ 0.05 m at a few offshore wind turbine sites and by >0.1 m in the shallow southern exit of Nantucket Sound and on the eastern side of Block Island. At a few offshore wind turbine sites, the vertically averaged velocity shows some small-scale eddies, with a magnitude of ~ 0.02-0.10 m/s.

Near the surface, the speed of the wind-induced onshore current can be reduced by a value of ~ 0.1-0.2 m/s inside the offshore wind turbine facility area (Figure 3.33: upper panel). Around the northeastern edge of the offshore wind turbine facility area, however, the northeastward flow is intensified, which produces a significant surface divergence around the 40-m isobath. Correspondingly, the offshore flow near the bottom weakens in the offshore wind turbine facility area in the same order of magnitude as that near the surface, and intensifies around the northeastern edge along the 40-m isobath. As a result, the flow convergence near the bottom over that area is enhanced (Figure 3.33: lower panel).

The difference in the significant wave height is much higher than surface elevation (Figure 3.34: upper panel). Within the offshore wind turbine facility area, the difference is in the range of ~ ±1.0 m, with a strip-like distribution in the along-shelf direction. The big difference is found around Block Island and also near the southern shelf of Nantucket Sound and the coast of Narragansett Bay, Rhode Island and Buzzard Bay, MA.

The change of the bottom stress varies significantly in space. It is reduced by values of ~ 0.3-0.4 N/m^2 between the 40- and 50-m isobaths in the region west of 70.5°W and increased by values of ~ 0.1-0.3 N/m^2 around the northeastern edge between the 30- and 40-m isobaths (Figure 3.34: lower panel). A big difference is also found over the

southwestern and eastern tips of Martha's Vineyard, the western side of Nantucket Island, and the eastern shelf region of Nantucket Shoals as well as around Block Island.

The model results clearly show that the change of the marine environment due to the deployment of wind turbines is much more significant around Block Island than in the offshore shelf off Massachusetts and Rhode Island. We will discuss the change around Block Island later in Section 3.3.

3.2.2 Hydrodynamic simulation with NS-FVCOM

The hydrodynamic simulation refers to the model run with NS-FVCOM only. In this experiment, surface waves are not included. With the same purpose described in section 3.1.2, this experiment is made to examine the relative contribution of wave-current interaction on surface elevation, vertically averaged velocity (in proportion to the transport), near-surface and near-bottom velocities, and bottom stress.

3.2.2.1 Without wind turbines

For the case without the presence of wind turbines, the model-computed surface elevation for the model run without surface waves exhibits the same spatial and temporal variation patterns as those found in the experiment with the inclusion of wave-current interaction (Figure 3.35: upper panel). The difference is in magnitude. As the hurricane moves towards the coast, wave-current interaction can produce a higher surface elevation in the shallow region in Nantucket Sound, Buzzard Bay, and Narragansett Bay as well as around Block Island, but lower surface elevation in the offshore region between the 40-m and 60-m isobaths (Figure 3.35: lower panel). The difference is larger than 0.2 m.

The model-computed vertically averaged, near-surface and near-bottom velocities for the model run without surface waves are also very similar to those obtained for the model run with the inclusion of wave-current interaction (Figures 3.36-3.38: upper panels). The difference in the vertically averaged velocity for the cases with and without surface waves was remarkable around islands and near the coast region, but was insignificant in the offshore region (Figure 3.36: lower panel). The maximum velocity difference can be up to ~ 1.0 m/s in the shallow region in Nantucket Sound. The difference in the near-surface velocity for these two cases shows a similar feature, large in the shallow region where the water depth is less than 40 m (Figure 3.37: lower panel). The wave-current interaction can produce a large offshore flow component in Nantucket Sound, with a magnitude of up to 1.0 m/s. This process tends to slow down the onshore movement of water in that region. The velocity change due to wave-current interaction has an opposite direction between the bottom and the surface. This process can strengthen the near-surface onshore velocity component and slow down the offshore water movement near the bottom (Figure 3.38: lower panel).

The model-computed bottom stress for the model run without surface waves shows a general similar spatial distribution pattern as that for the model run with the inclusion of

wave-current interaction (Figure 3.39: upper panel). However, removing the contribution of surface waves leads to a smaller bottom stress in the strong current regions around Nantucket Sound, the northeastern slope east of Nantucket Sound and Shoals, near the coast, and in the offshore region between the 40-m and 60-m isobaths as well as around Block Island (Figure 3.39: lower panel). If only the offshore wind turbine facility area and Block Island are considered, our results suggest that the assessment for the change in the bottom stress and sediment due to the deployment of wind turbines should take wave-current interaction into account.

3.2.2.2 With wind turbines

After adding wind turbines, the spatial distribution of surface elevation during the hurricane for the model run without surface waves remains the same pattern as that for the model run with the inclusion of wave-current interaction (Figure 3.40: upper panel). The impact of wave-current interaction on surface elevation found in the case with wind turbines are similar to that found in the case without wind turbines (Figure 3.40: lower panel).

The spatial distribution of the vertically averaged velocity remains unchanged after adding wind turbines (Figure 3.41: upper). The significant difference between the cases with and without wave-current interaction only occurs in the shallow region where the currents are strong, but not in the offshore region where wind turbines are located (Figure 3.41: lower panel).

It seems clear that wave-current interaction can cause a big difference in the near-surface velocity during the storm after wind turbines are added. In the case without wind turbines, the influences of wave-current interaction mainly occur in the shallow regions where the water depth is less than 40 m. After wind turbines are added, wave-current interaction tends to increase the onshore component of the velocity and also enhance the offshore component in the shallow region (Figure 3.42). Near the bottom, wave-current interaction have a very small impact on the flow in the offshore turbine facility area, which exhibits the same spatial distribution pattern as that for the model run without wind turbines.

With the inclusion of wind turbines, the model-computed bottom stress for the model run without surface waves shows the same spatial distribution pattern as that obtained for the model run with the inclusion of wave-current interaction (Figure 3.43). The major difference is in magnitude. Wave-current interaction can produce a larger bottom stress. The difference in the bottom stress between the case with and without surface wave can be 0.6 N/m^2 or larger (Figure 3.43: lower panel).

3.2.2.3 Difference

The difference in the surface elevation between the cases with and without wind turbines significantly differs for the model runs with and without wave-current interaction. In the wave-current interaction case, we found that during Hurricane Bob,

the influence of wind turbines on surface elevation is not significant. However, in the case without surface waves, adding wind turbine can cause a lower surface elevation near the coastal area off Narragansett Bay and over the shelf south of Nantucket Sound, and a higher surface elevation on the eastern shelf of Nantucket Sound, although its influence on the offshore wind turbine facility area is small (Figure 3.45: upper panel). The surface elevation between the cases with and with wind turbines can be up to 0.2 m.

The difference in the vertically averaged velocity between the case with and without wind turbines is also different for the model runs with and without wave-current interaction. In the wave-current interaction case, the major difference is found around Block Island and at local sites inside the offshore wind turbine facility area. However, when the surface waves are not considered, the difference shifts towards the eastern shelf and the southwestern shelf of Martha's Vineyard outside the wind turbine facility area, with a velocity difference of up to 0.1-0.2 m/s (Figure 3.45: lower panel).

The similar feature is also found for the near-surface and near-bottom velocities. In the wave-current interaction case, influences of wind turbines on the near-surface and near-bottom velocities are mainly within the wind turbine facility area. However, in the case without surface waves, adding wind turbines can significantly increase the offshore and onshore velocity components near the surface and bottom, respectively (Figure 3.46). This influence is regional, but no longer local within wind turbines.

The difference in the bottom stress between the cases with and with wind turbines for the model run without surface waves shows significantly different spatial distribution and magnitude as those for the model run with the inclusion of wave-current interaction. In the wave-current interaction case, the influence of wind turbines during the storm is mainly around the edge of the offshore wind turbine facility area and in the shallow region where the current is strong. However, in the case without surface waves, the influence spreads over the entire northern shelf region, with a very complex spatial distribution pattern (Figure 3.47). The change of the bottom stress in the shallow region outside the wind turbine facility area can be up to 0.6 N/m^2 or even larger.

3.2.3 Surface wave simulation with NS-SWAVE

As the same as the February 1978 storm case, the surface wave simulation described here refers to the model run with NS-SWAVE only, in which the wave-current interaction process is not taken into account. The experiments are made to estimate the contribution of the feedback of wave-current interaction to the significant wave height described in the case with the inclusion of wave-current interaction.

3.2.3.1 Without wind turbines

Running NS-SWAVE without coupling with NS-FVCOM produces the same spatial distribution and temporal variation of surface waves as those obtained using the coupled NS-FVCOM and NS-SWAVE system (Figure 3.48: upper). The major difference in significant wave height between the cases with and without the inclusion of wave-current

interaction is in the shallow region around the coast where the water depth is shallower than 40 m. Wave-current interaction can produce a higher significant wave height, with a value of >1.0 m near the coast and lower significant wave height in the offshore shelf region (Figure 3.48: lower panel). This influence can be regional, and varies significantly along and cross isobaths.

3.2.3.2 With wind turbines

Adding wind turbines does not change the spatial distribution of the significant wave height (Figure 3.49: upper panel). Due to the presence of wind turbines, the difference in the significant wave height between the experiments with and without the inclusion of wave-current interaction is slightly weaker in the case with wind turbines than in the case without turbines (Figure 3.49: lower panel), although the maximum difference near the coast between the two cases is very close.

3.2.3.3 Difference

The difference in the significant wave height between the cases with and without wind turbines is larger in the shallow region where the water depth is less than 40 m and around the outer edge of the offshore wind turbine facility area (Figure 3.50). As the same as in the wave-current interaction case, the difference between the cases with and without wind turbines is much larger around Block Island. Compared with the case with the inclusion of wave-current interaction, we can see that the change in surface waves due to the presence of wind turbines can be underestimated if no feedback of wave-current interaction to the wave simulation is accounted.

3.3 Block Island

Five wind turbine foundations are already installed in the southwestern area of Block Island. Differing from the offshore wind turbines, these five wind turbines are close to the coast. The experiment results for the February 1978 nor'easter storm and the August 1991 Hurricane Bob cases show that these near-coastal wind turbines can have a more significant impact on the local marine environment condition than the offshore wind turbines. To provide a quantitative assessment of this impact, we zoomed in on the Block Island area here to discuss the wind turbine-resulting possible change of surface elevation, currents, waves and bottom stress around the island due to nor'easter storms and hurricanes.

3.3.1 The February 1978 nor'easter storm

During the February 1978 nor'easter storm, the strong northeasterly wind blew over the shelf off Massachusetts and Rhode Island, which was directly towards the eastern coast of Block Island. Under the condition without wind turbines, at the time of the maximum wind, the surface elevation was about 0.25 m higher on the eastern side than western side (Figure 3.51: top-left). As a result, the water moved towards the eastern coast, split northward and southward, and flowed around the island. These two around-island flow branches encountered at the southwest top of the island and pushed the water

offshore (Figure 3.51: top-right). This current pattern remained the same when five turbines are added, but the flow convergence at the southwest tip is intensified (Figure 3.51: middle-right) and the surface elevation rose by 0.25 m on the lee side of the island (Figure 3.51: middle-left). The differences between the two cases show that the turbine-induced change of surface elevation varied in space. On the front side facing the wind, it can be up to ~ 0.10 m, while on the lee side of the island, it can be about ~ 0.25 m (Figure 3.51: bottom-left). The change in the vertically averaged velocity occurs mainly around the southwest tip of the island and in the wind turbine facility area, with magnitude of ~ 0.1-0.3 m/s.

Around Block Island, the water was vertically well mixed during the storm. Under the condition without wind turbines, the flow is surface-intensified, with the same spatial distribution pattern near the surface and the bottom (Figure 3.52: top). Adding five wind turbines does not change the around-island flow pattern, but it does influence the magnitude of the flow around the southwest tip of the island and the wind turbine facilityarea (Figure 3.52: middle). The differences between the two cases show that at the time of the maximum wind, the near-surface flow is intensified around the southwest and southeast tips of the island with a magnitude change of ~ 0.5-1.0 m/s, and weakened around the wind turbine facility area with a magnitude change of ~ 0.2-0.3 m/s (Figure 3.52: bottom-left). The change of the near-bottom flow mainly occurs around the wind turbine facility area, where adding turbines produces the small-scale flow convergences around individual turbines (Figure 3.52: bottom-right).

The storm generated a significant wave height up to ~ 6-7 m over the eastern side shelf of the island, but only about 1-3 m around the coast of the island. Under the condition without wind turbines, the significant wave height is higher on the front side shelf of the island than on the lee side shelf of island, even though the significant wave height was similar around the island coast (Figure 3.53: top-left). Although this surface wave distribution pattern remained the same under the condition with wind turbines, the significant wave height was considerably higher on the eastern side of the wind turbine facility area (Figure 3.53: middle-left). The difference in the significant wave height between the two cases can be up to ±1.0 m around the island (Figure 3.53: bottom-left). At the time of the maximum wind, the presence of five wind turbines can cause the significant wave height to increase by a value of ~ 1.0 m around the wind turbine facility area and in the eastern offshore region, and to drop by a value of ~ -1.0 m around the eastern and southern coast areas of the island.

Strong storm winds produced a large bottom stress around the island. Under the condition without wind turbines, at the time of the maximum wind, two maximum bottom stress areas occurred around the southern side and northern tip of the island, with a value exceeding 2.0 N/m^2 (Figure 3.53: top-right). The model-produced bottom stress under the condition with five wind turbines remains the same spatial distribution (Figure 3.53: middle-right), but the magnitude around the wind turbine facility area and around the island can change significantly. The maximum difference can be up to ~ 0.6 N/m^2 or larger (Figure 3.53: bottom-right).

3.3.2 The August 1911 Hurricane Bob

When the August 1991 Hurricane Bob moved towards Narragansett Bay, its pathway was very close to Block Island. Under the condition without wind turbines, at 18:00:00 GMT August 19, the wind at Block Island was westerly (eastward) with a magnitude of > 20 m/s. The surface elevation increased onshore, with a relatively high surface elevation of ~ 1.0 m around the coast of the island (Figure 3.54: top-left). The vertically averaged velocity shows that the water flowed towards the island on the southern side and split into two around-island flow branches: one flowed northward and another flowed westward, with a magnitude of ~ 1.0 m/s (Figure 3.54; top-right). After five wind turbines are added, the surface elevation and vertically averaged velocity remain the same spatial distribution pattern (Figure 3.54: middle), but the surface elevation and vertically averaged velocity around the wind turbine facility area and the coast of the island differed. The differences in the two cases show that the surface elevation can be increased by a value of up to ~ 0.20 m around the eastern and southern coast of the island. This change of the surface elevation exhibits a significant spatial variation (Figure 3.54: bottom-left). For example, the surface elevation is increased by a value of ~ 0.10-0.20 m around the northern three wind turbines, but it drops by a vale of ~ 0.10-0.20 m around the southern two wind turbines. Similarly, the northward vertically averaged velocity on the southeastern and western coasts of the island is increased with a magnitude of up to ~ 0.5-1.0 m/s.

Similar to the February 1978 nor'easter storm case, the water around Block Island was also vertically well mixed when and after Hurricane Bob passed. The velocity was surface-intensified, with the same spatial distribution near the surface and bottom (Figure 3.55: top). Near the surface, the around-island velocity was up to ~ 1.0 m/s, while near the bottom, it was up to ~ 0.1 m/s. Adding five wind turbines does not change the horizontal and vertical distributions of the velocity, but can significantly influence its magnitude around the wind turbines (Figure 3.55: middle). This influence occurs not only around the wind turbine facility area, but also can cover the entire coastal region of the island near the surface and bottom (Figure 3.55: bottom). Near the surface, the change can be up to 1.0 m/s. Even near the bottom, it can be up to 0.5-1.0 m/s.

Under the condition without wind turbines, with strong eastward winds, the surface waves propagated towards the northwest from the southern offshore region. The significant wave height was higher on the southern and eastern shelves of the island and lower on the northwestern and northern shelves of the island (Figure 3.56: top-left), with the tendency to become smaller towards the coast of the island. The significant wave height over the southern offshore shelf exceeded 12 m, and was around 2-3 m around the island coast. Adding five wind turbines does not change the propagation direction of surface waves and regional-scale spatial distribution of significant wave height, but it does significantly influence the wave height around the island (Figure 3.56: middle-left). The turbine-induced change in the significant wave height exhibits a significant spatial variation around the island, which can cause a ~ 1.0 m rise or drop in the region (Figure 3.56: bottom-left).

The hurricane produced a large bottom stress on the eastern and southern sides of the island with a maximum value exceeding 2.0 N/m^2 (Figure 3.56: top-right). Between large bottom stress areas was a lower bottom stress zone. Adding five wind turbines can significantly increase the bottom stress on the eastern and southern sides of the island including in the wind-turbine facility area. (Figure 3.56: middle-right). For example, over the three-wind turbine facility area is a small bottom stress zone, but turns into the high bottom stress zone after wind turbines are added. The turbine-induced change of the bottom stress exhibits a significant spatial variation, with a value of > 0.6 N/m^2 in the turbine facility area (Figure 3.56: bottom-right). This influence is not limited locally around the turbine facility area, but can cover the entire coastal region of the island.

3.4 Results of Lagrangian-particle tracking

One of the major concerns regarding fisheries is whether or not the offshore wind turbines can alter the dispersal and settling of the scallop larvae that are transported from the upstream spawning area on Georges Bank and Nantucket Shoals to the Middle Atlantic Bight. In this contract work, we have considered the extreme influence condition under nor'easter storms and hurricanes. Releasing the particles in and out of the wind turbine facility area can help us address the questions on the impact of the deployment of the offshore wind energy facility on the larval transport inside and through this area under extreme weather conditions.

To estimate the change of the particle dispersion rate after adding wind turbines, we calculate the dispersion rate of particles at every tracking time interval for the case with and without wind turbines. In this calculation, the *x* (east-west) and *y* (south-north) components of the dispersion rate are defined as

$$A_x = 0.5\frac{\Delta V_x}{\Delta t}; A_y = 0.5\frac{\Delta V_y}{\Delta t} \qquad (7)$$

where

$$\Delta V_x = V_x(t+\Delta t) - V_x(t);\ \Delta V_y = V_y(t+\Delta t) - V_y(t)$$

and

$$V_x(t) = \frac{1}{N}\sum_{i=1}^{N}[x_i(t) - x_c(t)]^2\ ;\ V_y(t) = \frac{1}{N}\sum_{i=1}^{N}[y_i(t) - y_c(t)]^2\ ;$$

$$x_c(t) = \frac{1}{N}\sum_{i=1}^{N} x_i\,(t);\ y_c(t) = \frac{1}{N}\sum_{i=1}^{N} y_i\,(t).$$

Here *N* is the total number of particles released in each case and *i* is the index for individual particle.

It should be pointed out here that the Lagrangian-particle tracking experiment conducted in this contract is mainly focused on the impact of the offshore wind farm on larvae transport and dispersion through the offshore wind turbine region under storm weather conditions. Scallop recruitment is a function of spawning, fertilization success,

and survival of early life stages of scallop larvae and early settlement stages. Adult scallops are broadcast spawners. After fertilization, the non-motile zygote stages develop through the trochophore stage and then prodisochonch stage and start to migrate upward towards the sea surface (Gallager et al., 1996; McGarvey et al., 1992; Cragg, 2006). The pelagic veliger stage begins around Day 4 and terminates as the pediveligers, with foot and byssus threads, settle and attach to particles on the seafloor about 40-50 days later. During the pelagic phase, changes in the depth-specific current-driven larval dispersal and retention are a primary factor in controlling interannual variability in spatfall and ultimately recruitment (McGarvey et al., 1993). While early prodisochonch larvae (4 to ~40 days) actively swim between the surface and thermocline, late-stage pediveligers (40 to 50 days) cross the thermocline and descend towards the bottom in preparation for settlement (Gallager et al., 1996; Pearce et al., 1996).

To assess the impact of the development of an offshore wind energy facility on the scallop larval transport and dispersion requires an individual-based model (IBM) for scallop population consisting of four pelagic phases (egg, trochophore, veliger and pediveliger) (Tian et al., 2009a). Individual development in the model is based on age: eggs <2 days, trochophores 2–4 days, veligers 5–40 days, and pediveligers > 40 days (Stewart and Arnold, 1994). Behavioral vertical migration is specified for each life stage. Eggs are spawned on the seabed, are neutrally buoyant, and drift passively without vertical migration. Contrary to the existing models, trochophores have no directionality in their swimming and only randomly spin. Once the first shell is formed (prodisoconch) and the larvae form the 'D' configuration, then their center of gravity is below the velum, which propels them in the vertical direction upwards (Gallager, 1993; Gallager et al., 1996). Veligers are essentially subject to current drift in the surface layers above the thermocline, but actively swim and alternately sink producing a distinct migration pattern. Veligers are sensitive to light transitions, not to any prolonged state of light intensity such as day or night (Gallager et al., 1996). Larvae between the ages of 5 and 45 days vertically migrate to the surface and then back to the thermocline both when the sun comes up and when it sets (Gallager et al., 1996). In addition, larvae respond to algal density (food) in a concentration-dependent way by spending more time at depths where algal density is higher (Gallager et al., 1996). Larvae also respond to ephemeral pulses of turbulence greater than 10-7 W.Kg-1 by withdrawing their velum and sinking rapidly until the turbulent energy has subsided (Pearce et al., 1998). This extensive suite of swimming behaviors has never been captured in a model to date (e.g. Stewart and Arnold, 1994 and Tian et al., 2009a treated larvae as particles with a random walk) and can contribute greatly to the overall transport potential of larvae since they are constantly responding to stimuli and changing their depth. Late-stage pediveligers (>45 days) migrate downwards to the seabed (1.7 mm s-1) to settle, but may remain at the thermocline for more than 100 days and delay metamorphosis if thermal conditions are inappropriate (Pearce et al., 1996). Such a delay in settlement can lead to higher retention if larvae are in a gyre that extends beyond the shelfbreak only to return several days later, particularly in the MAB. Mortality throughout the pelagic phase can be carefully parameterized based on data and conditions provided in the literature (e.g. Gallager et al., 1986a,b, 1988).

Our contract project is focused on 1) developing the high-resolution subdomain model that is capable of resolving the small-scale physical processes within offshore

wind turbine facility areas with nesting to the regional NECOFS system and 2) using this model to examine the impact of the offshore wind facility on the local and regional environments during storm conditions. This contract does not include the effort to run an IBM scallop population model and assess the impact of the development of the offshore wind energy facility on the connectivity of scallop larval transport between Georges Bank/Great South Channel and Mid-Atlantic Bight.

3.4.1 The February 1978 nor'easter storm

For the February 1978 Nor'easter case, we conducted two types of particle tracking experiments. In the first type experiment, a total of 100 particles are released in two regions: 1) over the eastern shelf outside the wind turbine facility area (hereafter referred to as "Case 1") and 2) within the offshore wind turbine facility area (hereafter referred to as "Case 2"). The particle-releasing region for Case 1 is close to the area where a high scallop aggregation is observed over the western shelf of the Great South Channel (Figure 1.2). In this case, the particles are released near the surface with a separation scale of ~ 1.4 km in the east-west direction and 3.2 km in the south-north direction at 00:00:00 GMT February 1 and then traced in the surface velocity field for 11 days ending at 00:00:00 GMT February 11. For Case 2, the particles are released with a separation scale of 2.5 km in the east-west direction and 5.5 km in the south-north direction within the wind turbine facility area at the same time as those for Case 1. These two experiments are repeated for the cases without the inclusion of wind turbines. In the second type experiment, the high-density distributed particles are released around individual wind turbines. This type experiment is aimed at examining the impact of small-scale variability of the flow field around wind turbines on particle trajectories. Three locations are selected, which are referred to as Case 3, Case 4 and Case 5. In each of Case 3-5, 210 particles are released with a spatial separation scale of ~ 50 m around an individual wind turbine. The starting and ending track times are the same as those used in Cases 1-2. These particle-tracking experiments are also repeated for the case without wind turbines.

For particles released outside the wind turbine facility area (Case 1), the results clearly show that in the case without wind turbines, particles are advected southward along local isobaths in the regions between 40 and 60 m (Figure 3.57: upper panel). At the tracking ending time, particles can arrive in the area close to 40.6^{o}N, 72°W. When wind turbines are added, the particles show no problems to go through the wind turbine facility area (Figure 3.57: lower panel). No particles are trapped within the wind turbine facility area. This suggests that under the nor'easter storm condition with strongly northeasterly winds, the deployment of the offshore wind turbines in this region will not have a significant influence on the southwestward water transport from the upstream Nantucket Shoals, Great South Channel and Georges Bank area to the Mid-Atlantic Bight. However, adding the wind turbine facility does cause the trajectories of particles to be more dispersive in both the along-isobath and cross-isobath directions. The particles move southwestward at a faster speed, and trajectories of some particles dispersed offshore from the 60-m isobath to the 80-m isobath. At the tracking ending time, particles can arrive in the area near 40.4^{o}N, 72.5°W. In this case, during the tracking period, the mean of the change in the spatial dispersion rate after adding wind turbines is ~ 0.44×10^{5}

m^2/s, with a maximum value up to ~ 1.6×10^5 m^2/s. This maximum value is the same order of magnitude as the maximum dispersion rate of the particles that are released in the case without wind turbines (Table 3.1).

For particles released within the proposed wind turbine facility area (Case 2), the results show that in the case without wind turbines, the trajectories of particles exhibit a significant cross-shelf variation during the storm, but eventually move southwestward along the shelf. At the tracking ending time, a large portion of particles has arrived in the area centered near 40.3°N, 72.5°W (Figure 3.58: upper panel). When the wind turbines are added, the trajectories of particles remain a similar distribution pattern, except an increase of the cross-shelf dispersion (Figure 3.58: lower panel). At the tracking ending time, most of the particles had arrived in the area centered near 40.2°N, 72.8°W. Under this storm event, no particles are trapped in the wind turbine facility area. In this case, during the tracking period, the mean of the change in the spatial dispersion rate after adding wind turbines was ~ 0.21×10^5 m^2/s, with a maximum value up to ~ 1.10×10^5 m^2/s (Table 3.1).

In Cases 3-5, the particles are released with a high-density distribution in a small region around individual wind turbines. The particle trajectories between the cases with and without wind turbines are shown in Figures 3.59-3.62. The results clearly show that the particle trajectories for these two cases significantly differed, which is believed due to the small-scale variability of the flow field around the wind turbines. In these three cases, the spatial dispersion is reduced in the case with wind turbines, which differ from what we observed in Cases 1 and 2. The mean of the change in the spatial dispersion rate after adding wind turbines is ~ 0.01×10^5 m^2/s, but the maximum value can be up to ~ 0.08×10^5 m^2/s for Case 3, ~ 0.10×10^5 m^2/s for Case 4 and ~ 0.06×10^5 m^2/s for Case 5 (Table 3.1), respectively.

The particle-tracking experiments described above suggest that the deployment of wind turbines in the proposed offshore region will not have a significant influence on the near-surface southwestward larval transport from the upstream Nantucket Shoals, Great South Channel, and Georges Bank area to the Mid-Atlantic Bight, although it can significantly change the cross-shelf larval dispersion. All past nor'easter storms are characterized with strong northeasterly winds. To a certain extent, the experiment made for the February 1978 nor'easter storm can be representative of the winter-spring storm condition in this region.

3.4.2 The August 1991 Hurricane Bob

For August 1991 Hurricane Bob, we also released particles in two regions: 1) over the southern shelf outside the wind turbine facility area and 2) within the offshore wind turbine facility area. Hurricane Bob moved toward the coast on the left side of the proposed offshore wind turbine facility area, during which the strong cyclonic wind pushed the water onshore. The first experiment is made to examine how trajectories of particles, which originated over the outer shelf, can be influenced when wind turbines are added. The second experiment is made to examine if the particles can be more trapped in

the offshore wind turbine facility area after these turbines are deployed. In both experiments, 100 particles are released near the surface with a uniform space distribution at 00:00:00 GMT August 16 and tracked over a 5-day period ending at 00:00:00 GMT August 21.

For the first case, the results show that in the case without wind turbines, all particles first move southward along local isobaths and then northeastward with a tide- and wind-induced relatively large oscillation (Figure 3.63: upper panel). This pattern remains unchanged after the offshore wind turbines are added. However, the particles move slowly, with small oscillation amplitude (Figure 3.63: lower panel). At tracking ending time, particles can reach the 50-m isobath in the case without wind turbines, but only arrive on the 60-m isobath in the case with wind turbines. This result is consistent with what we found in the change of the near-surface velocity field after wind turbines are added. The presence of wind turbines can reduce the onshore flow during this hurricane.

For the second case, the results show that in the case without wind turbines, particles almost move around the release area and only a few particles are able to leave the region and enter Nantucket Sound (Figure 3.64: upper panel). When wind turbines are added, the particles tend to be more trapped in and around the release area where the offshore wind turbine are (Figure 3.64: lower panel). The trapped feature of particles in that area is due to the hurricane-induced cyclonic wind, but the wind turbines can reduce the spatial dispersion of particles in that region.

3.1. Difference between dispersion rates for cases with and without wind turbines.

February 1978 Nor'easter storm		
Dispersion rate	Maximum difference ($\times 10^5$ m^2/s)	Mean difference ($\times 10^5$ m^2/s)
Case 1	1.60	0.44
Case 2	1.10	0.21
Case 3	0.08	0.01
Case 4	0.10	0.01
Case 5	0.06	0.01
August 1991 Hurricane Bob		
Case 1	1.17	0.18
Case 2	0.83	0.15

When Hurricane Bob moved through the offshore region, it created a strong near-inertial oscillation with a maximum speed up to ~1.5 m/s (Figure 3.65). At latitude of 40.5°N, the inertial period is 18.48 hours. The oscillation period found in particle trajectories is around 19 hours, which is within the inertial period in that region. The comparison results between the cases with and without wind turbines clearly show that adding wind turbines can significantly reduce the storm-induced inertial oscillation in the current field in the offshore region, within or outside of the wind turbine facility area. The oscillation speed reduced from ~ 1.5 m/s to ~ 1.0 m/s after wind turbines are added, which accounts for a reduction of ~ 33% (Figure 3.65).

The hurricanes strike this region with a much lower frequency than the nor'easter storms. Recording to past records, the hurricane generally pass over the study region with a time scale of shorter than 2 days. The influence of the hurricane on particle trajectories should be a short-term variation but will not change the general feature of the larval transport in this region.

4. Summary

A high-resolution, wind turbine-resolving, subdomain FVCOM model is developed and used to conduct an assessment of the possible impact of the future offshore wind energy facility on the local and regional physical environments under storm conditions. This high-resolution model is named "NS-FVCOM", which is fully coupled with the FVCOM surface wave model (named "NS-SWAVE). The February 1978 nor'easter storm and the August 1991 Hurricane Bob are selected as representatives of extratropical and tropical storms, respectively, and the numerical experiments were made under the conditions without and with wind turbines. The modeling assessment is first carried out by running the coupled NS-FVCOM and NS-SWAVE system with the inclusion of wave-

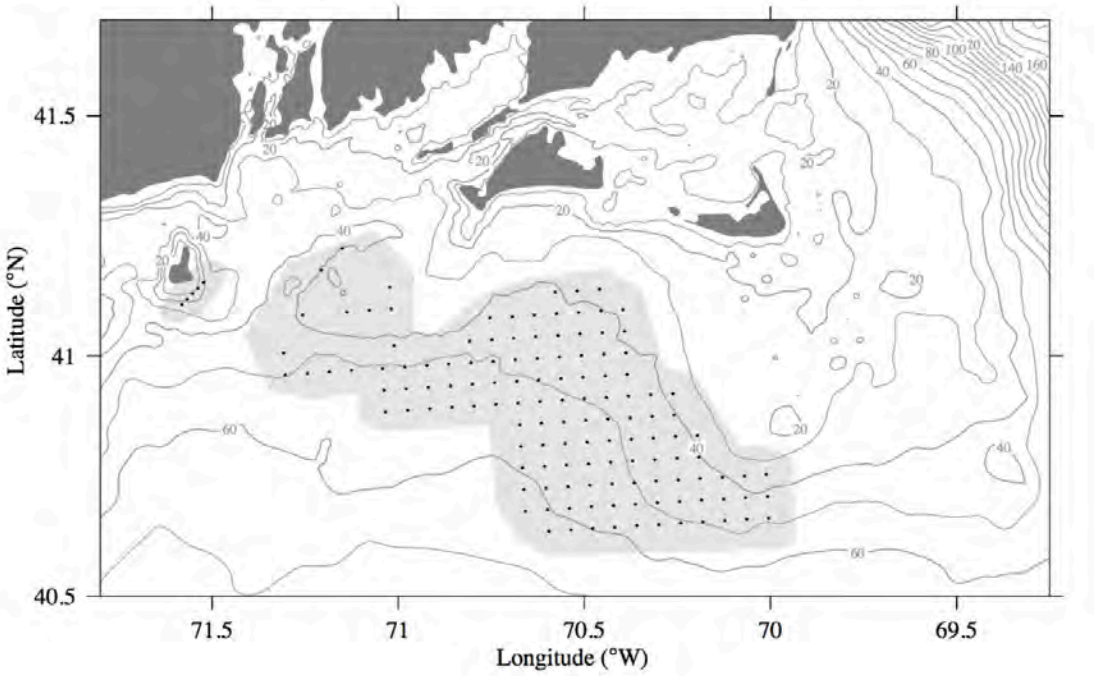

Figure 4.1: Definition of 1) the offshore wind turbine facility area (covered by a large gray shadow), 2) the Block Island wind turbine facility area (covered by a gray shadow zone on the eastern shelf of Block Island, and 3) the region outside the wind turbine facility.

current interaction, and then either hydrodynamic simulation with NS-FVCOM only or surface wave simulation with NS-SWAVE only. The purpose of running the model under different dynamical setups is to quantitatively estimate the relative contribution of wave-current interaction to hydrodynamics variables and significant wave heights under the conditions without and with wind turbines.

To help summarize our major finding, we have defined two areas and one region in our analysis: 1) the offshore wind turbine facility area, 2) the Block Island wind turbine facility area and 3) the region outside the wind turbine facility area (Figure 4.1). A quantitative assessment is approached by calculating the mean and maximum differences in these three areas and region between the cases with and without the inclusion of wind turbines. The results are summarized in Tables 4.1-4.4.

Table 4.1: Summary of offshore wind turbine-induced possible environmental changes for the February 1978 nor'easter storm case.

Variable difference	**Inside the wind turbine facility**		**Outside the wind turbine facility**	
	Mean	**Max**	**Mean**	**Max**
Elevation (m)	-0.04	0.08(-0.01)	-0.03	0.18(-0.05)
Vertically averaged velocity speed (m/s)	-0.03	2.09(-1.01)	-0.00	0.54(-0.57)
Velocity averaged velocity direction (degree)		172.40°		75.98°
Near-surface velocity speed (m/s)	-0.04	0.58(-0.86)	0.00	0.71(-1.01)
Near-surface velocity direction (degree)		172.48°		95.05°
Near-bottom velocity speed (m/s)	-0.04	0.66(-0.44)	0.01	0.64(-0.51)
Near-bottom velocity direction (degree)		82.82°		143.28°
Significant wave height (m)	-0.34	2.11 (-5.53)	-0.08	2.35(-2.84)
Bottom stress (N/m^2)	-0.05	2.30 (-0.47)	0.01	2.87(-2.82)

Table 4.1 summarizes the mean and maximum difference of the surface elevation, vertically averaged, near-surface and near-bottom velocities, significant wave height, and bottom stress between the cases with and without wind turbines inside the offshore wind turbine facility and in the region outside the wind turbine facility for the 1978 nor'easter storm case. The model results show that the influence of the deployment of offshore wind turbines on the physical environment exhibits a significant spatial-varying pattern, not only in a local scale within the wind turbine facility but also can be over a regional scale covering the outside region over the shelf and near the coast. The impact is more significant on currents, surface waves, and bottom stress than surface elevation.

The spatial distributions of these differences are described in Section 3.1. The major finding is that near the surface, the deployment of the offshore wind turbines can produce a cyclonic circulation with a magnitude of ~ 0.2 m/s around the wind turbine facility and multiple small-scale cyclonic eddies near the surface inside the wind turbine facility. It also can intensify the offshore flow by a magnitude of ~ 0.3 m/s near the bottom. The influence can extend over the shallow region and outer slope, with the same order of magnitude as those found inside the wind turbine facility.

Table 4.2 summarizes the same variables as those in Table 4.1, but for the August 1991 Hurricane Bob case. The model results also suggest that the influences of the deployment of offshore wind turbines can have a regional impact, not only inside the wind turbine facility but also in the region outside. Similar to the February 1978 nor'easter storm, the change is generally small in surface elevation and vertically averaged velocity, but significant in surface waves, near-surface and near-bottom velocities. Influences also vary significantly in space, with the same order of magnitude inside and outside the wind turbine facility.

Table 4.2: Summary of offshore-wind turbine-induced possible environmental changes for the August1991 Hurricane Bob case.

Variable difference	**Inside the wind turbine facility**		**Outside the wind turbine facility**	
	Mean	**Max**	**Mean**	**Max**
Elevation (m)	-0.01	0.15(-0.10)	-0.01	0.36(-0.16)
Vertically averaged velocity speed (m/s)	-0.02	2.22 (-0.98)	0.00	0.97(-0.58)
Vertically averaged velocity direction (degree)		176.54°		137.26°
Near-surface velocity speed (m/s)	0.06	1.35(-1.07)	0.00	1.06(-0.69)
Near-surface velocity direction (degree)		179.96°		136.64°
Near-bottom velocity speed (m/s)	0.04	0.96(-0.63)	0.00	0.58(-0.35)
Near-bottom velocity direction (degree)		179.64°		35.33°
Significant wave height (m)	-0.01	2.65 (-12.61)	-0.08	2.65(-3.51)
Bottom stress (N/m^2)	0.05	6.00 (-2.40)	-0.01	7.00 (-2.64)

Tables 4.3 and 4.4 summarize the mean and maximum difference of surface elevation, vertically averaged, near-surface and near-bottom velocities, significant wave heights and bottom stress inside the Block Island wind turbine facility area for the February 1978 nor'easter storm and the August 1991 Hurricane Bob cases. The strong northeasterly wind blew over the island during the February 1978 nor'easter storm, while it was dominated by a strong westerly wind during August 1991 Hurricane Bob. Although wind directions were different in these two cases, the model experiment results show that the wind turbine facility on the eastern shelf off Block Island can cause more significant local and regional impacts than offshore wind facilities over the outer shelf off Massachusetts and Rhode Island. The changes due to wind turbines vary with the intensity and direction of the storm winds, which exhibit a significant spatial variation.

Table 4.3: Summary of possible environmental changes inside the wind turbine zone on the eastern shelf off Block Island for the February 1978 nor'easter storm case.

Variable difference	**Inside the wind turbine facility**

	Mean	Max
Elevation (m)	-0.05	0.16(-0.20)
Vertically averaged velocity speed (m/s)	0.01	0.85(-1.15)
Vertically averaged velocity direction (degree)		170.30°
Near-surface velocity speed (m/s)	0.10	1.04(-1.45)
Near-surface velocity direction (degree)		171.82°
Near-bottom velocity speed (m/s)	-0.09	1.55(-0.66)
Near-bottom velocity direction (degree)		148.14°
Significant wave height (m)	0.07	3.49 (-4.79)
Bottom stress (N/m^2)	-0.35	28.17(-1.28)

Table 4.4: Summary of possible environmental change within the wind turbine zone on the eastern shelf off Block Island for the August 1991 Hurricane Bob case.

Variable difference	Inside the wind turbine facility	
	Mean	Max
Elevation (m)	-0.05	0.41(-0.43)
Vertically averaged velocity speed (m/s)	-0.49	1.72(-0.80)
Vertically averaged velocity direction (degree)		179.56°
Near-surface velocity speed (m/s)	-0.48	1.75(-0.65)
Near-surface velocity direction (degree)		179.48°
Near-bottom velocity speed (m/s)	-0.29	1.44(-0.57)
Near-bottom velocity direction (degree)		176.02°
Significant wave height (m)	0.56	5.57(-7.29)
Bottom stress (N/m^2)	-1.71	16.78(-2.53)

The particle-tracking experiments are made to examine if the deployment of the offshore wind turbines can affect the larval transport from the upstream Nantucket Shoals, Great South Channel and Georges Bank area to the Mid-Atlantic Bight. The results show that particles, which are released in the upstream area or inside the wind turbine facility areas during the nor'easter storm for the cases without and with wind turbines, have similar trajectories: all of them move southwestward along local isobaths. In view of the large-scale variability, the presence of wind turbines can increase the spatial dispersion and speed of larval movement, but will not block the larvae within the wind turbine facility area. However, when looking at small-scale variability, the presence of wind turbines can also decrease the spatial dispersion. The mean of the change in the spatial dispersion rate through the wind turbine region was in the range of $0.01\text{-}0.44\times10^5$ m^2/s, with a maximum value up to ~ 1.6×10^5 m^2/s. This maximum value was the same order of magnitude as the maximum dispersion rate of the particles that were released in the case without wind turbines.

The assessments are carried out by the coupled NS-FVCOM and NS-SWAVE system with consideration of wave-current interaction. The results are compared with those obtained by the model run with either hydrodynamics only or surface wave model only. The comparison between these experiment results clearly shows that the impact of the offshore wind turbines on the local and regional physical environment can significantly

differ in cases with and without wave-current interaction. The difference occurs mainly on surface, and near-surface and near-bottom velocities. Since nor'easter storms and hurricanes can produce very large surface waves in the offshore shelf region, the modeling assessment of the impact of the future offshore wind energy facilities on the marine environment should be done with consideration of the wave-current interaction process.

5. Acknowledgments

This project is supported by the Bureau of Safety and Environmental Enforcement (BSEE), the United State Department of the Interior (DOI); on behalf of the Bureau of Ocean Energy Management (BOEM) under contract number M14PS00040. We would like to thank Ms. Callie Hall, the Coordinator at BOEM, who has provided us valuable advice and suggestions for modeling experiments. The high-resolution, turbine-resolving FVCOM model was developed as a subdomain model of NECOFS. The development and operation of NECOFS are supported by the NERACOOS under the NOAA IOOS program.

6. References

Altimari, Daniela, 1998 "Blizzard Of 1978: Feb. 6-7, 1978: The Blizzard Of '78 Shut Down The State And Made Heroes Out Of Those With Four-Wheel Drive", *Hartford Courant*, February 25, 1998

Beardsley, R. C., C. Chen and Q. Xu, 2013. Coastal flooding in Scituate (MA): a FVCOM study of the Dec. 27, nor'easter*, Journal of Geophysical Research,* 118, doi: 10.1002/2013JC008862.

Bernier, N. and K. R. Thompson, 2006. Predicting the Frequency of Storm Surges and Extreme Sea Levels in the Northwest Atlantic, *Journal of Geophysical Research*, 111, C10009, doi:10.1029/2005JC003168.

Bretschneider, C. L., 1972. A non-dimensional stationary hurricane wave model, paper presented at 4th Offshore Technology Conference, Houston, Texas.

Chen, C., Paola Malanotte-Rizzoli, Jun Wei, Robert C. Beardsley, Zhigang Lai, Pengfei Xue, Sangjun Lyu, Qichun Xu, Jianhua Qi, and Geoffrey W. Cowles, 2009a. Application and comparison of Kalman filters for coastal ocean problems: An experiment with FVCOM, *Journal of Geophysical Research*, 114, C05011, doi:10.1029/2007JC004548.

Chen, C, G. Gao, J. Qi, A. Proshutinsky, R. C. Beardsley, Z. Kowalik, H. Lin and G. Cowles, 2009b. A new high-resolution unstructured-grid finite-volume Arctic Ocean model (AO-FVCOM): an application for tidal studies, *Journal of Geophysical Research*, doi: 10.1029/2008jc004941.

Chen, C., H. Huang, R. C. Beardsley, Q. Xu, R. Limeburner, G. W. Cowles, Y. Sun, J. Qi, and H. Lin, 2011. Tidal dynamics in the Gulf of Maine and New England Shelf: An application of FVCOM, *Journal of Geophysical Research*, 116, C12010, doi:10.1029/2011JC007054.

Chen, C. R. C. Beardsley, R. A Luettich Jr, J. J. Westerink, H. Wang, W. Perrie, Q. Xu, A. S. Dohahue, J. Qi, H. Lin, L. Zhao, P. Kerr, Y. Meng and B. Toulany, 2013a. Extra tropical storm inundation testbed: intermodal comparisons in Scituate, Massachusetts, *Journal of Geophysical Research,* 118, doi:10.1002/jgrc.20397.

Chen, C., R. C. Beardsley, G. Cowles, J. Qi, Z. Lai, G. Gao, D. Stuebe, H. Liu, Q. Xu, P. Xue, J. Ge, R. Ji, S. Hu, R. Tian, H. Huang, L. Wu, H. Lin, Y. Sun, L. Zhao, 2013b. An unstructured-grid, finite-volume community ocean model FVCOM user manual (3rd edition), *SMAST/UMASSD Technical Report-13-0701*, University of Massachusetts-Dartmouth, pp 404.

Chen, C., G. Gao, Y. Zhang, R. C. Beardsley, Z. Lai, J. Qi, H. Lin. 2016. Circulation in the Arctic Ocean: Results from a high-resolution coupled ice-sea nested Global-FVCOM and Arctic-FVCOM system, *Progress in Oceanography*. 141 (2016) , 60-80.

Cowles, G., S. J. Lentz, C. Chen, Q. Xu, and R. C. Beardsley, 2008. Comparison of observed and model-computed low frequency circulation and hydrography on the New England Shelf, *Journal of Geophysical Research,* 113, C09015, doi:10.1029/2007JC004394

Cragg, S. M., 2006. Development, physiology and ecology of scallop larvae. In: S.E. Shumway and G.J. Parsons (Eds.) Scallops: Biology, Ecology and Aquaculture. Elsevier, Amsterdam, pp. 45-122.

Gallager, S. M., and R. Mann, 1986a. Growth and survival of larvae of Mercenaria mercenaria (L.) Crassostrea virginica (Gmelin) and Placopecten magellanicus relative to lipid content of eggs and broodstock conditioning. *Aquaculture*, 56(2): 105-121.

Gallager, S. M., R. Mann, and G. L. Sasaki, 1986b. Lipid as an index of growth and viability in three species of bivalve larvae. *Aquaculture*, 56(2), 81-103.

Gallager, S. M., 1988. Visual observations of particle manipulation during feeding in larvae of bivalve molluscs. Bull. Mar. Sci., 43(3), 344-365.

Gallager, S. M., 1993. Hydrodynamic disturbances produced by small zooplankton: a case study for veliger larvae of bivalve molluscs. *J. Plankton Res*., 15(11), 1277-1296..

Gallager, S. M., 1996. Ciliary suspension-feeding and particle selection in mollusc larvae. *J. Shellfish Res*., 15(2), 506-510.

Gallager, S. M., J. L. Manuel, D. A. Manning and R. O' Dor, 1996. Ontogenetic changes in the vertical distribution of scallop larvae Placopecten megellanicus in 9 m-deep mesocosms as a function of light, food, and temperature stratification. *Mar. Biol*., 124, 679-692.

Donelan A.M., F.W. Dobson, S.D. Smith, and R.J. Anderson, 1993. On the dependence of sea surface roughness on wave development, *Journal of Physical Oceanography*, 23, 2143-2149, doi: 10.1175/1520-0485(2001)031.

Dudhia et al., 2003 Dudhia, J., 1993: A nonhydrostatic version of the Penn State/NCAR mesoscale model: Validation tests and simulation of an Atlantic cyclone and cold front, *Mon. Wea. Rev*., 121,1493–1513.

Earls, Alan R., and Dukakis, Michael S., Greater Boston's Blizzard of 1978, Arcadia Publishing, 2008, ISBN 978-0-7385-5519-5

Fairall, C. W., E. F. Bradley, D. P. Rogers, J. B. Edson, and G. S. Young, 1996: Bulk parameterization of air–sea fluxes for Tropical Ocean Global Atmosphere Coupled Ocean–Atmosphere Response Experiment, *Journal of Geophysical Research*, 101(C2), 3747–3764.

Fairall, C. W., E. F. Bradley, J. E. Hare, A. A. Grachev, and J. B. Edson, 2003. Bulk parameterization of air-sea fluxes: updates and verification for the COARE algorithm, *J. Climate*, *16*, 571-591, doi: 10.1175/1520-0442(2003)016.

Freedman, A. 2010. Blizzard blasts coastal cities from Va. to Mass, The Washington Post-December 27, 2010.

Freedman, A., 2013. Blizzard of 2013 brings another threat: coastal flooding, Climate Central News published on February 8, 2013.

Gao, G., C. Chen, J. Qi, and R. C. Beardsley, 2011. An unstructured-grid, finite-volume sea ice model: Development, validation, and application, *Journal of Geophysical Research*, 116, C00D04, doi:10.1029/2010JC006688.

Grell, G. A., 1993: Prognostic evaluation of assumptions used by cumulus parameterizations, *Mon. Wea. Rev*., 121, 764–787.

Houston, S. H., W.A. Shaffer, M. D. Powell, and J. Chen, 1999. Comparisons of HRD and SLOSH surface wind fields in hurricanes: Implications for storm surge modeling, *Wea. Forecas.*, *14*(5), 671-686, doi: 10.1175/1520-0434(1999)014.

HydroQual, Inc. and Normandeau Associates, Inc. 1993. A water quality model for Massachusetts and Cape Cod Bays. Boston, Massachusetts Water Resource Authority. ENQUAD 93-05, 222pp.

Jelesnianski, C. P., 1966. Numerical computations of storm surges without bottom stress. *Mon. Wea. Rev.*, *94*, 279-394, doi: 10.1175/1520-0493(1967)095.

Lai, Z., C. Chen, G. Cowles, and R. C. Beardsley, 2010. A Non-Hydrostatic Version of FVCOM, Part II: Mechanistic Study of Tidally Generated Nonlinear Internal Waves in Massachusetts Bay, *Journal of Geophysical Research*, doi: 10.1029/2010JC006331.

Li, Y., P. S. Fratantoni, C. Chen, J. A. Hare, Y. Sun, R. C. Beardsley and R. Ji, 2015, Spatio-temporal patterns of stratification on the Northwest Atlantic shelf, *Progress in Oceanography*, 134, 123-137.

McCown, S, 2008. "Perfect Storm" Damage Summary". *National Climatic Data Center*. National Oceanic and Atmospheric Administration. http://www.ncdc.noaa.gov/oa /satellite/satelliteseye/cyclones/pfctstorm91/pfctstdam.html.

McGarvey, R., F. M. Serchuk and I. A. McLaren, 1992. Statistics of reproduction and early life history survival of the Georges Bank sea scallop (Placopecten magellanicus) population. *J. Northwest Atl. Fish. Sci*., 13, 83-99.

McGarvey, R., Serchuk, F. M. and I. A. McLaren, 1993. Spatial and parent-age analysis of stock-recruitment in the Georges Bank sea scallop (Placopecten magellanicus) population. Can. *J. Fish. Aquat. Sci*., 50, 564-574.

Melvin, G. D., M. J. Dadswell, and R. A. Chandler, 1985. Movement of scallop (Placopecten magellaniucs) (Gmelin, 1791) (Mollusca: Pectinidae) on Georges Bank. *Can Atl Fish Sci Advis Comm Res Doc 95*.

Mellor, G.L., 2011. Wave Radiation Stress. *Ocean Dynamics*, doi: 10.1007/s10236-010-0359-2.

Mellor, G. L., and T. Yamada, 1982. Development of a turbulence closure model for geophysical fluid problem, *Rev. Geophys. Space Phys., 20,* 851-875, doi: 10.1029/RG020i004p00851.

Naidu, K. S., and G. Robert, 2006. Fisheries sea scallop. Placopecten magellanicus. In: Shumway S. E., Parsons G.J. (eds) Scallops: biology, ecology and aquaculture. Elsevier, Amsterdam, p 869–905.

Pasch, R., and L. Avila, 1992. Atlantic hurricane season of 1991. *Mon. Wea. Rev., 120*, 2671-2687.

Phadke, A. C., C. D. Martino, K. F. Cheung, and S. H. Houston, 2003. Modeling of tropical cyclone winds and waves for emergency management, *Ocean Eng.*, *30*(4), 553-578, doi: 10.1016/S0029-8018(02)00033-1.

Posgay J. A., 1981. Movement of tagged scallops on Georges Bank. *Fish Rev*., 43:19–25.

Powell, M. D. and P. G. Black, 1990. The relationship of hurricane reconnaissance flight-level measurements to winds measured by NOAA's oceanic platforms, *J. Wind Eng. Ind. Aerodyn.*, *36*(1-3), 381-392.

Qi, J., C. Chen, R. C. Beardsley, W. Perrie, Z. Lai and G. Cowles, 2009. An unstructured-grid finite-volume surface wave model (FVCOM-SWAVE): implementation, validations and applications, *Ocean Modelling*, 28, 153-166. doi:10.1016/j.ocemod. 2009.01.007.

Shearman, K., and S. J. Lentz (2004), Observations of tidal variability on the New England shelf, Journal of Geophysical Research, 109, C06010, doi:10.1029/2003JC001972.

Smagorinsky, J., 1963. General circulation experiments with the primitive equations, Mon. *Wea. Rev., 91*, 99-164, doi: 10.1175/1520-0493(1963)091.

Stewart, P. L. and S. H. Arnold, 1994. Environmental requirements of the sea scallop (Placopectenmagellanicus) in eastern Canada and its response to human impacts. Can. Tech Rep. Fish. Aquat. Sci. 2005, 1– 36.

Sun, Y., C. Chen, R. C. Beardsley, Q. Xu, J. Qi, and H. Lin, 2013. Impact of current-wave interaction on storm surge simulation: A case study for Hurricane Bob, *Journal of Geophysical Research* 118, 2685-2701, doi:10.1002/jgrc.20207.

Sun, Y., C. Chen, R. C. Beardsley, D. Ullman, B. Butman and H. Lin, 2016 Surface circulations in Block Island Sound and adjacent coastal and shelf regions: A FVCOM-CODAR comparison. *Progress in Oceanography*, in revision.

Tian, R. C., C. Chen, K. D. E. Stokesbury, B. J. Rothschild, Q. Xu, S. Hu, G. W. Cowles, B. P. Harris, and M. C. Marino II, 2009. Modeling the connectivity between sea scallop populations in the Middle Atlantic Bight and over Georges Bank. *Marine Ecology Progress Series* 390, 147-160.

Tian, R. C., C. Chen, K. D. E. Stokesbury, B. J. Rothschild, Q. Xu, G. W. Cowles, B. P. Harris and M. C. Marino II, 2009a. Sensitivity analysis of sea scallop (Placopectenmagellanicus) larvae trajectories to hydrodynamic model configuration on Georges Bank and adjacent coastal regions. Fish. Oceanogr., 18, 173-184.

Vickery, P. J., P. F. Skerlj and L. A. Twisdale, 2000. Simulation of Hurricane Risk in the U. S. using empirical track model. *Journal of Structural Engineering*, 126 (10), 1222-1237.

Warner J. C., Sherwood C. R., Signell R. P., Harris C., Arango H G, 2008. Development of a three-dimensional, regional, coupled wave, current, and sediment-transport model. *Computers and Geosciences*, 34, 1284-1306.

Wu, L, C. Chen, F. Guo, M. Shi, J. Qi, and J. Ge, 2010. A FVCOM-based unstructured grid wave, current, sediment transport model, I. model description and validation, *J. Ocean. Univ. China, 10*(1), 1-8, doi: 10.1007/s11802-011-1788-3.

Zhang, Y., C. Chen, R. C.Beardsley, G. Gao, Z. Lai, B. Curry, C. M. Lee, H. Lin, J. Qi, and Q. Xu, 2016a. Studies of the Canadian Arctic Archipelago water transport and its relationship to basin-local forcings: results from AO-FVCOM, *Journal of Geophysical Research*, in revision.

Zhang, Y., C. Chen, R. C.Beardsley, G. Gao, J. Qi, and H. Lin, 2016b. Seasonal and Interannual Variability of the Arctic Sea Ice: A Comparison between AO-FVCOM and observations*, Journal of Geophysical Research*, to be submitted.

Zhang, Y, G. Gao, C. Chen, Y Zhang, R. C.Beardsley, J. Qi, W. Perrie[4], and H. Lin, 2016. Applications of an unstructured grid surface wave model (FVCOM-SWAVE) to the Arctic Ocean: effects of ice-induced wave attenuation, *Journal of Geophysical Research*, submitted.

7. Appendix

7.1 Description of the model source codes, forcing, and initial/boundary condition files

We have saved all the model source codes, forcing, and initial/boundary condition files into the flash disk and delivered it to BOEM. The total of the size of this product is larger than 100 GB, and all in a folder named "SETUP".

The folder "SETUP" includes the model source codes and run-set up controlling parameter input files, model grids, external forcing and initial/boundary conditions for the 1978 nor'easter storm and the 1991 Hurricane Bob simulation cases. These files are required as deliverables for Task 3.

External forcing includes the surface wind stress, net surface heat flux, shortwave irradiance, precipitation and evaporation, and air pressure (for Hurricane Bob).

The boundary condition consists of sea elevation, 3-D current velocity, temperature, salinity and wave spectral density at the nesting nodes and cells connecting to the regional domain NECOFS. The boundary data are directly output from NECOFS.

In "Setup", there are two folders named 'INPUT and "code_and_run".

1. INPUT:

This folder includes the grid and external forcing for the 1978 nor'easter storm and the 1991 Hurricane Bob simulation cases. In this folder, there are two sub-folders named "197802" and "199108".

1.1) 197802

This sub-folder includes two additional sub-folders named:

a. BOEM_C/input/n1978: The grid, forcing and boundaries for the cases without wind turbines;

b. BOEM_F/input/n1978: The grid, forcing and boundaries for the cases with wind turbines.

1.2) 199108

This sub-folder includes two additional sub-folders named:

a. BOEM_C/input/n1991: The grid, forcing and boundaries for the cases without wind turbines;

b. BOEM_F/input/n1991: The grid, forcing and boundaries for the cases with wind turbines.

In each folder of "197802/BOEM_C/input/n1978", "199108/BOEM_C/input/n1991", 197802/BOEM_F/input/n1978, and 199108/BOEM_F/input/n1991", there are 7 files with the same names for the cases without and with wind turbines in model domain. They are:

auxiliary_data.nc: The bottom roughness input file;
boem_cor.dat: The Coriolis parameter input file;
boem_dep.dat: The mean water depth input file;
boem_grd.dat: The model grid mesh input file;
boem_obc.dat: The nesting boundary node IDs input file;
boem_sigma.dat: The vertical level setup input file;
boem_spg.dat: The open boundary sponge node number and IDs.

In the folder 197802/BOEM_C/input/n1978, there are 4 additional NetCDF files. They are:

boemc_restart.nc: Restart file (00:00:00 GMT Feb. 1 1978);

boem_forcing.nc: External forcing file (00:00:00 GMT Feb. 1– 00:00:00 GMT Feb. 11, 1978);

nestnode02.nc: Nesting boundary file for elevation, current, temperature and salinity;

nestnode02_wave.nc: Nesting boundary file for wave spectral density.

In the folder 197802/BOEM_F/input/n1978, there are 4 additional NetCDF files. They are:

boem02_restart.nc: Restart file (00:00:00 GMT Feb. 1 1978);

boem_forcing.nc: External forcing file (00:00:00 GMT Feb. 1 – 00:00:00 GMT Feb. 11, 1978);

nestnode02.nc: Nesting boundary file for elevation, current, temperature and salinity;

nestnode02_wave.nc: Nesting boundary file for wave spectral density.

In folders 199108/BOEM_C/input/n1991, there are 4 additional NetCDF files. They are:

boem_restart_19910816.nc: Restart file (00:00:00 GMT Aug. 16 1991);

boem_forcing.nc: External forcing file (00:00:00 GMT Aug. 16 —00:00:00 GMT Aug. 21, 1991);

nestnode02.nc: Nesting boundary file for elevation, current, temperature and salinity nestnode02_wave.nc: Nesting boundary file for wave spectral density.

In folders 199108/BOEM_F/input/n1991, there are 4 additional NetCDF files. They are:

boem_restart_19910816.nc: Restart file (00:00:00 GMT Aug. 16 1991);

boem_forcing.nc : External forcing file (00:00:00 GMT Aug. 16 –00:00:00 GMT Aug. 21, 1991);

nestnode02.nc: Nesting boundary file for elevation, current, temperature and salinity;

nestnode02_wave.nc: Nesting boundary file for wave spectral density.

2. code_and_run

This folder includes the model source code and control parameters for model run. It contains two sub-folders named “197802” and “199108”

2.1) 197802

There are two sub-folders:
a. BOEM_C: For the case without wind turbines;
b. BOEM_F: For the case with wind turbines.

2.2) 199108

There are two sub-folders:
a. BOEM_C: For the case without wind turbines;
b. BOEM_F: For the case with wind turbines.

In each folder BOEM_C above, there are three directories, including:
boemc_current_only: The model without wave;
boemc_wave_current: The model with the wave-current interaction;
boemc_wave_only: The model with wave only.

In each folder BOEM_F, there are three directories, including:
boem_current_only: The model without wave;
boem_wave_current: The model with the wave-current interaction;
boem_wave_only: The model with wave only.

In each sub-folder listed above (boemc_* and boem_*), there are two additional folders, including:
FVCOM_source: The source code for the model run
run: Files for controlling model parameters

Inside the folder “run”, there are 1 or 3 files:
boem01_run.nml: Namelist for the controlling model parameters;
INPUT: Controlling model parameters file for surface wave;
swaninit: The wave initial file.

Model executive steps:

1) Link input files under folder “boemc_*” or “boem_*”. For example:

Link INPUT/197802/BOEM_C/input under the folder “boemc_current_only”, “boemc_wave_current” and “boemc_wave_only”, separately.

2) Create folder “output/n1978” or “output/n1991” under the folder “boemc_*” or “boem_*”.

3) Link the execute file 'fvcom' in the folder “run”, and executive a run job by typing

mpiexec -np <number of node> ./fvcom --casename=boem01

If it is run on the cluster, one needs to run a script file.

7.2 Description of the deliverable product files and database

The model outputs for all experiments over the simulation periods have been saved at hourly intervals on a portable external disk. The database includes the results obtained from the model runs for the February 1978 nor'easter storm and the August 1991 Hurricane Bob. In each case, there are three types of model output: 1) the experiments using the coupled NS-FVCOM and NS-SWAVE system with the inclusion of wave-current interaction, 2) the hydrodynamic simulation using NS-FVCOM only and 3) the surface wave simulation using the NS-SWAVE only. In each of these experiments, we have included the model outputs under the conditions without and with wind turbines.

All output files are in the NetCDF format, including physical variables of surface elevation, horizontal and vertical velocities, water temperature, water salinity, significant wave height and peak period, horizontal diffusion coefficient and vertical eddy viscosity. The definition of each file is explained in the "Readme" file included in the deliverables.

In addition to figures included in the report, we have also plotted the hourly distributions of surface elevation, significant wave height, vertically averaged velocity, near-surface and near-bottom velocities, and bottom stress for all the cases.

A Fortran program used for particle-tracking is included in the deliverable.

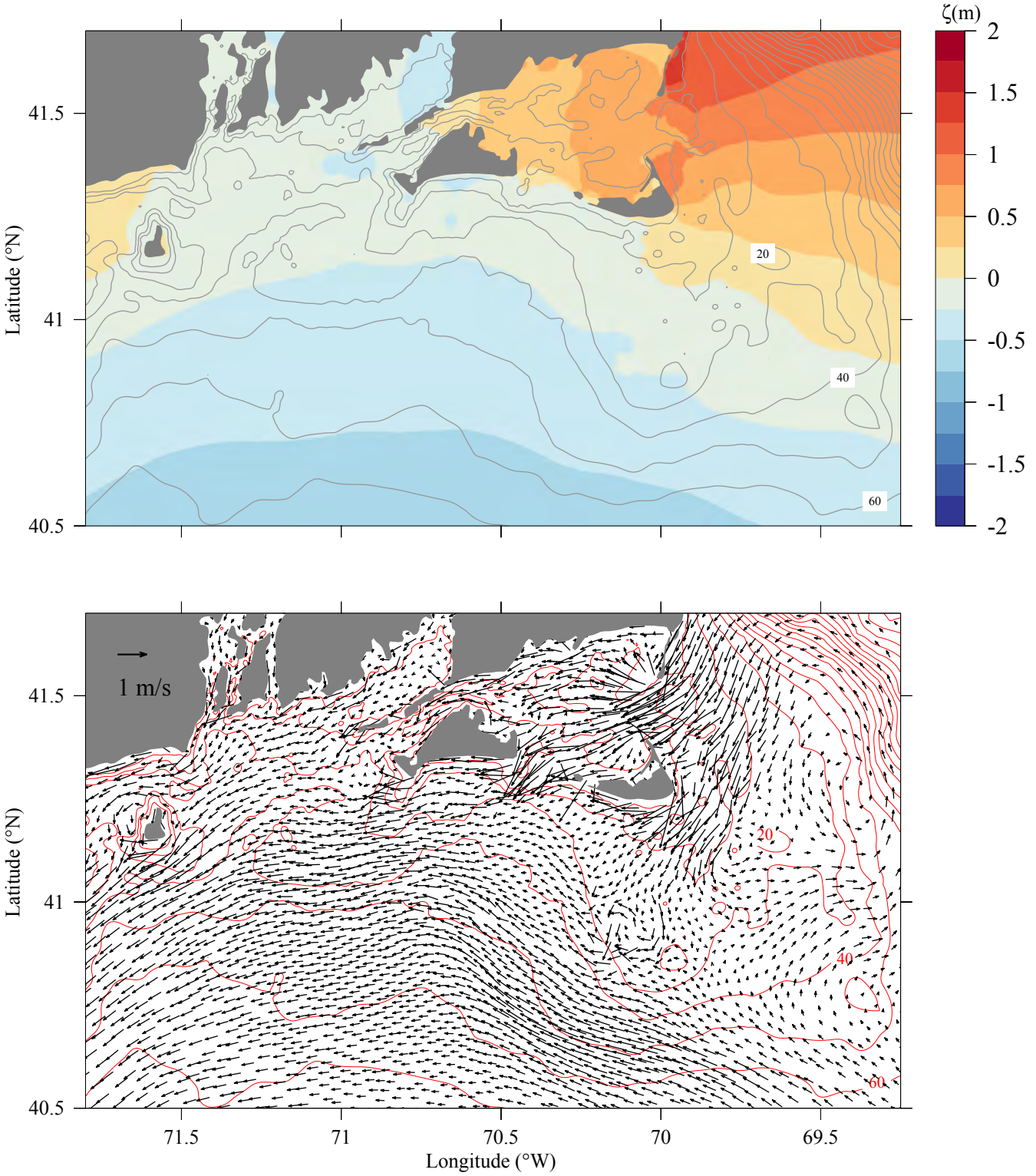

Figure 3.1: Snapshots of the distributions of the model-computed surface elevation (upper panel) and vertically averaged velocity(lower panel) over the New England Shelf at 03:00:00 GMT, February 7, 1978 under the condition without wind turbines for the experiment with the inclusion of wave-current interactions.

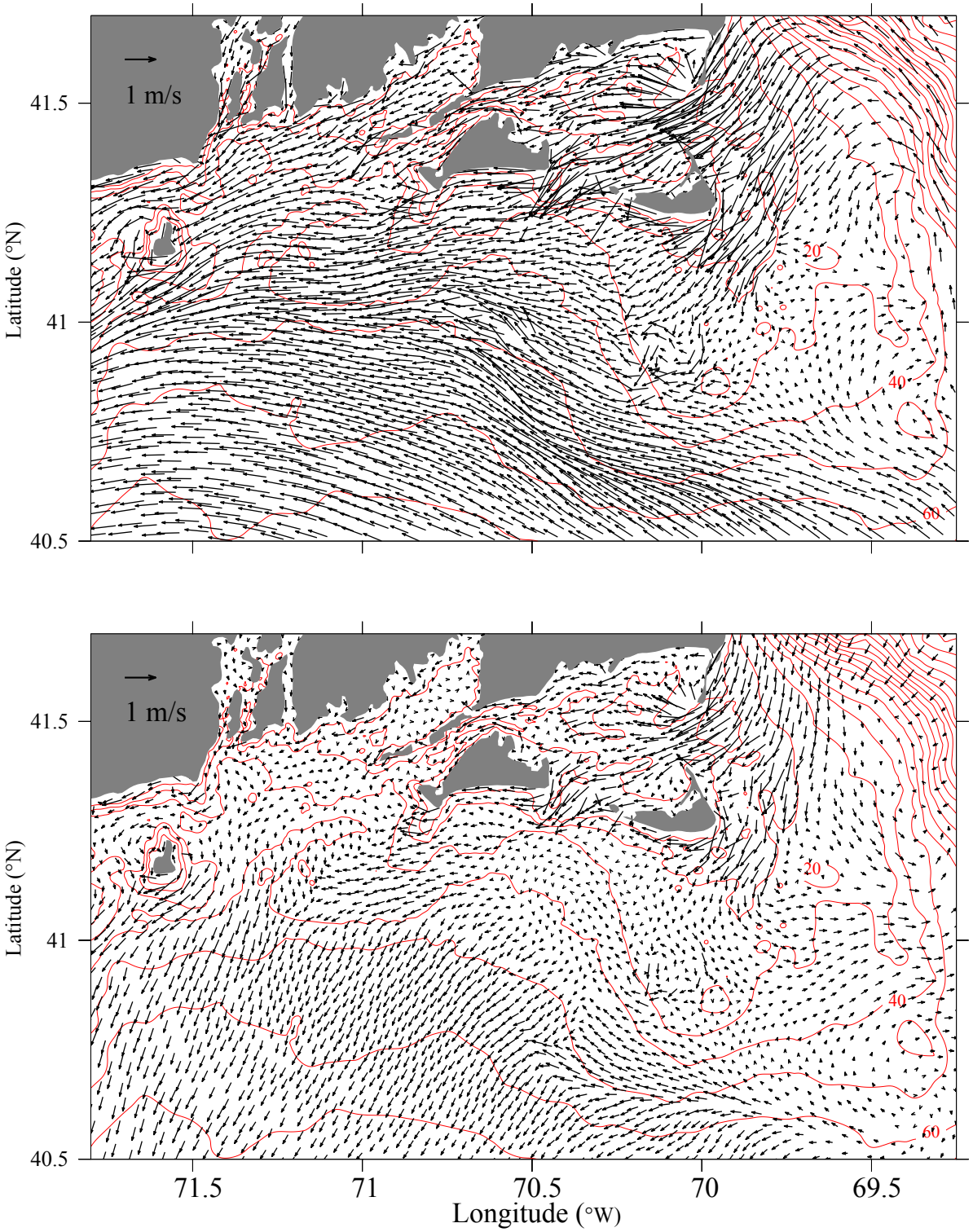

Figure 3.2: Snapshots of the distributions of the model-computed near-surface (upper panel) and near-bottom (lower panel) velocities over the New England Shelf at 03:00:00 GMT, February 7, 1978 under the condition without wind turbines for the experiment with the inclusion of wave-current interactions.

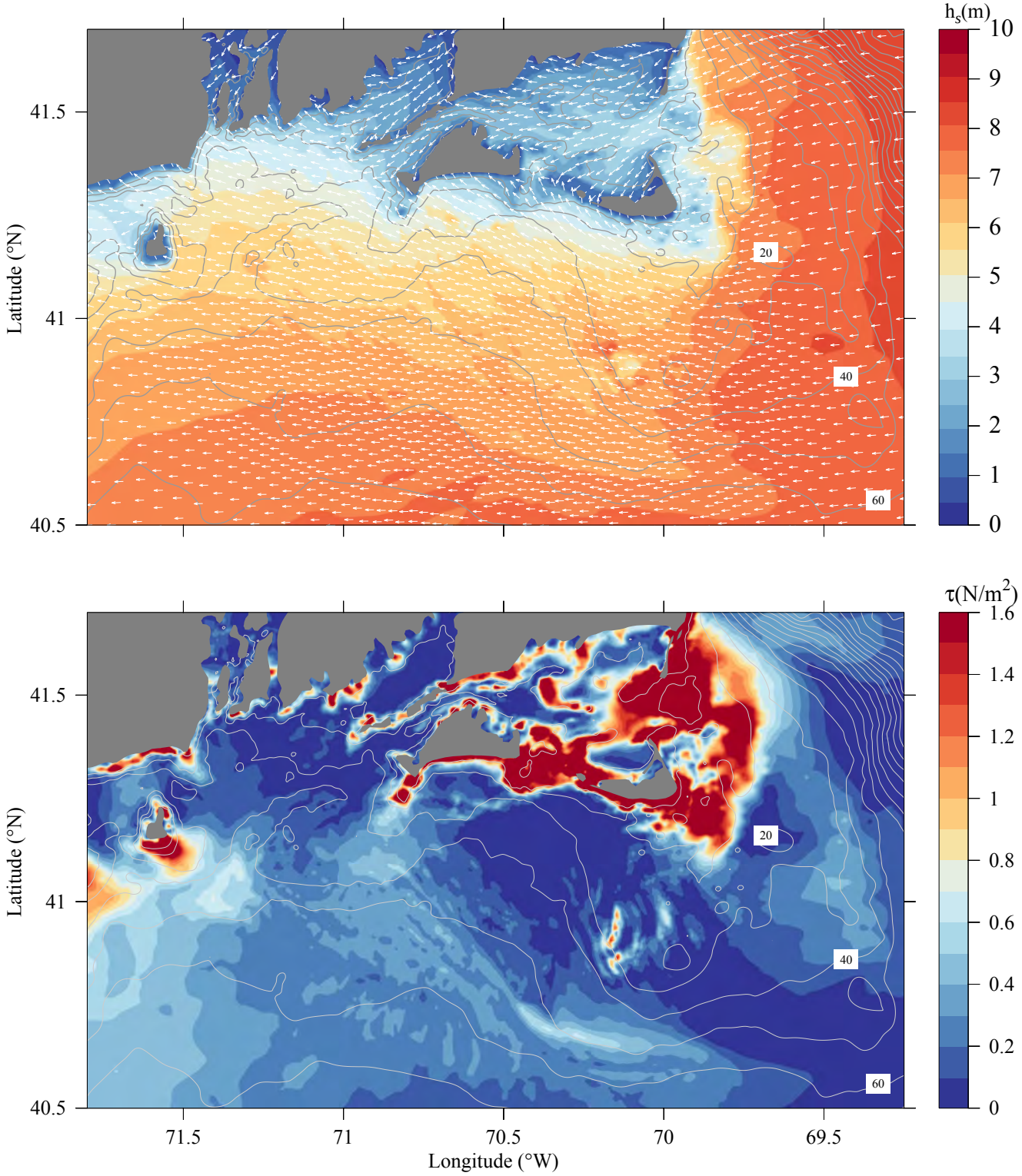

Figure 3.3: Snapshots of the distributions of the model-computed significant wave height (upper panel) and bottom stress (lower panel) over the New England Shelf at 03:00:00 GMT, February 7, 1978 under the condition without wind turbines for the experiment with the inclusion of wave-current interactions.

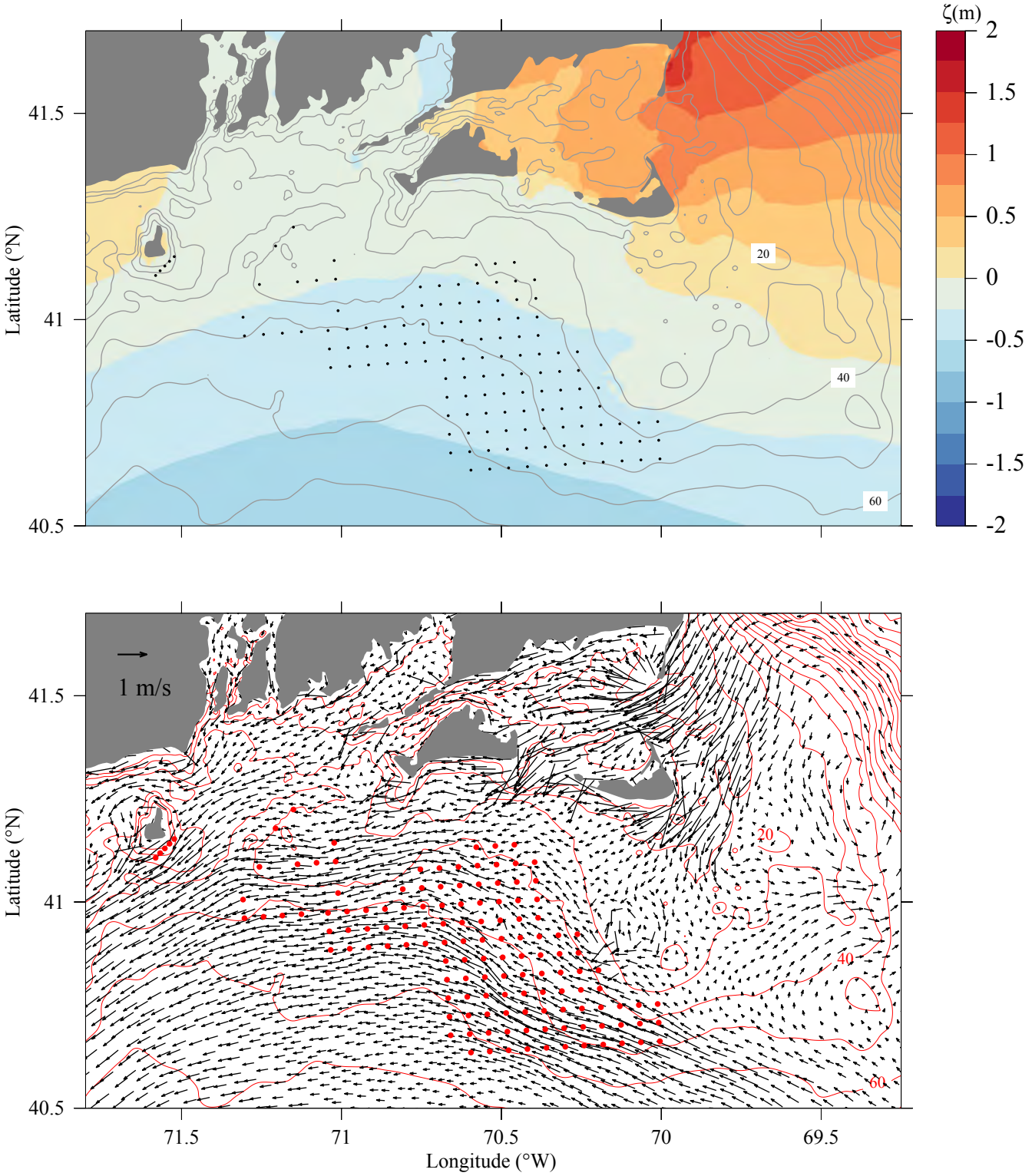

Figure 3.4: Snapshots of the distributions of the model-computed surface elevation (upper panel) and vertically averaged velocity (lower panel) over the New England Shelf at 03:00:00 GMT, February 7, 1978 under the condition with wind turbines for the experiment with the inclusion of wave-current interactions.

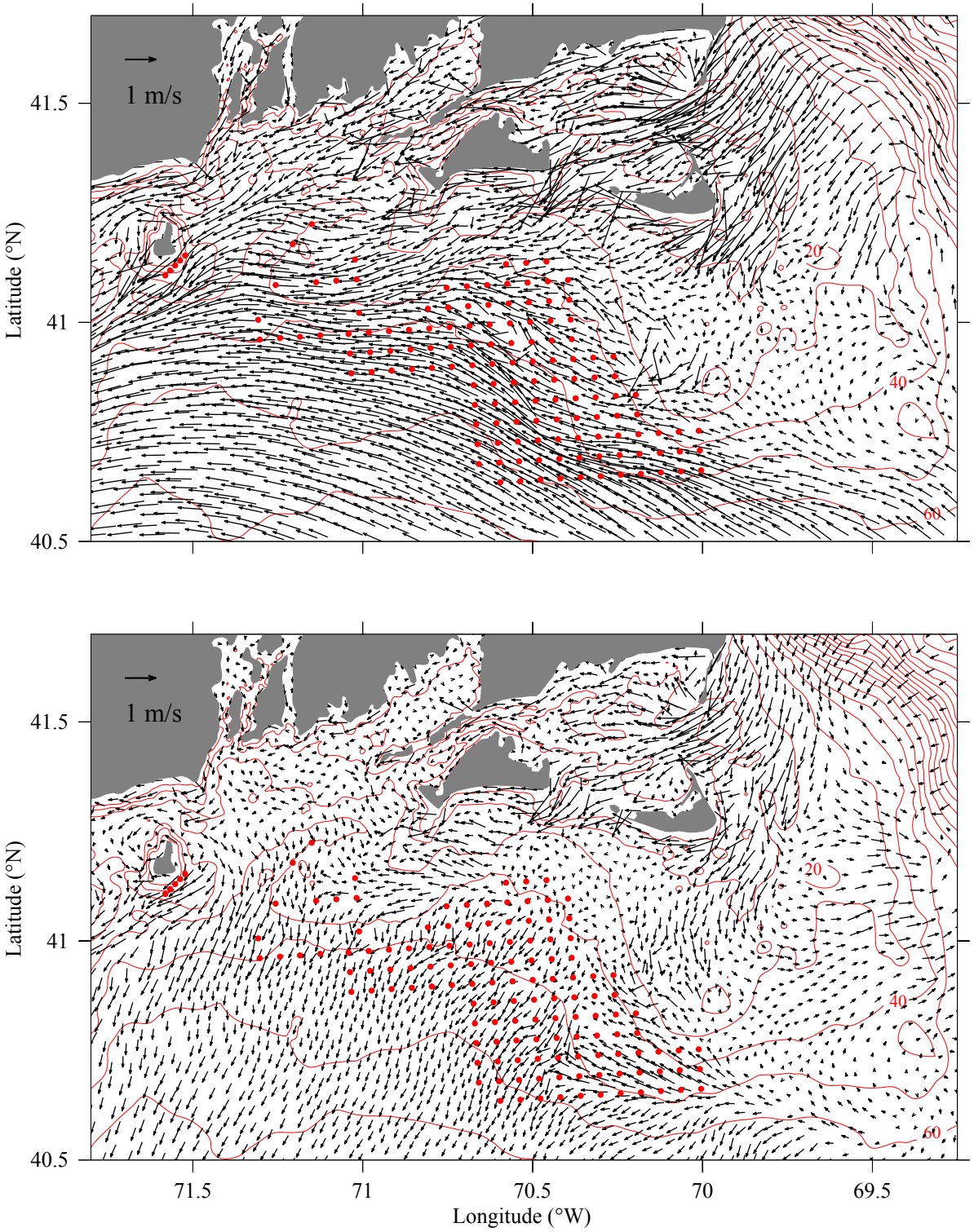

Figure 3.5: Snapshots of the distributions of the model-computed near-surface (upper panel) and near-bottom (lower panel) velocities over the New England Shelf at 03:00:00 GMT, February 7, 1978 under the condition with wind turbines for the experiment with the inclusion of wave-current interactions.

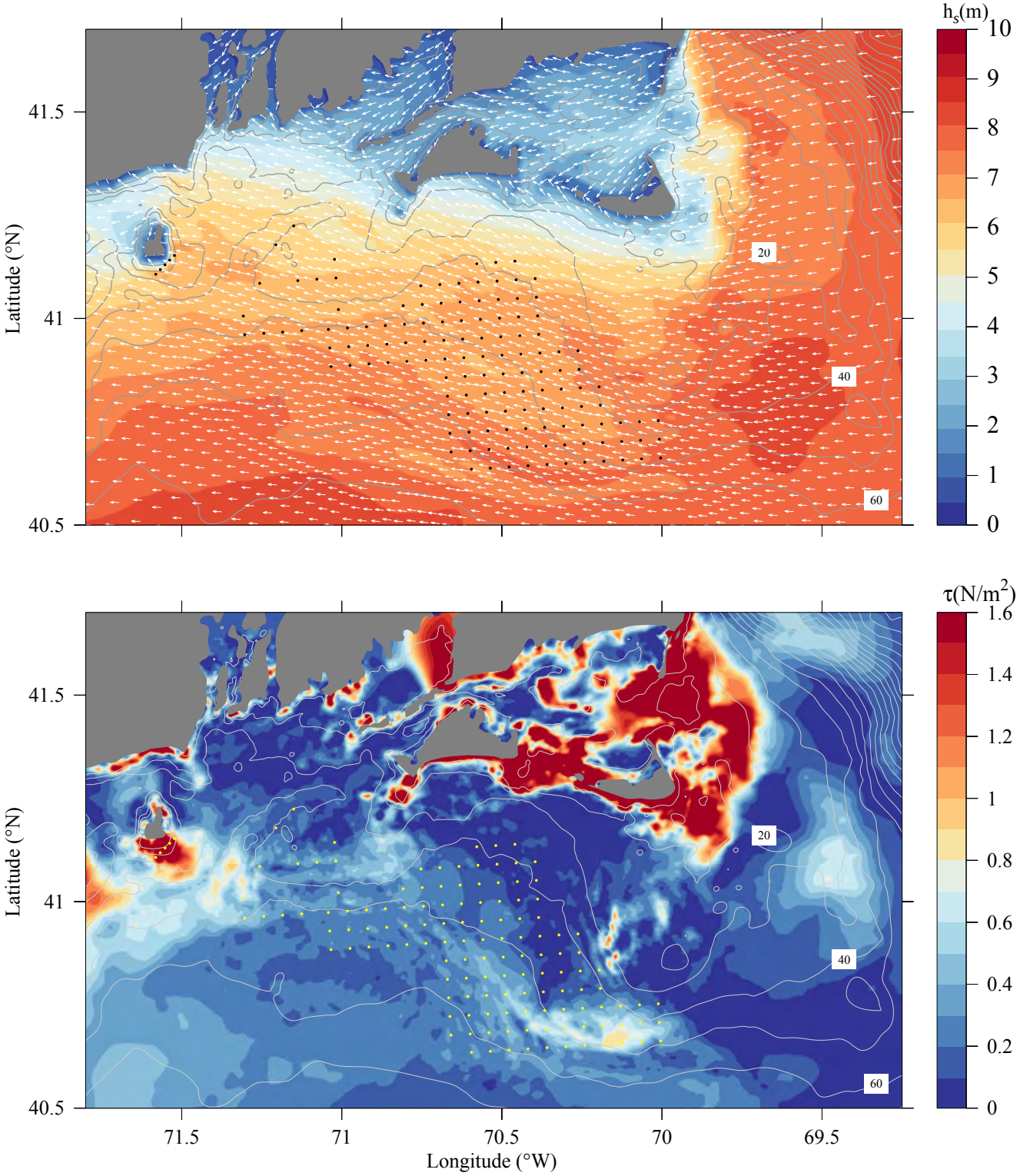

Figure 3.6: Snapshots of the distributions of the model-computed significant wave height (upper panel) and bottom stress (lower panel) over the New England Shelf at 03:00:00 GMT, February 7, 1978 under the condition with wind turbines for the experiment with the inclusion of wave-current interactions.

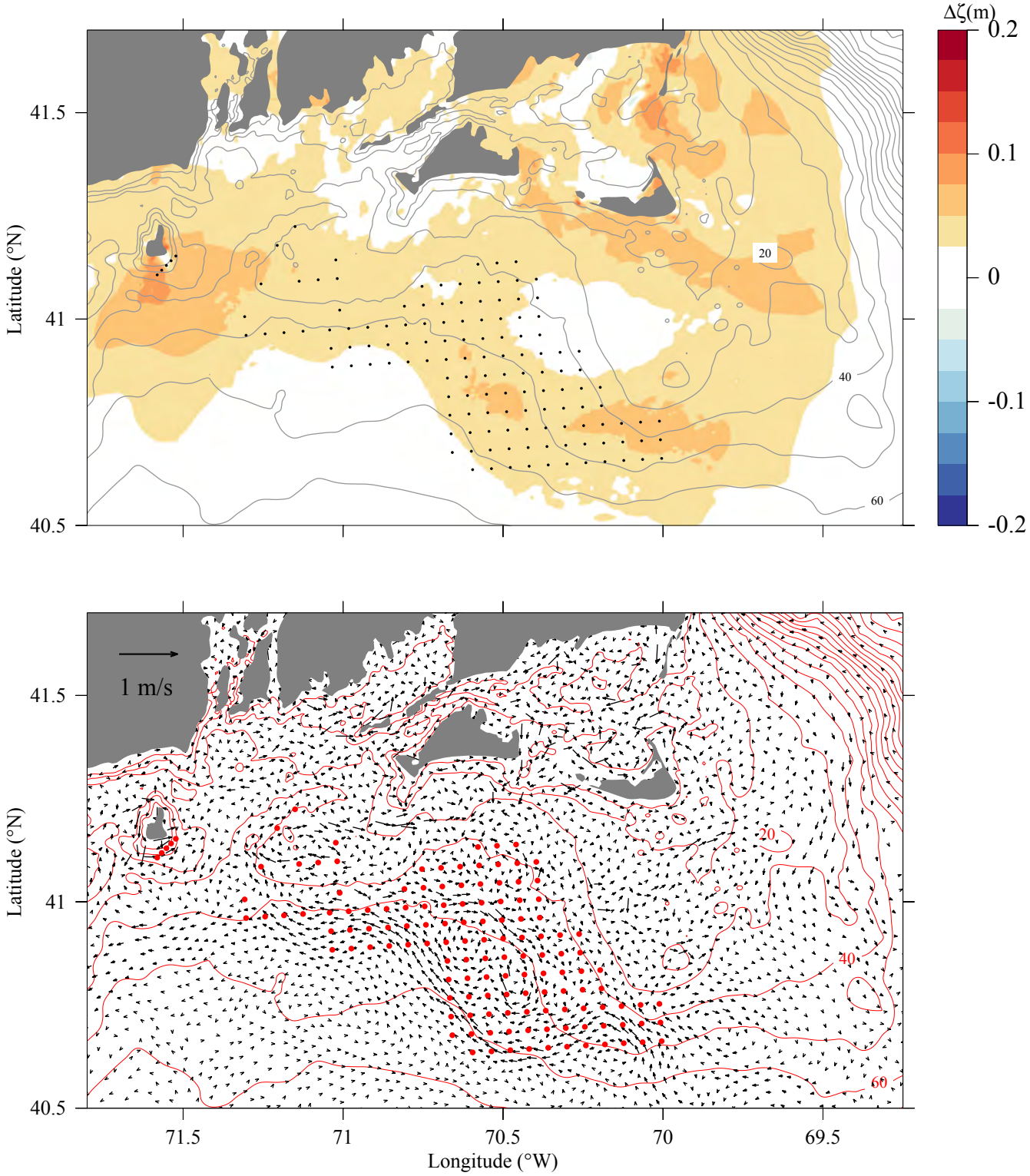

Figure 3.7: Difference of the sea surface (upper panel) and vertically averaged velocity (lower panel) between the two cases under the conditions with and without wind turbines at 03:00:00 GMT, February 7, 1978 for the experiment with the inclusion of wave-current interactions.

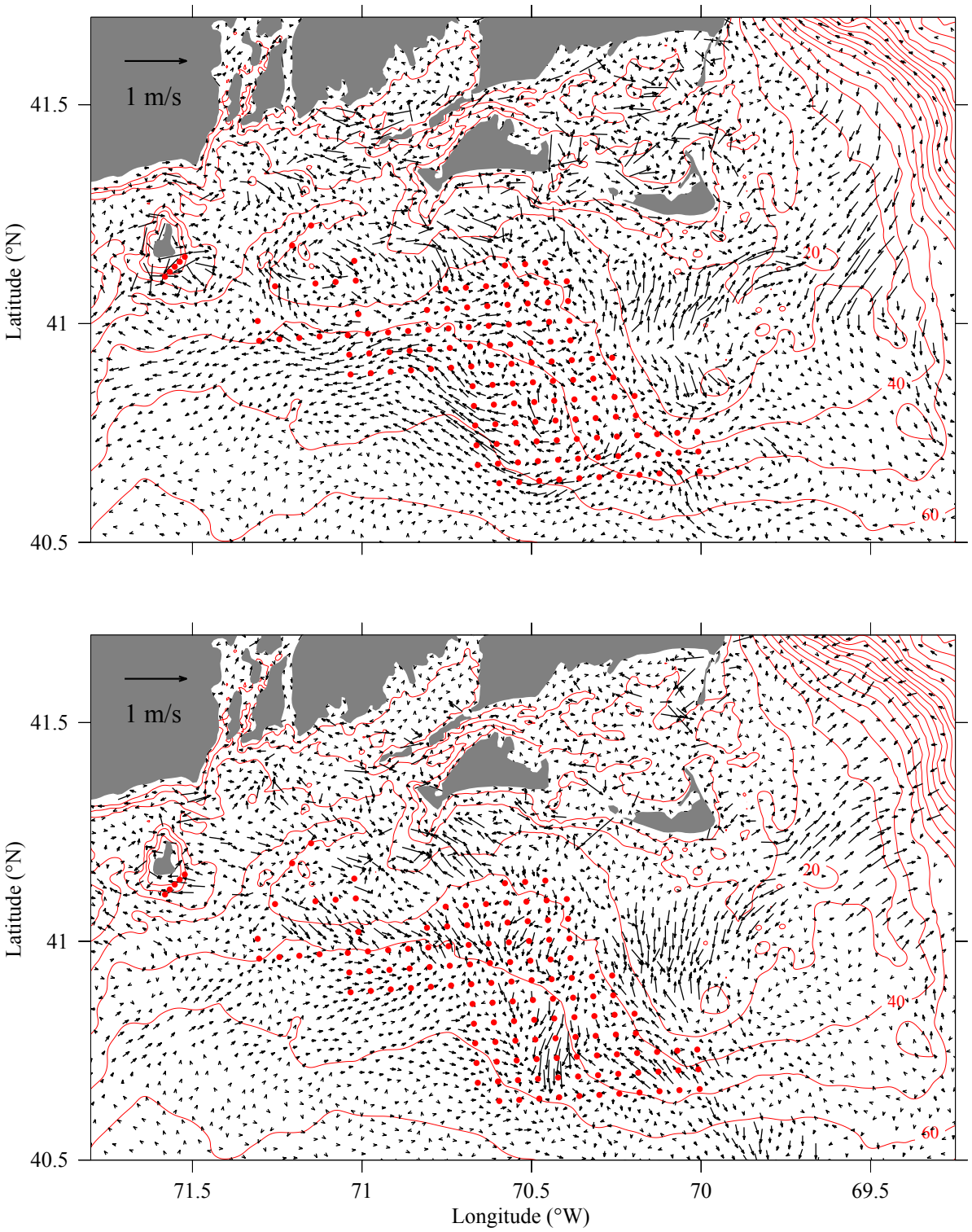

Figure 3.8: Difference of the near-surface (upper) and near-bottom (lower) velocities between the two cases under the conditions with and without wind turbines at 03:00:00 GMT, February 7, 1978 for the experiment with the inclusion of wave-current interactions.

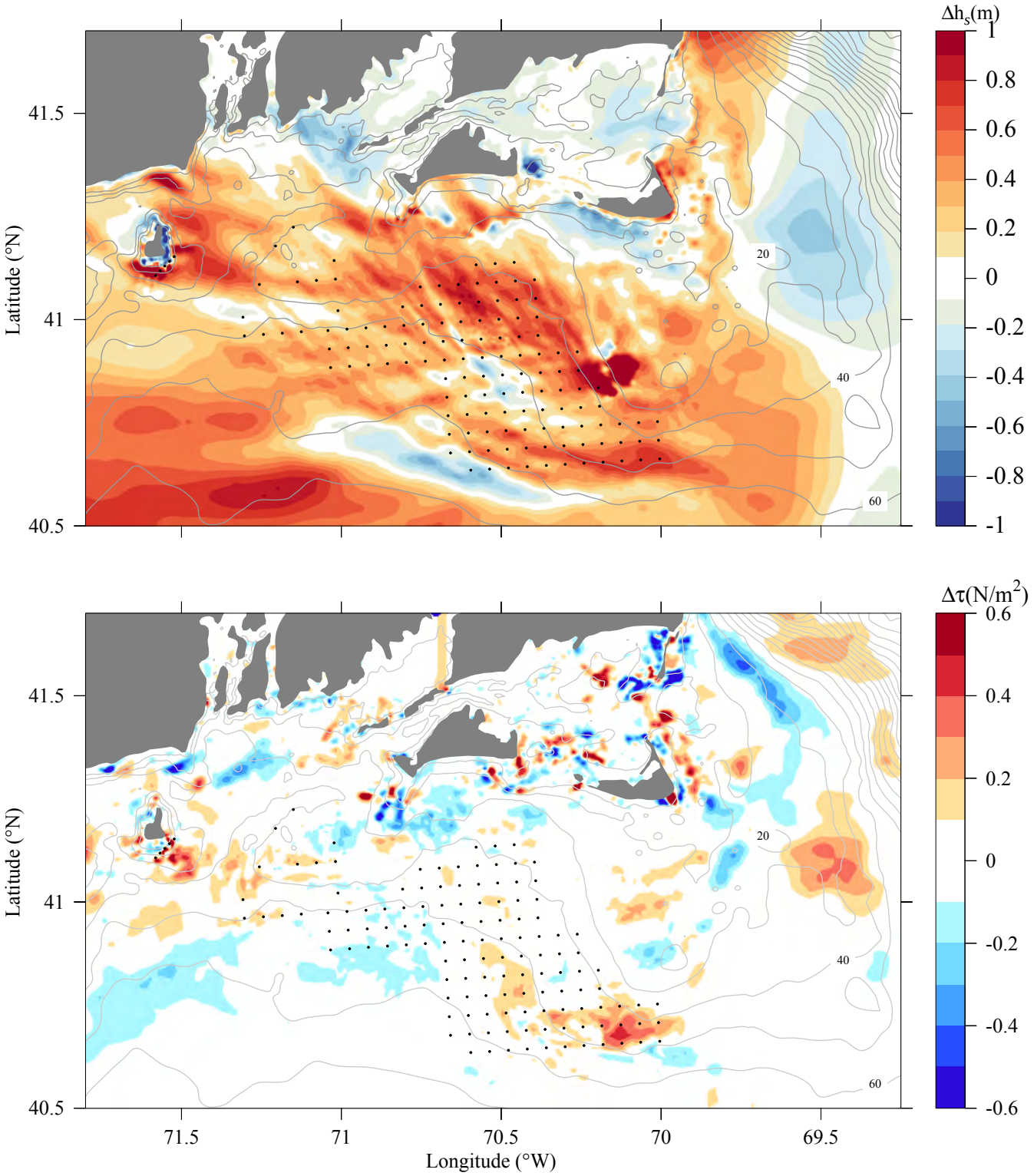

Figure 3.9: Difference of the significant wave height (upper panel) and bottom stress (lower panel) between the two cases under the conditions with and without wind turbines at 03:00:00 GMT, February 7, 1978 for the experiment with the inclusion of wave-current interactions.

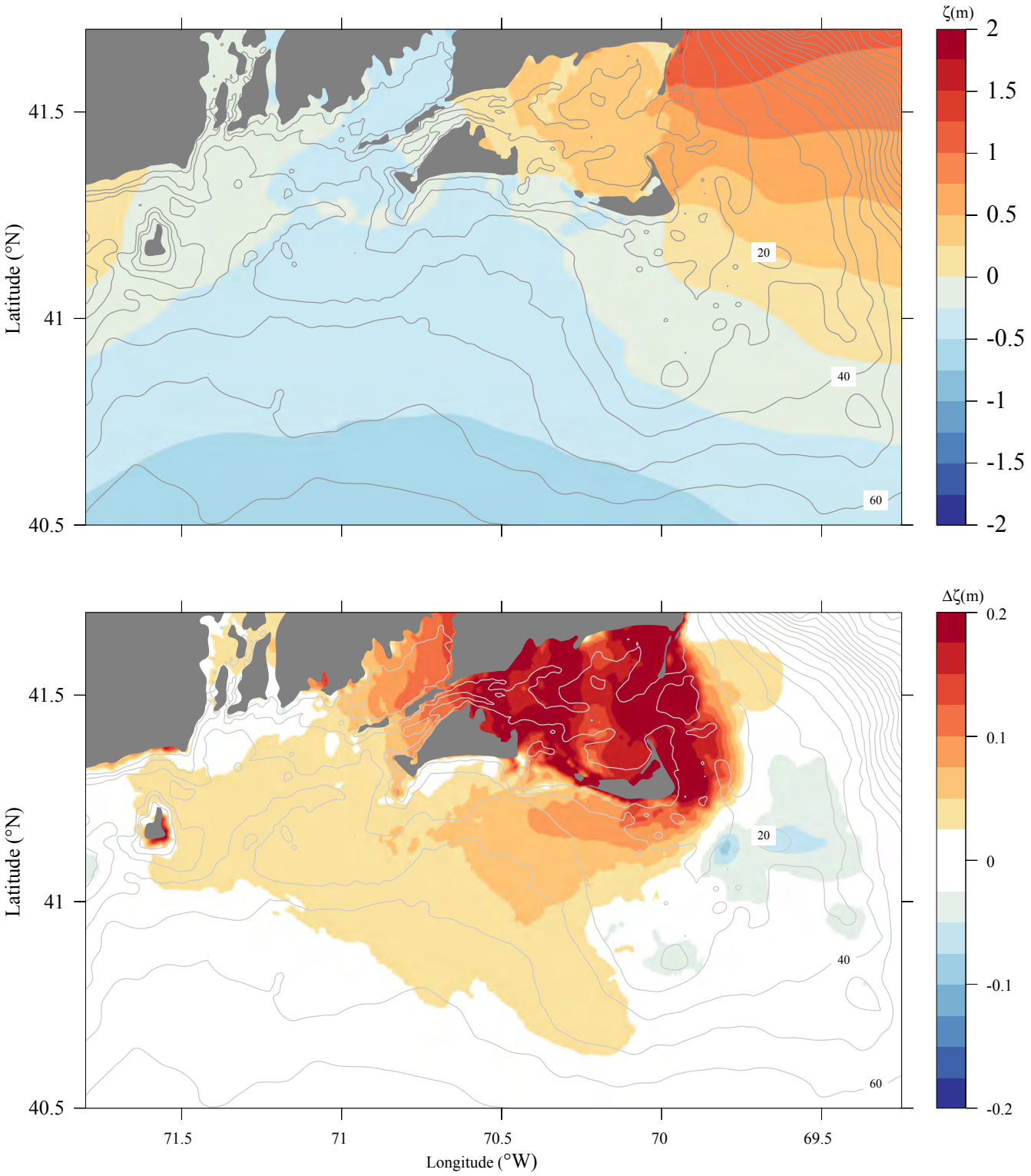

Figure 3.10: Upper panel: a snapshot of the distribution of the surface elevation over the New England Shelf at 03:00:00 GMT, February 7, 1978 under the condition without wind turbines for the hydrodynamic simulation experiment with NS-FVCOM. Lower panel: the difference of the surface elevation between the two cases with and without the inclusion of current-wave interactions at the same time.

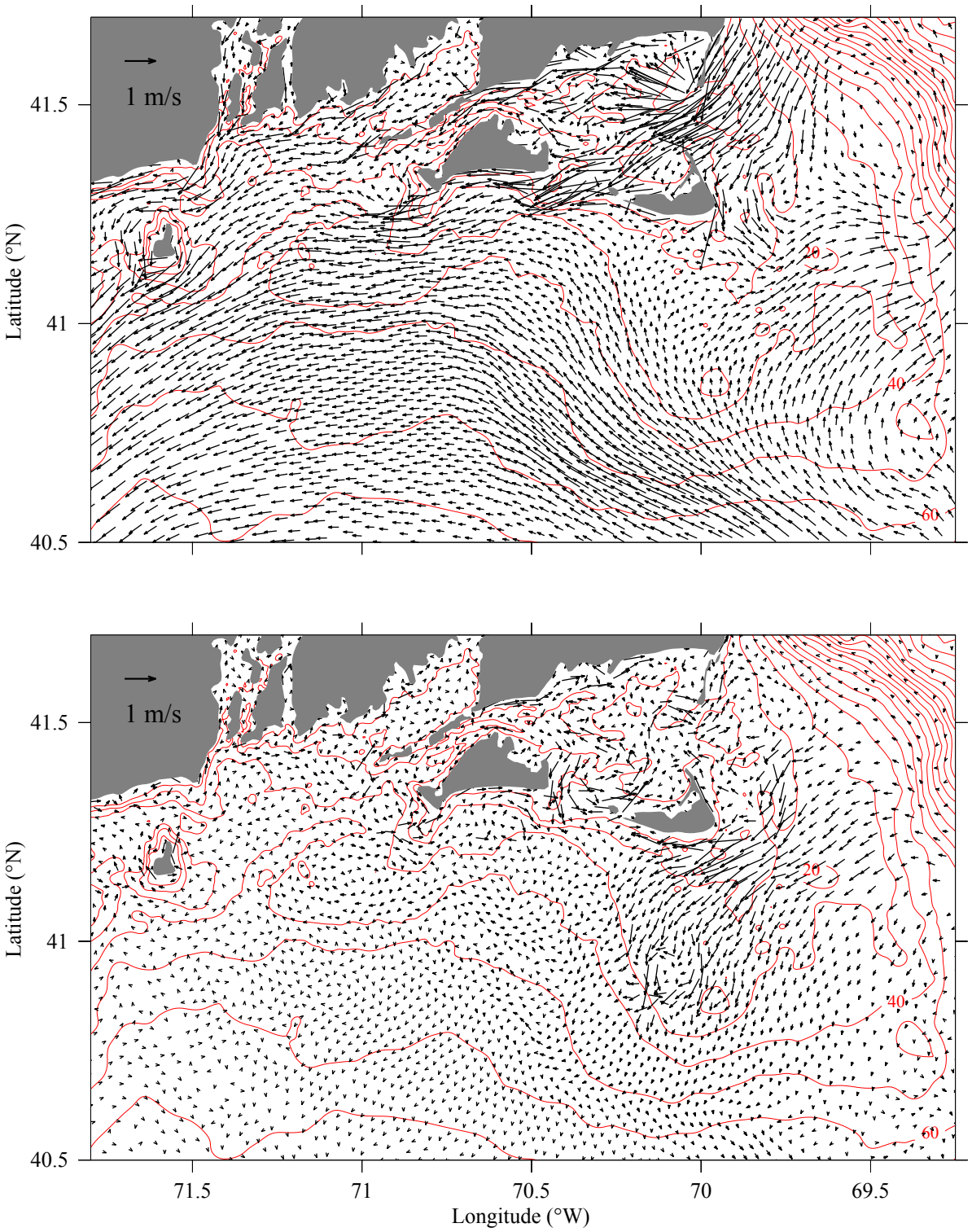

Figure 3.11: Upper panel: a snapshot of the distribution of the vertically averaged velocity over the New England Shelf at 03:00:00 GMT, February 7, 1978 under the condition without wind turbines for the hydrodynamic simulation experiment with NS-FVCOM. Lower panel: the difference of the vertically averaged velocity between the two cases with and without the inclusion of current-wave interactions at the same time.

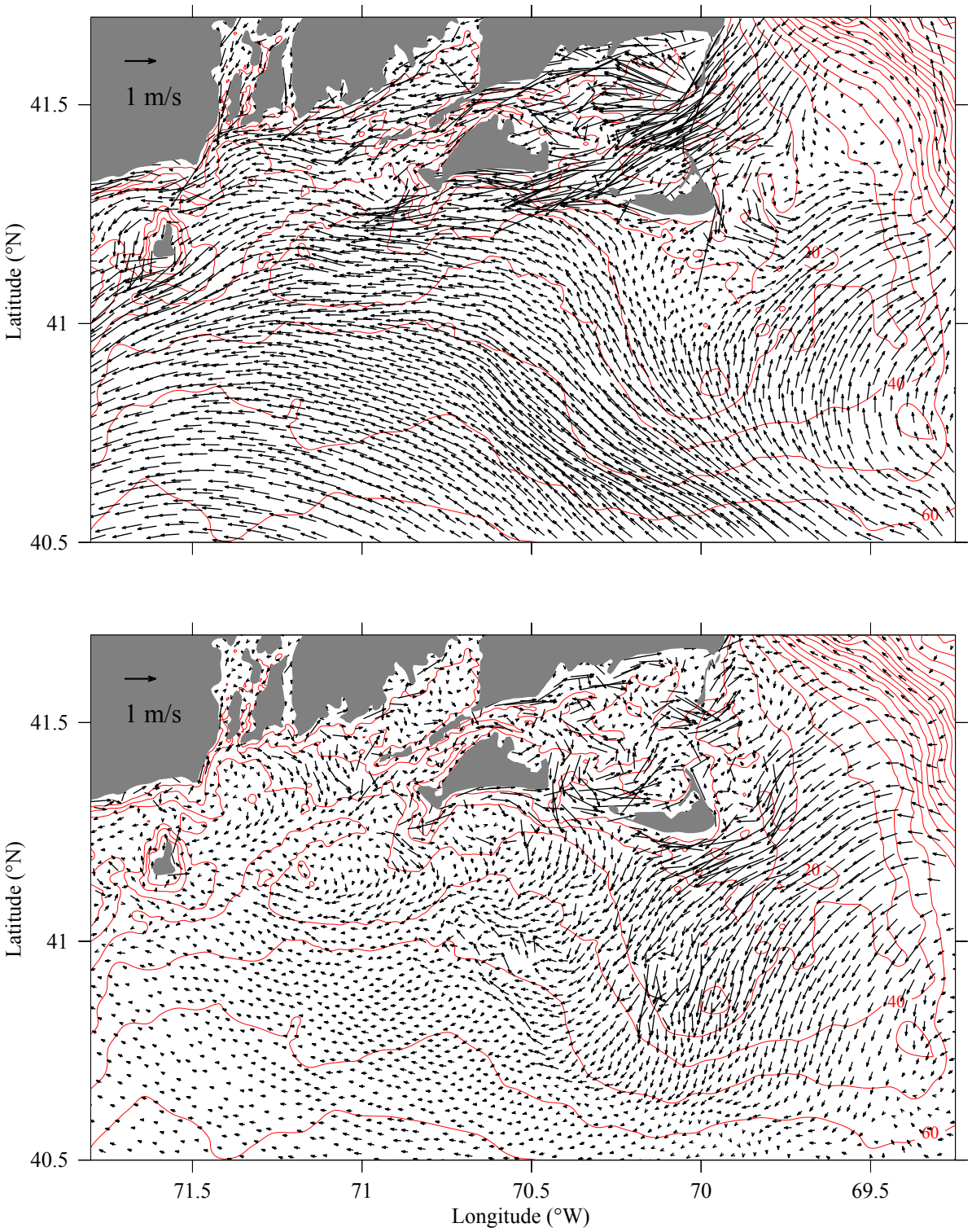

Figure 3.12: Upper panel: a snapshot of the distribution of the near-surface velocity over the New England Shelf at 03:00:00 GMT, February 7, 1978 under the condition without wind turbines for the hydrodynamic simulation experiment with NS-FVCOM. Lower panel: the difference of the near-surface velocity between the two cases with and without the inclusion of current-wave interactions at the same time.

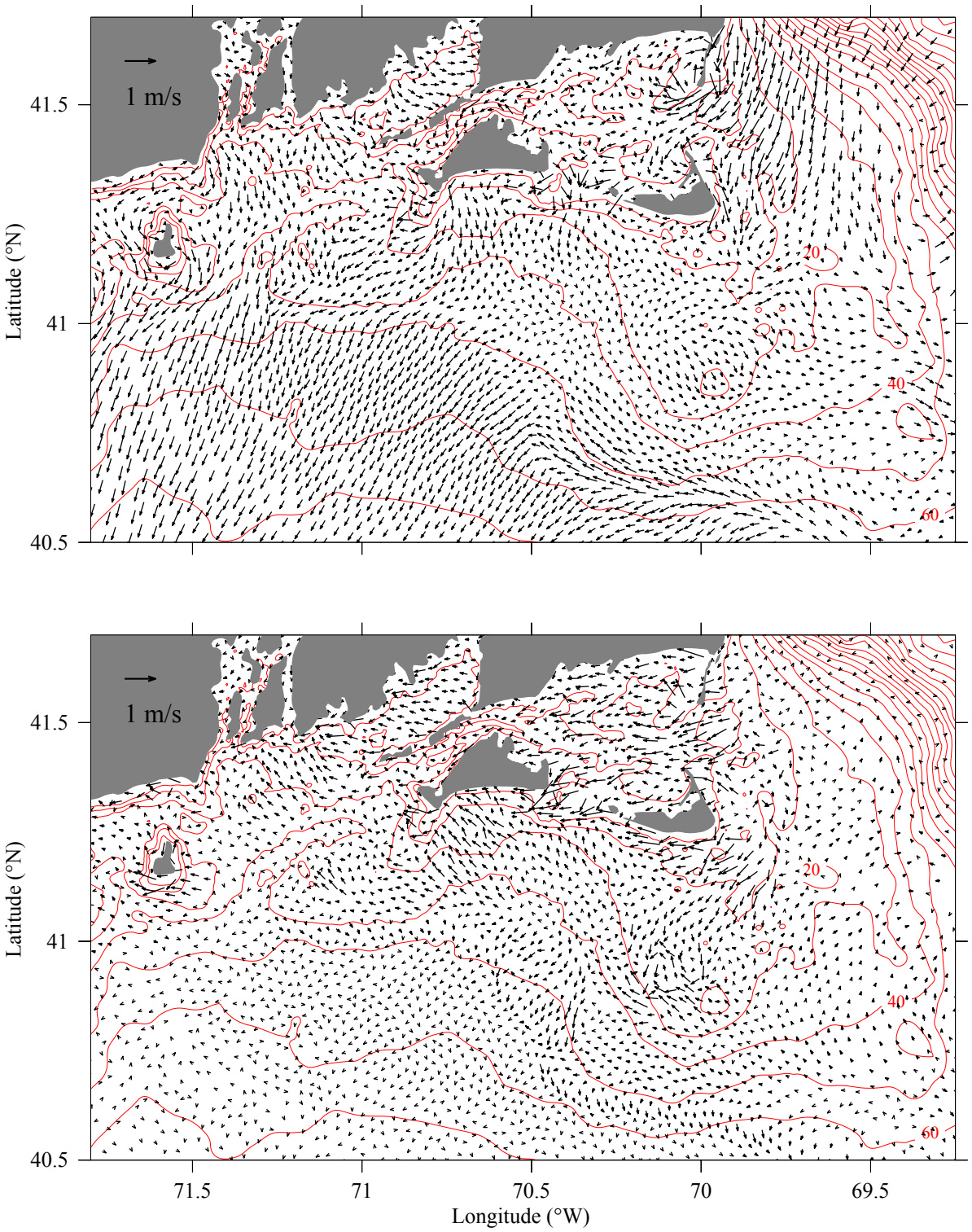

Figure 3.13: Upper panel: a snapshot of the distribution of the near-bottom velocity over the New England Shelf at 03:00:00 GMT, February 7, 1978 under the condition without wind turbines for the hydrodynamic simulation experiment with NS-FVCOM. Lower panel: the difference of the near-bottom velocity between the two cases with and without the inclusion of current-wave interactions at the same time.

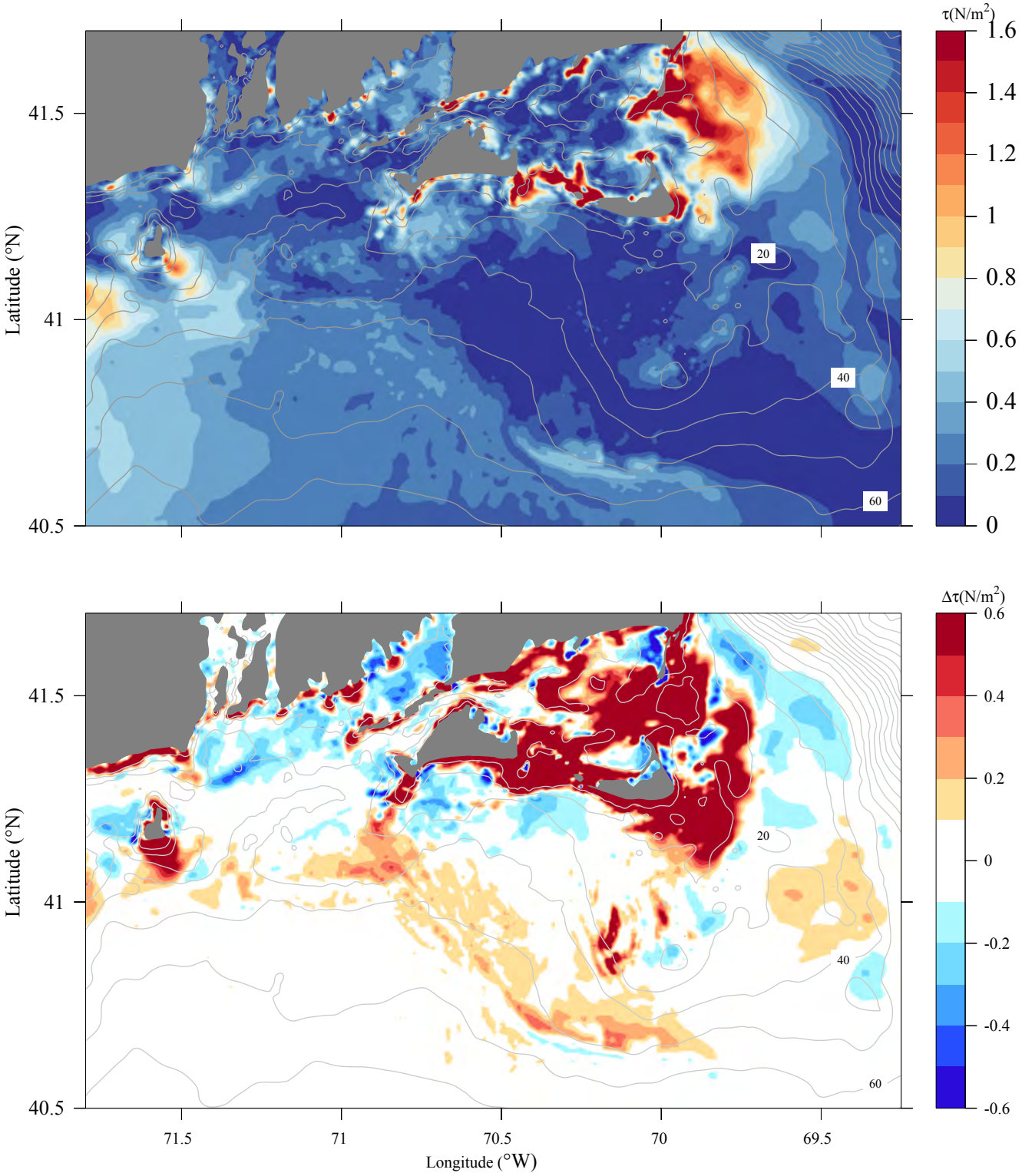

Figure 3.14: Upper panel: a snapshot of the distribution of the bottom stress over the New England Shelf at 03:00:00 GMT, February 7, 1978 under the condition without wind turbines for the hydrodynamic simulation experiment with NS-FVCOM. Lower panel: the difference of the bottom stress between the two cases with and without the inclusion of current-wave interactions at the same time.

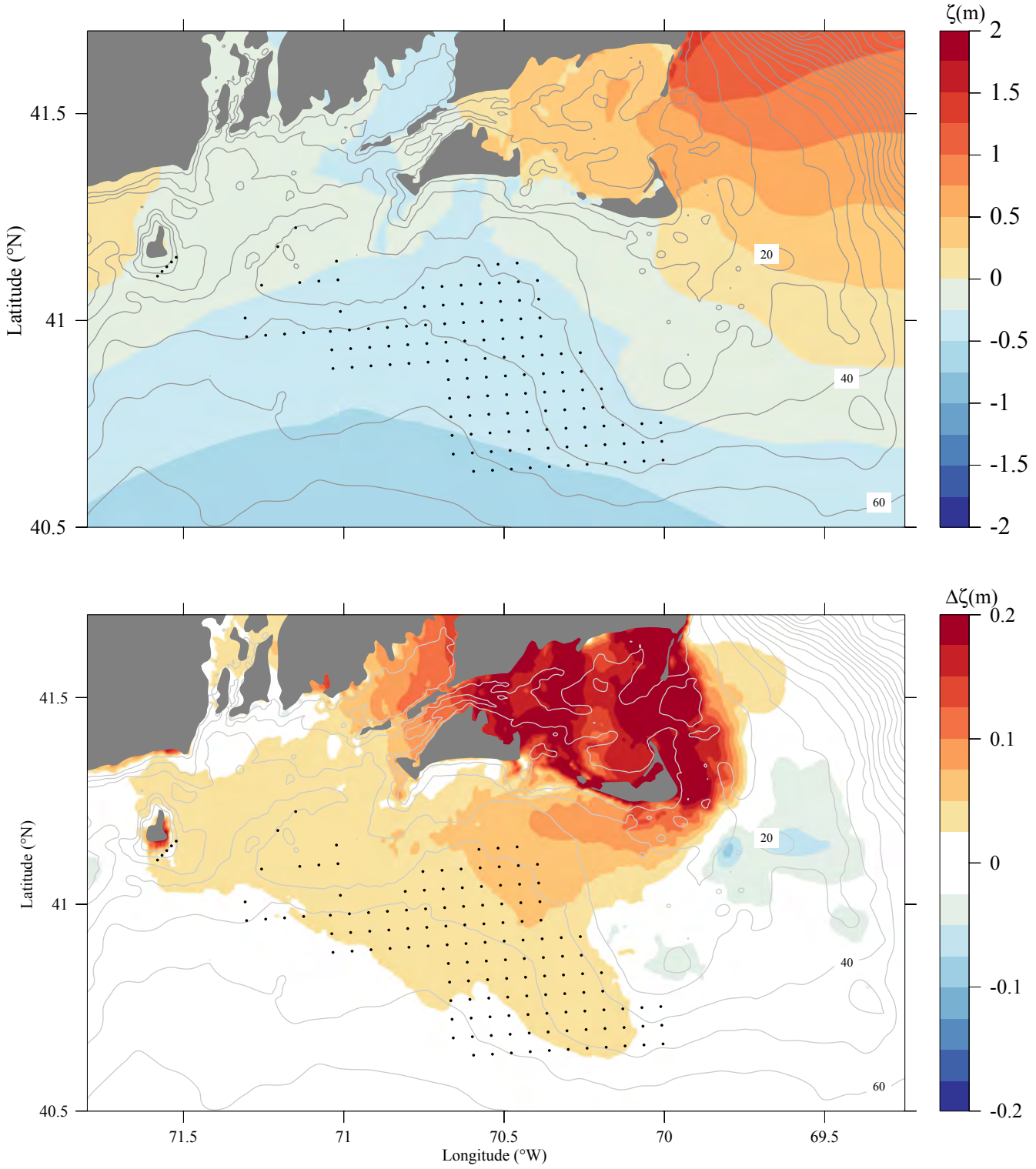

Figure 3.15: Upper panel: a snapshot of the distribution of the surface elevation over the New England Shelf at 03:00:00 GMT, February 7, 1978 under the condition with wind turbines for the hydrodynamic simulation experiment with NS-FVCOM. Lower panel: the difference of the surface elevation between the two cases with and without the inclusion of current-wave interactions at the same time.

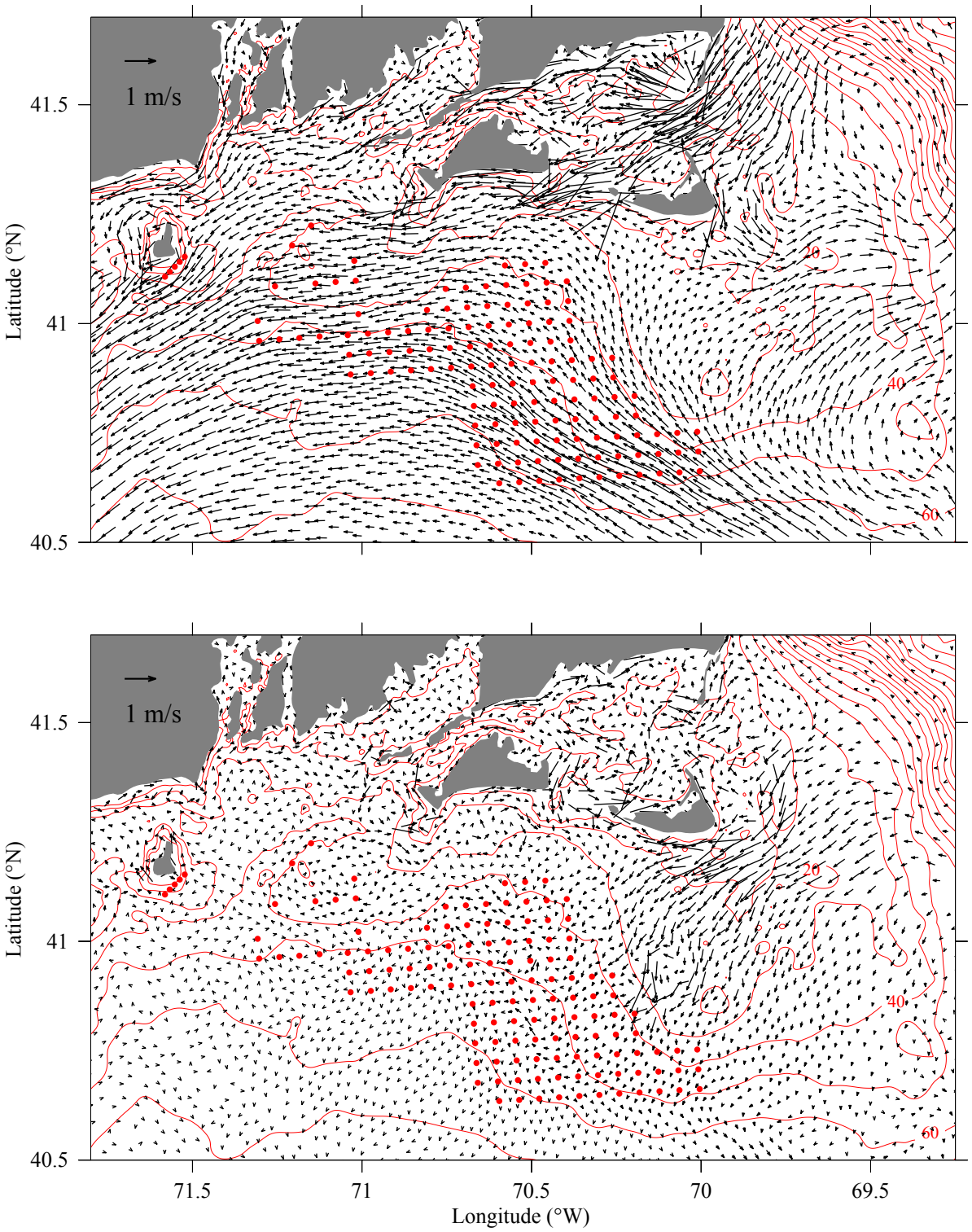

Figure 3.16: Upper panel: a snapshot of the distribution of the vertically averaged velocity over the New England Shelf at 03:00:00 GMT, February 7, 1978 under the condition with wind turbines for the hydrodynamic simulation experiment with NS-FVCOM. Lower panel: the difference of the vertically averaged velocity between the two cases with and without the inclusion of current-wave interactions at the same time.

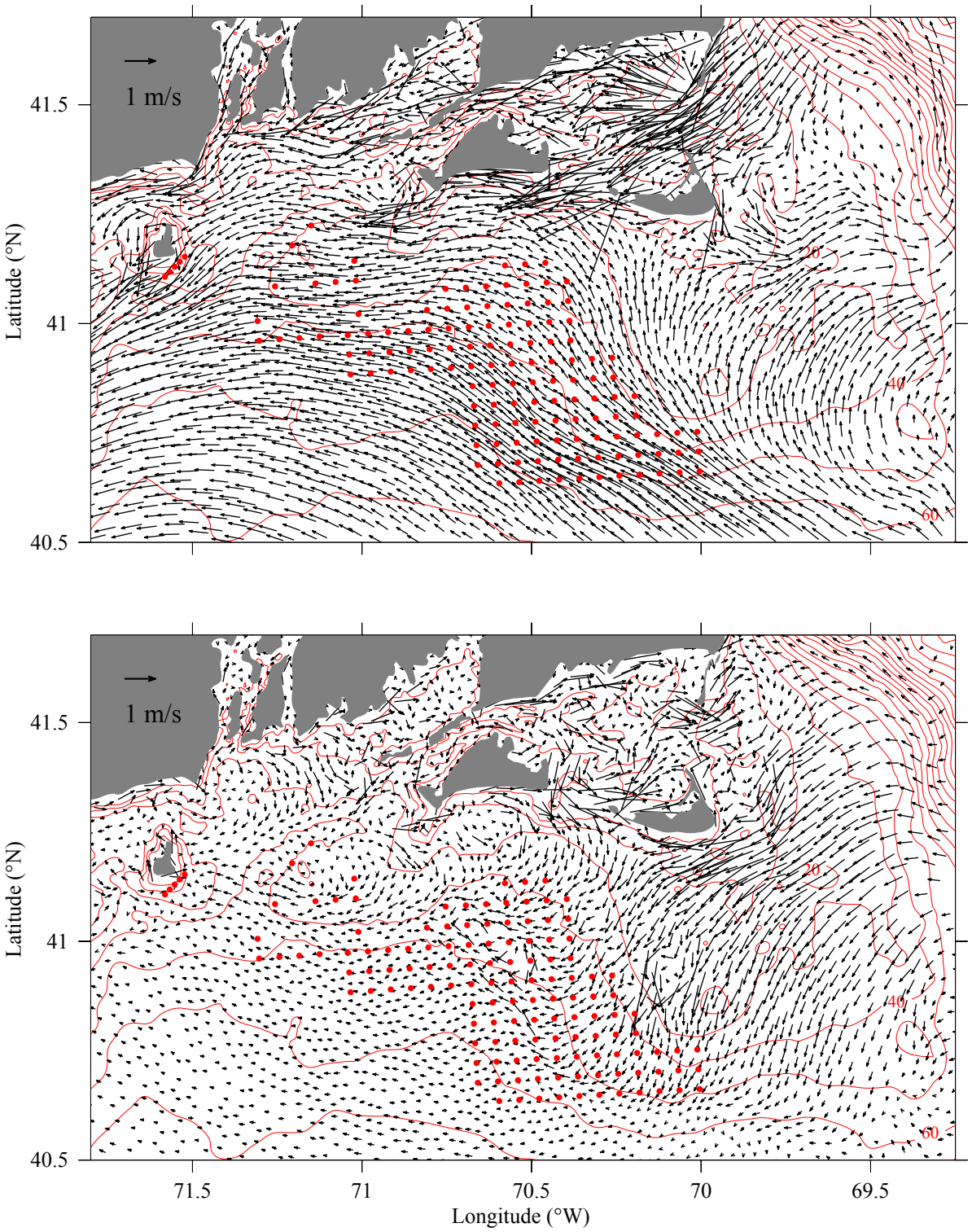

Figure 3.17: Upper panel: a snapshot of the distribution of the near-surface velocity over the New England Shelf at 03:00:00 GMT, February 7, 1978 under the condition with wind turbines for the hydrodynamic simulation experiment with NS-FVCOM. Lower panel: the difference of the near-surface velocity between the two cases with and without the inclusion of current-wave interactions at the same time.

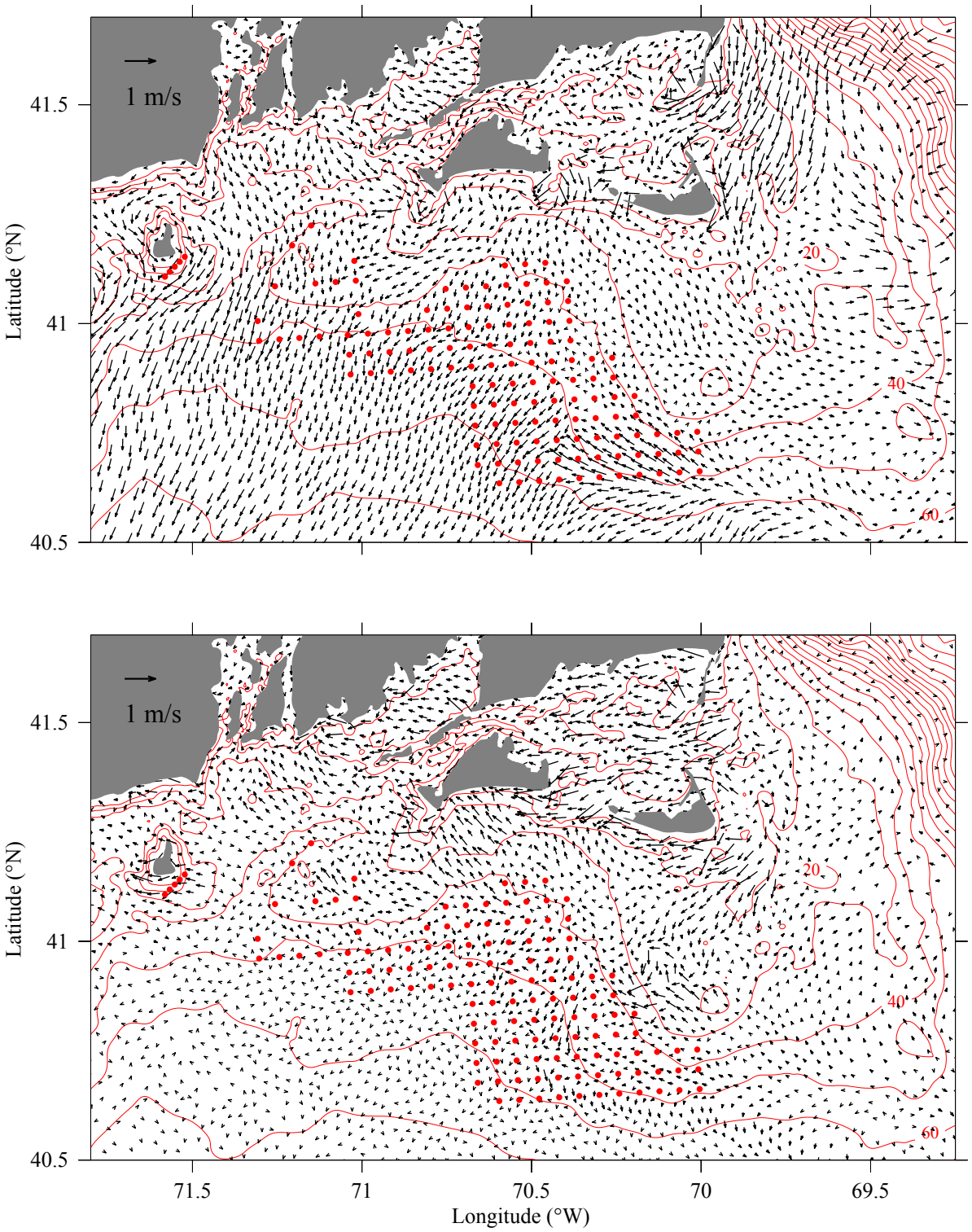

Figure 3.18: Upper panel: a snapshot of the distribution of the near-bottom velocity over the New England Shelf at 03:00:00 GMT, February 7, 1978 under the condition with wind turbines for the hydrodynamic simulation experiment with NS-FVCOM. Lower panel: the difference of the near-bottom velocity between the two cases with and without the inclusion of current-wave interactions at the same time.

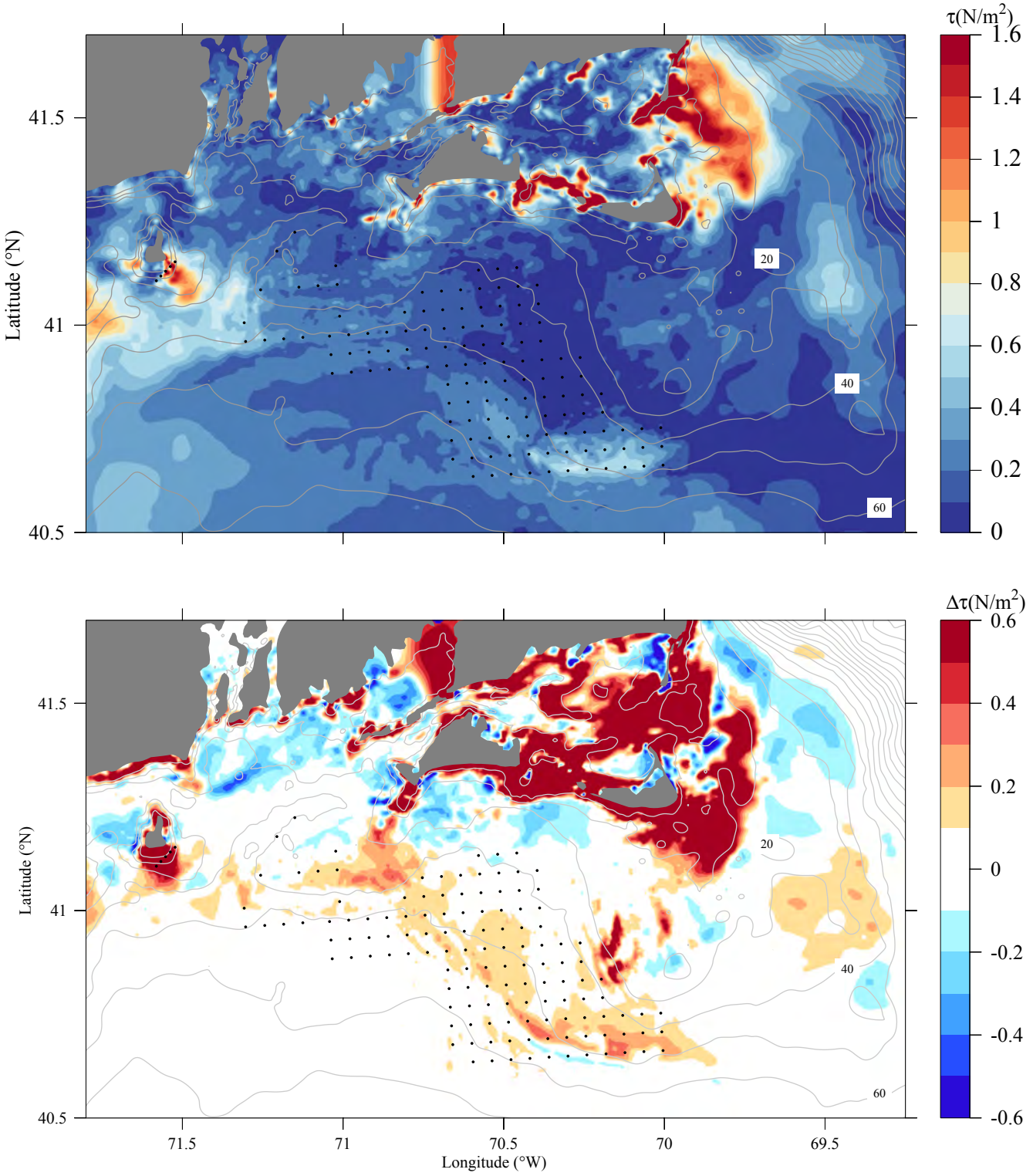

Figure 3.19: Upper panel: a snapshot of the distribution of the bottom stress over the New England Shelf at 03:00:00 GMT, February 7, 1978 under the condition with wind turbines for the hydrodynamic simulation experiment with NS-FVCOM. Lower panel: the difference of the bottom stress between the two cases with and without the inclusion of current-wave interactions the time same.

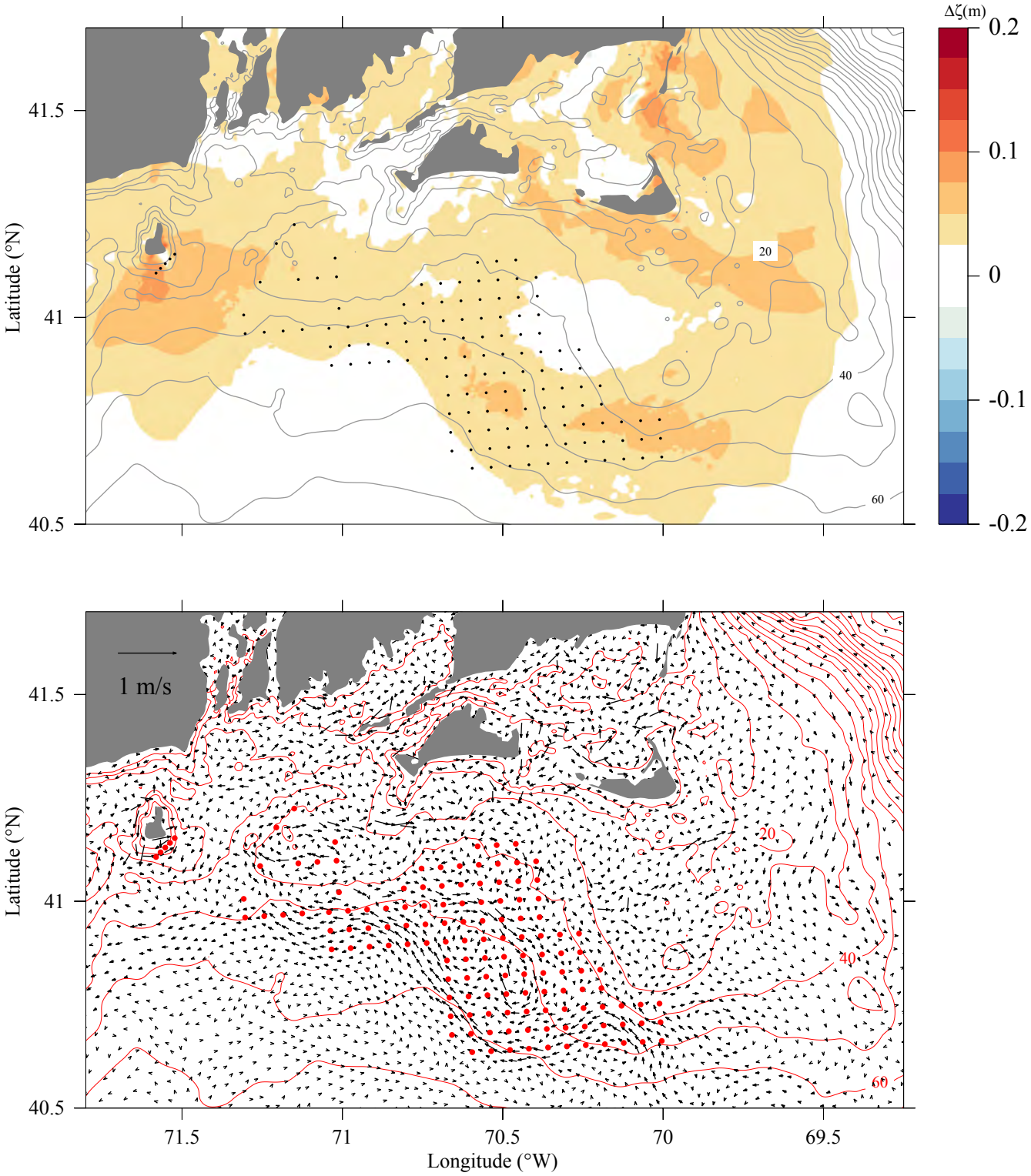

Figure 3.20: Differences of the surface elevation and vertically averaged velocity between the two cases under the conditions with and without wind turbines at 03:00:00 GMT, February 7, 1978 for the hydrodynamic simulation with NS-FVCOM.

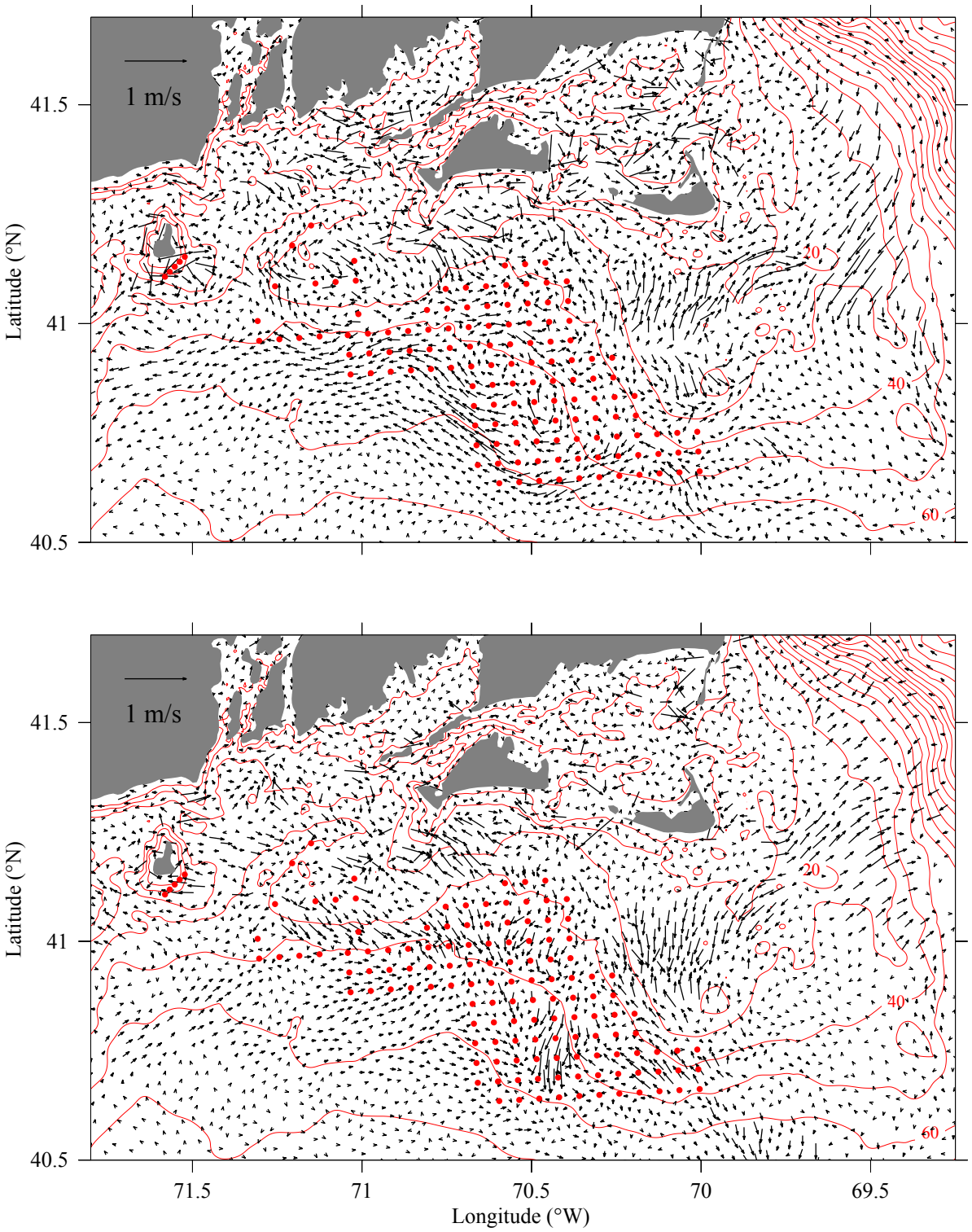

Figure 3.21: Differences of the near-surface (upper) and near-bottom (lower) velocities between the two cases under the conditions with and without wind turbines at 03:00:00 GMT, February 7, 1978 for the hydrodynamic simulation with NS-FVCOM.

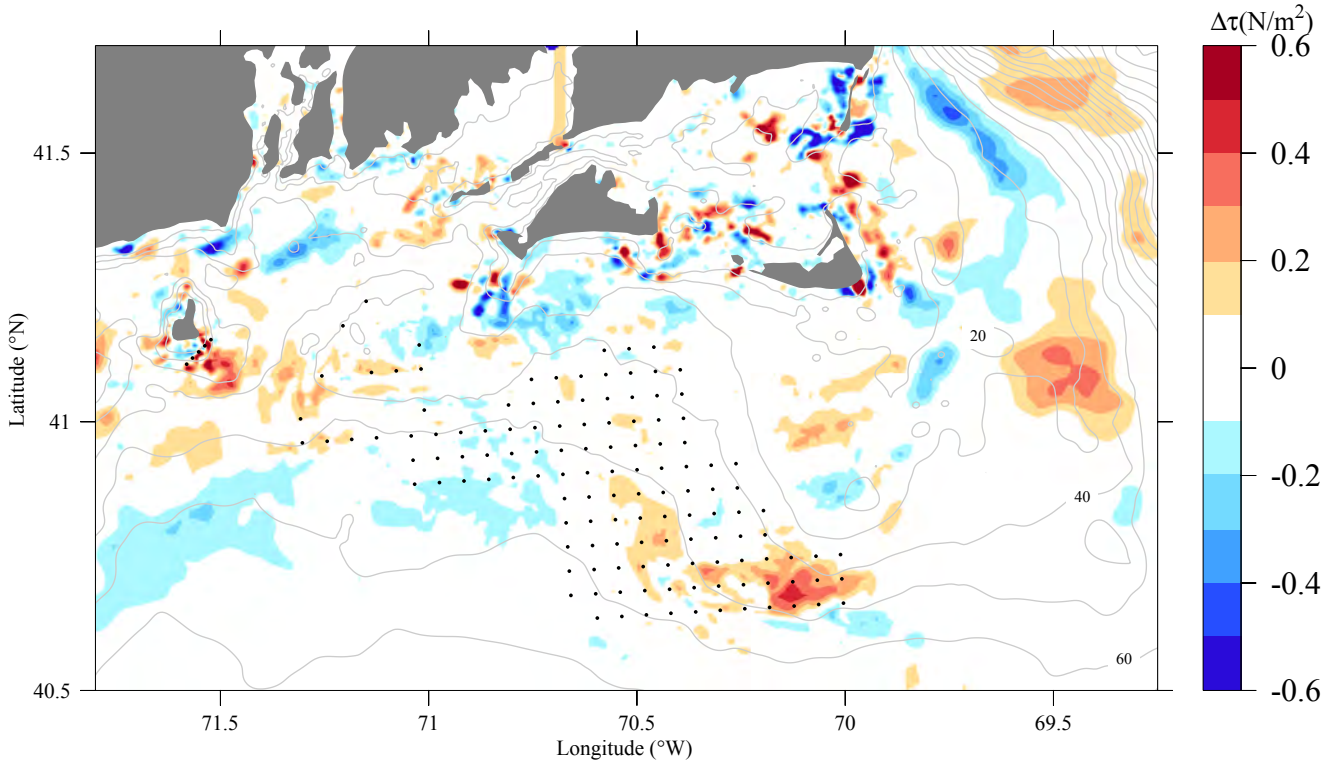

Figure 3.22: Difference of the bottom stress between the two cases under the conditions with and without wind turbines at 03:00:00 GMT, February 7, 1978 for the hydrodynamic simulation with NS-FVCOM.

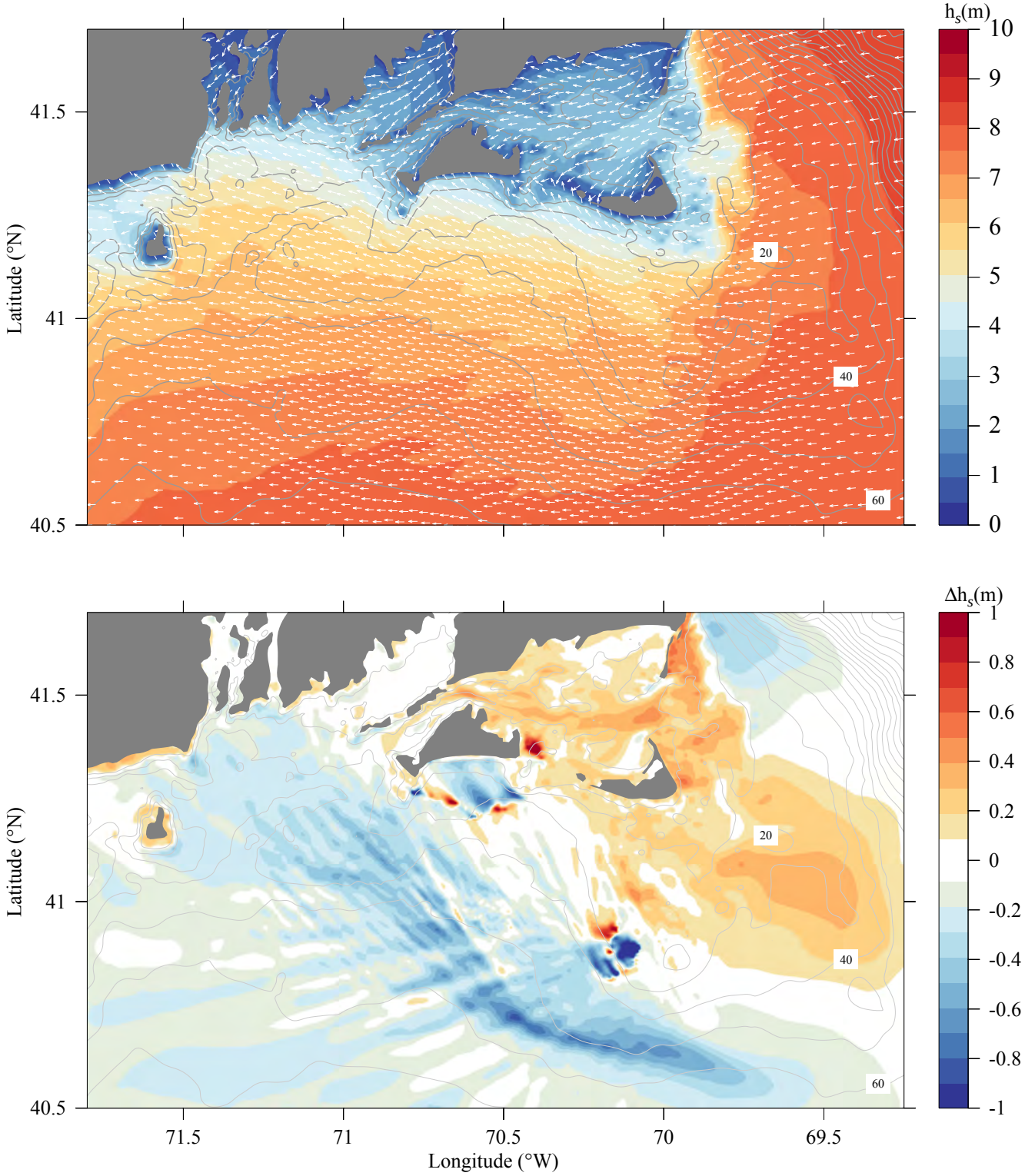

Figure 3.23: Upper panel: a snapshot of the distribution of the significant wave height over the New England Shelf at 03:00:00 GMT, February 7, 1978 under the condition without wind turbines for the surface wave simulation experiment with NS-SWAVE. Lower panel: the difference of the significant wave height between the two cases with and without the inclusion of current-wave interactions at the same time.

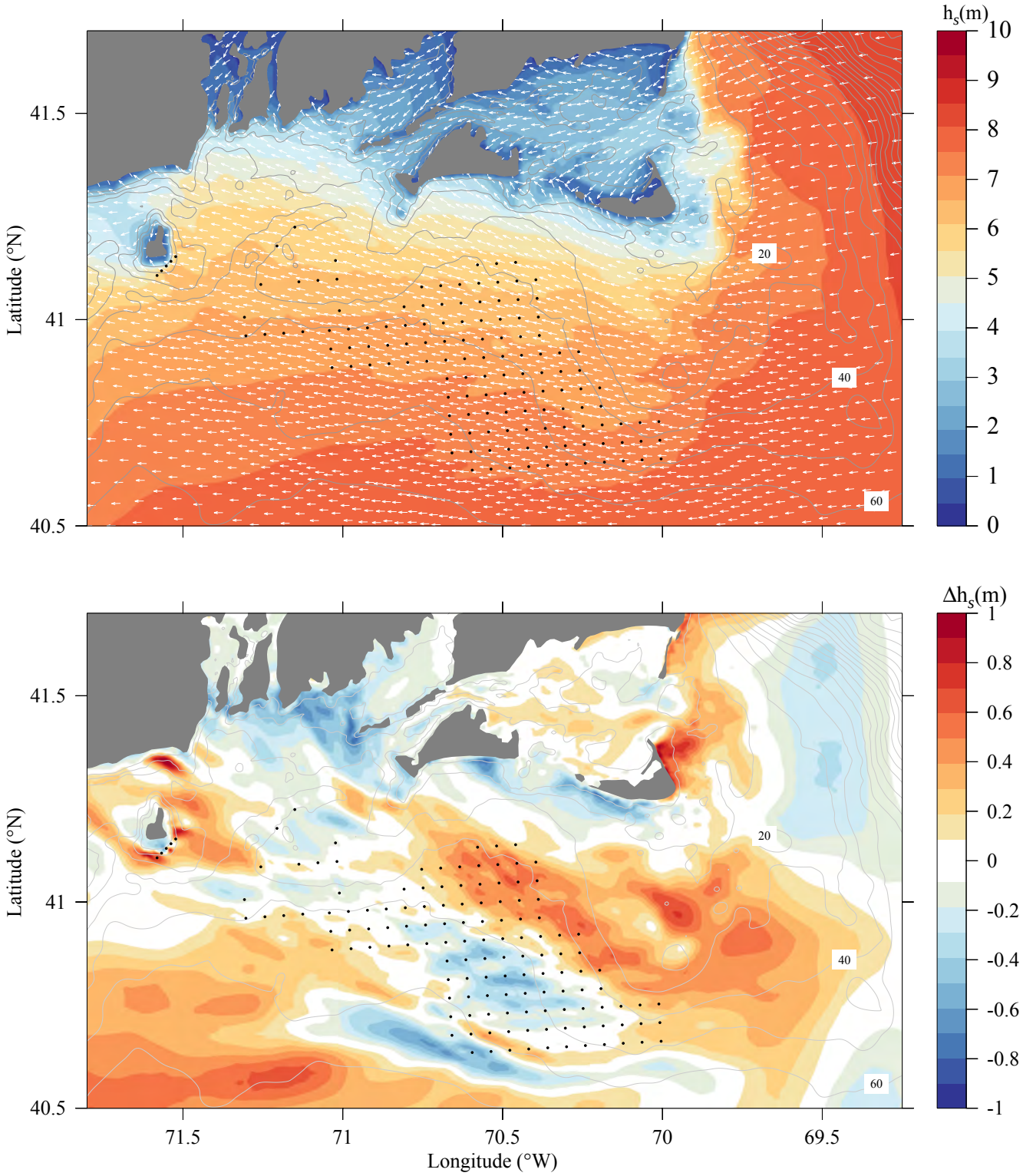

Figure 3.24: Upper panel: a snapshot of the distribution of the significant wave height over the New England Shelf at 03:00:00 GMT, February 7, 1978 under the condition with wind turbines for the surface wave simulation experiment with NS-SWAVE. Lower panel: the difference of the significant wave height between the two cases with and without the inclusion of current-wave interactions at the time same.

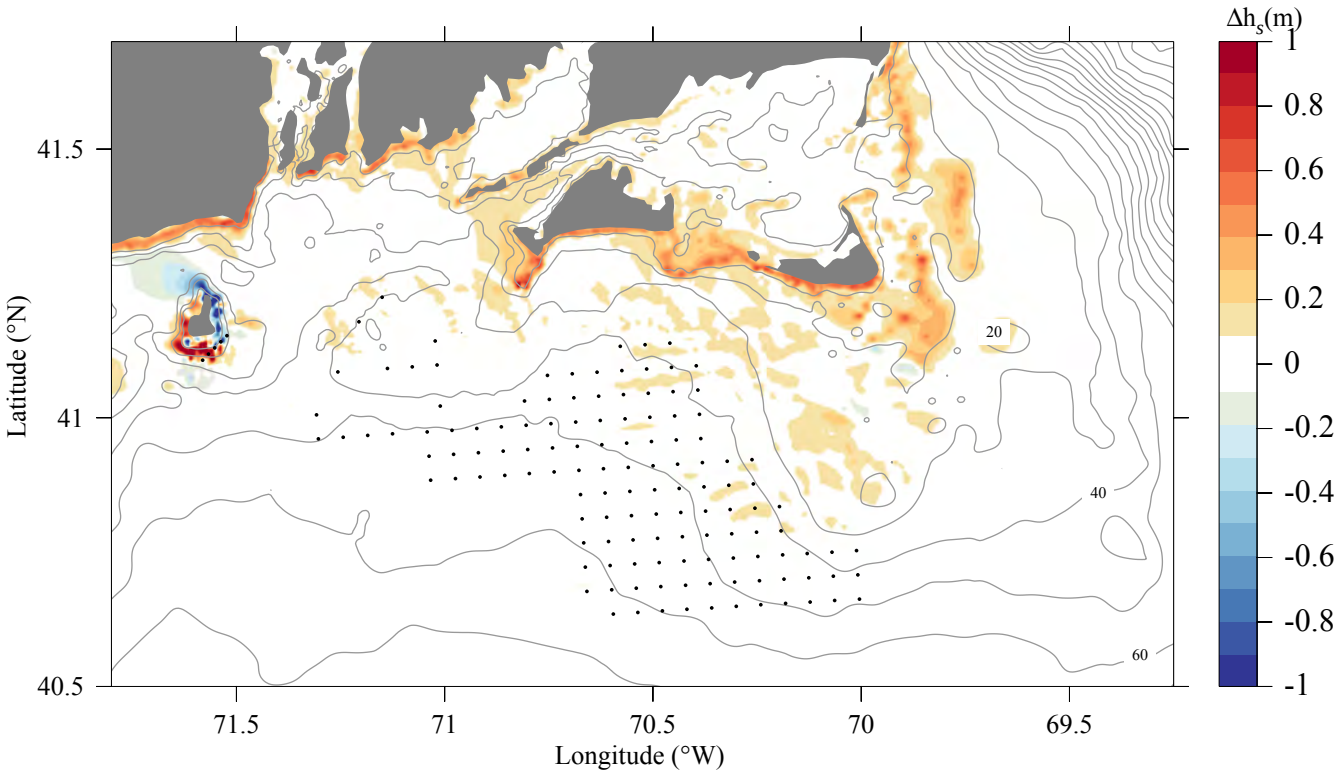

Figure 3.25: A snapshot of the distribution of the significant wave height over the New England Shelf at 03:00:00 GMT, February 7, 1978 under the conditions with and without wind turbines for the surface wave simulation experiment with NS-SWAVE.

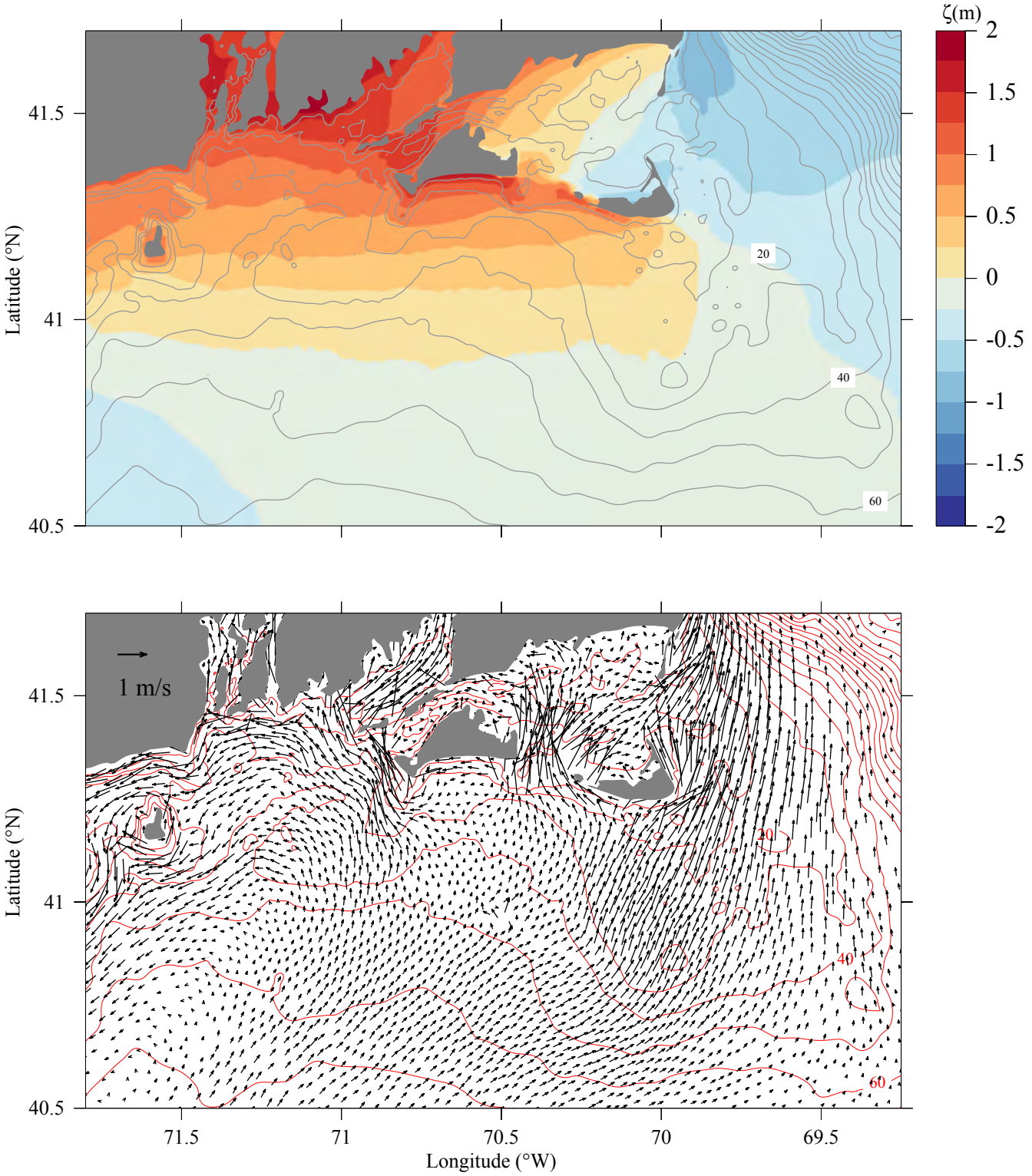

Figure 3.26: Snapshots of the distributions of the model-computed surface elevation (upper panel) and vertically averaged velocity (lower panel) over the New England Shelf at 18:00:00 GMT, August 19, 1991 under the condition without wind turbines for the experiment with the inclusion of wave-current interactions.

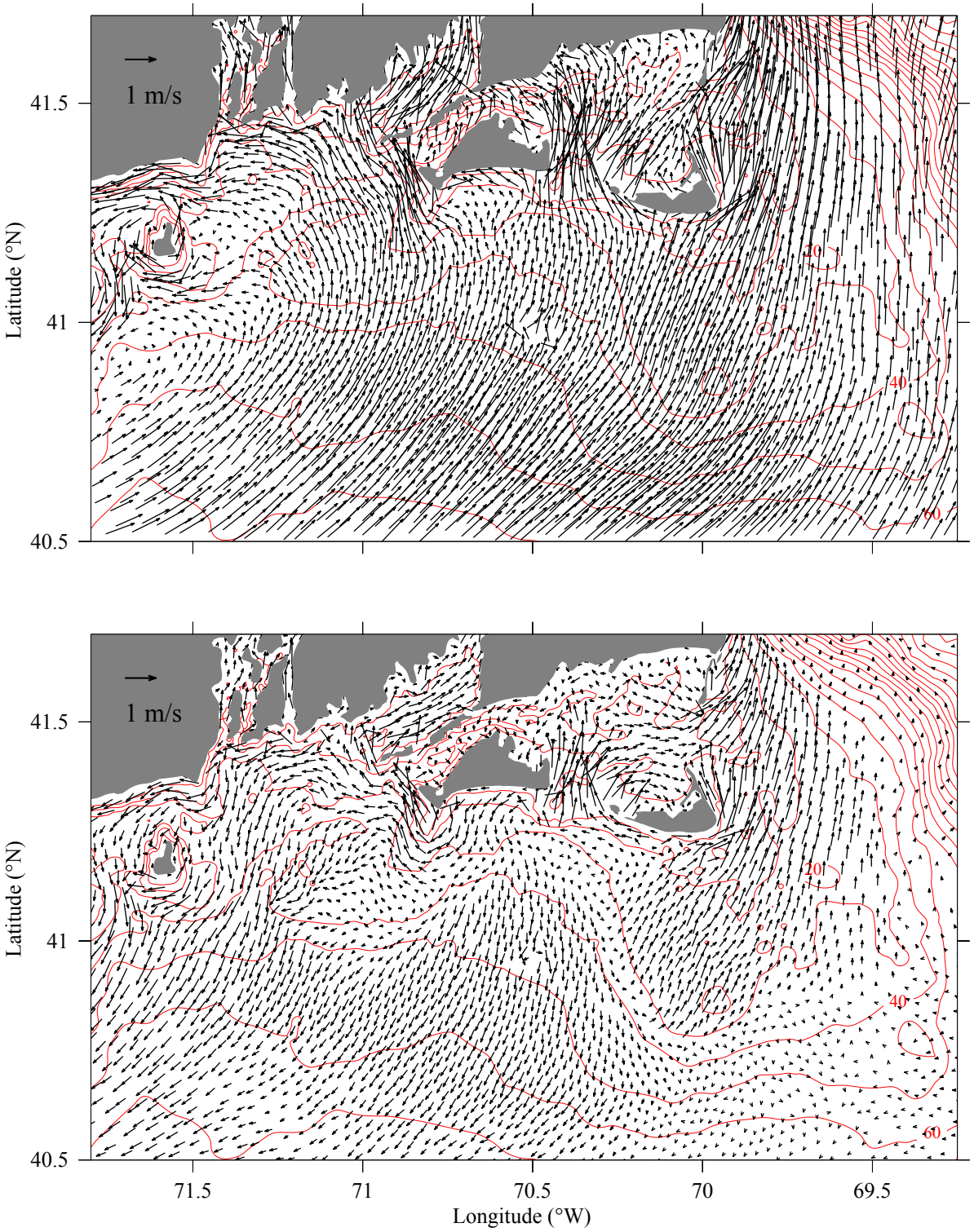

Figure 3.27: Snapshots of the distributions of the model-computed near-surface (upper panel) and near-bottom (lower panel) velocities over the New England Shelf at 18:00:00 GMT, August 19, 1991 under the condition without wind turbines for the experiment with the inclusion of wave-current interactions.

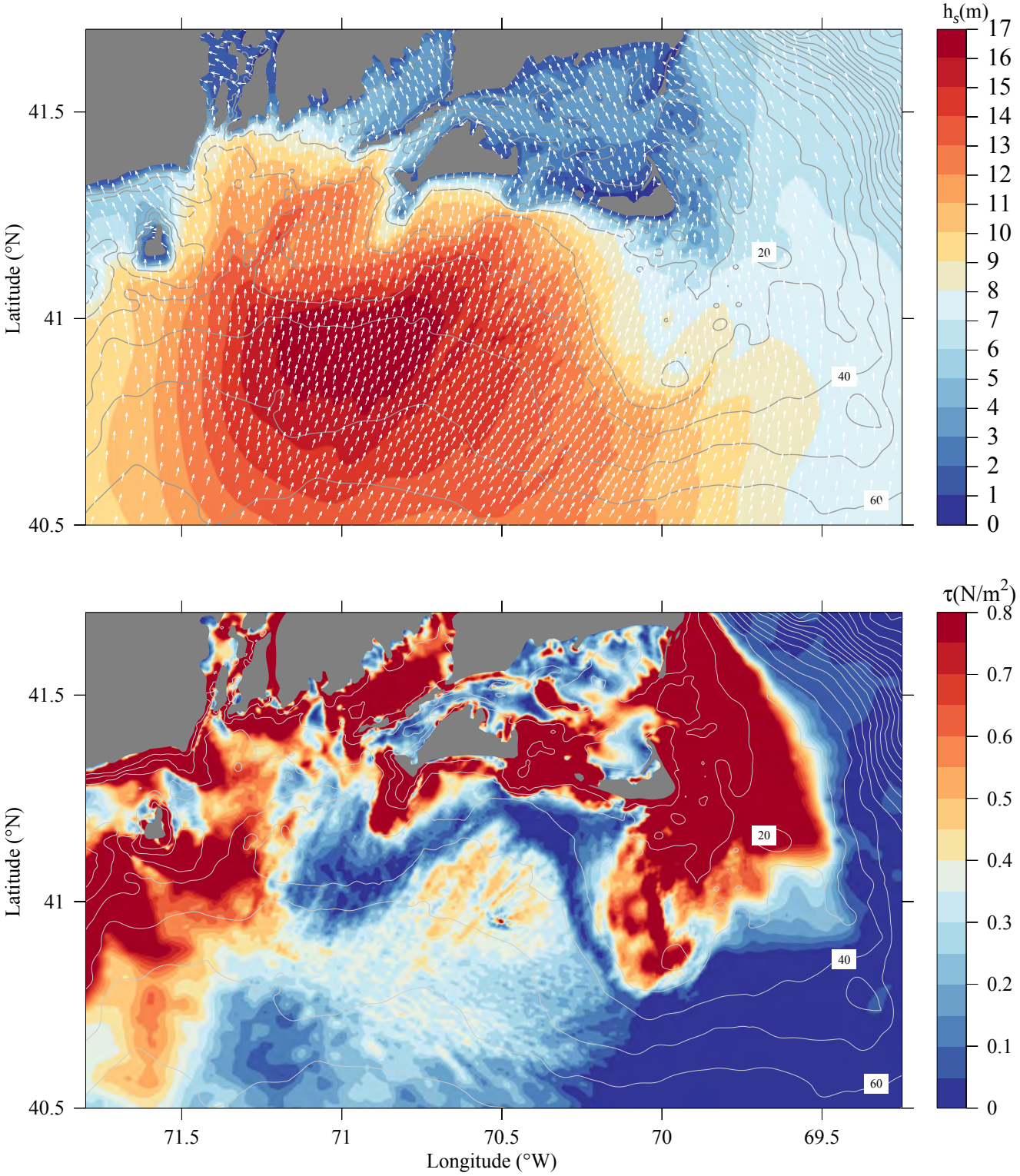

Figure 3.28: Snapshots of the distributions of the model-computed significant wave height (upper panel) and bottom stress (lower panel) over the New England Shelf at 18:00:00 GMT, August 19, 1991 under the condition without wind turbines for the experiment with the inclusion of wave-current interactions.

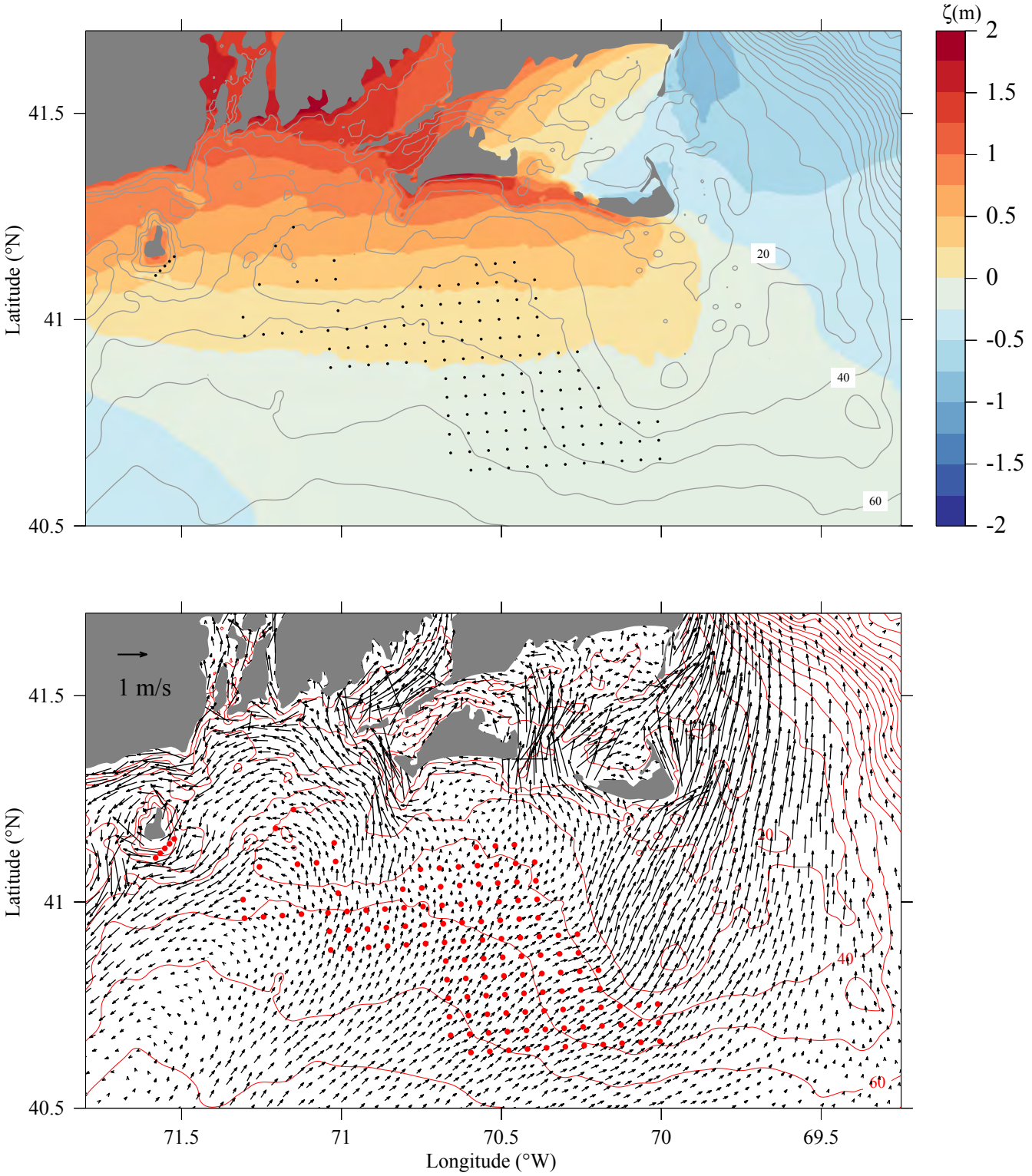

Figure 3.29: Snapshots of the distributions of the model-computed surface elevation (upper panel) and vertically averaged velocity (lower panel) over the New England Shelf at 18:00:00 GMT, August 19, 1991 under the condition with wind turbines for the experiment with the inclusion of wave-current interactions.

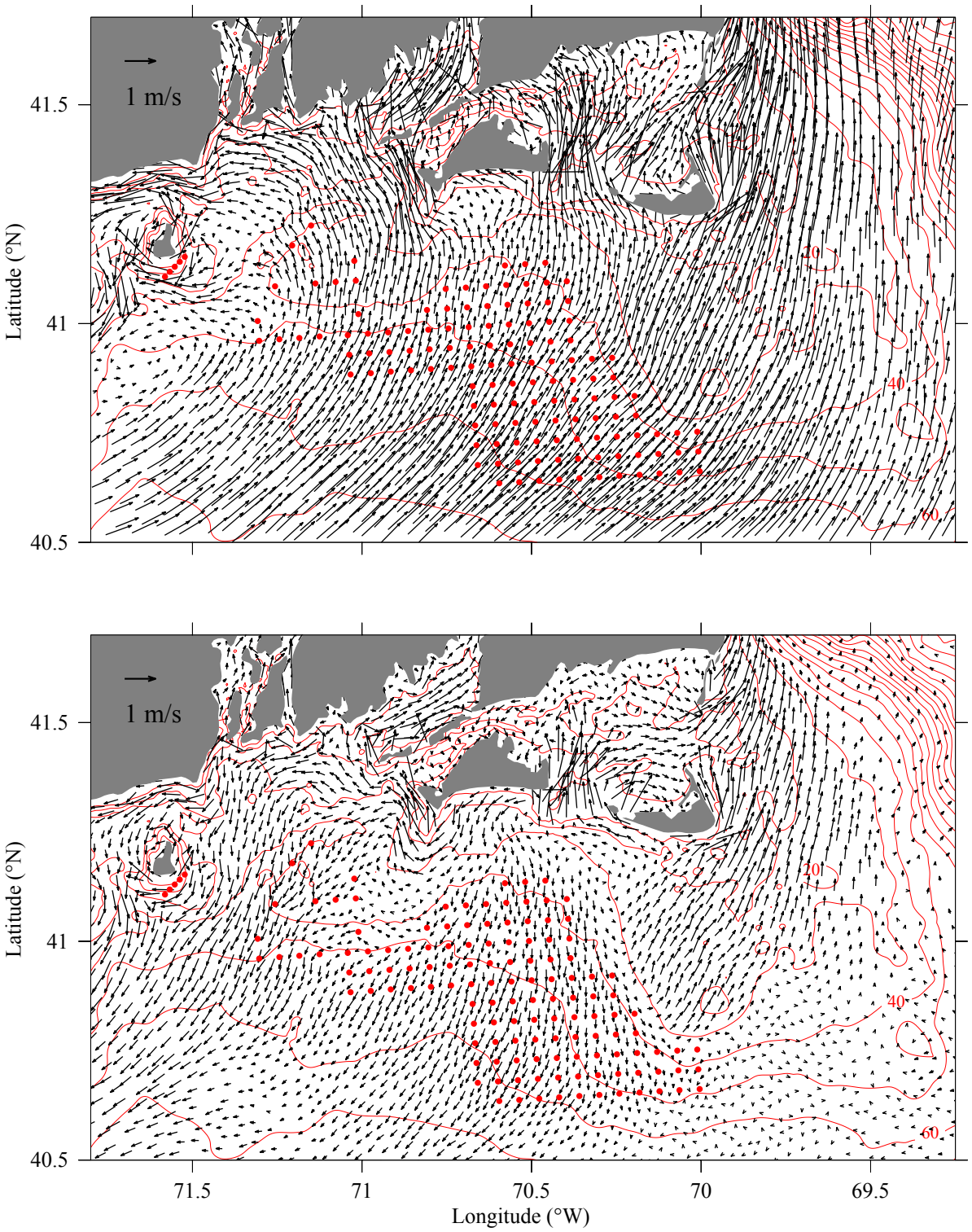

Figure 3.30: Snapshots of the distributions of the model-computed near-surface (upper panel) and near-bottom (lower panel) velocities over the New England Shelf at 18:00:00 GMT, August 19, 1991 under the condition with wind turbines for the experiment with the inclusion of wave-current interactions.

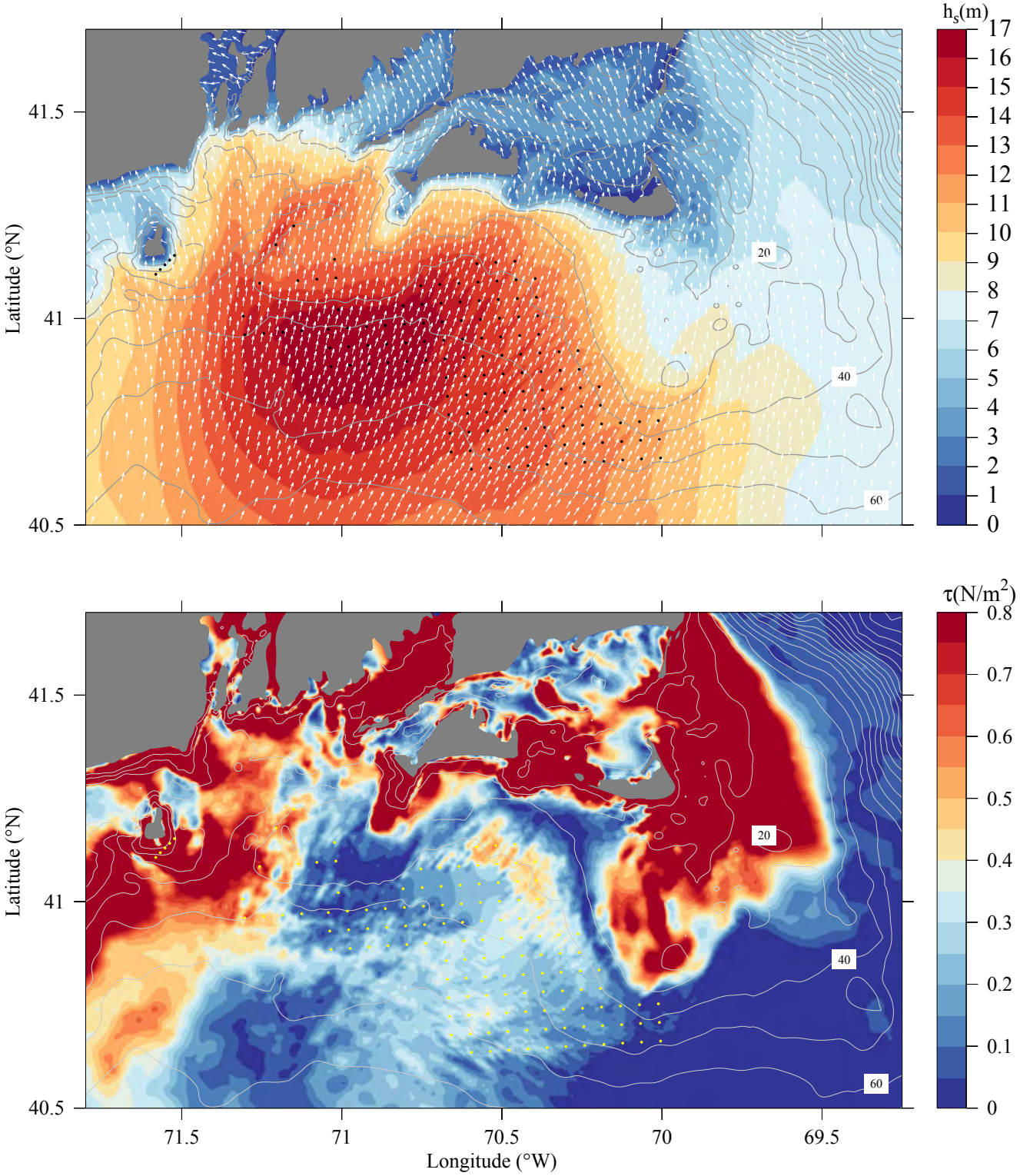

Figure 3.31: Snapshots of the distributions of the model-computed significant wave height (upper panel) and bottom stress (lower panel) over the New England Shelf at 18:00:00 GMT, August 19, 1991 under the condition with wind turbines for the experiment with the inclusion of wave-current interactions.

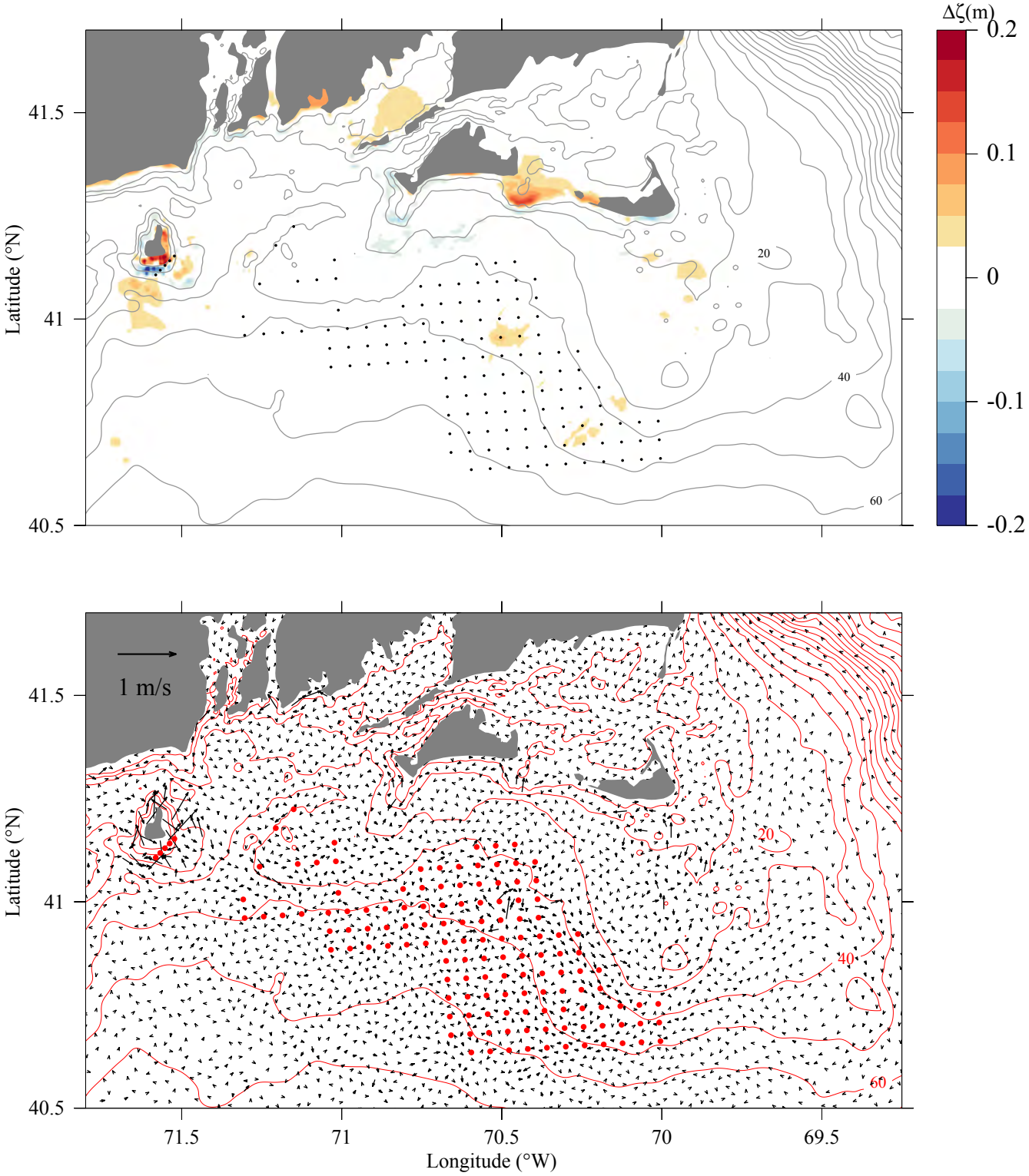

Figure 3.32: Difference of the sea surface (upper panel) and vertically averaged velocity (lower panel) between the two cases under the conditions with and without wind turbines at 18:00:00 GMT, August 19, 1991 for the experiment with the inclusion of wave-current interactions.

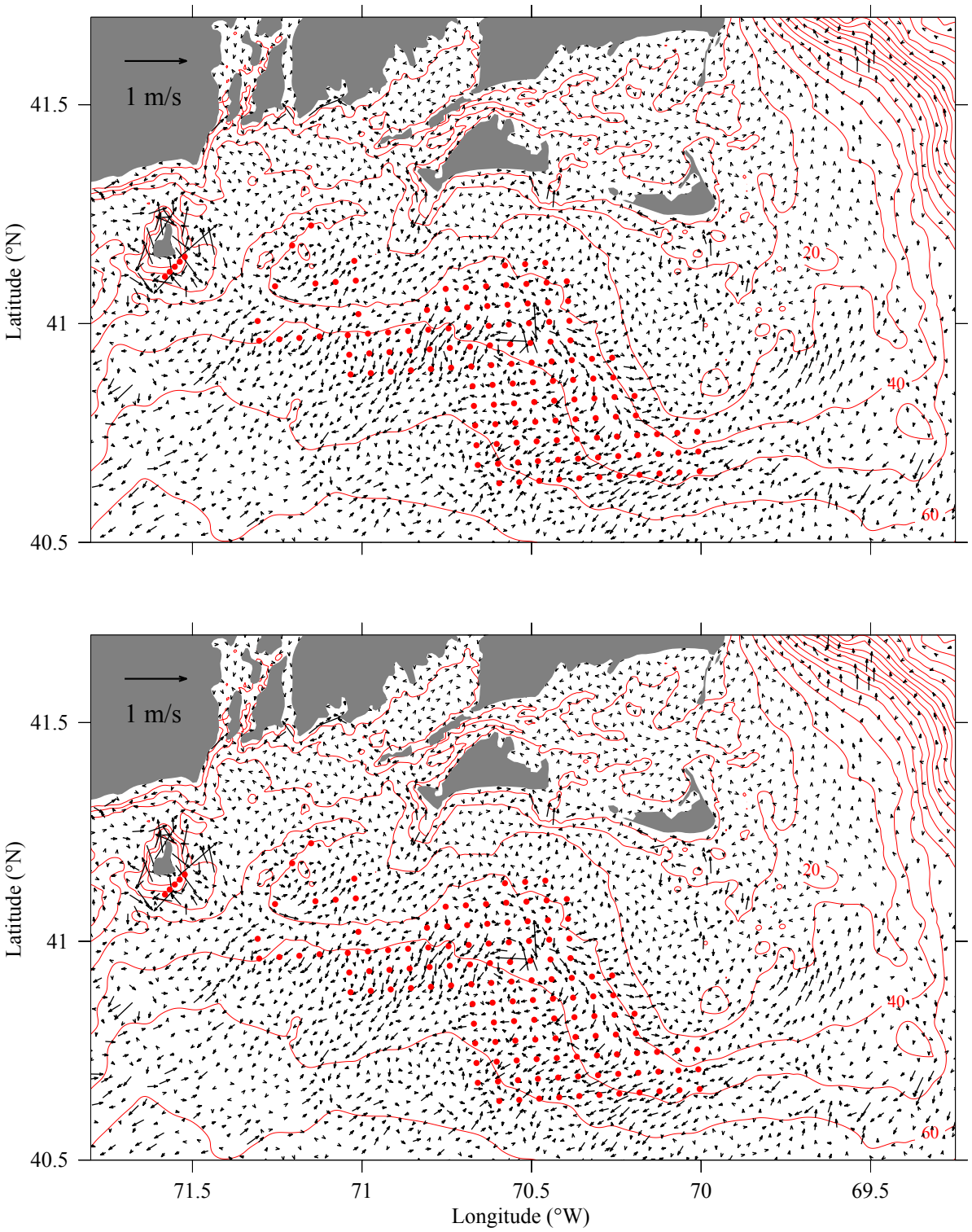

Figure 3.33: Difference of the near-surface (upper) and near-bottom (lower) velocities between the two cases under the conditions with and without wind turbines at 18:00:00 GMT, August 19, 1991 for the experiment with the inclusion of wave-current interactions.

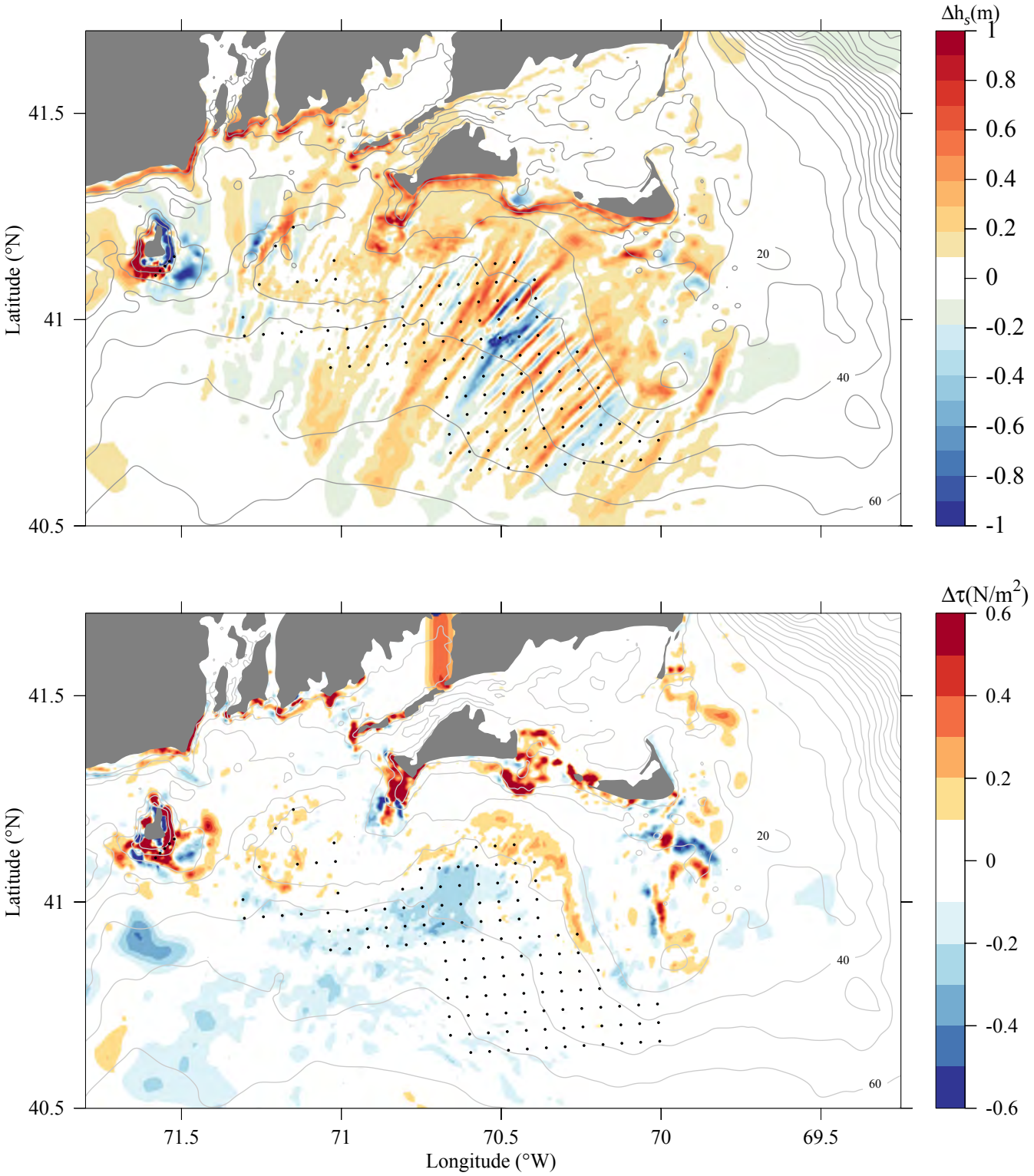

Figure 3.34: Difference of the significant wave height (upper panel) and bottom stress (lower panel) between the two cases under the conditions with and without wind turbines at 18:00:00 GMT, August 19, 1991 for the experiment with the inclusion of wave-current interactions.

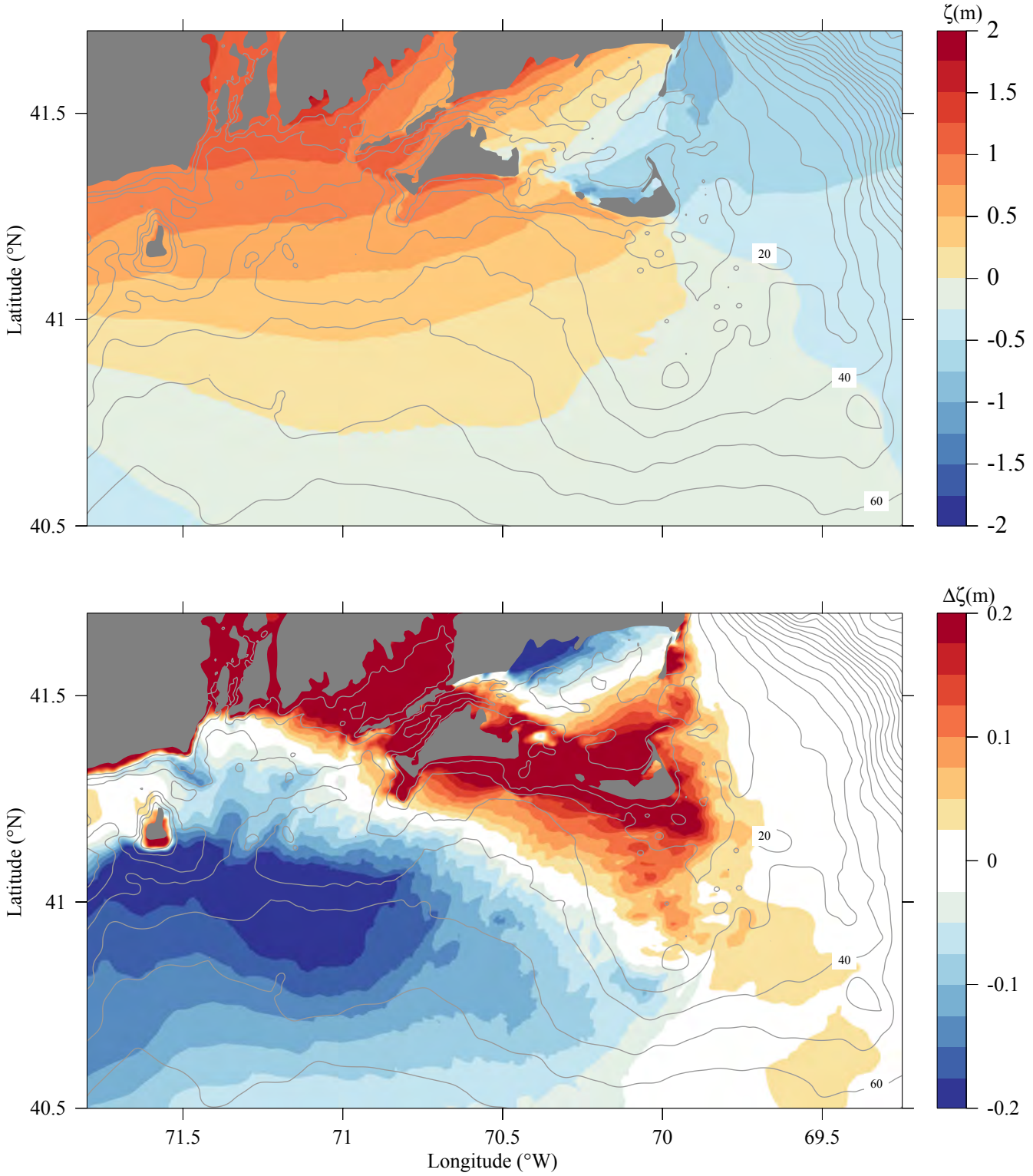

Figure 3.35: Upper panel: a snapshot of the distribution of the surface elevation over the New England Shelf at 18:00:00 GMT, August 19, 1991 under the condition without wind turbines for the hydrodynamic simulation experiment with NS-FVCOM. Lower panel: the difference of the surface elevation between the two cases with and without the inclusion of current-wave interactions at the same time.

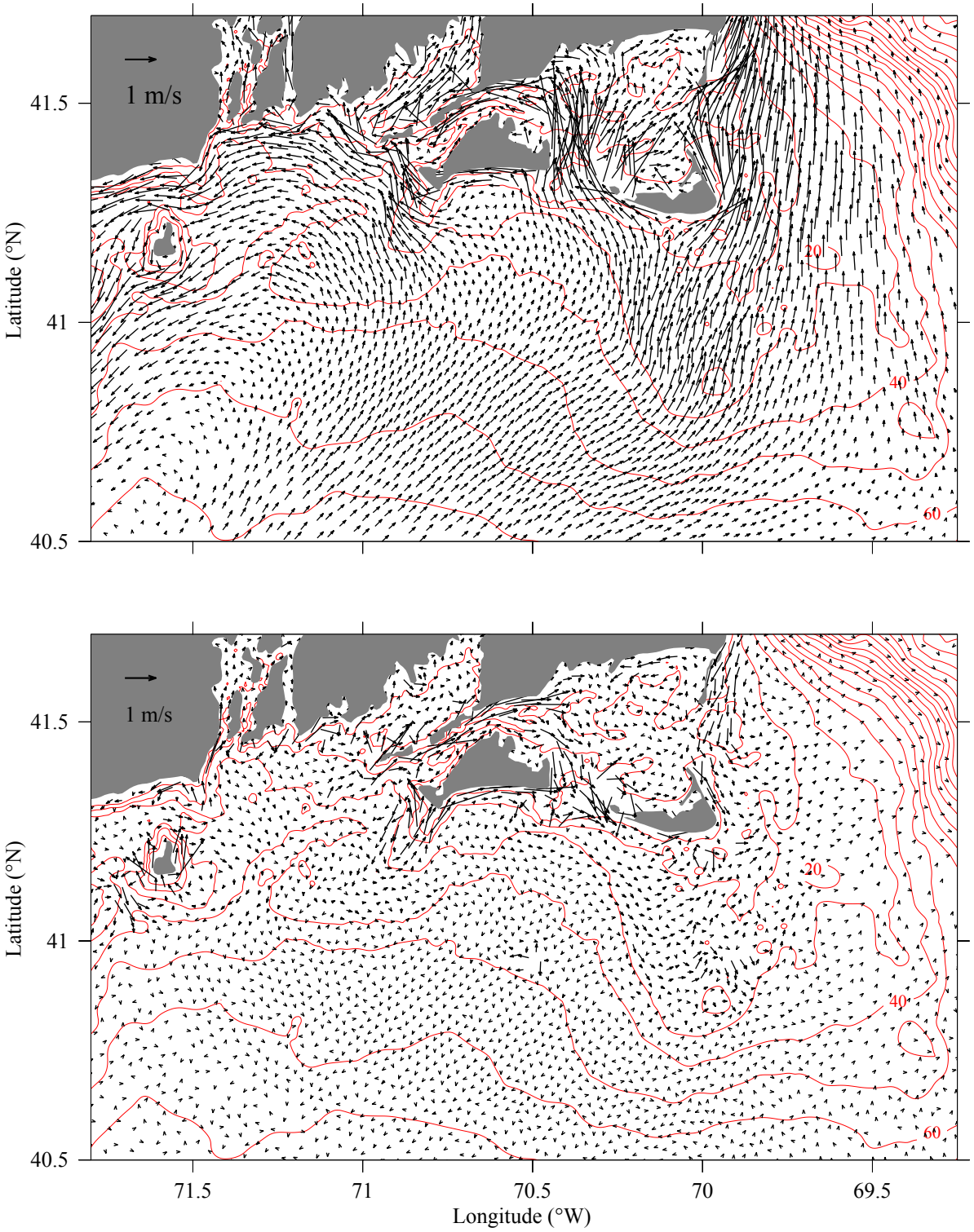

Figure 3.36: Upper panel: a snapshot of the distribution of the vertically averaged velocity over the New England Shelf at 18:00:00 GMT, August 19, 1991 under the condition without wind turbines for the hydrodynamic simulation experiment with NS-FVCOM. Lower panel: the difference of the vertically averaged velocity between the two cases with and without the inclusion of current-wave interactions at the same time.

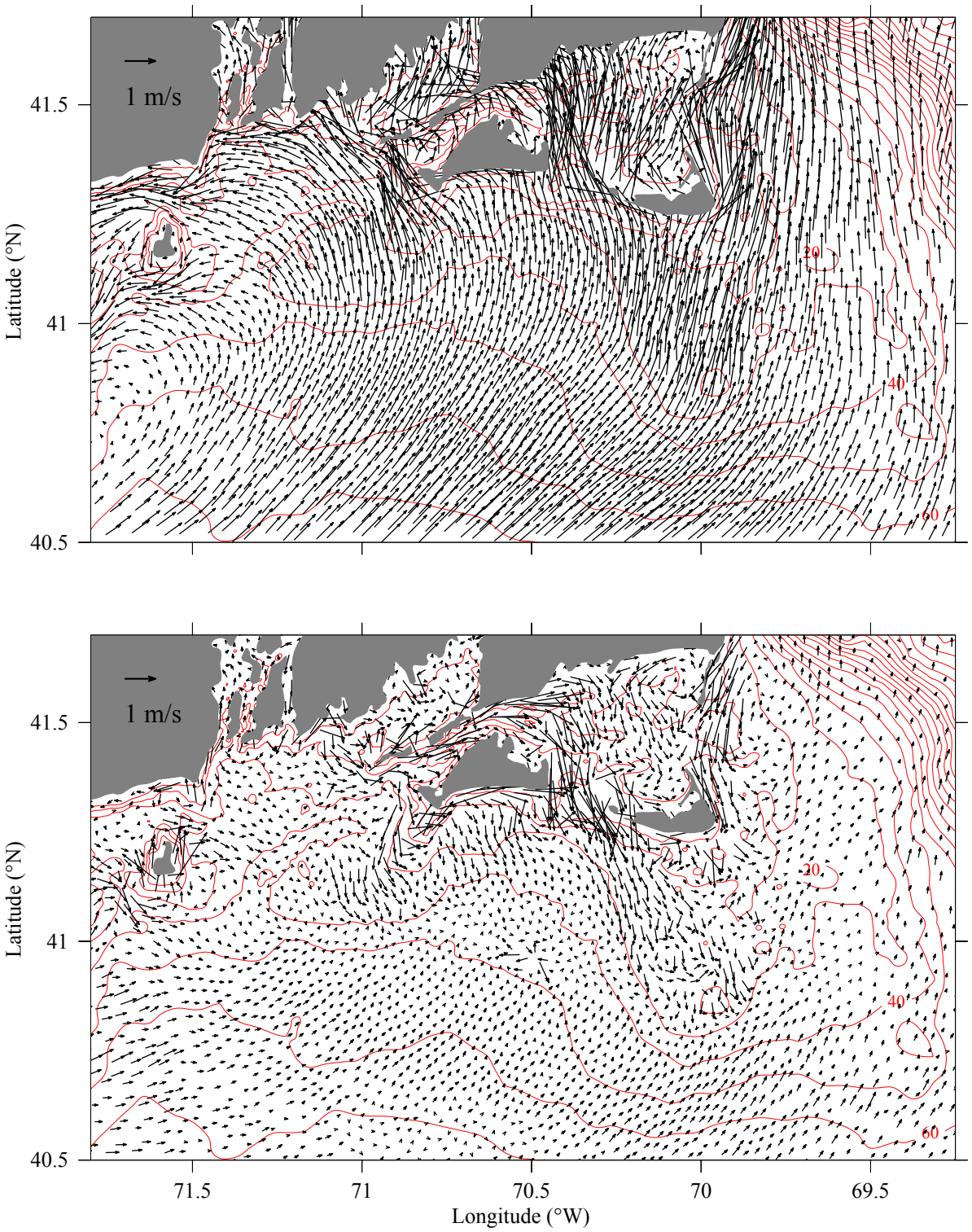

Figure 3.37: Upper panel: a snapshot of the distribution of the near-surface velocity over the New England Shelf at 18:00:00 GMT, August 19, 1991 under the condition without wind turbines for the hydrodynamic simulation experiment with NS-FVCOM. Lower panel: the difference of the near-surface velocity between the two cases with and without the inclusion of current-wave interactions at at the same time.

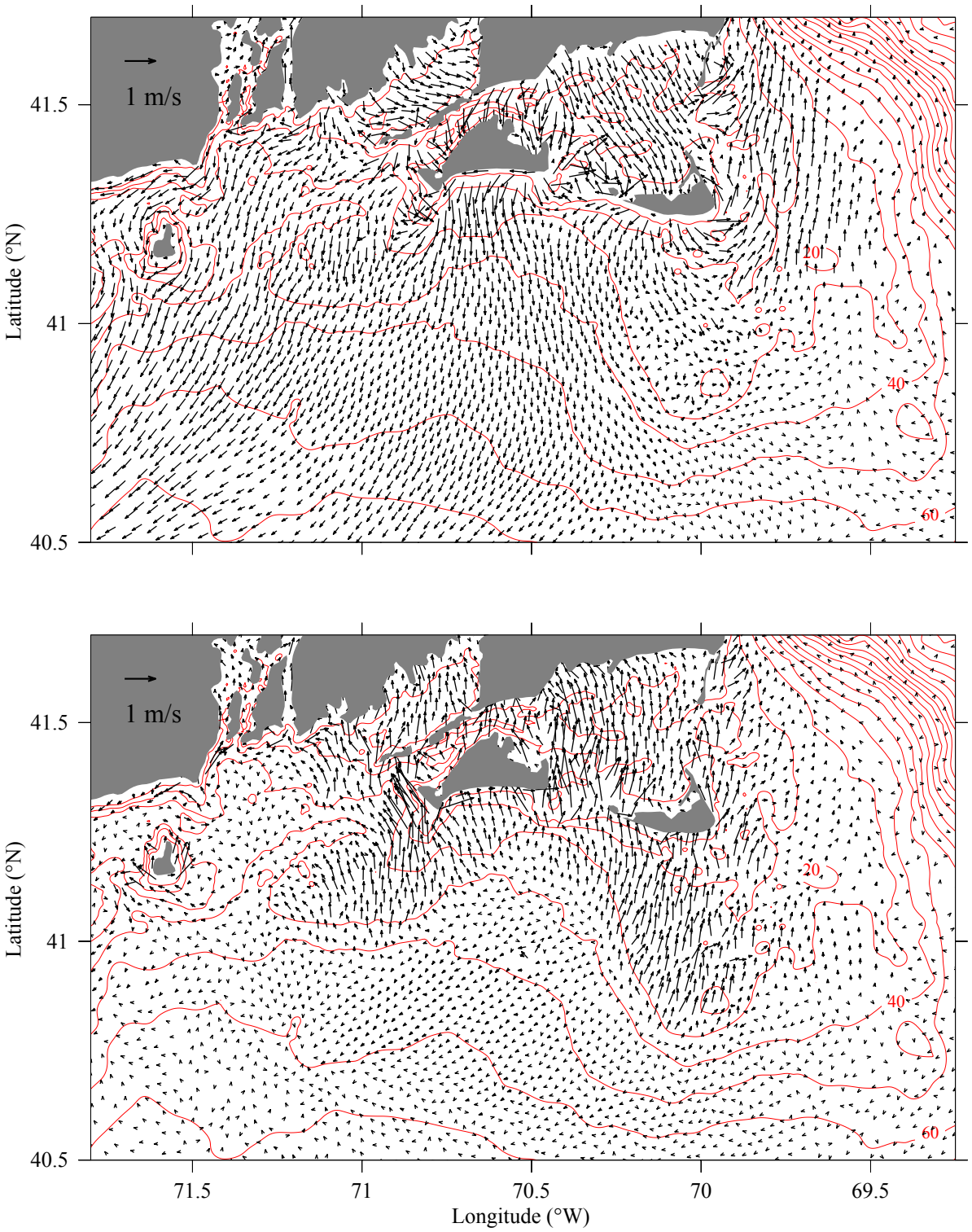

Figure 3.38: Upper panel: a snapshot of the distribution of the near-bottom velocity over the New England Shelf at 18:00:00 GMT, August 19, 1991 under the condition without wind turbines for the hydrodynamic simulation experiment with NS-FVCOM. Lower panel: the difference of the near-bottom velocity between the two cases with and without the inclusion of current-wave interactions at the same time.

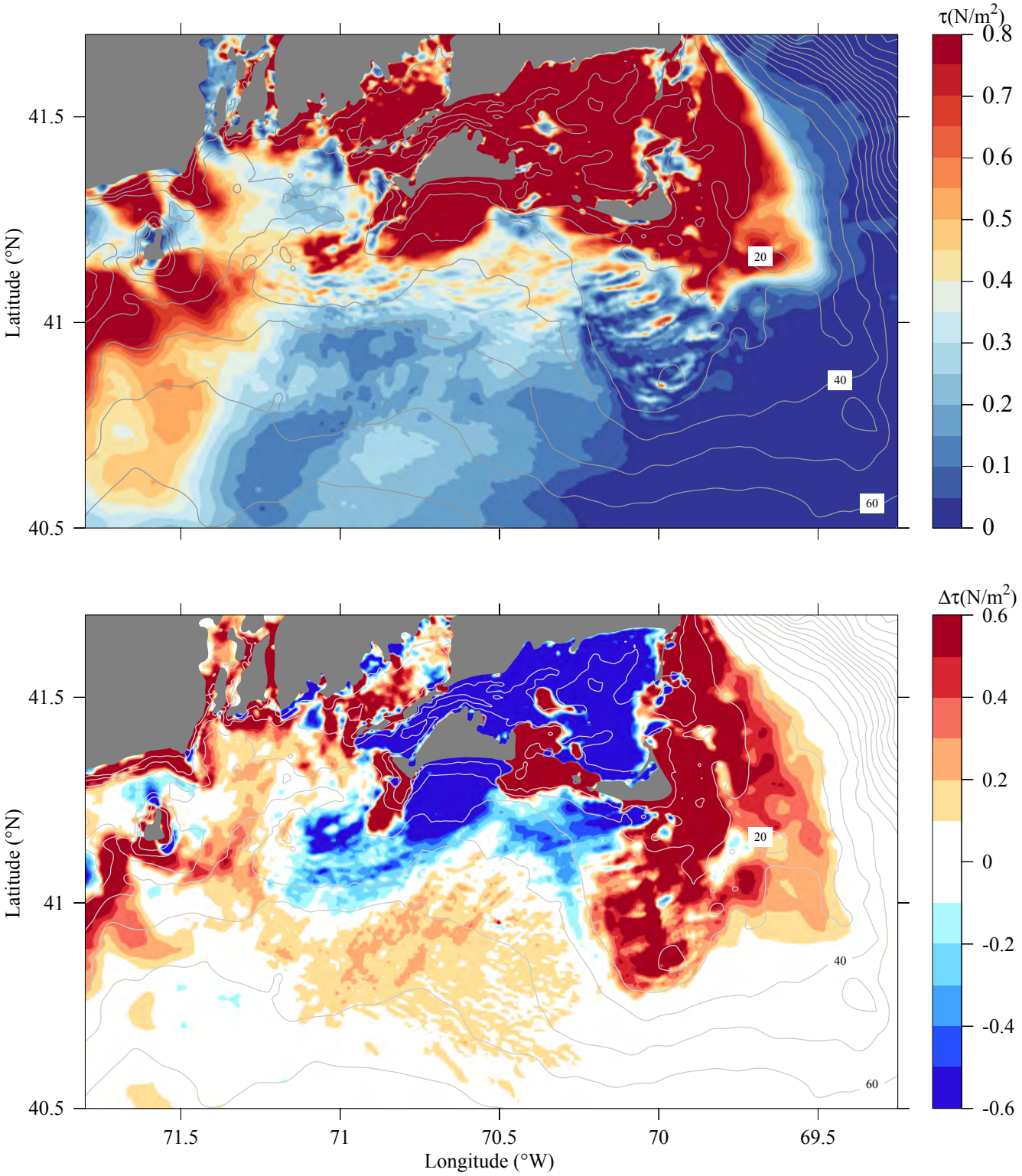

Figure 3.39: Upper panel: a snapshot of the distribution of the bottom stress over the New England Shelf at 18:00:00 GMT, August 19, 1991 under the condition without wind turbines for the hydrodynamic simulation experiment with NS-FVCOM. Lower panel: the difference of the bottom stress between the two cases with and without the inclusion of current-wave interactions at the same time.

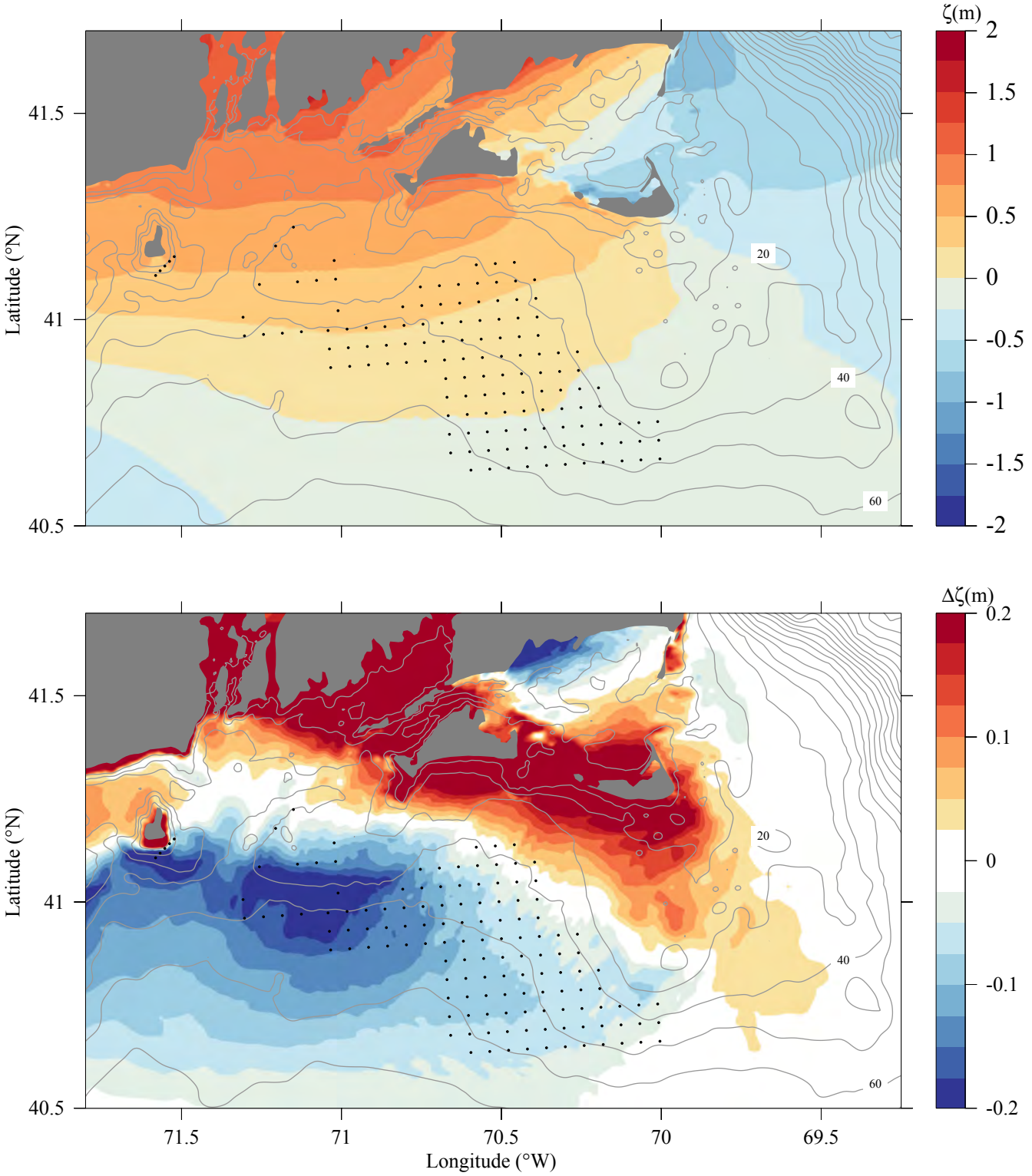

Figure 3.40: Upper panel: a snapshot of the distribution of the surface elevation over the New England Shelf at 18:00:00 GMT, August 19, 1991 under the condition with wind turbines for the hydrodynamic simulation experiment with NS-FVCOM. Lower panel: the difference of the surface elevation between the two cases with and without the inclusion of current-wave interactions at the same time.

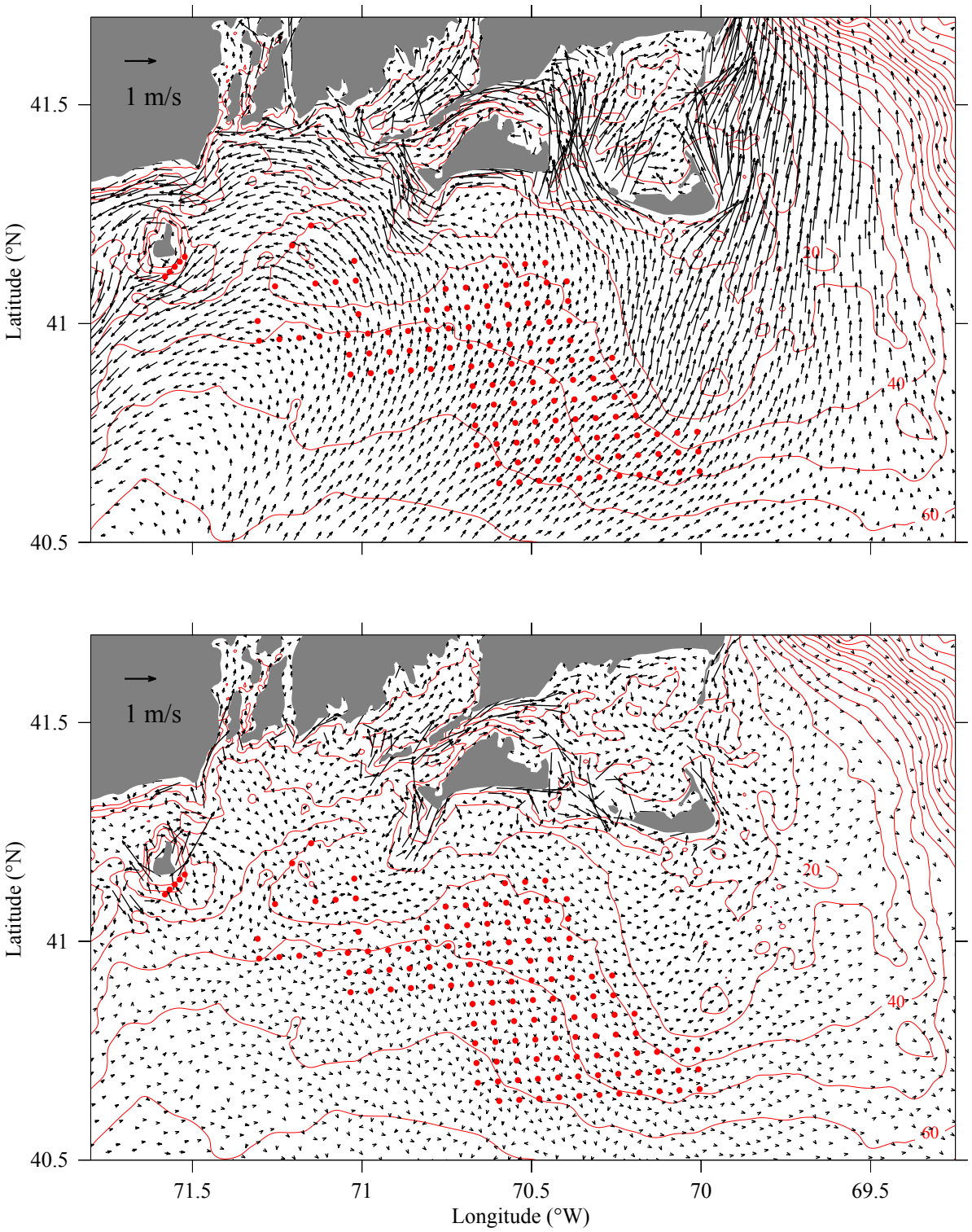

Figure 3.41: Upper panel: a snapshot of the distribution of the vertically averaged velocity over the New England Shelf at 18:00:00 GMT, August 19, 1991 under the condition with wind turbines for the hydrodynamic simulation experiment with NS-FVCOM. Lower panel: the difference of the vertically averaged velocity between the two cases with and without the inclusion of current-wave interactions at the same time.

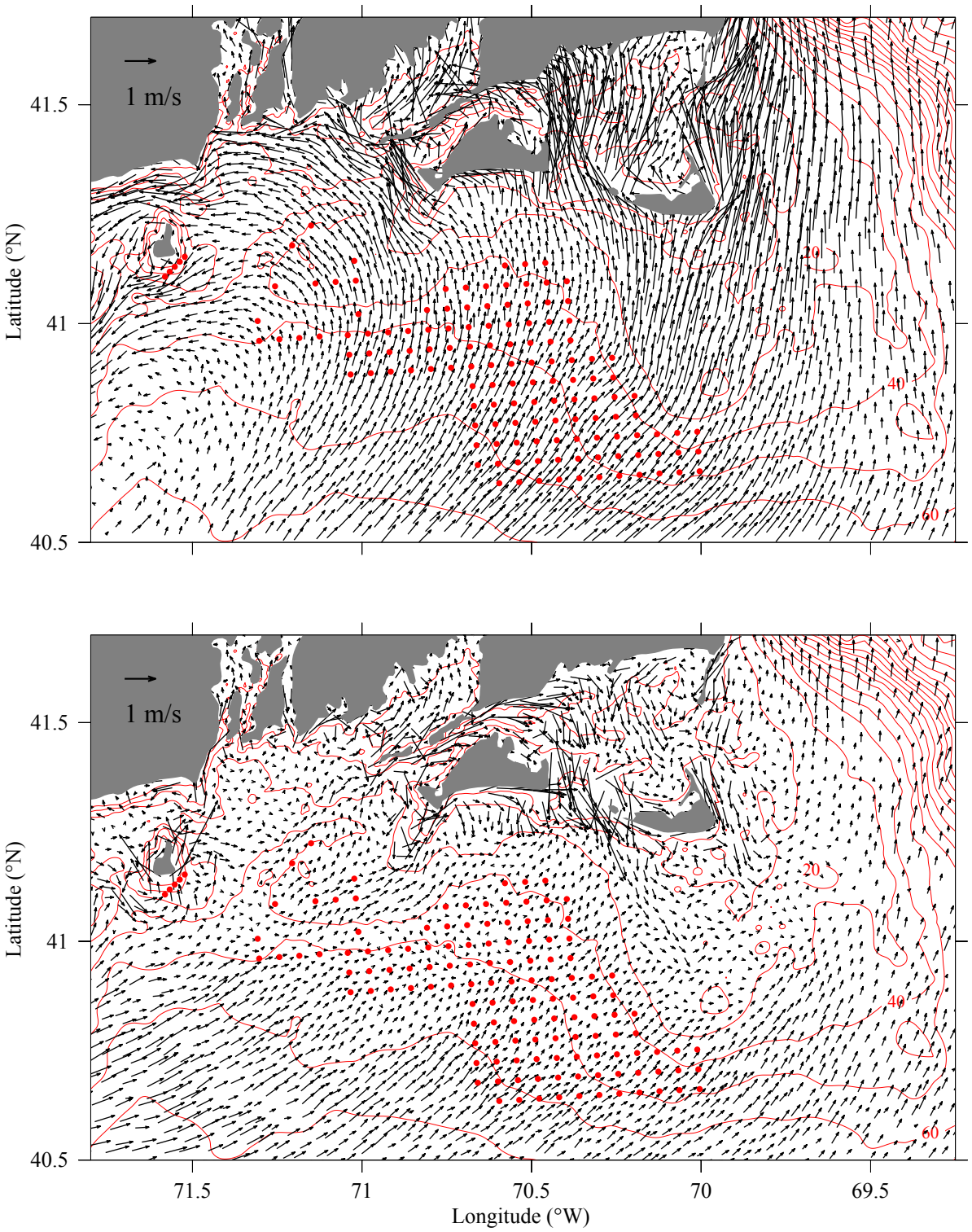

Figure 3.42: Upper panel: a snapshot of the distribution of the near-surface velocity over the New England Shelf at 18:00:00 GMT, August 19, 1991 for the hydrodynamic simulation experiment with NS-FVCOM under the condition with wind turbines. Lower panel: the difference of the near-surface velocity between the two cases with and without the inclusion of current-wave interactions at the same time.

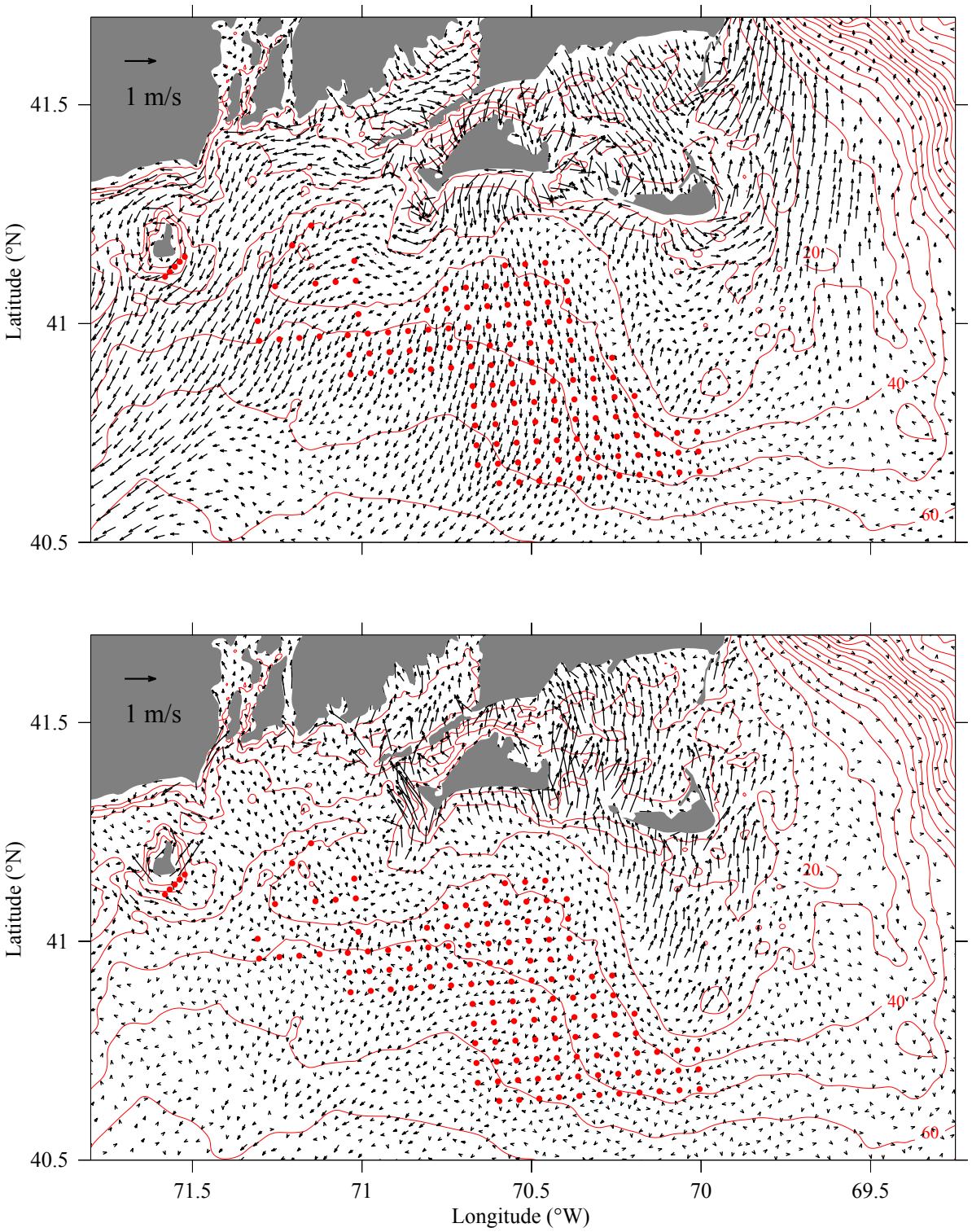

Figure 3.43: Upper panel: a snapshot of the distribution of the near-bottom velocity over the New England Shelf at 18:00:00 GMT, August 19, 1991 under the condition with wind turbines for the hydrodynamic simulation experiment with NS-FVCOM. Lower panel: the difference of the near-bottom velocity between the two cases with and without the inclusion of current-wave interactions at the same time.

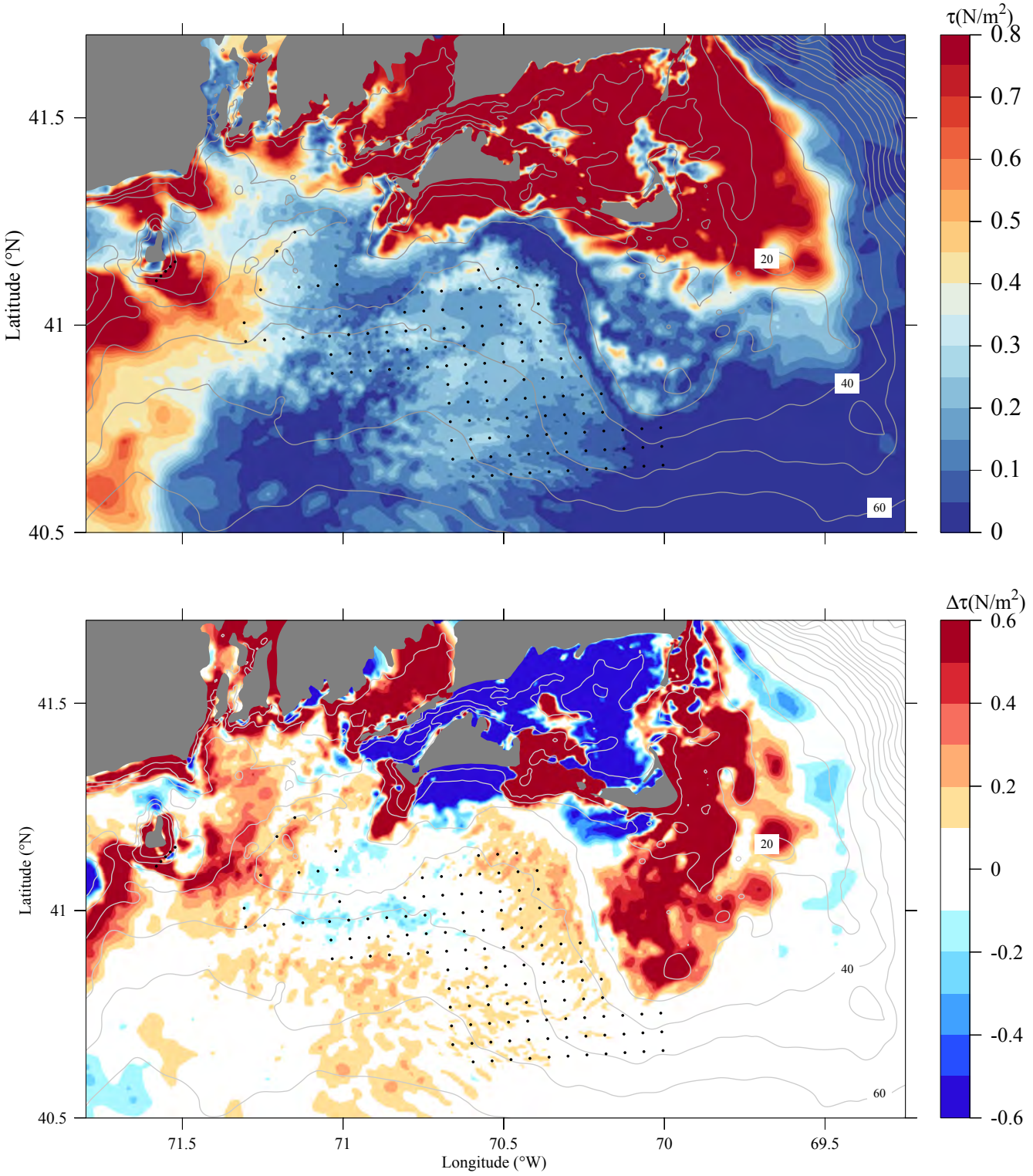

Figure 3.44: Upper panel: a snapshot of the distribution of the bottom stress over the New England Shelf at 18:00:00 GMT, August 19, 1991 under the condition with wind turbines for the hydrodynamic simulation experiment with NS-FVCOM. Lower panel: the difference of the bottom stress between the two cases with and without the inclusion of current-wave interactions at the same time.

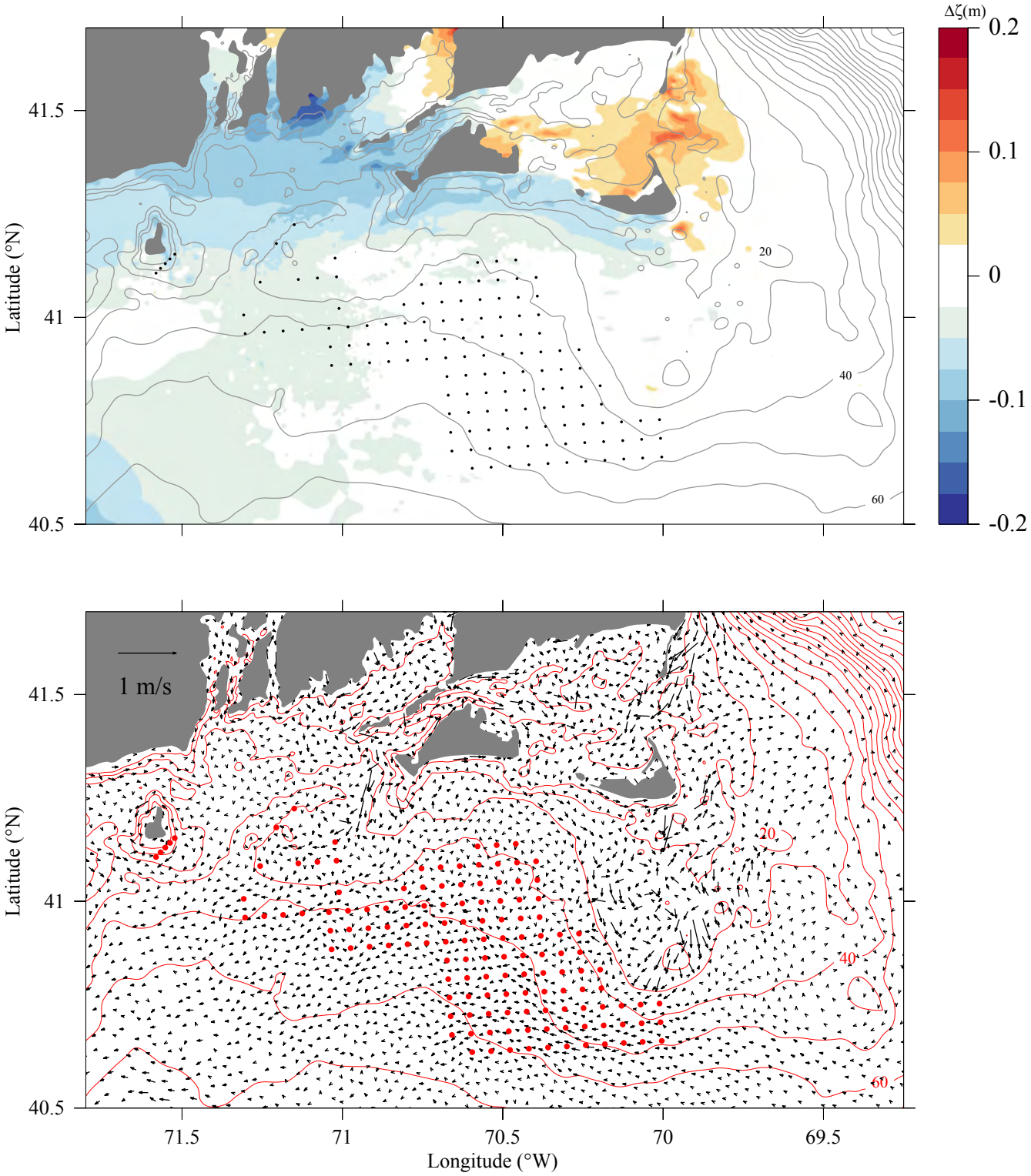

Figure 3.45: Differences of the sea surface (upper) and vertically averaged velocity vectors between the two cases with and without the inclusion of proposed offshore wind turbines at 18:00:00 GMT, August 19, 1991 for the hydrodynamic simulation experiment with NS-FVCOM.

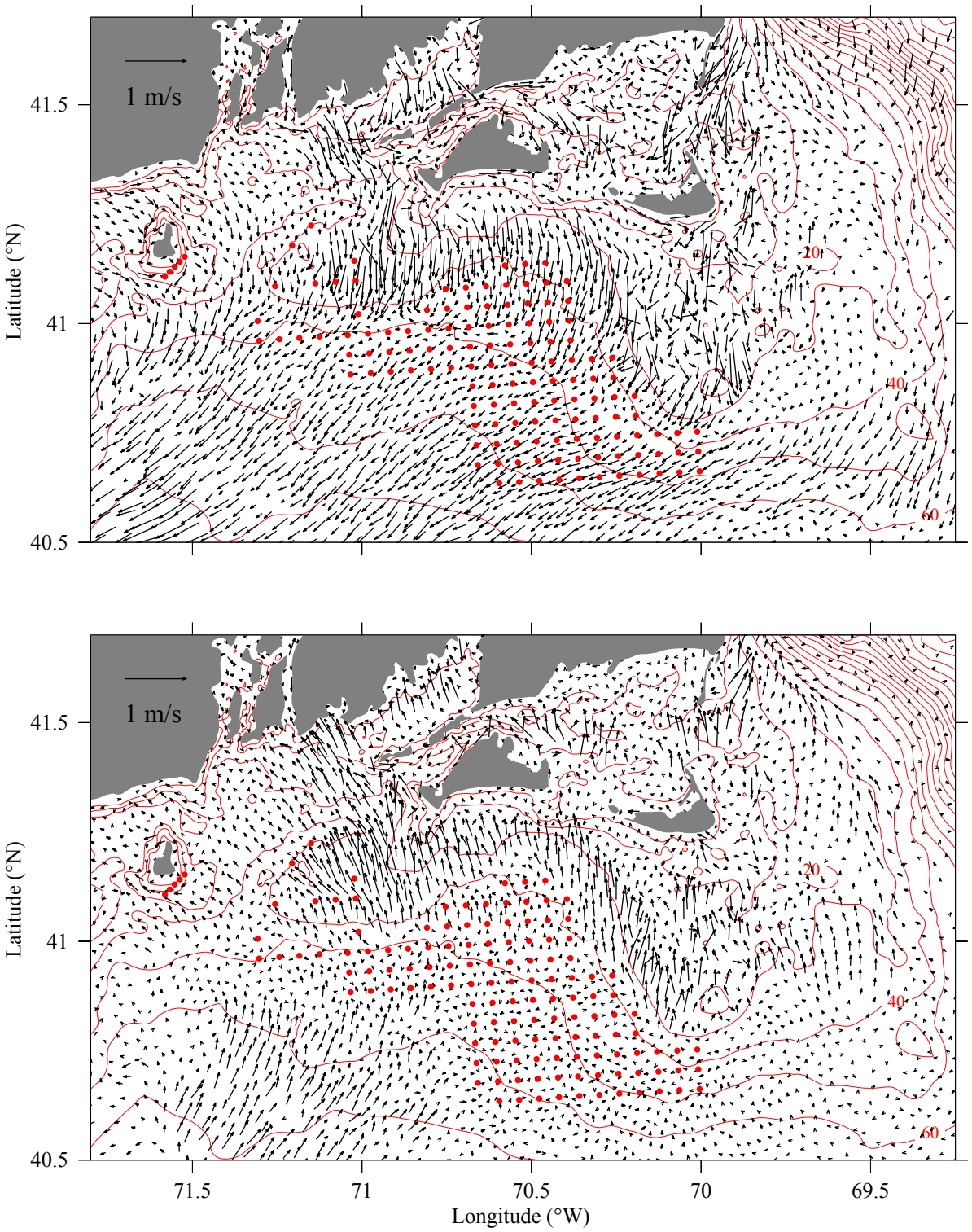

Figure 3.46: Differences of the near-surface and near-bottom velocities between the two cases with and without the inclusion of proposed offshore wind turbines at 18:00:00 GMT, August 19, 1991 for the hydrodynamic simulation experiment with NS-FVCOM.

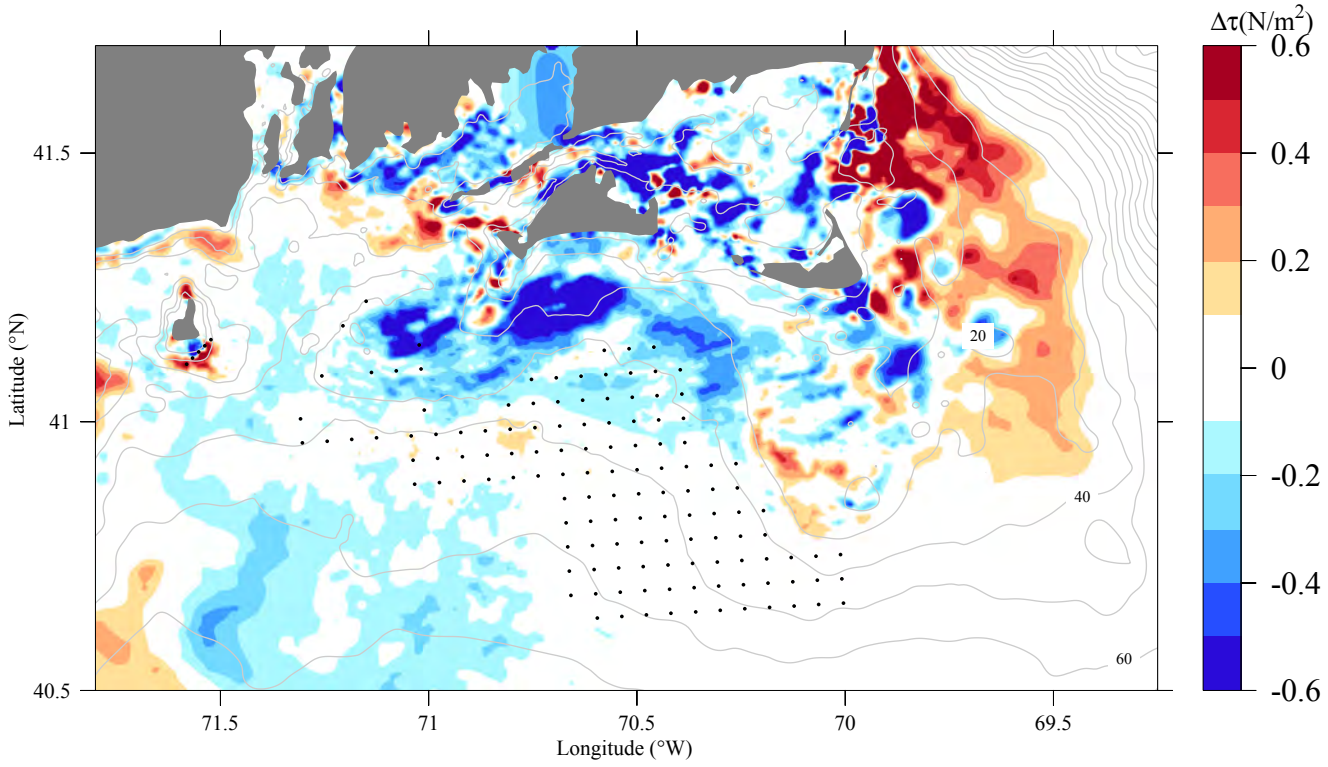

Figure 3.47: Difference of the bottom stress between the two cases under the conditions with and without wind turbines at 18:00:00 GMT, August 19, 1991 for the hydrodynamic simulation with NS-FVCOM.

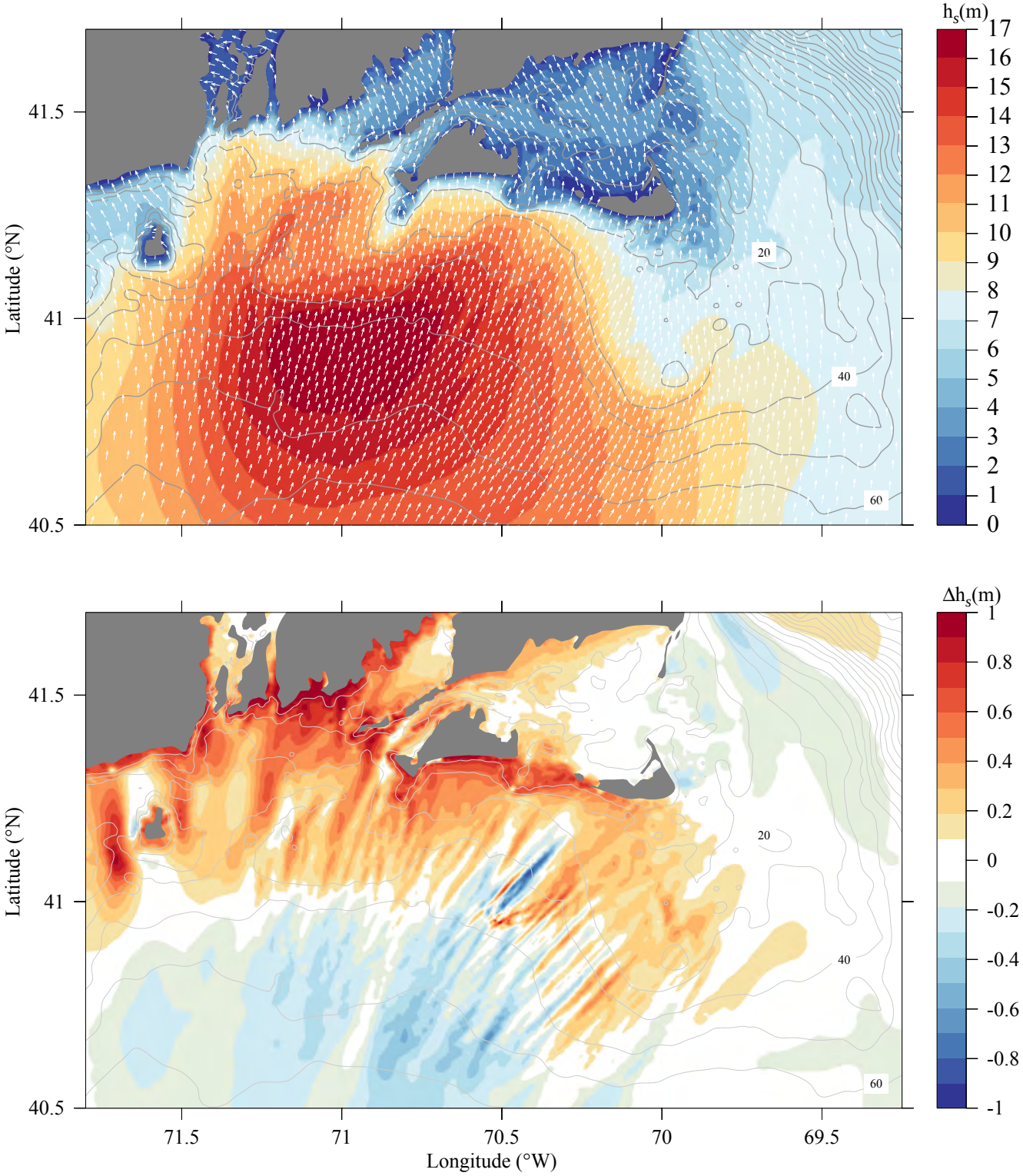

Figure 3.48: Upper panel: a snapshot of the distribution of the significant wave height over the New England Shelf at 18:00:00 GMT, August 19, 1991 under the condition without wind turbines for the surface wave simulation experiment with NS-SWAVE. Lower panel: the difference of the significant wave height between the two cases with and without the inclusion of current-wave interactions at the same time.

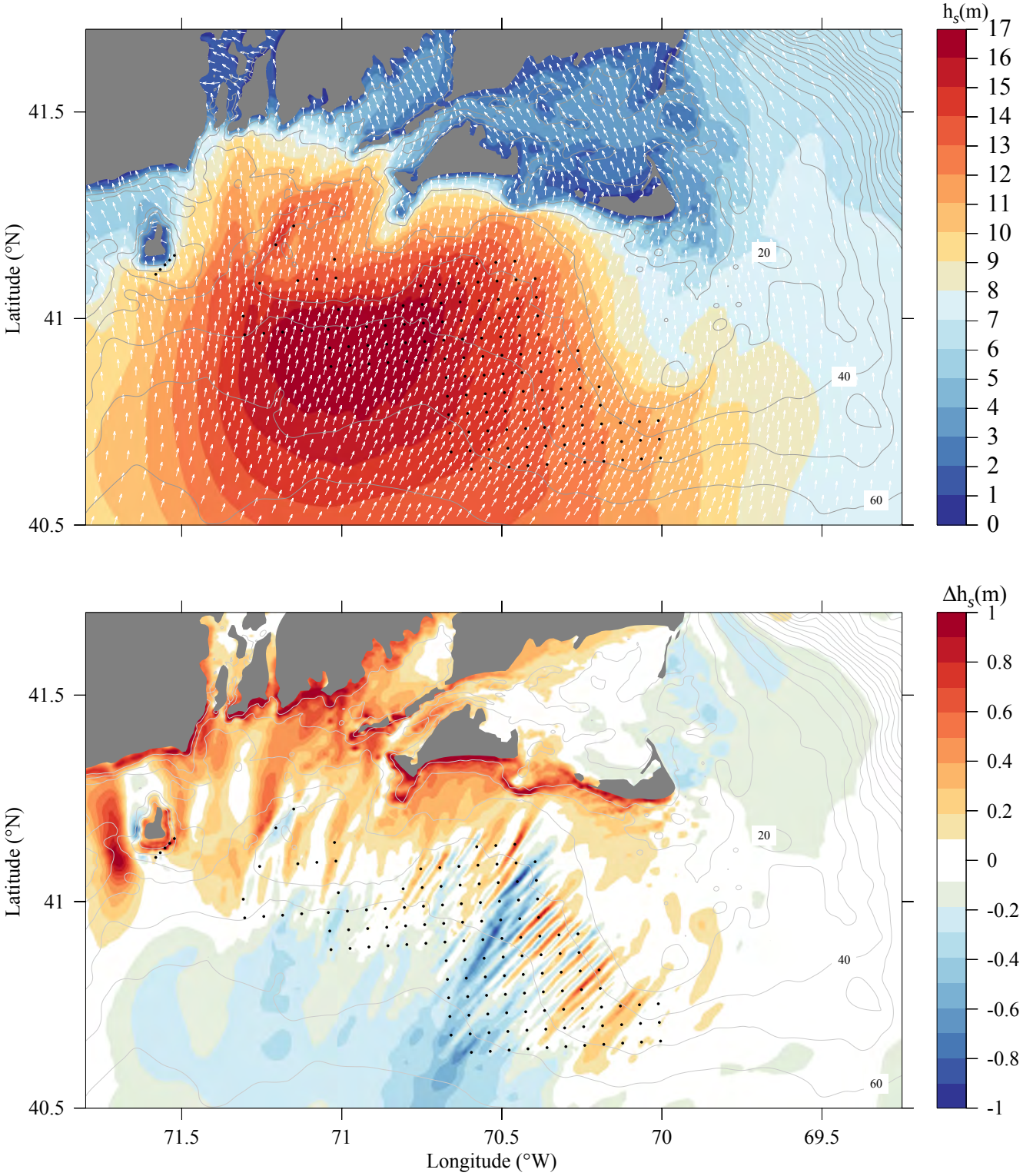

Figure 3.49: Upper panel: a snapshot of the distribution of the significant wave height over the New England Shelf at 18:00:00 GMT, August 19, 1991 under the condition with wind turbines for the surface wave simulation experiment with NS-SWAVE. Lower panel: the difference of the significant wave height between the two cases with and without the inclusion of current-wave interactions at the same time.

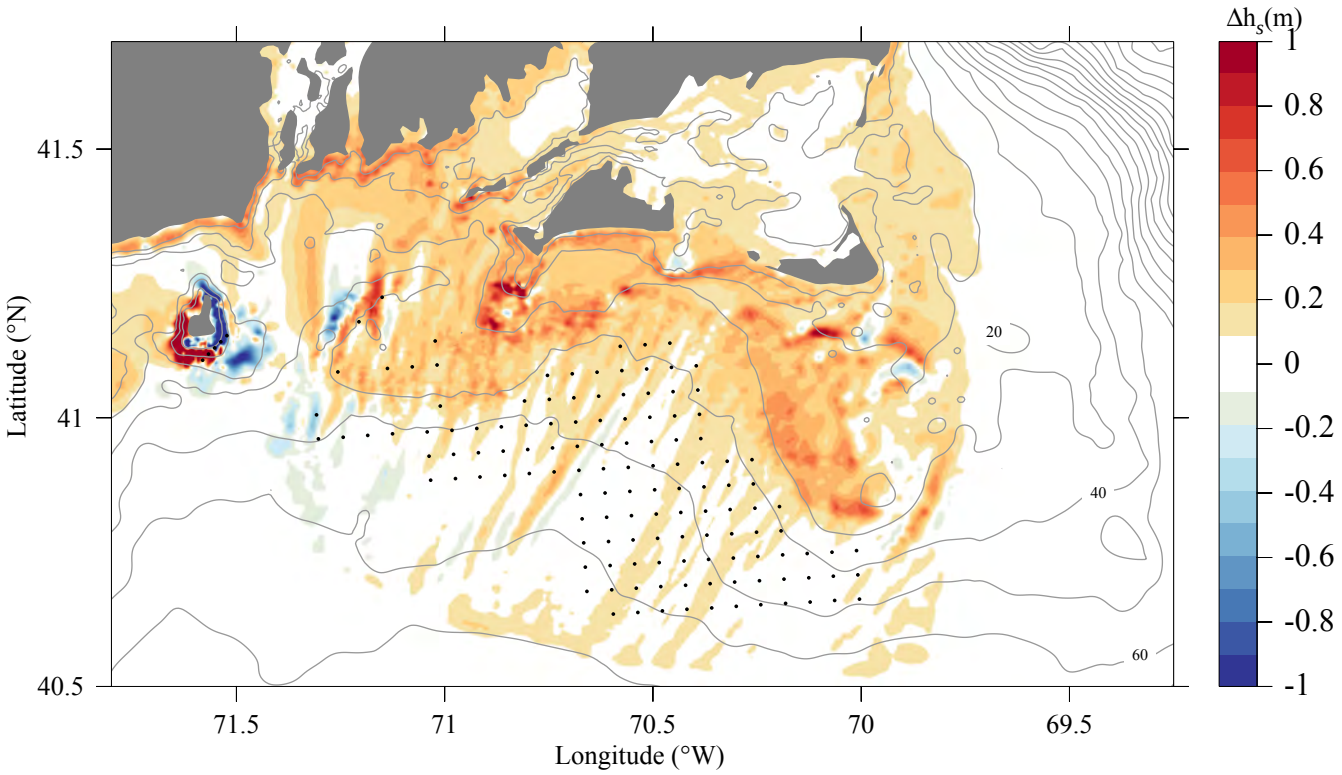

Figure 3.50: A snapshot of the distribution of the difference in significant wave height over the New England Shelf at 18:00:00 GMT, August 19, 1991 under the conditions with and without wind turbines for the surface wave simulation experiments with NS-SWAVE.

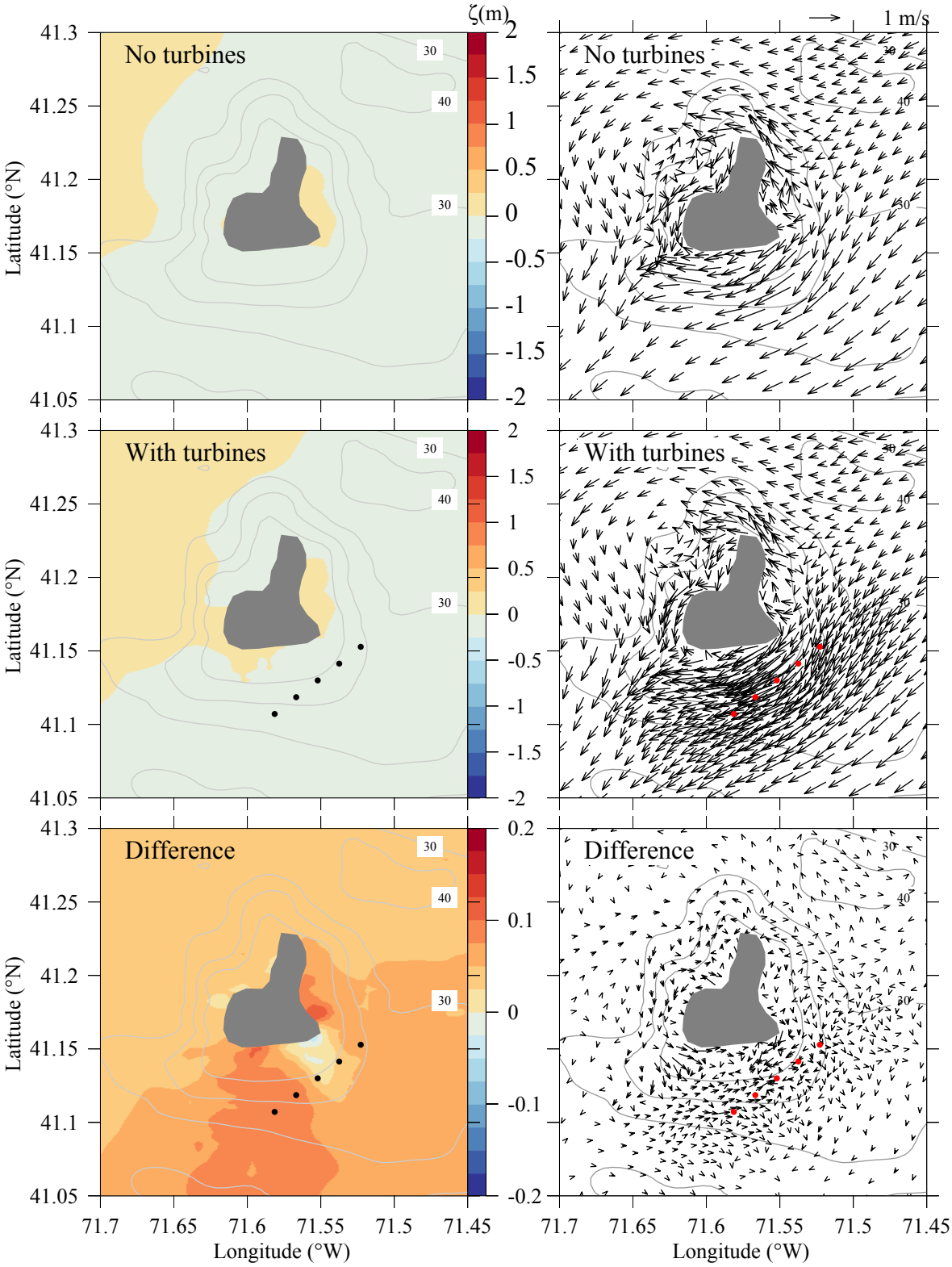

Figure 3.51: Snapshots of the distributions of the surface elevation, vertically averaged velocity, and differences over the New England Shelf at 03:00:00 February 7 1978 under the conditions without and with wind turbines for the experiment with the inclusion of wave-current interactions.

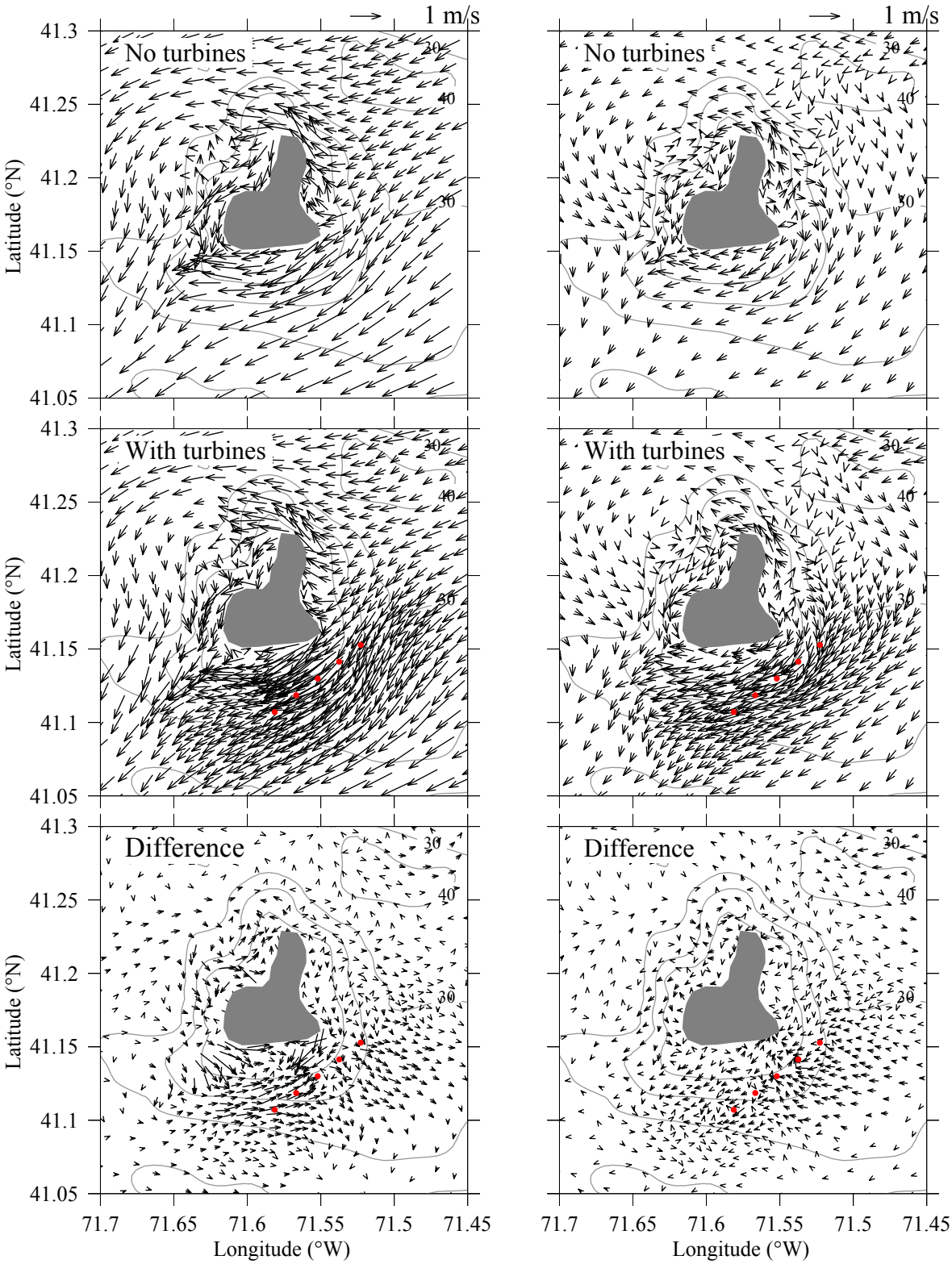

Figure 3.52: Snapshots of the distributions of the near-surface (left) and near-bottom (right) velocities and differences over the New England Shelf at 03:00:00 GMT, February 7, 1978 under the conditions without and with wind turbines for the experiment with the inclusion of wave-current interactions.

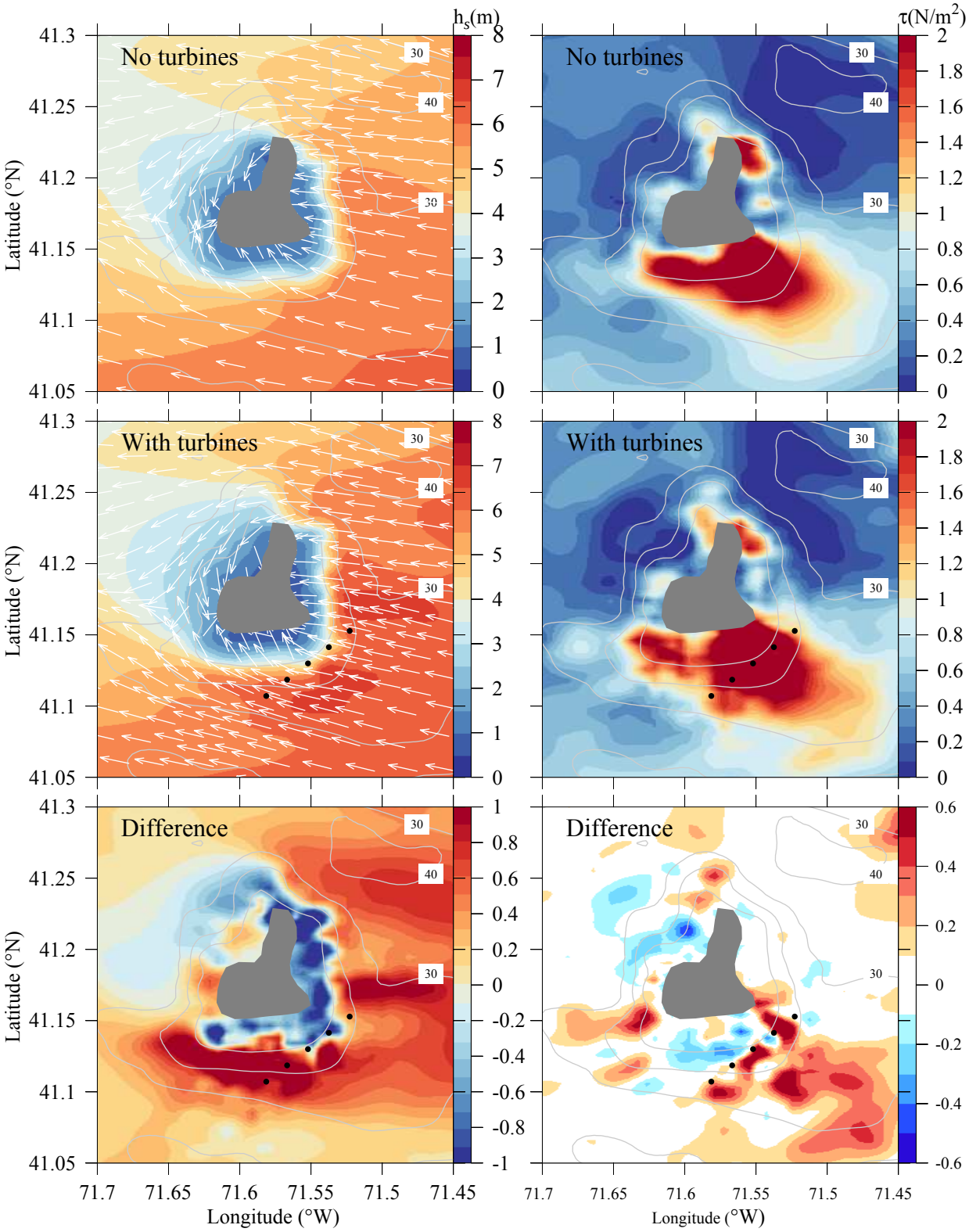

Figure 3.53: Snapshots of the distributions of the significant wave height, bottom stress and difference over the New England Shelf at 03:00:00 GMT, February 7, 1978 for the cases without and with the inclusion of proposed offshore wind turbines.

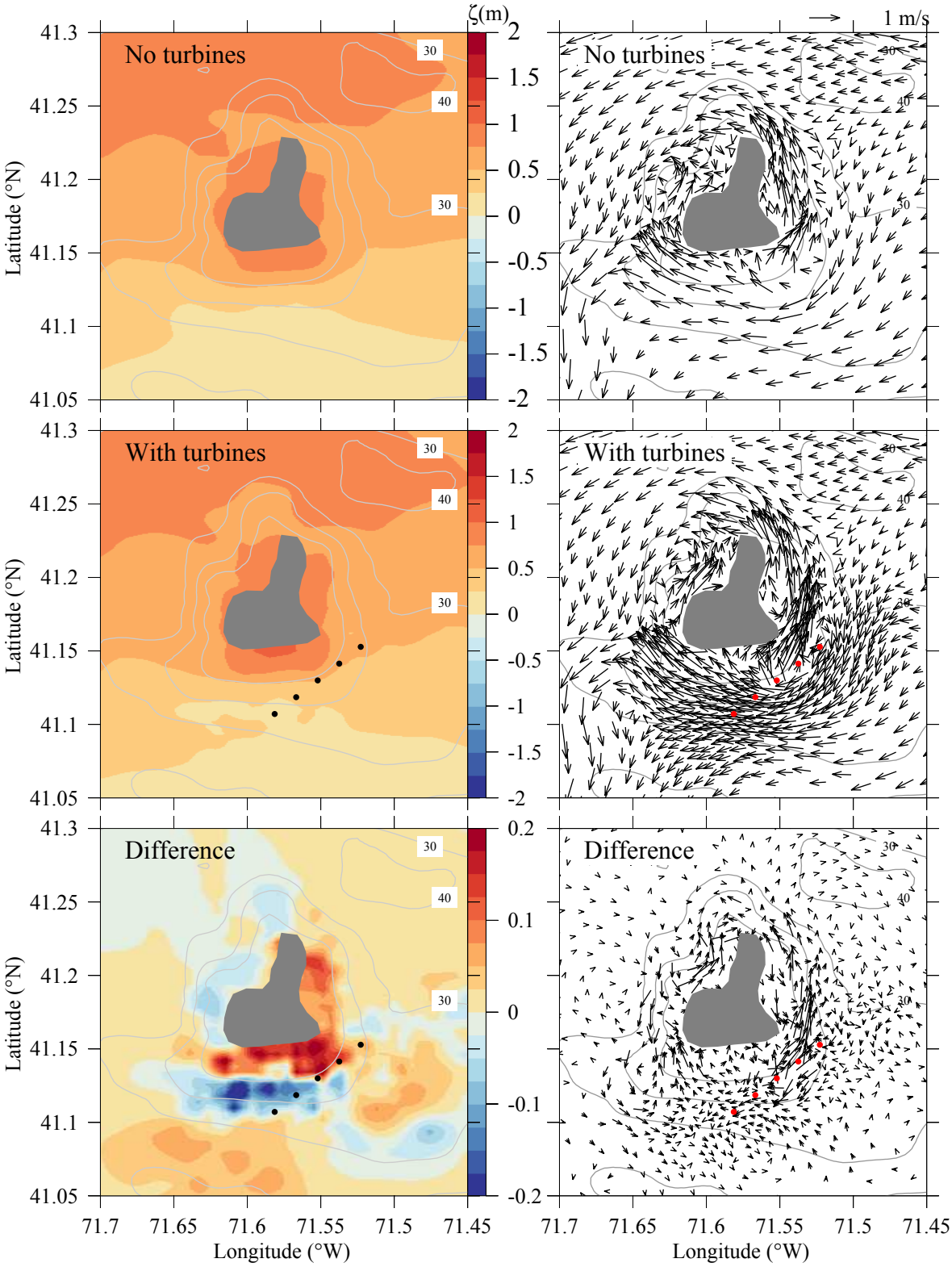

Figure 3.54: Snapshots of the distributions of the surface elevation, vertically averaged velocity and differences over the New England Shelf at 18:00:00 August 19 1991 under the conditions without and with wind turbines for the experiment with the inclusion of wave-current interactions.

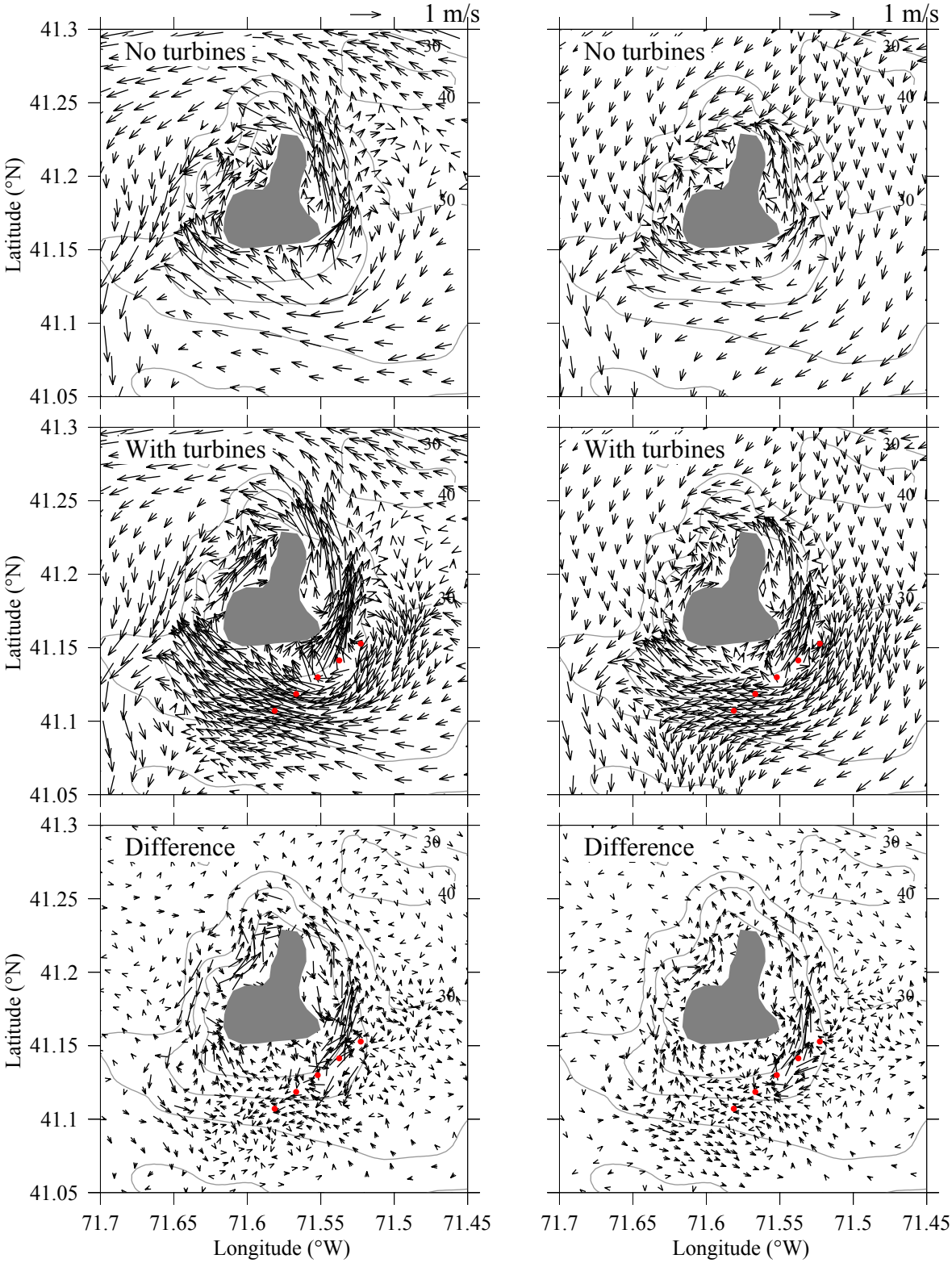

Figure 3.55: Snapshots of the distributions of the near-surface (left) and near-bottom (right) velocities and differences over the New England Shelf at 18:00:00 GMT, August 19, 1991 under the conditions without and with wind turbines for the experiment with the inclusion of wave-current interactions.

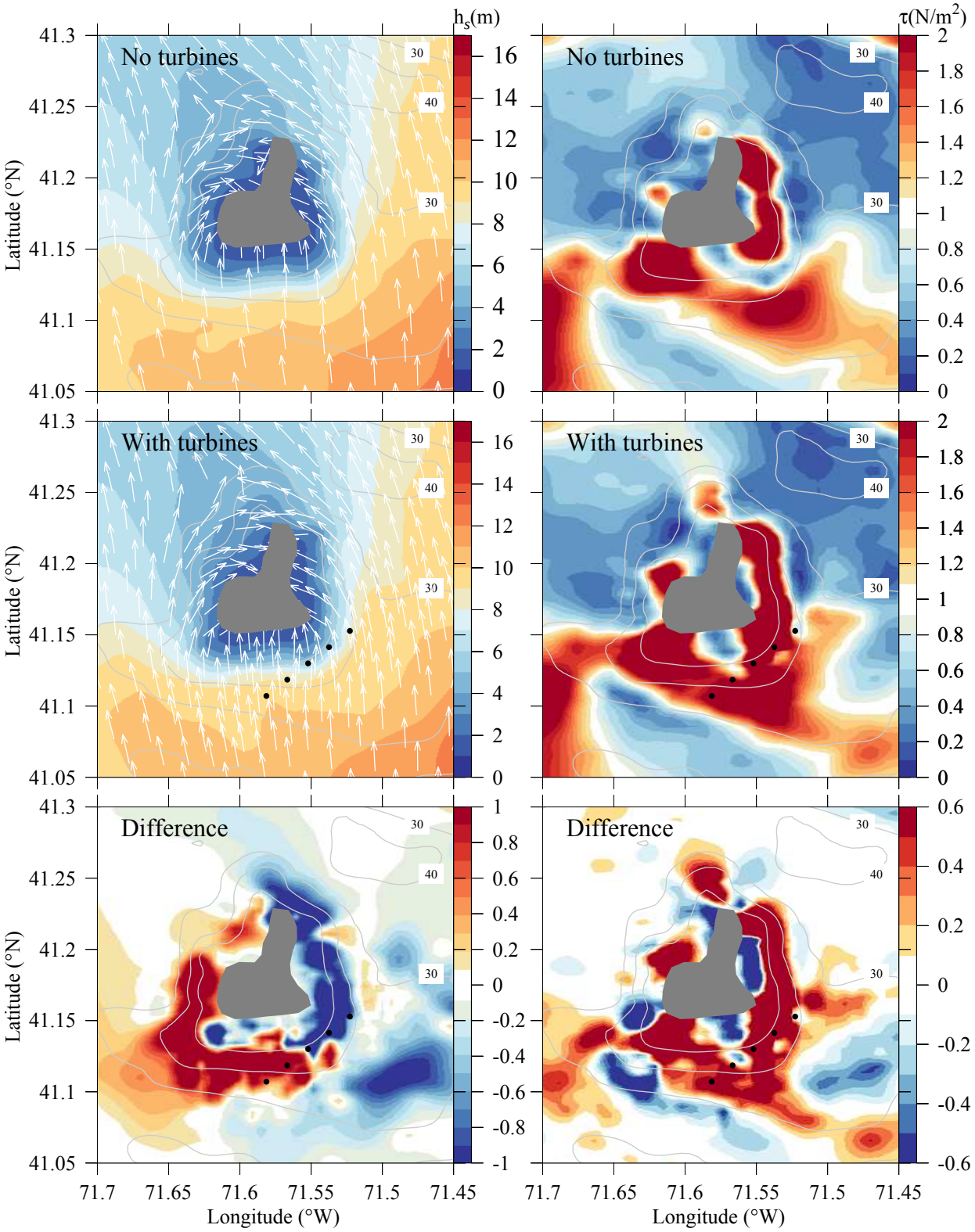

Figure 3.56: Snapshots of the distributions of the significant wave height, bottom stress and difference over the New England Shelf at 18:00:00 GMT, August 19, 1991 under the conditions without and with wind turbines for the experiment with the inclusion of wave-current interactions.

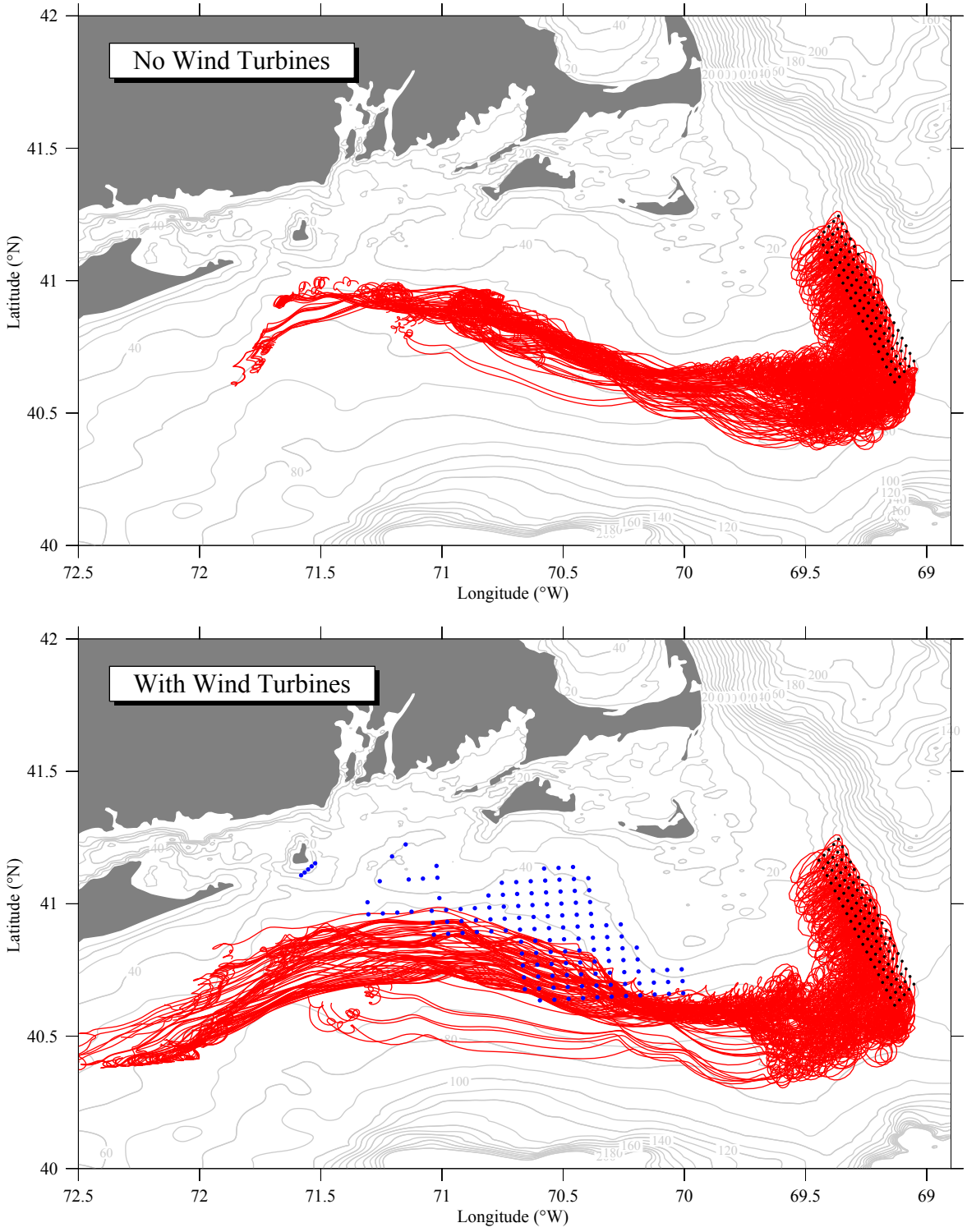

Figure 3.57: Model-predicted trajectories of particles for the cases without (upper) and with (lower) wind turbines. A total of 100 particles were released with separate scales of 1.4 km in the east-west direction and 3.2 km in the south-north direction over the western slope of the Great South Channel.
The tracking period: 00:00:00 GMT, February 1 to 00:00:00 GMT, February 11, 1978. Black dots are the locations where the particles were released.

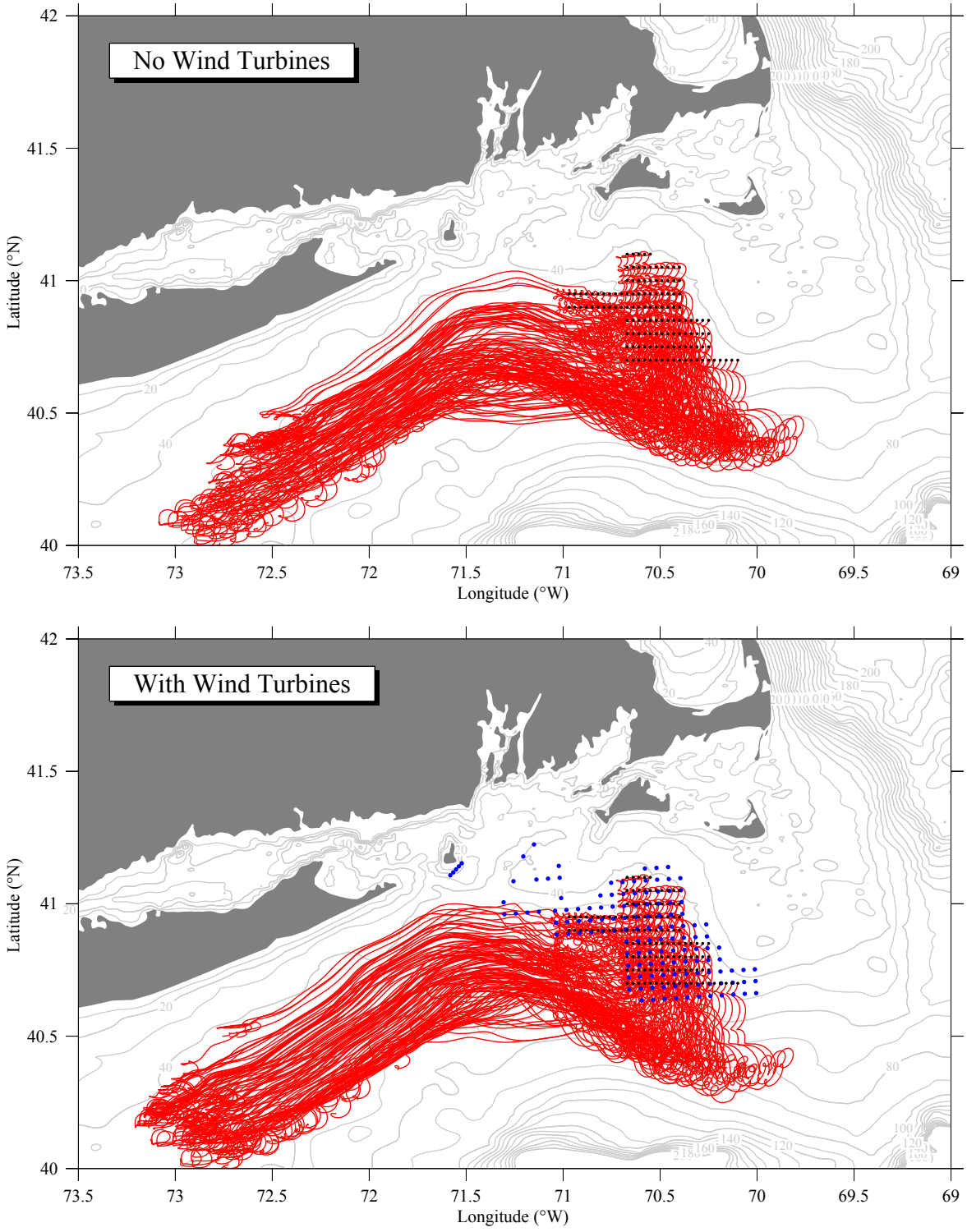

Fig. 3.58: Model-predicted trajectories of particles for the cases without (upper) and with (lower) wind turbines. In the wind turbine case, A total of 100 particles were released with separate scales of 2.5 km in the east-west direction and 5.5 km in the south-north direction within the wind turbine area. In the case without wind turbines, the same number of particles were released at the same locations. The tracking period: 00:00:00 GMT, February 1 to 00:00:00 GMT, February 11, 1978.

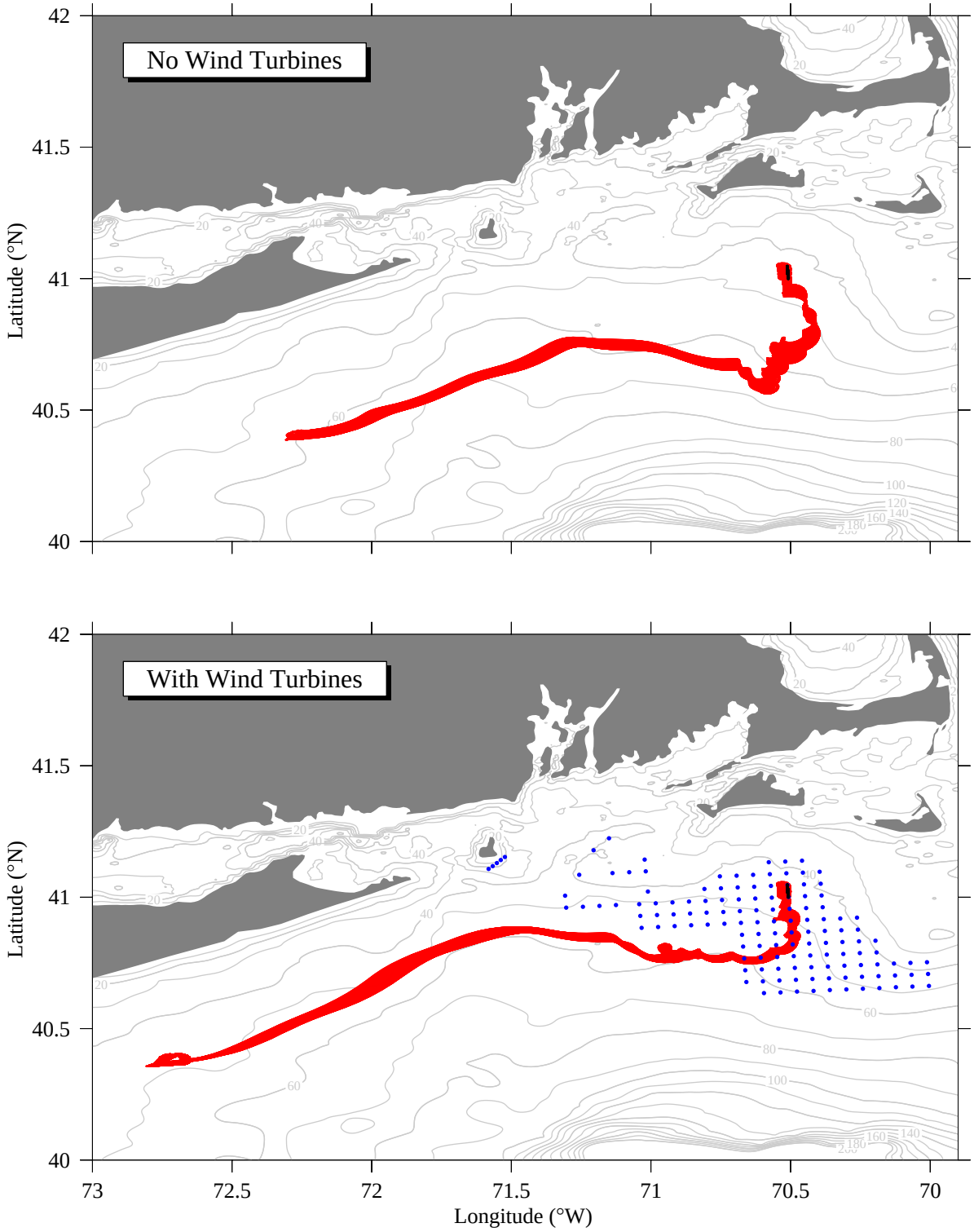

Figure 3.59: Model-predicted trajectories of the particles for the cases without (upper) and with (lower) wind turbines. In the wind turbine case, a total of 210 particles were released with a separation scale of 50 m on two lines east and west of a selected wind turbine, respectively. The same locations were selected in the case without wind turbines. Tracking period: 00:00:00 GMT, February 1 to 00:00:00 GMT, February 11, 1978

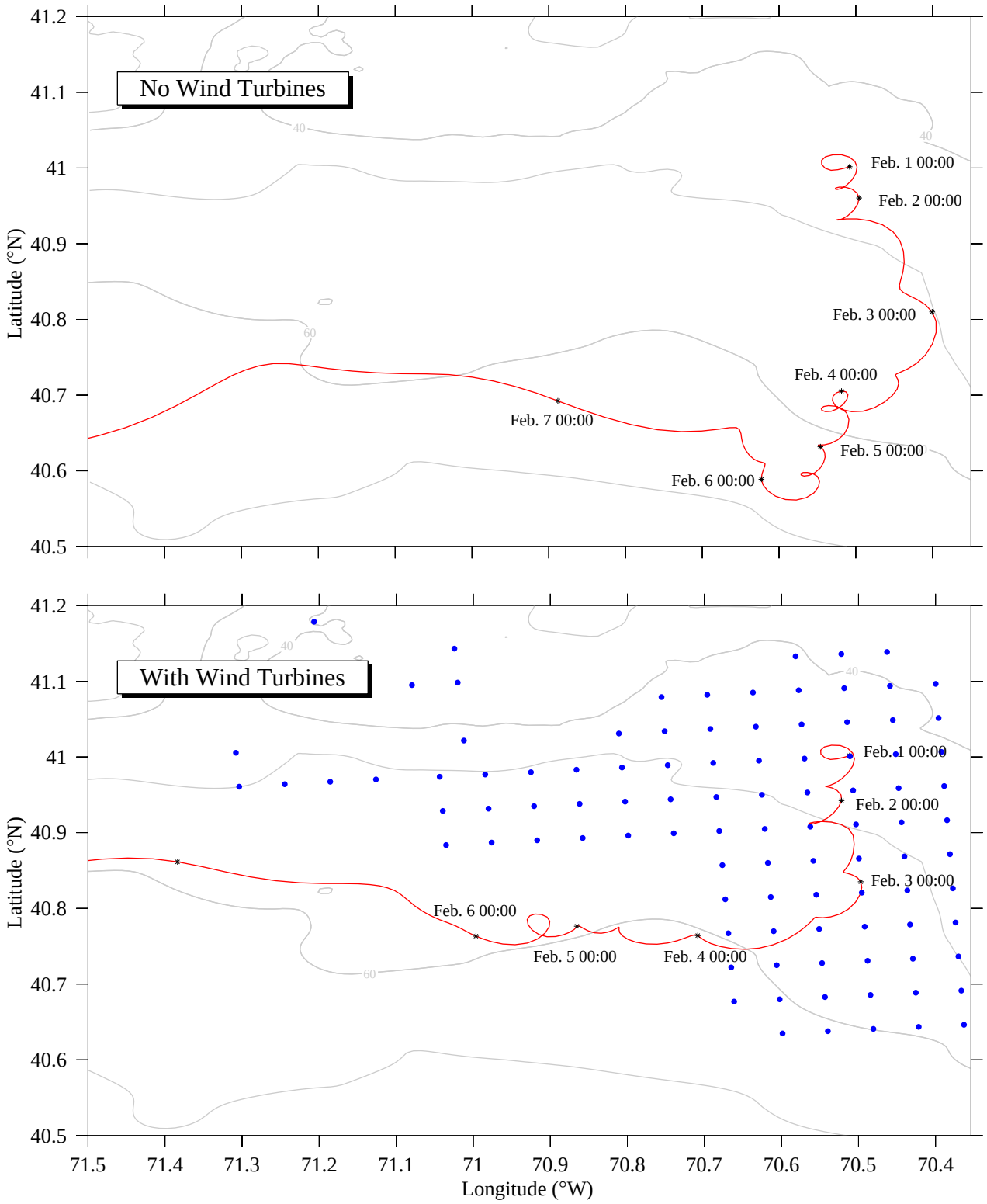

Figure 3.60: An enlarged view of a selected particle released in the case shown in Fig. 3.59. Symbol "*" is the daily location. Upper: no wind turbines. Lower: with wind turbines.

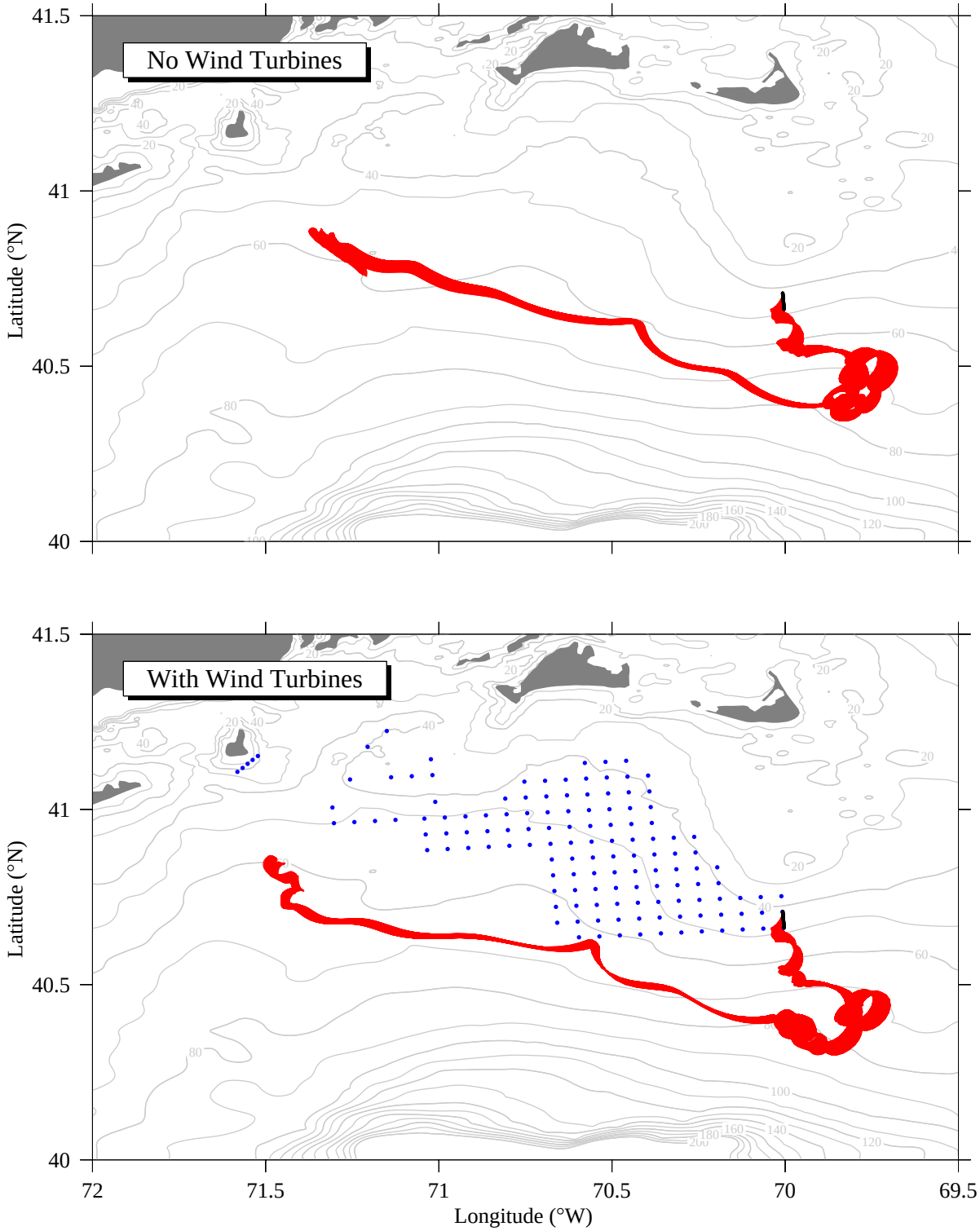

Figure 3.61: Model-predicted trajectories of the particles for the cases without (upper) and with (lower) wind turbines. In the wind turbine case, a total of 210 particles were released with a separation scale of 50 m on two lines east and west of a selected wind turbine shown in the figure. Tracking period: 00:00:00 GMT, February 1 to 00:00:00 GMT, February 11, 1978.

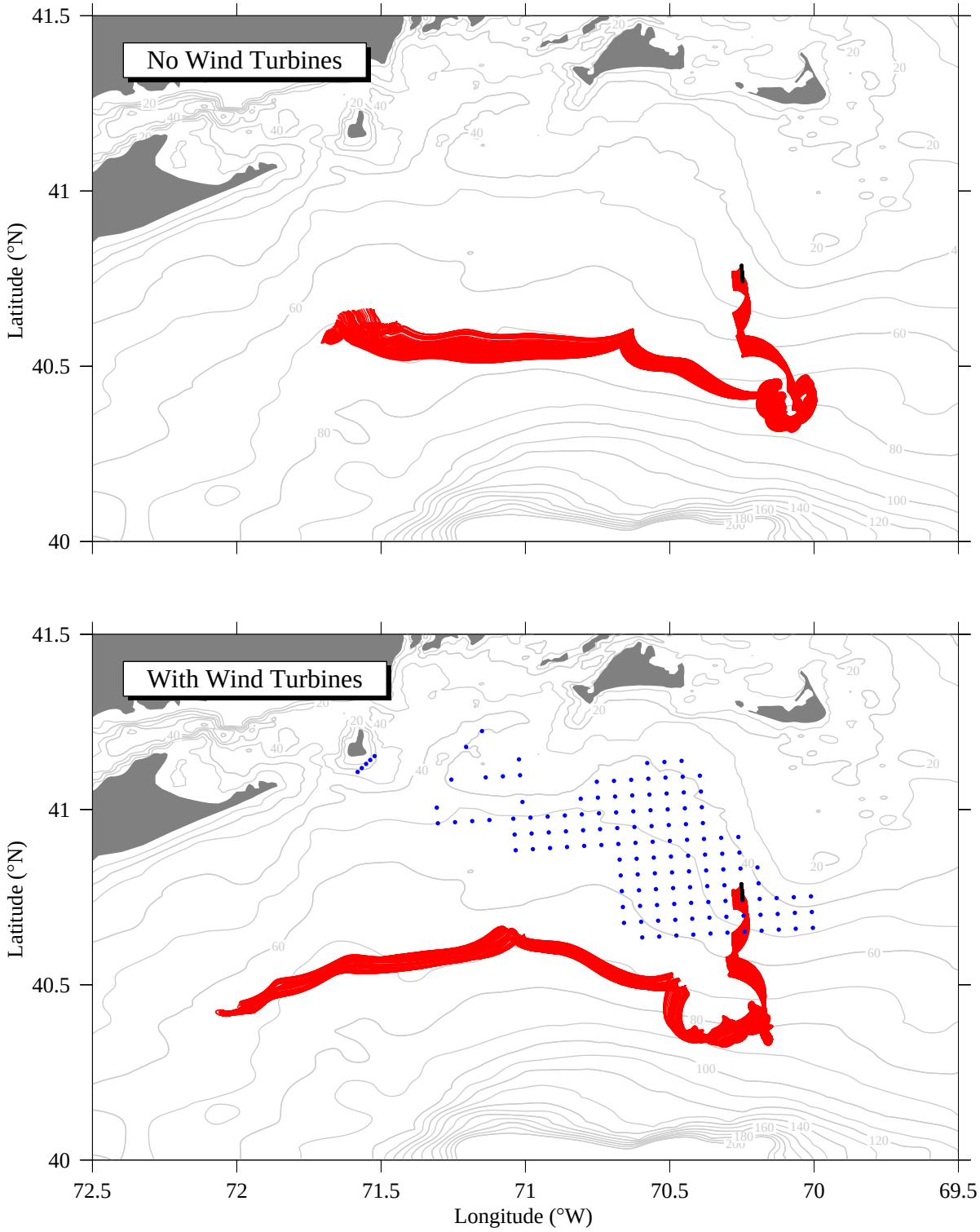

Figure 3.62: Model-predicted trajectories of the particles for the cases without (upper) and with (lower) wind turbines. In the wind turbine case, a total of 210 particles were released with a spatial separation scale of 50 m between two individual particles and from the distance related to the selected turbine on two lines east and west of a wind turbine shown in the figure. In the case without wind turbines, the number and location of particles remained the same. Tracking period: 00:00:00 GMT, February 1 to 00:00:00 GMT, February 11, 1978.

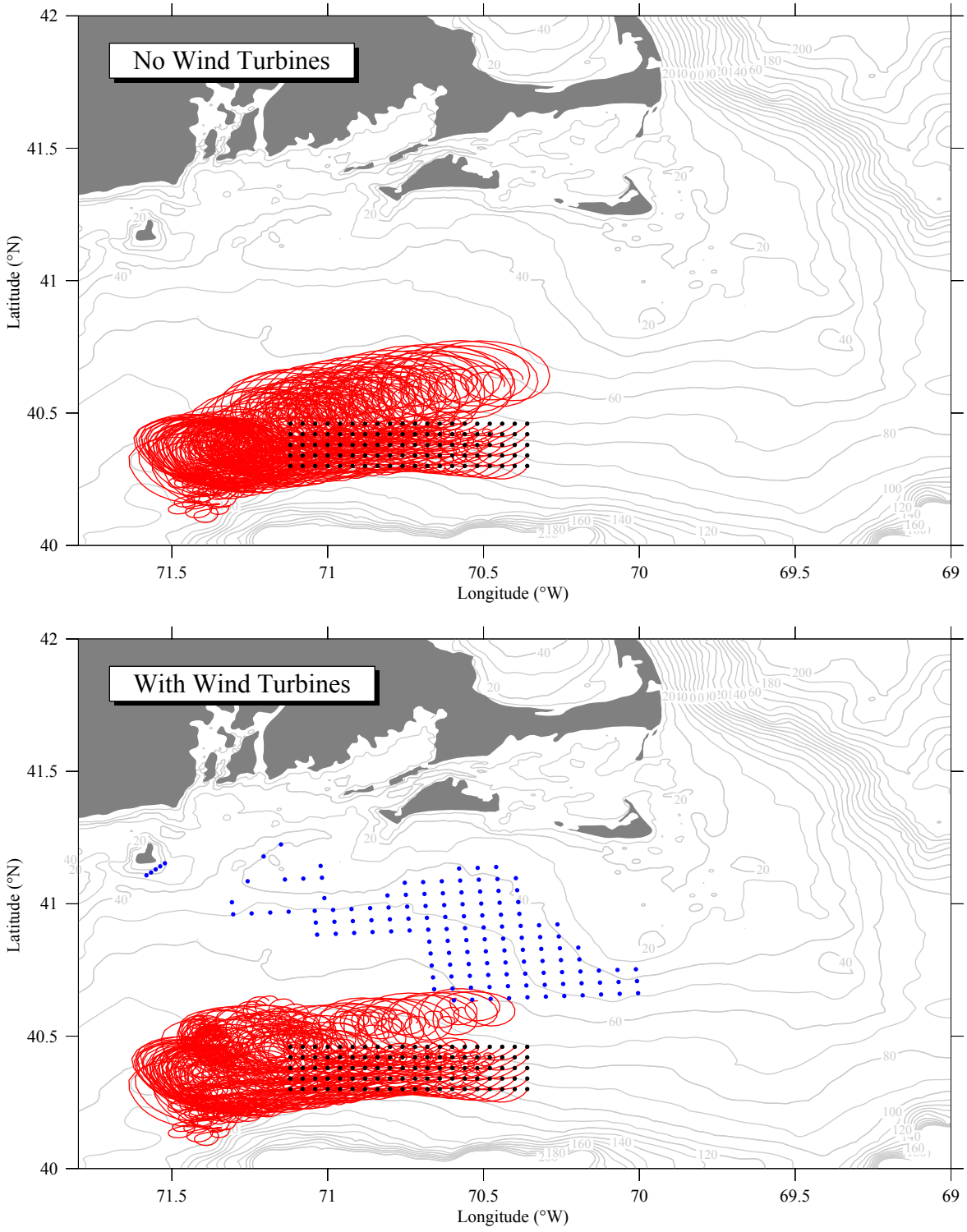

Figure 3.63: Trajectories of particles during the August 1991 Hurricane Bob period for the cases without (upper) and with (lower) wind turbines. In this case, a total of 100 particles were released with separation scales of 3.4 km in the east-west direction and 4.4 km in the north-south direction over the outer shelf region outside the wind turbine area. The tracking period: 00:00:00 GMT, August 16 to 00:00:00 GMT, August 21.

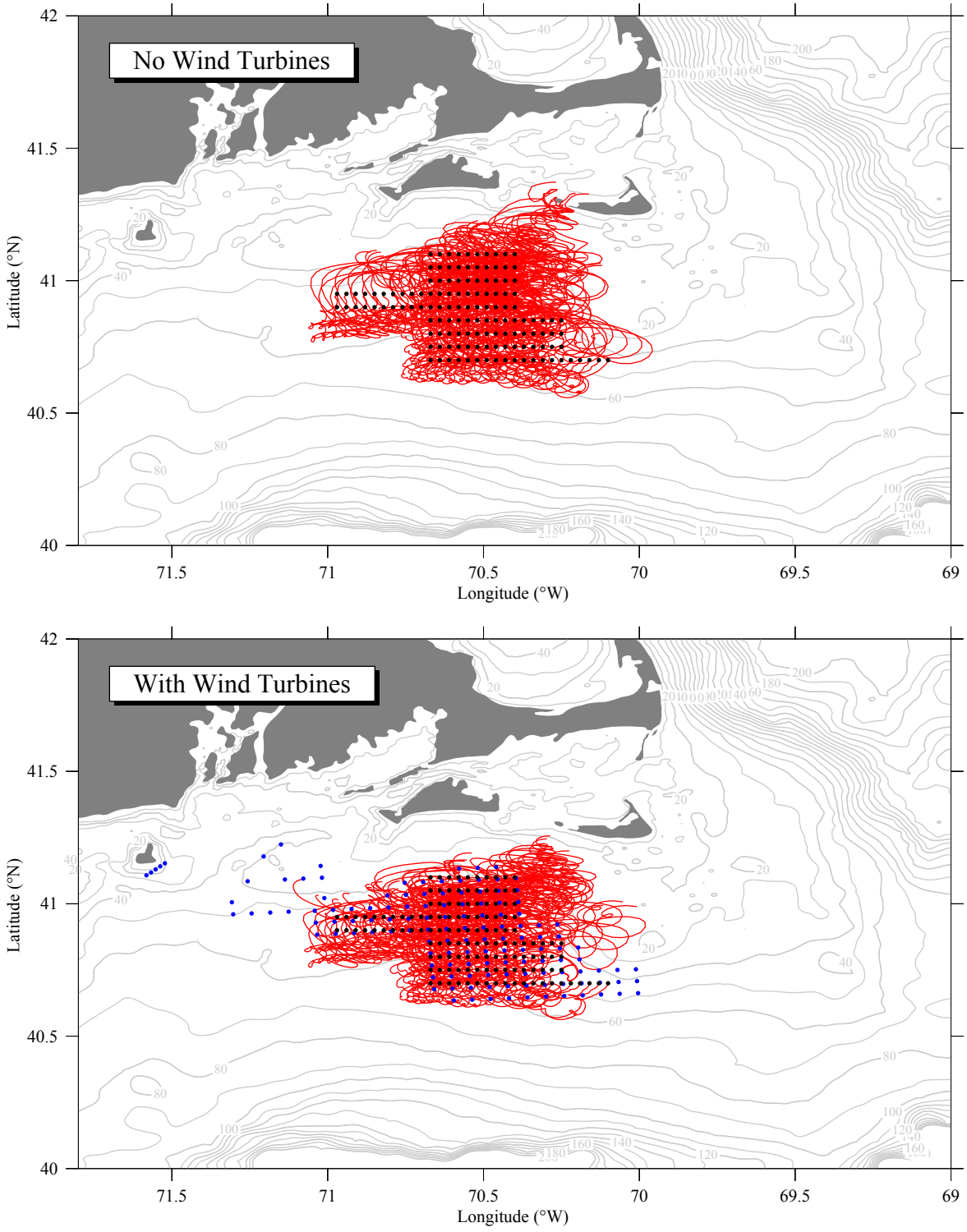

Figure 3.64: Trajectories of particles during the August 1991 Hurricane Bob period for the cases without (upper) and with (lower) wind turbines. In this case, a total of 100 particles were released with spatial separation scales of 2.5 km in th east-west direction and 5.5 km in the south-north direction within the wind turbine area. The tracking period: 00:00:00 GMT, August 16 to 00:00:00 GMT, August 21.

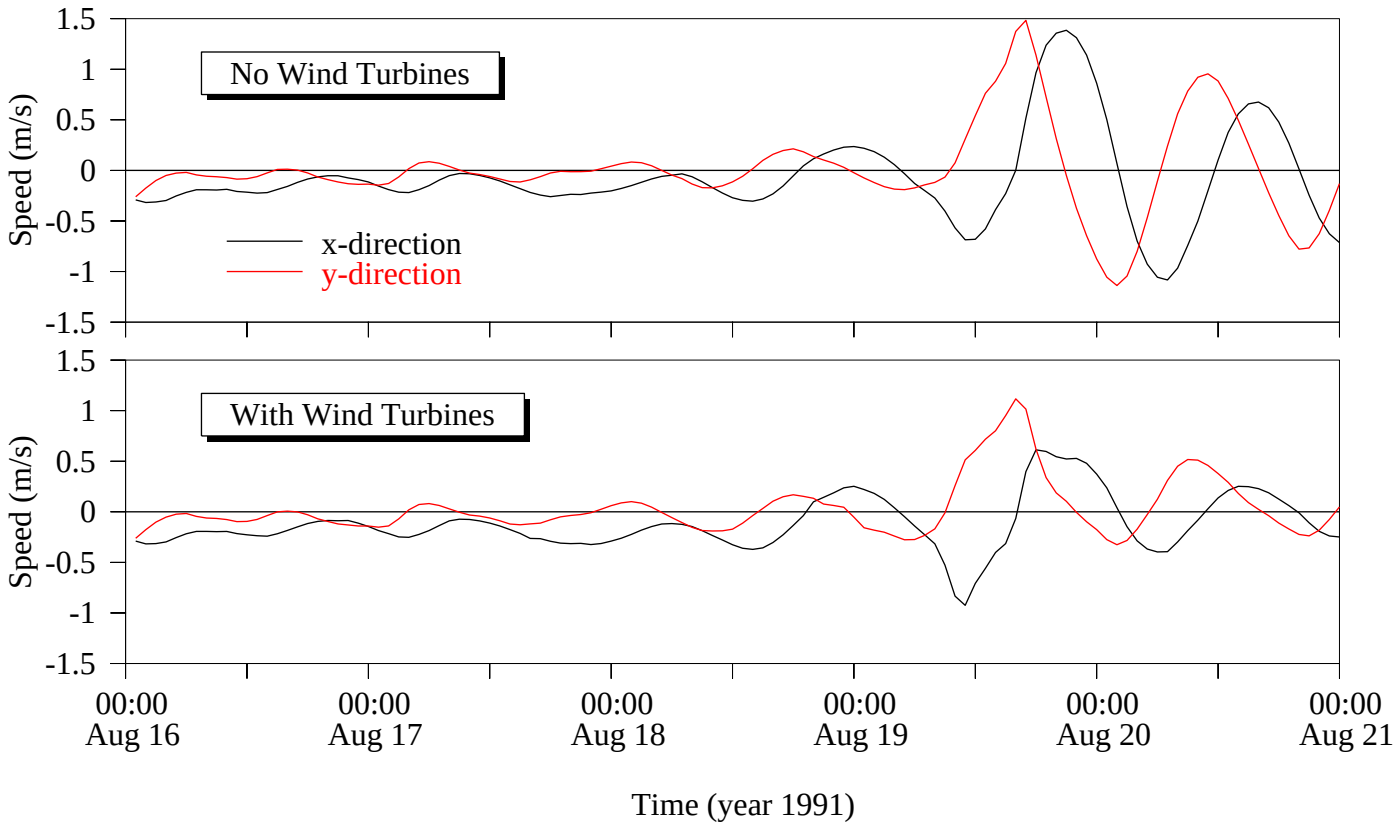

Figure 3.65: Time series of the x (eastward) and y (northward) components of a selected particle velocity with the same initial location for the case without and with wind turbines.

The Department of the Interior Mission

As the Nation's principal conservation agency, the Department of the Interior has responsibility for most of our nationally owned public lands and natural resources. This includes fostering the sound use of our land and water resources, protecting our fish, wildlife and biological diversity; preserving the environmental and cultural values of our national parks and historical places; and providing for the enjoyment of life through outdoor recreation. The Department assesses our energy and mineral resources and works to ensure that their development is in the best interests of all our people by encouraging stewardship and citizen participation in their care. The Department also has a major responsibility for American Indian reservation communities and for people who live in island communities.

The Bureau of Ocean Energy Management

The Bureau of Ocean Energy Management (BOEM) works to manage the exploration and development of the nation's offshore resources in a way that appropriately balances economic development, energy independence, and environmental protection through oil and gas leases,

www.boem.gov